DYNAMICS OF WATER AND NUTRIENTS IN

CLOSED, RECIRCULATING CROPPING SYSTEMS

IN GLASSHOUSE HORTICULTURE

With special attention to lettuce grown in irrigated sand beds

ii

Promotoren: dr. ir. R.A. Feddes
             hoogleraar in de bodemnatuurkunde, agrohydrologie en grondwaterbeheer

             dr. ir. P.A.C. Raats
             hoogleraar in de continuümmechanica

Dynamics of water and nutrients in closed, recirculating

cropping systems in glasshouse horticulture

With special attention to lettuce grown in irrigated sand beds

Marius Heinen

Proefschrift

ter verkrijging van de graad van doctor
op gezag van de rector magnificus
van de Landbouwuniversiteit Wageningen,
dr. C.M. Karssen,
in het openbaar te verdedigen
op dinsdag 25 maart 1997
des namiddags te vier uur in de Aula

Acknowledgement

Stellingen

1   Sturing van de watergift op basis van tensiometers in grove substraten stelt hoge eisen aan de nauwkeurigheid van het meetsysteem. Daarom kunnen beter watergehaltes worden gemeten, bijvoorbeeld met behulp van 'Time Domain Reflectometry' (TDR).
(Dit proefschrift)

2   Het moment van fertigeren dient niet alleen te worden bepaald door de waterbehoefte, maar mede op basis van de beheersing van concentratie of van geleidbaarheid van het substraatwater.
(Dit proefschrift)

3   Pas wanneer volledig sluitende massabalansen voor nutriënten kunnen worden opgesteld, kan met zekerheid geconcludeerd worden wat milieukundig (on)acceptabele verliezen zijn in de land- en tuinbouw.

4   Een gesloten teeltsysteem is een utopie.

5   Een Westlandse glastuinder die zijn gewas duurzaam in de grond wil telen kan het beste verhuizen naar een schone omgeving.

6   Goed, fundamenteel onderzoek is vrij, onafhankelijk, diep en kritisch nadenken. Veel uitkomsten van dat onderzoek kunnen niet van tevoren in projectvoorstellen worden aangegeven.
(gebaseerd op afscheidsrede 'Pleidooi voor meer nutteloosheid' van Prof. dr. ir. A. van den Beukel, TU Delft, 7 Februari, 1997)

7   Onverzadigde stroming bestaat niet.

8   Het betrekken van Nederlandse bodemfysici bij de aanleg van het substraatbed in de Amsterdamse Arena zou heel wat problemen hebben kunnen voorkomen.

9   Het feit dat slechts 0.0001% van al het water op de wereld in de bodem aanwezig is mag geen reden zijn om je hierom niet te bekommeren.
(Shafiqul Islam and Ted Engman, 1996. Why bother for 0.0001% of earth's water? Challenges for soil moisture research. EOS, Vol. 77: 420, 1996)

10   Het gebruik van 'ion-selective electrodes' (ISE) of van 'ion-sensitive field effect transistors' (ISFET) wordt pas interessant als deze naast een lange levensduur ook kleine meetfouten bezitten.
(Heinen M., 1992. Control of the composition of the nutrient solution in an automated NFT system: a simulation study. Acta Horticulturae 304: 281-289)

11   De argumentatie om het landbouwkundig onderzoek van LNV en DLO te centraliseren omdat dubbel werk, c.q. concurrentie niet goed is, is onjuist. Dat zoiets wel kan blijkt uit de drie viskramen die naast elkaar op de markt staan.

12   " ... it is more important to have beauty in one's equations than to have them fit the experiment ... "
(P.A.M. Dirac (1902-1984), Scientific American, May 1963)

13   Automatisering begint met au.

Stellingen behorende bij het proefschrift *"Dynamics of water and nutrients in closed, recirculating cropping systems in glasshouse horticulture. With special attention to lettuce grown in irrigated sand beds"* van Marius Heinen, Wageningen, 25 maart 1997.

Abstract

Heinen, M., 1997. Dynamics of water and nutrients in closed, recirculating cropping systems in glasshouse horticulture. With special attention to lettuce grown in irrigated sand beds. PhD Thesis, Wageningen Agricultural University, Wageningen, The Netherlands, 270 p., 80 figures, 30 tables, 216 references, English and Dutch summaries.

Due to the high leaching fractions commonly practised in glasshouse horticulture, environmental pollution is clearly a major concern. Switching from soil-based to closed, recirculating substrate-based cropping systems potentially offers a good solution to this problem. As an alternative to the usual trial-and-error method in designing these new systems and optimizing fertigation strategies, this thesis uses the approach of modelling processes in the root zone supported with some detailed experiments. For this purpose a two-dimensional simulation model is developed.

Water movement is described by the mixed volumetric water content-pressure head Richards equation, which is solved numerically using the control volume finite element method. When the entire flow domain is unsaturated, the solution is obtained by the alternating direction implicit method. Otherwise, the incomplete Cholesky conjugate gradient method is used. Nutrient transport occurs by convection, dispersion and diffusion. Water and nutrient uptakes by the roots are described by scaled-up versions of microscopic steady-rate solutions for uptake by a single root.

As a test case, large bedding cropping systems filled with coarse sand (median diameter 0.6 mm) were used. The hydraulic properties of the sand were determined by the equilibrium hanging water column and transient multi-step outflow methods. Hysteresis was taken into account. The main validation data were volumetric water content measured by the TDR method, pressure head, and drainage outflow. Water use, transpiration, root length density distribution and root radius were obtained in experiments as well, while other parameters were obtained from the literature. Additionally, data on lettuce growth and nutrient uptake are presented and in some cases compared with data obtained in nutrient film technique experiments and from the literature. Dry matter productions in the two systems were comparable, but nutrient uptake differed.

A reasonable agreement between simulated and measured data was obtained. The model was applied in some case studies. Coarse porous media usually have enough water available for long periods of evapotranspiration. However, high solute concentrations may develop near the surface of the substrate since solutes are left behind when water evaporates and the flow through these regions is limited. Therefore, it is advised to schedule fertigation based on salinity control rather than on water supply control. Saturated conditions at the bottom occur only for short periods, and aeration problems in coarse porous media are unlikely.

Additional keywords: control volume finite elements, evaporation, evapotranspiration, fertigation, hydraulic properties, hysteresis, multi-step outflow, nutrient balance, rockwool, root uptake, simulation model, soilless culture, TDR, transpiration

Voorwoord

Het proefschrift is klaar. Voorafgaande aan de inhoud wil ik de vele personen die fysiek en mentaal geholpen hebben zeer hartelijk bedanken.

Allereerst wil ik mijn promotoren Reinder Feddes en Pieter Raats bedanken voor hun inzet in de begeleiding. Pieter, jij was de initiator van het project waaruit dit proefschrift is ontstaan. Bij de aanvang van het project was nog niet duidelijk of het zou resulteren in een proefschrift. Maar jouw enthousiasme was een van de redenen dit proefschrift te schrijven. Reinder, jouw betrokkenheid bij dit proefschrift kwam pas later. Zo ben je niet betrokken geweest bij het experimentele werk. Toch kon je je vinden in de opzet van het onderzoek en het proefschrift. Jullie beider kritische opstellingen en de inhoudelijke discussies zijn zeer welkom geweest.

Bij de dagelijkse werkzaamheden heb ik zeer veel steun gehad aan een tweetal personen: Peter de Willigen en Anco van Moolenbroek. Peter, je was een grote hulp en aanspreekpunt met betrekking tot de modellering. We hebben samen de eerste aanzet voor het simulatiemodel geformuleerd, en de wortelopnamemodellen zijn van jouw hand. Anco, jij was de man achter de experimenten. Op afstand heb jij in ruime halve dagen zorg gedragen voor technisch werk, plantverzorging, en eerste resultaatverwerkingen. Je kon goed zelfstandig werken en goed omgaan met de vele ideeën en problemen die van mijn kant naar voren kwamen.

Naast de hierboven genoemde vier personen zijn er nog velen, die ik hieronder wil bedanken: Bram de Vos voor technische aspecten van meten, met name TDR, Kees Rappoldt voor aspecten van automatisch meten en de filosofie van computers en modellen, Wilfred Otten en Meine van Noordwijk voor de algemene discussies. Klaas Boersma en Gerrit Bargerbos waren verantwoordelijk voor de electronica. Hobbe Pijpker, John de Koning, Jellis de Jong, Eltjo Groendijk en Willem Smit construeerden alle benodigde onderdelen en apparatuur. Jan Zwiers, Gerard Brouwer, Klaas Harmanny, Mejid Lahmar en Falentijn Assink waren verantwoordelijk voor de fysische karakteriseringen en calibraties. Een aantal medewerkers van het PBG, voorheen PTG, te Naaldwijk ben ik ook dank verschuldigd: Cees Sonneveld en Cees de Kreij voor de algemene discussies met betrekking tot de inrichting van de kas en de proeven, Evert van Voorthuizen voor de hulp bij de drukke oogstmomenten, Jop Kipp, Wim Voogt, Gerrit Wever, Alex van den Bos voor de algemene discussies. Dank ook aan het centraal laboratorium van het AB-DLO voor het verwerken van de aangeleverde monsters. Ik ben de directie van het AB-DLO, voorheen IB-DLO, en alle successievelijke afdelings- hoofden (Pieter Raats, Jacques Neeteson, Kor Zwart, Oene Oenema) waaronder dit werk is uitgevoerd, dankbaar dat ik dit heb kunnen doen. Dank aan leden van de discussiegroep 2 van de C.T. de Wit Onderzoeksschool Produktie-Ecologie, en aan de leden van de stuurgroep 'GPP/MJP-G Gesloten Teelten', onder voorzitterschap van Henk van Oosten, voor de steun aan het project. Henk, je kon de dagelijkse gang van zaken in kas 306 bijna vanuit je stoel volgen, en telkens wanneer de kas even leeg stond vroeg je wanneer de volgende proef zou starten.

Dietmar Schwarz, herzlichen Dank für die intensive Arbeit, die du geleistet hast. Viele Stunden waren nötig, um das Wurzelsystem zu charakterisieren, und um die 'breakthrough' Kurve festzustellen.

John Nieber, I am grateful to have had the opportunity to discuss with you the general problems we have encountered in multi-dimensional modelling. Unfortunately, we were not able to solve the ADI problem. I am also thankful for the discussions I had with Peter Wierenga and Richard Hills about the same aspects.

Verder wil ik iedereen danken die geïnteresseerd en belangstellend waren naar de voortgang van mijn proefschrift.

Naast alle mentale werkzaamheden was de morele steun van Monique en mijn Ouders, en de fysieke inspannende ontspanning van mijn lunch-loopmaatjes onontbeerlijk.

Marius

Contents

JONGE SLA

Alles kan ik verdragen,
het verdorren van bonen,
stervende bloemen, het hoekje
aardappelen kan ik met droge ogen
zien rooien, daar ben ik werkelijk hard in.

Maar jonge sla in september,
net geplant, slap nog,
in vochtige bedjes, nee.

YOUNG LETTUCE

I can stand anything,
the shrivelling of beans,
flowers dying, I can watch
the potato patch being dug up
and not shed a tear - I'm
real hard in such things.

But young lettuce in September,
just planted, still tender,
in moist little beds, no.

Chapter 1

Introduction

1.1 Some aspects of glasshouse horticulture

The area of glasshouse horticulture in the Netherlands comprises only a small part of the total agricultural sector. In 1991 the total glasshouse horticultural area was about $10 \cdot 10^3$ ha (4500 ha vegetables, 5300 ha flowers, 200 ha others such as fruits) and the total agricultural area was about $770 \cdot 10^3$ ha (LEI and CBS, 1992). However, glasshouse horticulture contributed to 20% of the total agricultural financial yield and thus is an important sector. Both soil-based and soilless cropping systems exist. Under *soilless culture* is meant any cropping system in which the crop does not grow on a natural soil, but in which other artificial or natural substrates or no substrates are used. Examples are Nutrient Film Technique (NFT) - mostly used for research purposes -, rockwool slabs and potting systems. Around 1990 about 45% of all greenhouse cropping systems were soilless systems, but differences existed between crops: potting plants nearly 100%, vegetables about 50%, and cut flowers about 15%. Only a few firms used recirculating systems (NRLO, 1990). *Recirculating systems* are systems in which excess of water and dissolved nutrients, i.e. drain water, is collected and, mostly after sterilization, is reused. Soil-based systems are sometimes called *'open' systems*, since the bottom of the root zone is permeable to outflow - and inflow - of water and solutes. The presence of drains at the bottom of the root zone makes it possible to collect most, but not necessarily all, of the excess of water and solutes which can be reused. *Closed systems* are systems which have an impermeable bottom, e.g. a concrete floor, a plastic sheet or plastic gullies, so that all excess of water and solutes can be collected and reused. A big disadvantage of soil-based and non-recirculating soilless systems is that *excess of water, nutrients and pesticides* leach towards the groundwater or to open water systems, causing environmental pollution. Hence, the efficiency of nutrient use in these systems is often low. De Willigen and van Noordwijk (1987) and van Noordwijk (1990) stated that on average 40% to 80% of all nutrients applied to tomatoes and cucumber grown on non-recirculating rockwool slab systems lying on natural soils is leached from the root zone. Around 1990, the hazard for environmental pollution resulted in the Dutch policy[1] that all commercial horticultural growers had to change to closed management systems by the year 2000. Part of those closed management systems are closed, recirculating cropping systems.

---

[1] 'Nationaal MilieubeleidsPlan Plus NMP+', and 'StructuurNota Landbouw SNL'

1.2 Soilless culture

Apart from the reduction of environmental pollution, *soilless culture* has more *advantages*, but also *disadvantages* (see, e.g. FAO, 1990). *Advantages are*: control of nutrition and crop production, more uniform supply of water and nutrients, control of total salt content and pH in the root zone, reduced labour requirements since no cultivation and less or no weed management is needed, ease of sterilization of the root zone, sometimes improved yields, crop production in regions where the natural soil is unsuitable (e.g. soils with high natural salt contents), and more economic use of water. The better control possibility is due to the lower buffer capacities of the soilless culture systems. For example, the typical quantities of available nitrogen in the top 30 cm of greenhouse soils, in rockwool slabs and in NFT are 1875 mmol m^{-2}, 230 mmol m^{-2} and 68 mmol m^{-2}, respectively (Sonneveld, 1995). Potentially, a more even supply of water and nutrients can be achieved, however, the current equipment is still not good enough (Sonneveld, 1995). *Disadvantages are*: high investment costs and increased technical operation demands. It is remarkable that, at first sight, the simplest system NFT requires the highest investment costs. For example, in 1983 the estimated capital investment costs per hectare in the US were for sand culture, rockwool and NFT systems $ 50.000, $ 55.000 and $ 81.000, respectively (Jensen and Collins, 1985). In a study by Ruijs *et al.* (1990) for chrysanthemums, the investment costs[2] per hectare for several types of cropping systems ranged from *f* 250.000 (sand bed) to *f* 1.120.000 (NFT with moving gullies). The yearly inherent costs per hectare ranged for these systems from *f* 43.500 to *f* 189.000. In that study the systems were evaluated based on business economical, cropping system technical, environmental, and labour conditions and costs.

Soilless culture is being used for more than three centuries in *experiments*. Steiner (1985) reported that Robert Boyle published about plant growth in a water culture in 1666. The first sand cultures were used by A.F. Wiegmann in 1842 and L. Polstorff in 1842 (Steiner, 1985). *Studies on soilless cultures* are mainly descriptive: for example, determination of crop growth and development, and water and nutrient use and flows, both at the small conditioned scale at research stations, and at the level of a complete firm (e.g. Adams and Massey, 1984; van der Burg and Hamaker, 1984; Willumsen, 1984; Voogt, 1992; Sonneveld, 1994; van Moolenbroek, 1995) as well as at the regional scale (Hamaker, 1989; 1992). Such studies are valuable since they yield knowledge on the amounts of water and nutrients required by the crop. They do not yield insight, however, about the best management practice for supplying water and nutrients, nor about other root zone requirements. For these aspects insight is required how water, nutrient and gasses move through the root zone and where they are taken up. For example, van Noordwijk (1978) and van Noordwijk and Raats (1980, 1982) visualized flow patterns in rockwool slabs with dye tracer experiments, and discussed leaching requirements in relation to position

---

[2] In 1996 $ 1 ≈ *f* 1.7 (Dutch florin).

of drippers and drainage outlets. Raats (1980) theoretically described the use of water and
nutrient mass balances in closed and open cropping systems. The importance of physical
properties of the substrate is known also for longer periods (e.g. Chen *et al.*, 1980; Milks
et al., 1989; Wallach *et al.*, 1992a,b; Otten, 1994; da Silva *et al.*, 1995). More recently
also the importance of chemical properties becomes evident (Otten, 1994; de Kreij *et al.*,
1995; Gabriels *et al.*, 1995). Still, the use of physical and chemical knowledge of the
substrates to understand what happens in the substrate and which management strategy
is required to grow crops optimally on that specific substrate is scarce. A good example
of such a modelling approach based on physical and chemical properties of a potting
medium is described by Otten (1994).

The use of models and technical equipment in greenhouse horticulture is common
practice. It is not the place here to give a complete overview about that subject. A few
examples are: greenhouse climate control (e.g. Bot, 1991; Challa and van Straten, 1991),
modelling (evapo)transpiration (e.g. de Graaf and van den Ende, 1981; Bakker, 1986;
Stanghellini, 1987; Baille *et al.*, 1992), self-adaptive control of NFT (Chotai and Young,
1991; Chotai *et al.*, 1991; Young *et al.*, 1991), and control of composition of the nutrient
solution in NFT systems (e.g. Steiner, 1984; Okuya and Okuya, 1991; Heinen, 1992;
Heinen and Harmanny, 1992; van den Vlekkert, 1992).

1.3 Excess of water and nutrients

In all types of glasshouse cropping systems *excess of water and nutrients is supplied*,
partly because it ensures the grower that the plant has ample low cost water and nutrients
available, but mainly to remove accumulated nutrients or salts from the root zone.
Nutrients are commonly supplied dissolved in the irrigation water. This technique is
known as fertigation, derived from <u>ferti</u>lization and irri<u>gation</u>. However, the ratio of the
uptake of water and nutrients is usually not equal to that present in the supplied fertigation
or nutrient solution (de Willigen and van Noordwijk, 1987; Sonneveld, 1995). While
during a certain period absorption of nutrients occurs at a constant rate, water uptake may
vary, e.g. due to changes in incoming solar radiation, which is the main determining
factor for transpirative demand. Usually, the concentration of a nutrient in the fertigation
solution is such that the uptake concentration is less than the supply concentration (de
Willigen and van Noordwijk, 1987). This results in accumulation of nutrients in the root
zone, rather than in depletion. Since at higher total salt concentrations crop growth is
negatively affected, leaching is required. For some vegetable crops a high osmotic
pressure in the root zone is required for producing good quality products. In that case,
even a small leaching fraction results in a large amount of leaching of nutrients. Other
solutes present in the water may appear at too high concentrations as well. For example,
in coastal areas high concentrations of Na and Cl are present in the rain water. Especially
in closed, recirculating cropping systems these elements accumulate as time progresses.
Under such conditions the concentrations of these elements in the total system may

become too high, and the grower has to drain off - part of - the nutrient solution to open water or a sewer.

1.4 A new approach in research

In the intensively practised horticultural sector, environmental pollution is clearly one main matter of concern. Moreover, growing crops in soilless cropping systems may be a promising solution. Closed, recirculating cropping systems are not new. Examples are rockwool slabs in gullies for producing tomatoes, cucumbers, or sweet pepper, and potting plants produced on flooded benches. These are mostly crops with a low planting density, i.e. a few plants per unit area. For crops with a high planting density, such as lettuce, spinach, radish and some flowers, closed, recirculating, soilless cropping systems were still lacking around 1991. These types of crops require 'full-greenhouse' substrates. To reduce investment costs, a thin layer of a substrate is preferable. The natural soil in thin layers cannot be used, because, when frequently watered, it will remain too wet, causing aeration problems for the roots. Instead, coarse substrates need to be used. Up to now the design of closed, recirculating cropping systems and the development of fertigation management strategies for these systems are rather empirical. Knowledge of flow of water and transport of nutrients and gases in natural and artificial substrates is a helpful tool for the development and scientific foundation of such systems. Furthermore, knowledge on the development and functioning of root systems in substrates, the water and nutrient demand of crops, and the greenhouse climate are needed.

The *aim of this thesis* is to formulate and validate a simulation model for water movement and nutrient transport in closed, recirculating cropping systems. It should be a starting point for management models that can be used to obtain growth systems with minimal input of external materials - water, nutrients, pesticides -, with a high production of good quality, and with a minimal nuisance to the environment. Of course, this approach is not restricted to closed, recirculating cropping systems, but can also be applied for open, soil-based systems. The reason for choosing closed systems as the main object of study is that these systems are better defined and controllable.

The modelling approach is rather new. A good example of a comparable modelling approach based on physical and chemical properties of a potting medium has been described by Otten (1994). In fact, Otten's and my own research together give insight in the dynamics of water and nutrients in two different closed, recirculating cropping systems.

In this study I focussed on closed bedding systems, with a *sand bed system* as a test case in experiments. Sand or gravel bedding systems as cropping systems in horticulture are not new. They were, for example, used in the United States of America in the early seventies (Collins and Jensen, 1983; Jensen and Collins, 1985).

The present study is not meant to tackle all problems concerning closed, recirculating cropping systems. For example, no attention has been paid to the feasibility of sand bed systems for practical use, with respect to investment costs, energy and labour requirements, optimal plant nutrition schemes, sterilization, and use of pesticides. Examples of such studies can be found in other recent projects (see NRLO, 1990).

1.5 Objectives and layout of this thesis

This thesis consists of three main parts. In the first, theoretical, part I formulate a simulation model for water movement and solute or nutrient transport with the presence of root uptake (Chapters 2, 3 and 4). In the second part I describe experimental conditions and experimental results which were used to collect input data, boundary conditions and validation data and use these in the simulation model (Chapters 4, 5, 6, 7). In the third part I show how the simulation model can be used to give answers to practical problems, which is demonstrated in some case study problems (Chapter 8). The rationale for doing only a few experiments with only one system was to characterize and describe one system in detail.

For cropping systems with localized input and output of water and nutrients, one-dimensional simulation models for water movement and solute transport can usually not be used. An exception is, for example, the mainly one-dimensional process in potted plants as described by Otten (1994). The *sand bed system*, that was used for the experiments, consisted of a 15 cm layer of coarse sand overlying a drainage system that was located on top of a concrete greenhouse floor (Photo 1; Figure 1-1). A full description is given in Chapter 5. As is obvious from Figure 1-1, half the region between two drains is an element that repeats itself in this system. Due to symmetry reasons, I needed to consider only this region in the simulation model (Figure 1-1B). Water movement and nutrient transport will obviously be far from one-dimensional. The presence of the drippers and roots suggests three-dimensional water movement and solute transport. However, as a first rough approximation I decided to consider the processes in two dimensions for simplicity reasons. Since multi-dimensional models are scarce and always suitable for all kinds of problems, I decided to develop my own model.

In *Chapter 2* water movement is described by the Richards equation including a sink term for root water uptake (Section 2.1) and the general expressions for boundary and initial conditions are given, with special attention to the sand bed system (Section 2.2). Root water uptake is described by a macroscopic version of the steady rate description of water distribution around a single root (de Willigen and van Noordwijk, 1987) (Section 2.3). The governing transport equation for solute or nutrient transport including a sink term term for root uptake is given in Section 2.4, followed by the boundary and initial conditions (Section 2.5). Root nutrient uptake is, in analogy to water uptake, described
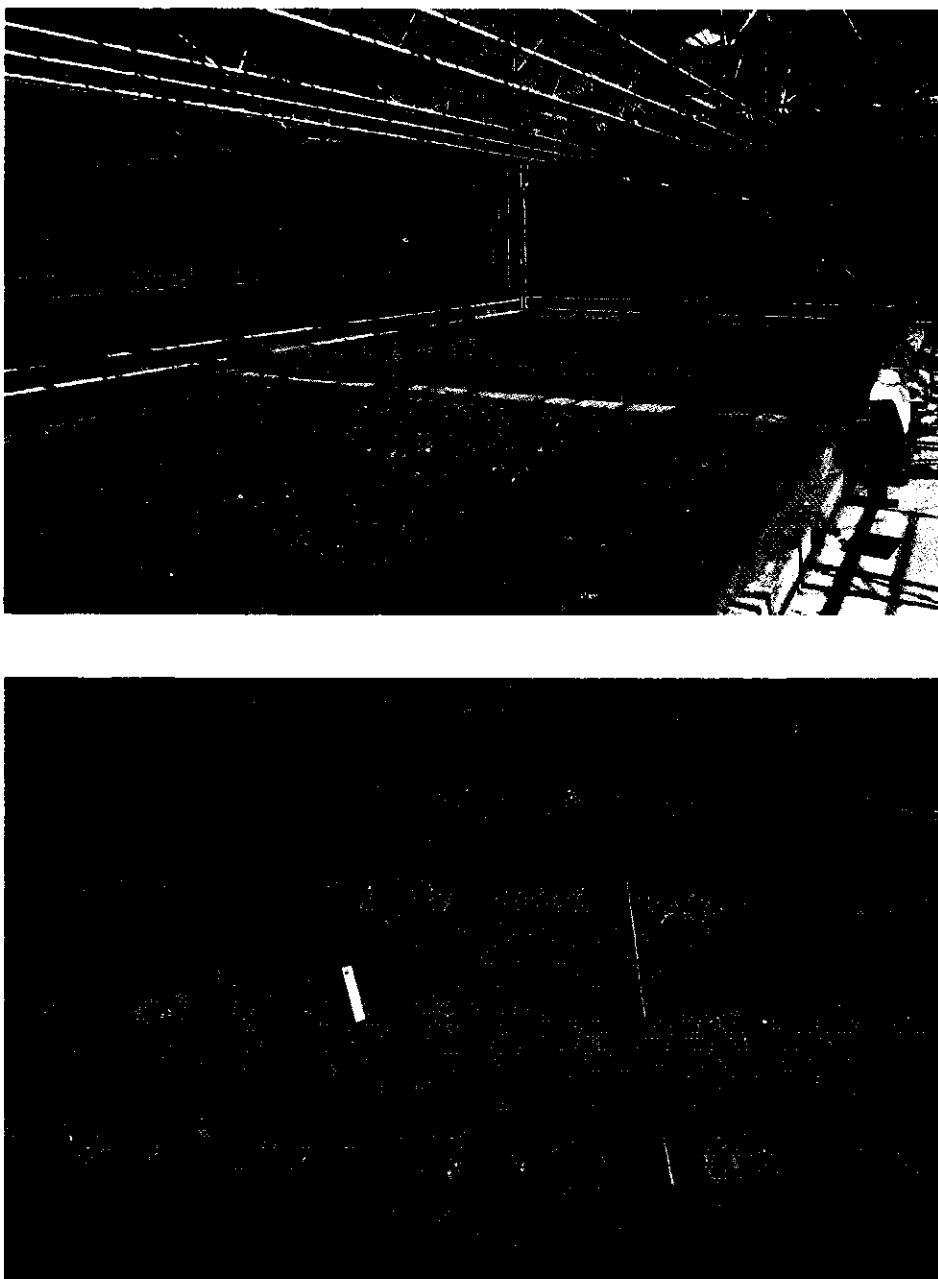
Photo 1 (Top) Overview of greenhouse compartment with lettuce growing in irrigated sand beds, and (Bottom) a detailed view of lettuce in coarse sand with a dense grid of drippers.
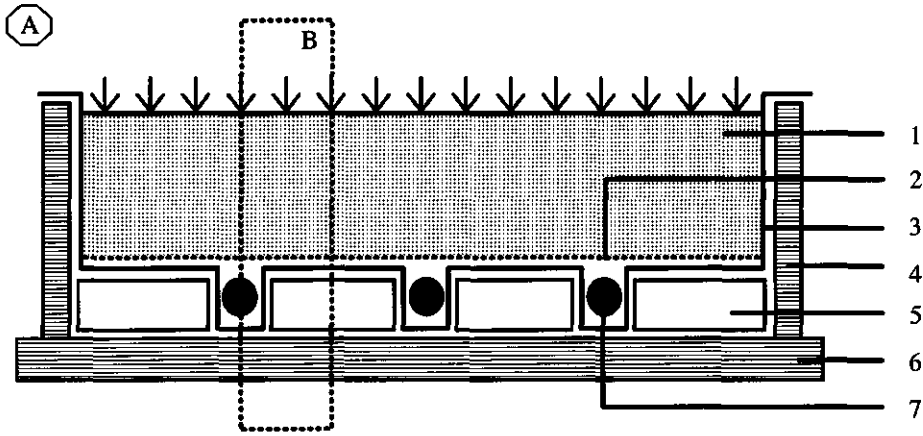
1: 15 cm coarse sand   5: extended polystyrene foam

2: anti rooting mat   6: concrete floor

3: impermeable plastic sheet   7: corrugated drain

4: concrete wall
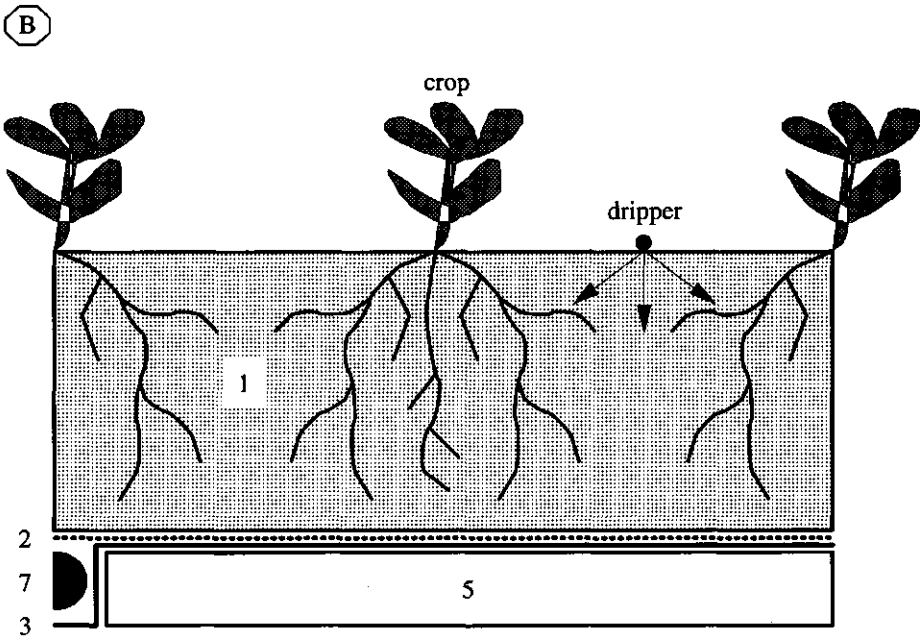
Figure 1-1 (A) Schematic representation of the sand bed cropping system and (B) an enlargement of half the region between two drains.

by a macroscopic version of a steady rate solution for concentration distribution around a single root (de Willigen and van Noordwijk, 1987, 1994a,b; Section 2.6).

In *Chapter* 3 the numerical solution of the governing water movement and nutrient transport equations is presented. Water movement is solved by a control volume finite element method including the mass conservative technique proposed by Celia *et al.* (1990) (Section 3.2). The procedure is described in detail, since this control volume method is not used very much. The resulting set of difference equations is written in matrix notation and is solved by either using the alternating direction implicit method or the incomplete Cholesky conjugate gradient method (Section 3.3). The problem of nutrient transport is solved explicitly based on new information about volumetric water content and water flux densities obtained from the water movement description (Section 3.4).

In *Chapter* 4 the mathematical functions for the hydraulic properties by van Genuchten (1980) and Mualem (1976) are used (Section 4.1). Hysteresis is considered in Section 4.2 where the modified dependent domain model of Mualem (1984) is applied to describe scanning curves. Also in this chapter the physical characterization of the coarse sand used as substrate in this study is presented (Section 4.3), which consists of particle weight fraction distribution, porosity, hydraulic conductivity at saturation, and the water retention and hydraulic conductivity characteristics.

In *Chapter* 5 the sand bed system is described: experimental layout (Section 5.1), measurement equipment (Section 5.2), and water supply control system (Section 5.3). In Section 5.4 a short description of the experiments is presented.

In *Chapter* 6 the growth (Section 6.1), rooting characteristics (Section 6.2), and water (Sections 6.3 and 6.4) and nutrient (Sections 6.5 and 6.6) balances of lettuce grown in irrigated sand beds are presented. Time courses of temperatures and electrical conductivity as measured in the sand beds are given in Sections 6.7 and 6.8, respectively.

In *Chapter* 7 measured and simulated conditions in the root zone are presented. First the input data are briefly described (Section 7.1). The in-situ water retention data are compared with the main envelopes of the water retention characteristic as determined in Chapter 4 (Section 7.2). The results with respect to the water part of the model refer to volumetric water content and drain outflow (Section 7.3) and pressure head (Section 7.4). The simulation model was calibrated for two parameters occurring in the solute transport module using breakthrough data (Section 7.5). As a demonstration the simulated dynamics of a solute are presented in Section 7.6.

In *Chapter* 8 I show examples of how the simulation model can be used in studying, designing, or optimizing a cropping system. Some practical questions are dealt with. What

is the maximum height of a phreatic surface and its time of disappearance during an irrigation-drainage cycle in a bedding system, and can these features be predicted by existing analytical solutions? (Section 8.1). What is the maximum allowable time span between two fertigation events, and what should determine that? In other words, how much water is available in the cropping system, and how are the concentrations of solutes affected when the substrate dries out? (Section 8.2). How much new solution must be flushed through the substrate to replace a resident solution by the new solution? (Section 8.3). Can the simulation model be used for other substrates and other cropping systems as well? In Section 8.1 different substrates will be used, and in Section 8.4 some simulation results for a rockwool slab cropping system will be presented.

Chapter 2

Water movement, nutrient transport

and root uptake : theory

Water movement in the root zone supplies the roots with water to fulfill partly or entirely the transpirative demand of the crop. Soil water is the medium for diffusive/dispersive transport of nutrients in the soil. With the water nutrients or other solutes are transported towards the root surface. Moreover, soil biological and soil chemical processes are strongly influenced by water content. Therefore, knowledge of the water content and water movement in the root zone is a prerequisite. In this chapter the basic mathematical formulations for water movement and nutrient transport are presented in Sections 2.1 and 2.4, respectively. Boundary and initial conditions for water movement and nutrient transport are discussed in Sections 2.2 and 2.5, respectively. Models for root water and nutrient uptake are given in Sections 2.3 and 2.6, respectively. I assume that the reader is familiar with some basics of soil physics, such as volumetric water content, flux density, porosity, and the head equivalent for soil water potential (see e.g., Hanks and Ashcroft, 1980; Hillel 1980a,b; Koorevaar *et al.*, 1983).

2.1 Water movement in porous media

Water movement in a porous medium always obeys the *law of conservation of matter*. Mathematically the continuity equation for incompressible water in rigid porous media in three dimensions is written as

$$\frac{\partial \theta}{\partial t} = -\nabla \cdot (\theta \mathbf{v}) - S_w$$

[2-1]

$$= -\nabla \cdot \mathbf{q} - S_w,$$

where θ is the volumetric water content ($L^3 L^{-3}$), t is time (T), $\nabla \cdot$ is the divergence operator (L^{-1}), $\mathbf{v}$ is the velocity (LT^{-1}) of the water, $\mathbf{q} = \theta \mathbf{v}$ is the volumetric water flux density ($L^3 L^{-2} T^{-1}$), and S_w is the volumetric sink (or source) strength for water ($L^3 L^{-3} T^{-1}$), e.g. root water uptake. In general, all dependent variables in this section, such as θ, $\mathbf{v}$, $\mathbf{q}$ and S_w, are functions of the independent variables x, y, z, and t, where x and y are the horizontal coordinates (L) and z is the vertical coordinate (L), taken positive downwards. For convenience, the spatial and temporal functional dependency is left out from the notation in this thesis. For saturated porous media, Darcy (1856) obtained experimentally that $\mathbf{q}$ is proportional to the gradient in water potential. Buckingham

(1907) extended Darcy's law to partially saturated porous media. With the water potential expressed as an head equivalent, (the extended) *Darcy's law* reads

$$\mathbf{q} = -K(\theta)\nabla H, \qquad\qquad [2\text{-}2]$$

where K is the hydraulic conductivity $(\mathrm{LT^{-1}})$ of the porous medium, ∇ is the gradient operator $(\mathrm{L^{-1}})$, and H is the hydraulic head (L) being the sum of the pressure head h (L) and the gravitational head z_g (L):

$$H = h(\theta) - z_g, \qquad\qquad [2\text{-}3]$$

where the minus sign results from z taken positive downwards. The dependent variables K, H and h depend on x, y, z and t. The relationships $h(\theta)$ and $K(h)$ are subject to hysteresis, while $K(\theta)$ is considered not to be subject to hysteresis (Miller and Miller, 1956); the hydraulic properties are discussed in Chapter 4. The direction of flow is opposite to the gradient in total head, which explains the minus sign in Eq. [2-2]. Richards (1931) combined Darcy's law and the continuity equation to obtain the governing non-linear partial differential flow equation for water in porous media. *For variably saturated, heterogeneous, isotropic, rigid, isothermal porous media and incompressible water, the Richards equation is given by*

$$\frac{\partial\,\theta(h)}{\partial\,t} = \nabla\cdot\left[\,K(\theta)\nabla h(\theta)\,\right] - \frac{\partial K(\theta)}{\partial z} - S_w. \qquad\qquad [2\text{-}4]$$

In unsaturated porous media $h < h_a$, with h_a being the air-entry value, and in saturated porous media $h \geq h_a$; I assume $h_a = 0$. For given relationships between K-θ-h (see Chapter 4) and for given initial and boundary conditions (see Section 2.2) and the sink strength (see Section 2.3), the problem is fully defined and can be solved, provided that flux boundary conditions are not ill-posed. However, due to the non-linear relationships between K-θ-h, analytical solutions are available only for special cases. For most practical problems numerical techniques must be applied, as is done in Chapter 3.

In this thesis I will use the mixed θ-h form of the Richards equation (Eq. [2-4]). In many other studies the Richards equation is rewritten, so that it has only one dependent variable, either θ or h. The θ-based form or diffusivity form of the Richards equation is restricted to unsaturated, homogeneous porous media and processes not involving hysteresis, and, therefore, not attractive to be used. The h-based form of the Richards equation reads

$$C(h)\frac{\partial h}{\partial t} = \nabla\cdot\left[\,K(h)\nabla h\,\right] - \frac{\partial K(h)}{\partial z} - S_w, \qquad\qquad [2\text{-}5]$$

where the differential moisture capacity C $(\mathrm{L^{-1}})$ is defined as

$$C = \frac{\mathrm{d}\,\theta}{\mathrm{d}\,h}. \qquad\qquad [2\text{-}6]$$

The h-based form of the Richards equation can handle partially saturated, heterogeneous

porous media and is used mostly. However, although Eq. [2-5] is exactly equal to Eq. [2-4], problems with respect to mass balance are experienced when solving it numerically. This is not the case when solving Eq. [2-4] numerically, as is done in this thesis (Chapter 3).

It is convenient to introduce here the matric flux potential ϕ (L^2T^{-1}) as it will be used later in this chapter (Gardner, 1958, Raats, 1970):

$$\phi(h) = \int_{h_{ref}}^{h} K(\eta)\,d\eta, \qquad [2\text{-}7]$$

where h_{ref} is some reference value for h and η (L) is a dummy variable of integration.

2.2 Boundary and initial conditions for water movement

The governing flow equation can be solved for given boundary and initial conditions. A general form of the boundary conditions can be given as (e.g. McCord, 1991)

$$\mu h + v \frac{\partial(h-z)}{\partial n_\Gamma}\bigg|_\Gamma = B, \qquad [2\text{-}8]$$

where μ, v and B are given functions evaluated on the boundary Γ of the region which are dependent on x, y, z and t, n_Γ is the coordinate normal to Γ, and $\partial/\partial n_\Gamma|_\Gamma$ is the exterior normal derivative operator. The following types are distinguished:

- for $\mu \neq 0$ and $v = 0$, Eq. [2-8] represents a first-type or *Dirichlet* boundary condition,
- for $\mu = 0$ and $v \neq 0$, Eq. [2-8] represents a second-type or *Neumann* boundary condition, and
- for $\mu \neq 0$ and $v \neq 0$, Eq. [2-8] represents a third-type or *Cauchy* boundary condition.

In this thesis I use only the Dirichlet and Neumann conditions.

The *Dirichlet* condition, with $\mu = 1$, $v = 0$ and $B = h_\Gamma$ in Eq. [2-8], is given as

$$h = h_\Gamma, \qquad [2\text{-}9]$$

where h_Γ is the prescribed pressure head at the boundary.

The *Neumann* condition, with $\mu = 0$, $v = K_\Gamma$ and $B = q_\Gamma$ in Eq. [2-8], is given as

$$K_\Gamma \frac{\partial(h-z)}{\partial n_\Gamma} = q_\Gamma, \qquad [2\text{-}10]$$

where q_Γ is the prescribed volumetric flux density at the boundary, for example, known irrigation rate or no flow across an impermeable boundary. An alternative form of the Neumann condition is the specified hydraulic gradient condition, i.e with $\mu = 0$, $v = 1$ and

$B = B_\Gamma$ in Eq. [2-8], where B_Γ is the specified hydraulic gradient at the boundary. This Neumann condition is given as

$$\left.\frac{\partial h}{\partial n_\Gamma}\right|_\Gamma = B_\Gamma .$$ [2-11]

In the cross-sectional view of the sand bed system (Figure 1-1A) a sequence of repeating regions can be distinguished, i.e. half of the region between two drains (Figure 1-1B). The boundary conditions for this region are as follows (Figure 2-1). The *upper boundary condition* at the porous medium-atmosphere interface is a Neumann or prescribed volumetric flux density:

$$\left.q_z\right|_{z=0} = q_0, \quad 0 \leq x \leq X,$$ [2-12]

where q_z is the vertical component of the volumetric flux density, q_0 is the prescribed volumetric flux density across the top boundary, and X is the total width (L) of half the region between two drains, i.e., half the drain distance.

The *lower boundary* to the right hand side of the drain with radius x_D (L) is impermeable due to the presence of an impermeable foil, so that the boundary condition is that of no flow (Neumann):
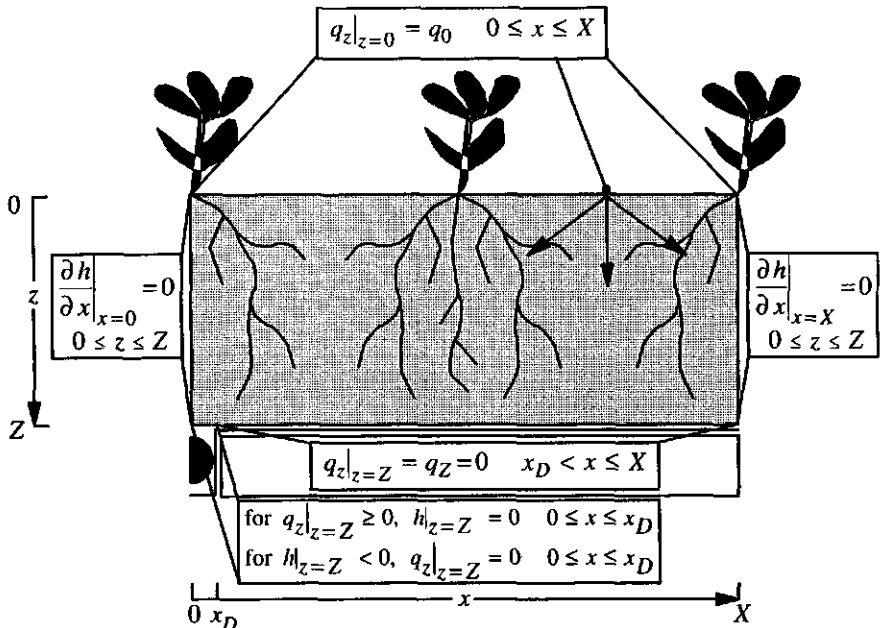
Figure 2-1 Half the region between two drains (see Figure 1-1) showing the boundary conditions for water movement.

$$q_z\big|_{z=Z} = q_Z = 0, \quad x_D < x \le X, \tag{2-13}$$

where q_Z is the prescribed volumetric flux density across the bottom boundary, and Z is the total depth (L) of the layer of substrate.

In this thesis *drains* are considered as well. The drains are located in an impermeable base of the flow domain. Water flowing into the drain is assumed to be discharged fast so that the drain never runs full. The air pressure inside the drain is assumed to be always atmospheric. Water flows into the drain at atmospheric pressure and it is assumed that no water can enter from the drain back into the porous medium. Thus, the *drain condition* to be used is that of a *horizontal seepage face*. Seepage face conditions have been used by others as well (e.g. Rubin, 1968; Neuman *et al.*, 1974; Cooley, 1983; Simunek *et al.*, 1994). In case the porous medium is saturated at the drain there will be outflow and the boundary condition at the drain will be of Dirichlet type, i.e. $h = 0$. As soon as the substrate at the drain location becomes unsaturated, the boundary condition at the drain will be that of no-flow Neumann type, i.e. $q_z = 0$. The seepage face may be partly of Neumann type and partly of Dirichlet type. The *seepage face conditions* are

$$\text{for } q_z\big|_{z=Z} \ge 0, \quad h\big|_{z=Z} = 0, \quad 0 \le x \le x_D, \tag{2-14}$$

or

$$\text{for } h\big|_{z=Z} < 0, \quad q_z\big|_{z=Z} = 0, \quad 0 \le x \le x_D. \tag{2-15}$$

Due to symmetry considerations *the left at x = 0, and right at x = X, boundaries* for all z are no flow boundaries, i.e. of Neumann type:

$$\frac{\partial h}{\partial x}\bigg|_{x=0} = 0, \quad 0 \le z \le Z, \tag{2-16}$$

and

$$\frac{\partial h}{\partial x}\bigg|_{x=X} = 0, \quad 0 \le z \le Z. \tag{2-17}$$

The *initial condition* is that of given initial pressure head h_0 distribution

$$h\big|_{t=0} = h_0(x, y, z). \tag{2-18}$$

2.3 Root water uptake

De Willigen and van Noordwijk (1987) developed a microscopic model for root water uptake. For one root surrounded by a hollow cylinder of substrate, the rate q_2 (LT^{-1}) of water movement from the substrate towards the root surface is equal to the uptake rate q_1 (LT^{-1}) by the root, which in turn is equal to the actual transpiration rate T (LT^{-1}):

$$q_1 = q_2 = T.$$ [2-19]

In this analysis the amount of water needed for growth and turgor regulation is disregarded.

Now consider one layer of substrate of thickness Δz (L) with equally distributed, parallel roots perpendicular to the porous medium surface. Each root with a radius of R_0 (L) is surrounded by a part of the substrate which can be represented by an equivalent hollow cylinder. The outer radius of this equivalent hollow cylinder R_1 is simply related to the root length density L_{rv} (LL^{-3}), i.e. root length per unit volume of porous medium, according to

$$R_1 = \left(\sqrt{\pi L_{rv}} \right)^{-1}.$$ [2-20]

Now it is possible to extend the single root model to a layer with known root length density. Within Δz there is supposed to be no vertical gradient in h, so that only radial flow towards the root surface is considered. In what follows, expressions for the three terms of Eq. [2-19] will be given. I do not use vector notation for fluxes to or away from individual roots, but only the magnitudes of the fluxes, with flow towards or into the root being positive. A schematic representation of the geometry and notation convention for root water uptake is given in Figure 2-2.

The *uptake rate* q_1 by roots from one layer of thickness Δz with a given root length density L_{rv} is given as (see also e.g. Gardner, 1960)

$$q_1 = \Delta z \, L_{rv} K_1 (h_{rs} - h_r),$$ [2-21]

where K_1 is the root hydraulic conductance (LT^{-1}), h_r is the root pressure head assumed to be uniform over the whole root system, and h_{rs} is the pressure head at the root-substrate interface. Considering h_r to be uniform is justified as follows. The change in water potential from roots to leaves is small compared to the change in water potential between leaves and atmosphere (e.g. Hillel, 1980b; his Figures 6.7 and 6.8). Moreover, the gradient in the root xylem vessels is small according to Poiseuille's law

$$\frac{\Delta h}{\Delta z} = \frac{8 \, q_1 \, \eta_l}{r_x^2 \, \rho_l g} + 1,$$ [2-22]

where η_l is the viscosity of water ($= 10^{-2} \, \mathrm{g\,cm^{-1}\,s^{-1}}$), ρ_l is the density of water ($= 1.0$
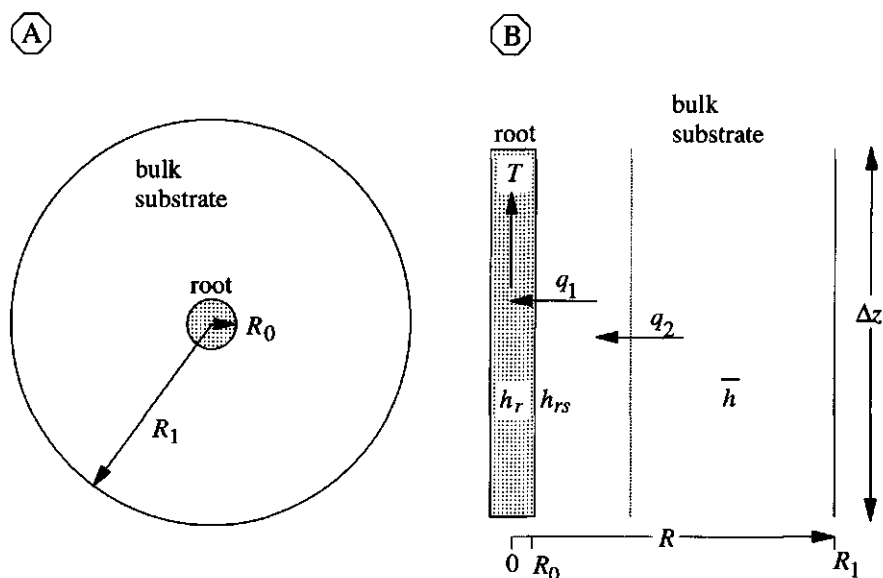
Figure 2-2 Geometry and notation convention for root water uptake model; (A) horizontal and (B) vertical cross sections through root and substrate cylinder.

g cm^{-3}), r_x is the radius of a xylem vessel (cm), and g is the gravitational field strength (= 980 cm s^{-2}). Wind (1955) observed for grass a relationship between root radius and xylem vessel radius. For a root radius of 0.02 cm, r_x equals 16.3·10^{-4} cm. For a transpiration of 0.2 cm d^{-1} it then follows from Eq. [2-22] that the gradient in water potential inside the root xylem vessel is 1.00007. For root lengths of 15 cm (maximum vertical root length in sand bed system) a difference in water pressure head in the roots of only 15 cm suffices, which in most cases is much smaller than the absolute values of root water pressure heads of e.g. -5000 cm (e.g. Taylor and Klepper, 1978).

The variables q_1, L_{rv}, h_r, and h_{rs} are generally time-dependent. In principle, K_1 is dependent on h_r and t, but this is not considered in this thesis, i.e K_1 is assumed to be constant.

Due to the highly non-linear relationship in the hydraulic properties, it is not possible to obtain an analytical solution for water movement in the substrate around the root. However, de Willigen and van Noordwijk (1987) showed that a *steady-rate solution for the matric flux potential* (Eq. [2-7]) *distribution* $\phi(R)$ (L^{2}T^{-1}) can be used, given by (Figure 2-3)

Steady-rate matric flux potential ($\phi(R)-\phi(R_0)$) (cm^2 d^{-1})
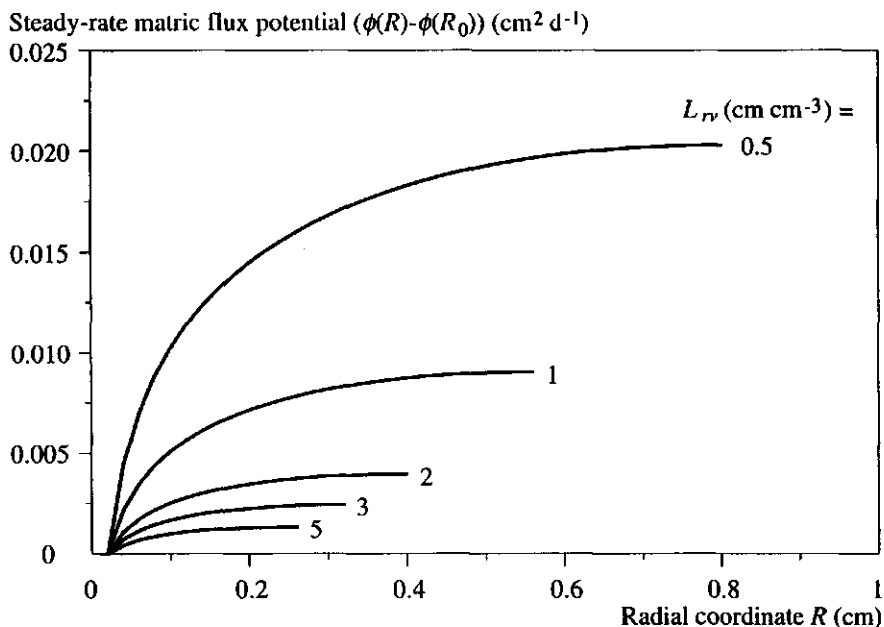
Figure 2-3   Steady-rate matric flux potential distribution ($\phi(R)-\phi(R_0)$) around a single root as
a function of the radial coordinate R according to Eq. [2-23] for five values of the
root length density L_{rv}; other parameters are: $R_0 = 0.02$ cm, $\Delta z = 10$ cm, and
$T = 0.2$ cm d^{-1}. The end points of the curves represent $R = R_1$.

$$\phi(R) \; = \; \phi(R_0) \; + \; \frac{T}{2\,\pi\,L_{rv}\,\Delta z}\left[\frac{\rho^2}{\rho^2-1}\,\ln\frac{R}{R_0} \; - \; \frac{\left(R/R_0\right)^2 - 1}{2\left(\rho^2-1\right)}\right], \qquad [2\text{-}23]$$

where R is the radial coordinate (L), and ρ is a dimensionless reduced radius of the
substrate cylinder surrounding each root defined by $\rho = R_1/R_0$.

The *rate q_2 at which water arrives at the root surface* is proportional to the difference
between the average matric flux potential in the hollow soil cylinder surrounding the root $\overline{\phi}$
and the matric flux potential ϕ_{rs} at the soil/root interface:

$$q_2 \; = \; \Delta z\,\pi L_{rv}\,\frac{(\rho^2-1)}{G_0(\rho)}\left(\overline{\phi} - \phi_{rs}\right), \qquad [2\text{-}24]$$

with $\overline{\phi}$ defined as

$$\overline{\phi} = \frac{\int\limits_{R_0}^{R_1} 2\,r\,\phi(R)\,\mathrm{d}R}{R_1^2 - R_0^2}\,, \qquad\qquad [2\text{-}25]$$

and $G_0(\rho)$ is a dimensionless geometry function given by

$$G_0(\rho) = \frac{1}{2}\left(\frac{1-3\rho^2}{4} + \frac{\rho^4 \ln\rho}{\rho^2-1} \right). \qquad\qquad [2\text{-}26]$$

$G_0(\rho)$ is a special case of the geometry function $G(\rho,\sigma)$ given in Section 2.6 (Eq. [2-50]; Figure 2-7).

The *actual transpiration rate* T can be assumed to be a function of the potential transpiration rate T_p (LT^{-1}) and the root water pressure head h_r according to

$$T = f_r(h_r)\,T_p\,. \qquad\qquad [2\text{-}27]$$

For example, Campbell (1985, 1991) gave the following reduction function (Figure 2-4)
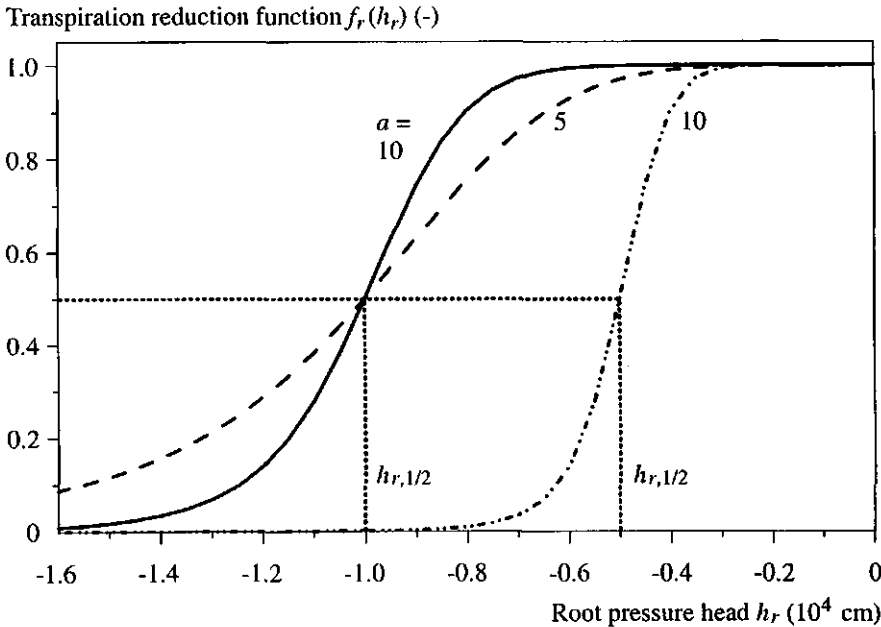
Figure 2-4 The transpiration reduction function, Eq. [2-28], as a function of the root pressure head for three sets of parameter values $h_{r,1/2}$ and a.

$$f_r(h_r) = \left[1 + \left(\frac{h_r}{h_{r,1/2}} \right)^a \right]^{-1}, \qquad\qquad [2\text{-}28]$$

where $h_{r,1/2}$ is a species-dependent plant pressure head at which, $T = 0.5 T_p$ and a is a species-dependent dimensionless constant.

The root water uptake model is solved by finding h_r, h_{rs} and T for given pressure head in the substrate so that Eq. [2-19], with Eqs. [2-21], [2-24] and [2-27]+[2-28], is satisfied. Due to the non-linear relationships between h and ϕ and between T and h_r, the solution has to be found iteratively. The root water uptake can be used as the sink strength S_w. Here the single root model was extended to a single layer with given root length density. It can be extended to multi-layers or to compartments, each with its own root length density (see Chapter 3, Subsection 3.2.5).

The $\phi(h)$ relationship is hysteretic, and the root water uptake module should account for that. Explicit formulations for $K(h)$ scanning curves are not available to my knowledge. Principally, one could derive these scanning curves from the $\theta(h)$ and $K(\theta)$ relationships. This needs further research and is not included in this thesis. Both $\overline{\phi}$ and ϕ_{rs} will be obtained from the main drying $K(h)$ relationship, and thus will be overestimated. As long as the difference between h of the bulk soil in the hollow soil cylinder and h_{rs} is not too large, it is anticipated that the error in disregarding hysteresis will be small. Such situations can be expected under wet conditions.

Under very wet conditions, e.g. in greenhouse substrates, the steady-rate solution for water distribution around a root can also be expressed in terms of volumetric water content according to

$$\theta(R) = \theta(R_0) + \frac{T}{2\pi \Delta z L_{rv} D_w} \left[\frac{\rho^2}{\rho^2 - 1} \ln \frac{R}{R_0} - \frac{(R/R_0)^2 - 1}{2(\rho^2 - 1)} \right]. \qquad [2\text{-}29]$$

Note that Eq. [2-29] is similar to Eq. [2-23], except for the presence of the diffusivity D_w ($L^2 T^{-1}$). Under these wet conditions the gradient in θ may be very small or negligible, so that $\overline{\phi} \approx \phi_{rs}$ and thus $h_{rs} \approx h$. In that case $q_2 = 0$, and the solution of the water uptake model is restricted to finding q_1 and h_r. In that case, the plant pressure head can be computed from

$$h_r = h - \frac{T}{K_1 L_{rv} \Delta z}. \qquad\qquad [2\text{-}30]$$

2.4 Nutrient transport in porous media

The *continuity or mass balance equation for nutrient transport* at any point in a rigid porous medium is given by (e.g. Bolt, 1982)

$$\frac{\partial Q}{\partial t} = -\nabla \cdot \mathbf{q}_s - S_s,$$ [2-31]

where Q is the total density (ML^{-3}) of the nutrient present in the porous medium, $\mathbf{q}_s$ is the nutrient mass flux density ($ML^{-2}T^{-1}$), and S_s is a mass sink (or source) strength ($ML^{-3}T^{-1}$) for a solute or nutrient, e.g. root nutrient uptake. In general, all dependent variables in this section are dependent on x, y, z and t. Equation [2-31] must be used for each nutrient separately. The nutrient can be present in solution, at the adsorption complex, or as a precipitate. In this thesis I assume that precipitation does not occur and that the porous medium is inert, i.e. it has no adsorption complex for all nutrients present, so that Q is given as

$$Q = \theta c,$$ [2-32]

where c is the nutrient concentration (ML^{-3}). *Nutrient transport is by mass flow with the water and by diffusion and dispersion due to gradients in concentration*, so that $\mathbf{q}_s$ is given as

$$\mathbf{q}_s = \mathbf{q}\,c - \mathbf{D}_h \cdot \nabla c,$$ [2-33]

where $\mathbf{D}_h$ is the hydrodynamic dispersion tensor (L^2T^{-1}) being the sum of the dispersion and diffusion tensors, and it is symmetric for isotropic porous media. Using Eqs. [2-32] and [2-33], Eq. [2-31] can be written as

$$\frac{\partial \theta c}{\partial t} = -\frac{\partial q_i c}{\partial x_i} + \frac{\partial}{\partial x_i}\left(\theta D_{ij} \frac{\partial c}{\partial x_j} \right) - S_s, \quad i,j = 1, 2, 3,$$ [2-34]

where subscripts i and j refer to the three perpendicular coordinate axes. The expression for D_{ij} for partially saturated porous media is given by (Bear and Verruijt, 1987; Simunek *et al.*, 1994)

$$\theta D_{ij} = a_T |\mathbf{q}| \delta_{ij} + \left(a_L - a_T \right)\frac{q_i q_j}{|\mathbf{q}|} + \theta D_0 \, \tau(\theta)\, \delta_{ij},$$ [2-35]

where a_L and a_T are the longitudinal - along a streamline - and transversal - perpendicular to a streamline - dispersivities (L), respectively, $|\mathbf{q}|$ represents the absolute magnitude of $\mathbf{q}$ (LT^{-1}), δ_{ij} is the Kronecker delta function with $\delta_{ij} = 1$ when $i = j$ and $\delta_{ij} = 0$ when $i \neq j$, D_0 is the molecular diffusion coefficient in free water (LT^{-1}; see also Eq. [5-17]), and τ is the tortuosity factor (1) which accounts for the increased path length in porous media, which is a function of θ. I use the broken-line $\tau(\theta)$ relationship from Barraclough and Tinker (1981; their Figure 1) given by

$$\tau(\theta) = \begin{cases} f_1\,\theta + f_2 & \theta \geq \theta_l \\[2mm] \dfrac{\theta\bigl(f_1\,\theta_l + f_2\bigr)}{\theta_l} & \theta < \theta_l \end{cases} \quad ,$$

[2-36]

where f_1, f_2 and θ_l are dimensionless parameters. Barraclough and Tinker (1981) obtained two sets of data, one for clay soils, and one for sand and loamy soils, for which the parameters occurring in Eq. [2-36] were determined (Table 2-1).

Table 2-1 Values for the dimensionless parameters θ_l, f_1 and f_2 occurring in Eq. [2-36] derived from data of Barraclough and Tinker (1981; their Figure 1).

Parameter	Sand or loam	Clay
θ_l	0.12	0.20
f_1	1.58	0.99
f_2	-0.17	-0.17

According to Bear and Verruijt (1987) a_L is 10 to 20 times larger than a_T. In one-dimensional studies only one dispersivity is determined. For example, Beven *et al.* (1993; their Table 5) summarized values measured in partially saturated undisturbed field core samples or plots, ranging from 0.0087 m to 1.116 m. In this thesis I determined a_L and a_T from a calibration procedure using breakthrough data (Chapter 7, Section 7.5).

2.5 Boundary and initial conditions for nutrient transport

In general, the boundary conditions for nutrient transport can be of the same type as those for water movement (see Section 2.2), for example, Dirichlet and Neumann conditions. In this thesis, where half of the region between two drains is considered, the following specific conditions were used (Figure 2-5). At the *upper boundary*, the substrate-atmosphere interface, there is no nutrient flux, except at the positions where fertigation takes place

$$\text{for } q_z\big|_{z=0} > 0, \quad q_{sz}\big|_{z=0} = c_f q_z\big|_{z=0}, \quad 0 \leq x \leq X,$$

[2-37]

and

$$\text{for } q_z\big|_{z=0} \leq 0, \quad q_{sz}\big|_{z=0} = 0, \quad 0 \leq x \leq X,$$

[2-38]

$$\text{for } q_z\big|_{z=0} > 0, \quad q_{sz}\big|_{z=0} = c_f q_z\big|_{z=0} \quad 0 \le x \le X$$

$$\text{for } q_z\big|_{z=0} \le 0, \quad q_{sz}\big|_{z=0} = 0 \quad\quad\quad\quad 0 \le x \le X$$

$$\frac{\partial c}{\partial x}\bigg|_{x=0} = 0 \quad 0 \le z \le Z$$

$$\frac{\partial c}{\partial x}\bigg|_{x=X} = 0 \quad 0 \le z \le Z$$

$$q_{sz}\big|_{z=Z} = q_Z = 0 \quad x_D < x \le X$$

$$\text{for } q_z\big|_{z=Z} > 0, \quad q_{sz}\big|_{z=Z} = c_D q_z\big|_{z=Z} \quad 0 \le x \le x_D$$

$$\text{for } q_z\big|_{z=Z} \le 0, \quad q_{sz}\big|_{z=Z} = 0 \quad\quad\quad\quad 0 \le x \le x_D$$
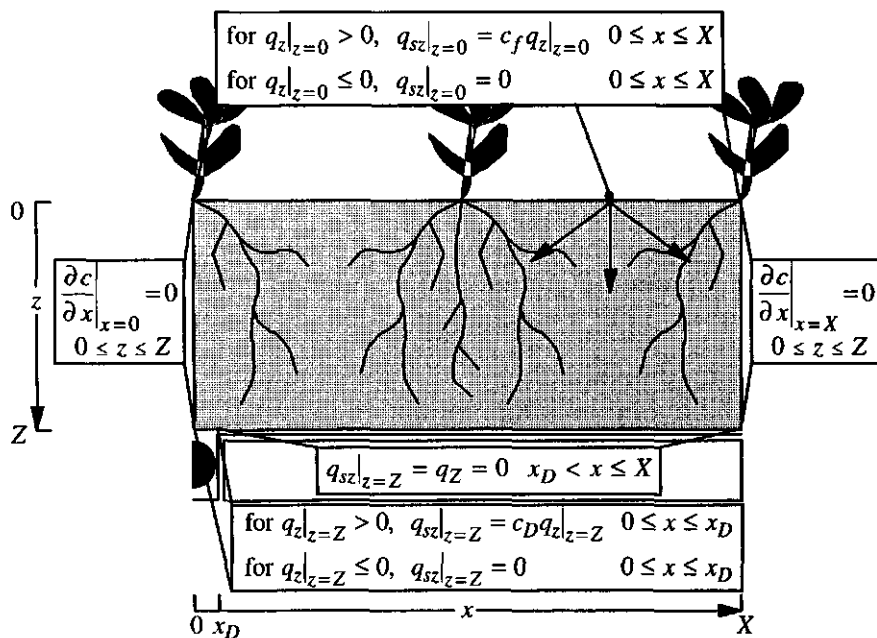
Figure 2-5 Half the region between two drains (see Figure 1-1) showing the boundary conditions for nutrient transport.

where q_{sz} is the vertical component of the nutrient mass flux density, and c_f is the concentration of the nutrient in the fertigation water.

The *lower boundary* to the right of the drain is impermeable due to the presence of an impermeable foil, so that the condition is that of no flow

$$q_{sz}\big|_{z=Z} = 0, \quad x_D < x \le X. \tag{2-39}$$

As for the water there can be only nutrient outflow to the *drain* and no inflow

$$\text{for } \quad q_z\big|_{z=Z} > 0, \quad q_{sz}\big|_{z=Z} = c_D q_z\big|_{z=Z}, \quad 0 \le x \le x_D, \tag{2-40}$$

or

$$\text{for } \quad q_z\big|_{z=Z} \le 0, \quad q_{sz}\big|_{z=Z} = 0, \quad 0 \le x \le x_D, \tag{2-41}$$

where c_D is the nutrient concentration at the drain location.

Due to symmetry, the *left, at* $x = 0$, *and right, at* $x = X$, boundaries ($0 \le z \le Z$) are no flow boundaries

$$\frac{\partial c}{\partial x}\bigg|_{x\,=\,0} = 0, \quad 0 \le z \le Z, \qquad\qquad [2\text{-}42]$$

and

$$\frac{\partial c}{\partial x}\bigg|_{x\,=\,X} = 0, \quad 0 \le z \le Z. \qquad\qquad [2\text{-}43]$$

The *initial condition* is that of given initial concentration c_0 distribution

$$c\big|_{t\,=\,0} = c_0(x,y,z), \qquad\qquad [2\text{-}44]$$

or that of given amount Q_{m0} (M)

$$Q_m\big|_{t\,=\,0} = Q_{m0}(x,y,z). \qquad\qquad [2\text{-}45]$$

The amount Q_m and the density Q are related according to

$$Q = Q_m V, \qquad\qquad [2\text{-}46]$$

where $V = \Delta x \Delta y \Delta z$ is the volume (L^3) of the porous medium.

2.6 Root nutrient uptake

De Willigen and van Noordwijk (1987, 1994a,b) developed a microscopic model for nutrient uptake. Like for root water uptake, one can consider a layer of substrate of thickness Δz with equally distributed, parallel roots perpendicular to the porous medium surface, i.e with uniform root length density L_{rv}. Root nutrient uptake is assumed to be primarily dictated by the requirement of the plant, denoted as S_{sr} ($ML^{-3}T^{-1}$). Required uptake cannot occur when the diffusion and mass flow processes in the substrate cannot resupply enough nutrient to the root. De Willigen and van Noordwijk (1994b) obtained a *steady-rate approximate solution for the concentration profile around the root for the zero-sink condition* given as (Figure 2-6)

$$c(R) = -\frac{S_{sr}}{2\,\pi\Delta z\,L_{rv}\,D}\left(\frac{R^{2\sigma+2}-R^{2\sigma}}{2\,(\rho^{2\sigma+2}-1)} + \frac{\rho^{2\sigma+2}(1-R^{2\sigma})}{2\,\sigma(\rho^{2\sigma+2}-1)}\right), \qquad [2\text{-}47]$$

where D is the diffusion coefficient (L^2T^{-1}), and σ is the dimensionless water uptake by the root defined as

$$\sigma = -\frac{q_1}{4\,\Delta z\,\pi L_{rv}\,D}. \qquad\qquad [2\text{-}48]$$

Concentration c (mg cm^{-3})
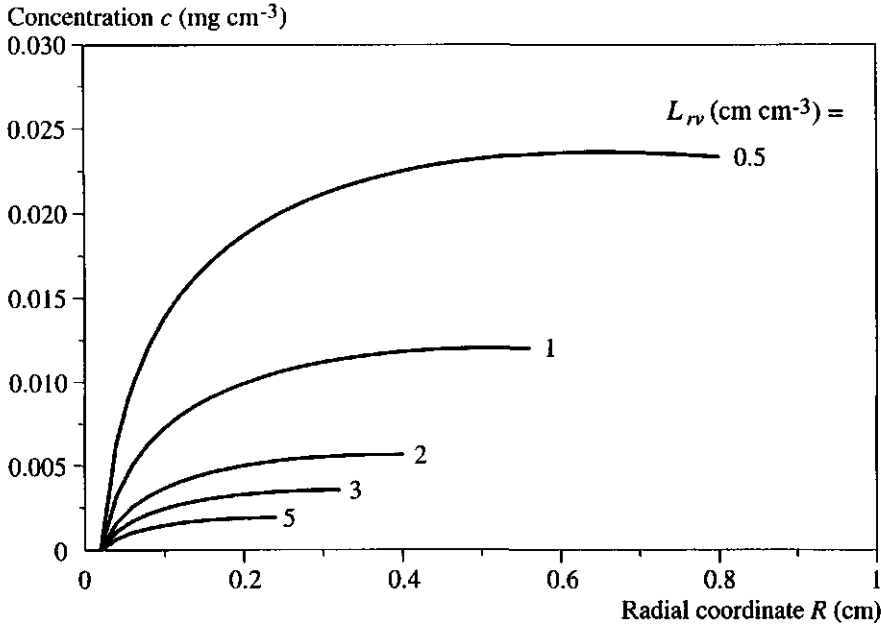
Figure 2-6   Zero-sink steady-rate concentration $c(R)$ distribution around a single root as a function of the radial coordinate according to Eq. [2-47] for five values of the root length density L_{rv}; other parameters are: R_0 = 0.02 cm, Δz = 10 cm, q_1 = T = 0.2 cm d^{-1}, D = 0.1 cm^2 d^{-1} (a typical value according to de Willigen and van Noordwijk, 1987), and S_{sr} = 0.03 mg cm^{-2} d^{-1}. The end points of the curves represent $R = R_1$.

Near the end points of the lines in Figure 2-6, i.e. at $R = R_1$, c decreases with increasing R. This occurs especially at low L_{rv} and high T_a, and is due to the replenishment of solute-free water at $R = R_1$ used as boundary condition in the development of Eq. [2-47]. Then dilution occurs at $R = R_1$. An alternative water supply condition is uniform replenishment. A different, more complicated expression for $c(R)$ results, but the $c(R)$ of both expressions are about the same (de Willigen and van Noordwijk, 1994a). Therefore, I used the simple expression given by Eq. [2-47].

If the approximate concentration distribution given in Eq. [2-47] holds, it can be derived that the *maximum possible nutrient uptake rate* per unit surface area of substrate S_{sm} (ML^{-2}T^{-1}) is given as

$$S_{sm} = \pi \Delta z \, L_{rv} D \bar{c} \, \frac{(\rho^2 - 1)}{G(\rho, \sigma)}, \qquad [2\text{-}49]$$

where $\bar{c}$ is the average bulk concentration in the substrate layer, and the dimensionless

geometry function G is given by (de Willigen and van Noordwijk, 1994a,b)[1] (Figure 2-7)

$$G(\rho,\sigma) = \frac{1}{2(\sigma+1)}\left(\frac{1-\rho^2}{2} + \frac{\rho^2(\rho^{2\sigma}-1)}{2\sigma} + \frac{\rho^2(\rho^{2\sigma}-1)(\sigma+1)}{2\sigma(\rho^{2\sigma+2}-1)} + \right.$$

[2-50]

$$\left. + \frac{(1-\rho^{2\sigma+4})(\sigma+1)}{(2\sigma+4)(\rho^{2\sigma+2}-1)}\right),$$

where in the limit $\sigma \to 0$, i.e. transport is by diffusion only, Eq. [2-50] reduces to Eq. [2-26] (Section 2.3). The effect of σ on G seems to be small (Figure 2-7). For the parameters given in Figure 2-7 and $\bar{c} = 0.2$ mg cm^{-3}, the relative difference between S_{sm} for $\sigma = -0.02$ and for $\sigma = 0$ with respect to S_{sm} at $\sigma = -0.02$ according to Eq. [2-49] increases from 0.01 to 0.07 for ρ ranging from 2 to 40.
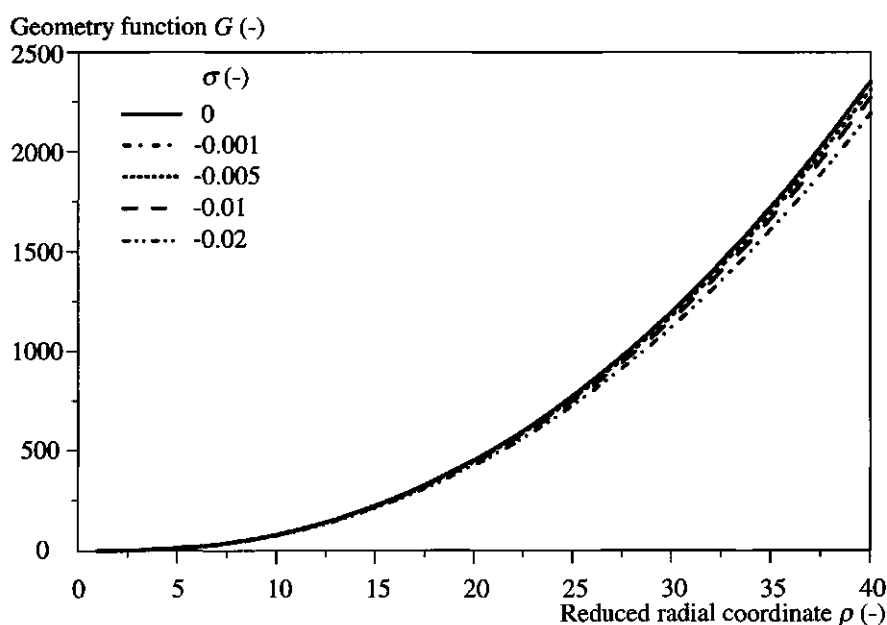
Figure 2-7   The geometry function G as a function of the reduced radius ρ according to Eq. [2-50] for five values of σ, i.e. 0, -0.001, -0.005, -0.01 and -0.02; for $D = 0.1$ cm^2 d^{-1} (de Willigen and van Noordwijk, 1987), $\Delta z = 10$ cm, and $L_{rv} = 2$ cm cm^{-3}, this corresponds to water uptake of 0, 0.025, 0.126, 0.25, 0.50 cm d^{-1}, respectively.

---

[1]   The expression given by de Willigen and van Noordwijk (1987; Eq. 9.29, p. 130) is incorrect (P. de Willigen, pers. comm.).

The *actual uptake rate* to be used as the sink strength S_s in Eq. [2-31] is equal to the minimum of the required uptake rate and the maximum uptake rate according to

$$S_s = \min\left(S_{sr}, \frac{S_{sm}}{\Delta z} \right) .$$

[2-51]

As for root water uptake, this approach can be extended to multi-layered porous media or media with compartments of uniform root length density (see Subsection 3.4.2).

Nutrient transport can be easily extended to include adsorption and/or precipitation, i.e. these amounts have to be included in Q. The root uptake models developed by de Willigen and van Noordwijk (1987, 1994a,b) are based on approximate steady-rate solutions. These authors showed that these approximations were very close to available analytical or numerical solutions for ranges of the parameter values they used. These models are based on regular root distributions. It is known that actual root distributions are non-regular and sometimes even clustered, and that partial root-substrate contact exists. De Willigen and van Noordwijk (1987) showed that the actual uptake under these conditions is lower than the uptake based on regular root distribution assumptions. Lower uptake due to non-uniformity and clustering of root distributions was also concluded by Rappoldt (1992) based on a different approach. For simplicity reasons, however, I decided to use the simple model.

2.7 Conclusions

In this chapter I have presented the general theory for water movement in porous media, i.e. the Richards equation. Solute transport is described as convective transport with the moving water and dispersive-diffusive transport due to gradients in concentration. The sink terms appearing in the water movement and solute transport equations represent root water and nutrient uptake. Scaled-up versions of microscopic root uptake models as formulated by de Willigen and van Noordwijk (1987, 1994a,b) are used as the sink terms. The boundary conditions for the two-dimensional sand bed system are given.

Chapter 3

Water movement, nutrient transport

and root uptake : numerical implementation

As mentioned in Chapter 2, the Richards equation has to be solved numerically in most cases. In this chapter the Richards equation is implicitly solved, using one of the possible numerical procedures, i.c. a sub-domain finite element method (Sections 3.1-3.3), where root water uptake is treated explicitly. The nutrient transport equation is explicitly solved in Section 3.4, making use of the new status of the water and explicitly known root nutrient uptake. In Section 3.5 the time-stepping procedure is described. For convenience, the functional dependence of the dependent variables is left out of the notation.

3.1 Introduction

In general, *numerical methods* can be divided in discrete domain methods, boundary methods and integral domain methods (Nieber and Feddes, 1996). They can be fully explicit, fully implicit, or a mixture of explicit and implicit such as the Crank-Nicholson method. A classical example of a *discrete domain method* is the *finite difference method* using the Taylor expansion series. The finite difference method is mathematically simple, but rather inflexible, and difficult to use in treating boundary conditions and in coping with irregular boundaries. The *boundary methods* seek a solution on the boundary of the solution domain. Only the boundary has to be considered and not the interior of the domain. Once the solution at the boundary is obtained, it is possible to obtain at selected interior points values of the dependent variable. It is favoured when the main interest is at the boundary of the solution domain, e.g. Pullan and Collins (1987) used it to determine the effectively wetted region from infiltration from buried and surface cavities. An example of an *integral domain method* is the *finite element method*. This method is physically correct due to the integral approach, but mathematically complex. Moreover, irregular flow domains and boundary conditions can be treated easily. In finite elements usually the method of weighted residuals is applied among which the Galerkin method (e.g. Simunek *et al.*, 1994) and subdomain method (Cooley, 1983) are well known. The first is mathematically more complex to handle than the second. A special case of the subdomain method is the *Control Volume* (CV) *method* with rectangular subdomains, which as applied in heat and fluid flow problems by Patankar (1980) and Meurs (1985). The CV method is easy to understand and lends itself to direct physical interpretation. The CV approximated equations are similar to finite difference equations. A method which results in similar numerical equations is the integrated finite difference method as

described by Narasimhan and Witherspoon (1976, 1977) and Narasimhan *et al.* (1977). However, unlike the CV method the integrated finite difference method still needs auxiliary nodes to handle boundary conditions. In the following the CV method will be used.

I consider the sand bed cropping system mentioned in Chapter 1 (Figure 1-1). There is a sequence of repeating elements, i.e. half of the region between two drains (Figure 1-1B). Water enters the substrate at certain positions (drip points) and can leave the flow domain at the drain position and at the substrate-atmosphere interface. Water is distributed in the root zone where spatially distributed roots are present. Under these conditions the flow pattern is multi-dimensional. In what follows I will use the two-dimensional (x, z) form of the mixed θ-h Richards equation, Eq. [2-4], written as

$$\frac{\partial}{\partial x}\left(K\frac{\partial h}{\partial x} \right) + \frac{\partial}{\partial z}\left(K\frac{\partial h}{\partial z} \right) - \frac{\partial K}{\partial z} - S_w - \frac{\partial \theta}{\partial t} = 0 . \qquad [3\text{-}1]$$

Since the flow domain is rectangular, the CV method with its rectangular subdomains can be applied.

The choice of a two-dimensional approach is questionable, since, for example, the water entry underneath a dripper is principly three-dimensional. For simplicity reasons, I decided to consider the drippers that close as if they behave as a line source. Moreover, three-dimensional models have a large disadvantage, since they require large storage and much computer time. Larabi and de Smedt (1994) ran their model on a super-computer.

3.2 The control volume method

In Subsection 3.2.1 a brief description of the method of weighted residuals is given. The control volume geometry is described in Subsection 3.2.2. The integration of the Richards equation and the boundary conditions are described in Subsections 3.2.3 and 3.2.4, respectively. In Subsection 3.2.5 the solution for root water uptake is presented. The description of the CV method is based on the work of Patankar (1980).

3.2.1 Method of weighted residuals

The *method of weighted residuals* can be briefly described as follows. Let a differential equation, e.g. Eq. [3-1] rewritten in h-based form, be represented by

$$\mathcal{L}(h) = 0 , \qquad [3\text{-}2]$$

where $\mathcal{L}$ is some differential operator. Assume a simple approximate solution h^* that contains a number of undetermined parameters. The substitution of h^* in the differential equation leaves a residual r defined as

$$r = \mathcal{L}(h^*) . \qquad [3\text{-}3]$$

The best solution is obtained when r is as small as possible over the whole region. It is proposed that the residual is distributed according to

$$\int_V w\,r\,\mathrm{d}V = 0,$$

[3-4]

where w is a *weighing function*, which is a function of space only, and V represents the complete flow domain under study. By choosing a succession of w values one can generate as many equations as needed for evaluating the parameters in h^*. In fact, a number of subdomains are chosen in V for each of which the Eq. [3-4] is set up. Different weighing functions w can be chosen. In the subdomain method the weighing function has the form $w = 1$ or $w = 0$. A number of weighted-residual equations can be generated by dividing V into subdomains further called Control Volumes (CV) and setting $w = 1$ within each CV and $w = 0$ everywhere else in V. Thus, integration over V as in Eq. [3-4] now becomes integration over the volume CV of the control volume. Using Eq. [3-1] and $w = 1$, and leaving out the superscript * for convenience, this yields

$$\int_{CV} \left[\frac{\partial}{\partial x}\left(K\frac{\partial h}{\partial x}\right) + \frac{\partial}{\partial z}\left(K\frac{\partial h}{\partial z}\right) - \frac{\partial K}{\partial z} - S_w - \frac{\partial \theta}{\partial t} \right] \mathrm{d}CV = 0,$$

[3-5]

where CV (L^3) is the volume of a CV. From now on, the dependent variables refer to the as yet unknown approximated numerical solution. The most attractive feature of the CV method formulation is that the resulting solution would imply that the *integral conservation mass is exactly satisfied* over each CV, any group of CV's and over the whole calculation domain.

3.2.2 Control volume geometry

There are several ways how the CV's and associated nodes can be located in the rectangular flow domain (Patankar, 1980). In this study I have chosen the *node centred* CV's (Figure 3-1A), as shown to be the best by Patankar (1980). The CV's have a unit thickness in the y-direction, i.e $\Delta y = 1$. The width of the columns and thickness of the layers can be variable throughout the flow domain. In this way the CV's can be located such that interfaces between two substrates or interfaces between boundary conditions can be located at the interfaces of CV's. At the boundaries, the nodes are on the boundaries itself - so-called half CV's are used. For each CV Eq. [3-5] integrated over time is to be solved. In what follows I use the following notation convention (Figure 3-1B). The nodes and the CV's are denoted by capital indexes (I,J), while small indices (i,j) refer to an interface between two CV's - for example, the interface between (I,J) and $(I+1,J)$ by (i,j), and that between (I,J) and $(I,J-1)$ by $(i,j-1)$. Column width and row thickness are denoted by Δx_I and Δz_J (with capital subscripts), respectively. The distance between nodes in the
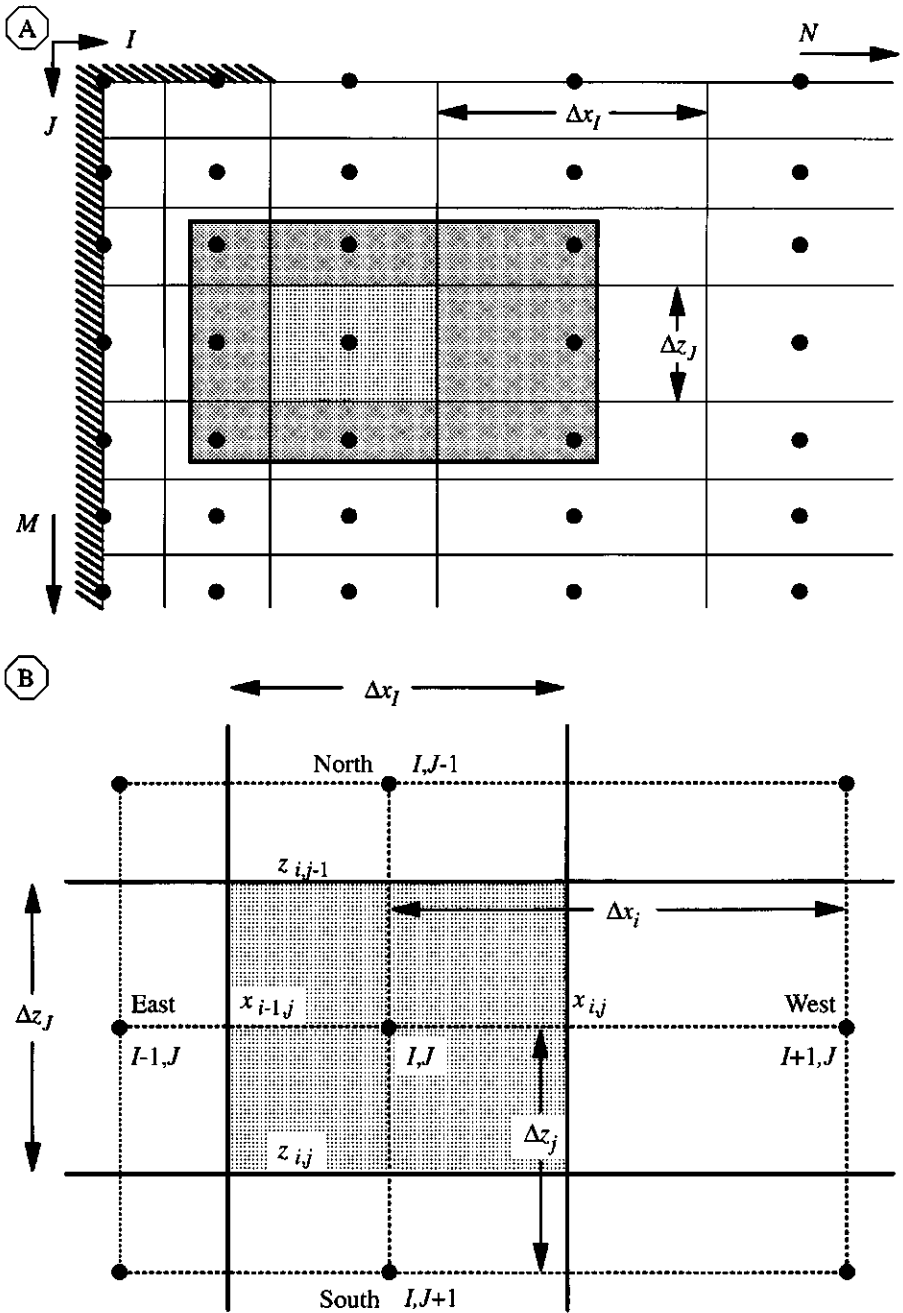
Figure 3-1 (A) Example of *node centred* control volumes with "half" control volumes at the boundaries; the hatched area in (A) is enlarged in (B) showing the Control Volume (CV) (shaded area) around node (I,J) including notation conventions.

x and z directions are denoted by Δx_i and Δz_j (with small subscripts), respectively, defined as

$$\Delta x_i = 0.5\left(\Delta x_I + \Delta x_{I+1}\right),$$ [3-6]

and

$$\Delta z_j = 0.5\left(\Delta z_J + \Delta z_{J+1}\right).$$ [3-7]

The neighbour nodes or corresponding interfaces are referred to by their 'geographical' position, i.e. West, East, North or South, for which the subscripts W, E, N and S are used, respectively (Figure 3-1B). In the x-direction there are N columns or nodes, and in the z-direction there are M layers or nodes. The volume of a CV equals $CV = \Delta x_I \, \Delta y \, \Delta z_J$, where Δx_I and Δz_J can be written as $\Delta x_I = (x_{i,j} - x_{i-1,j})$ and $\Delta z_J = (z_{i,j} - z_{i,j-1})$, respectively.

3.2.3 Integration of the mixed θ-h Richards equation

Equation [3-5], integrated over time, is solved numerically. The five terms on the left-hand side of Eq. [3-5] will be elaborated separately below. The variables are all evaluated at the new time $t+\Delta t$, where Δt is the time step (T), except when stated otherwise. Thus a fully implicit or backward Euler scheme is used.

Integrating the *first term* of Eq. [3-5] in the x-direction yields

$$\int_{z_{i,j-1}}^{z_{i,j}} \int_{y}^{y+\Delta y} \int_{x_{i-1,j}}^{x_{i,j}} \int_{t}^{t+\Delta t} \frac{\partial}{\partial x}\left(K\frac{\partial h}{\partial x}\right) dt \, dx \, dy \, dz = \left[K\frac{\partial h}{\partial x}\right]_{x_{i-1,j}}^{x_{i,j}} \Delta y \, \Delta z_J \, \Delta t .$$ [3-8]

In evaluating the (horizontal) flux-terms at the CV interfaces on the right-hand side of Eq. [3-8], one must assume a profile of h between the nodes, i.e. apply an interpolation. If it is assumed that h prevails over the CV, then the derivative of h is not defined at the CV interface (Figure 3-2A). To overcome this problem, I assume *a piece-wise-linear h profile*, i.e. linear interpolation (Figure 3-2B). Then the right-hand side of Eq. [3-8] can be written as

$$\left[K\frac{\partial h}{\partial x}\right]_{x_{i-1,j}}^{x_{i,j}} \Delta y \, \Delta z_J \, \Delta t = \left(K_{x,i,j}\frac{h_{I+1,J} - h_{I,J}}{\Delta x_i} - K_{x,i-1,j}\frac{h_{I,J} - h_{I-1,J}}{\Delta x_{i-1}}\right) \Delta y \, \Delta z_J \, \Delta t ,$$ [3-9]

where $K_{x,i,j}$ and $K_{x,i-1,j}$ are the hydraulic conductivities in the x-direction at the CV interfaces (i,j) and $(i-1,j)$, respectively. The hydraulic conductivities at the interfaces are unknown, only the hydraulic conductivities at the nodes are known. To evaluate K at the CV-interfaces several averaging methods have been proposed in the literature (e.g. Haverkamp and Vauclin, 1979; Ross and Bristow, 1990; Zaidel and Russo, 1992). In this study I use the *weighted geometric averaging* method. This simple method performed best in the one-dimensional problems studied by Haverkamp and Vauclin (1979). Since the width of the CV's may vary, the CV-interface is not situated halfway between two
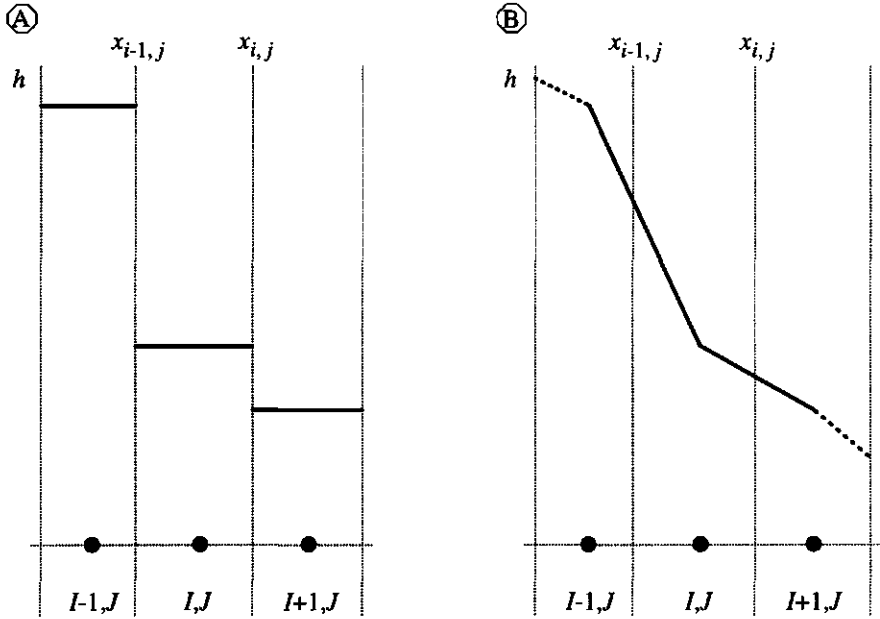
Figure 3-2 Profile assumptions for pressure head h between nodes: (A) step-wise profile; (B) piece-wise linear profile. The piece-wise linear profile is used for evaluating the fluxes at the control volume interfaces in the integration scheme.

nodes. Therefore, a distance weighing factor in the positive x-direction w_E (1) is defined as

$$w_{E,i} = \frac{\Delta x_{I+1}}{\Delta x_I + \Delta x_{I+1}} .$$ [3-10]

The *weighted geometric average* for $K_{x,i,j}$ is then given by

$$K_{x,i,j} = K_{I,J}^{1-w_{E,i}} K_{I+1,J}^{w_{E,i}} .$$ [3-11]

Likewise, integrating the *second term* of Eq. [3-5] but now in the z-direction yields

$$\int_{z_{i,j-1}}^{z_{i,j}} \int_{y}^{y+\Delta y} \int_{x_{i-1,j}}^{x_{i,j}} \int_{t}^{t+\Delta t} \frac{\partial}{\partial z}\left(K \frac{\partial h}{\partial z}\right) dt \, dx \, dy \, dz = \left[K \frac{\partial h}{\partial z}\right]_{z_{i,j-1}}^{z_{i,j}} \Delta x_I \Delta y \Delta t .$$ [3-12]

The (vertical) flux-term now is written as (cf. Eq. [3-9])

$$\left[K \frac{\partial h}{\partial z} \right]_{z_{i,j-1}}^{z_{i,j}} \Delta x_I \Delta y \Delta t \;=\; \left(K_{z,i,j} \frac{h_{I,J+1} - h_{I,J}}{\Delta z_j} - K_{z,i,j-1} \frac{h_{I,J} - h_{I,J-1}}{\Delta z_{j-1}} \right) \Delta x_I \Delta y \Delta t , \quad [3\text{-}13]$$

where $K_{z,i,j}$ and $K_{z,i,j-1}$ are the hydraulic conductivities in the z-direction at the CV interfaces (i,j) and $(i,j\text{-}1)$, respectively. Similar as above, the *weighted geometric average* for $K_{z,i,j}$ is given by

$$K_{z,i,j} \;=\; K_{I,J}^{1-w_{S,j}} K_{I,J+1}^{w_{S,j}} , \qquad\qquad [3\text{-}14]$$

with the distance weighing factor in the positive z-direction w_S (1) defined as

$$w_{S,j} \;=\; \frac{\Delta z_{J+1}}{\Delta z_J + \Delta z_{J+1}} . \qquad\qquad [3\text{-}15]$$

Integration of the *gravity term*, i.e. the *third term* of Eq. [3-5], yields

$$\int_{z_{i,j-1}}^{z_{i,j}} \int_y^{y+\Delta y} \int_{x_{i-1,j}}^{x_{i,j}} \int_t^{t+\Delta t} -\frac{\partial K}{\partial z} \, dt \, dx \, dy \, dz \;=\; -\left[K_{z,i,j} - K_{z,i,j-1} \right] \Delta x_I \Delta y \Delta t . \qquad [3\text{-}16]$$

Integration of the *sink strength term*, i.e. the *fourth term* of Eq. [3-5], yields

$$\int_{z_{i,j-1}}^{z_{i,j}} \int_y^{y+\Delta y} \int_{x_{i-1,j}}^{x_{i,j}} \int_t^{t+\Delta t} -S_w \, dt \, dx \, dy \, dz \;=\; -S_{w,I,J} \Delta x_I \Delta y \Delta z_J \Delta t . \qquad [3\text{-}17]$$

In Eq. [3-17] the sink strength is assumed to be explicitly known (see Subsection 3.2.5) and constant during the current time step for each control volume.

Integration of the *storage term*, i.e. the *fifth term* of Eq. [3-5], yields

$$\int_{z_{i,j-1}}^{z_{i,j}} \int_y^{y+\Delta y} \int_{x_{i-1,j}}^{x_{i,j}} \int_t^{t+\Delta t} -\frac{\partial \theta}{\partial t} \, dt \, dx \, dy \, dz \;=\; -\left[\theta_{I,J} - \theta_{I,J}^0 \right] \Delta x_I \Delta y \Delta z_J , \qquad [3\text{-}18]$$

where $\theta_{I,J}$ denotes the value of the water content at the end of the time step i.e. at time $t+\Delta t$, and θ^0 represents θ at time t.

At this time Eq. [3-1] is numerically approximated, but it is still expressed in two unknowns, i.e. θ and h. *The θ version of the storage term in Eq. [3-18] will be further elaborated using the procedure of Celia et al. (1990).* Due to the non-linear relationships

$K(\theta)$ and $\theta(h)$, the solution of the numerical equations has to be found by iteration. A modified Picard iteration procedure is applied here. Let the superscript k denote the values of h and θ at the k-th level of iteration, then for the next $(k+1)$ level θ^{k+1} is approximated by a truncated Taylor series with respect to h, about $h_{I,J}^{k}$

$$\theta_{I,J}^{k+1} \approx \theta_{I,J}^{k} + \frac{d\theta}{dh}\bigg|^{k} \left(h_{I,J}^{k+1} - h_{I,J}^{k}\right)$$

$$= \theta_{I,J}^{k} + C_{I,J}^{k}\left(h_{I,J}^{k+1} - h_{I,J}^{k}\right),$$

[3-19]

where $\theta_{I,J}^{k+1}$ is the water content corresponding to $h_{I,J}^{k+1}$. Substituting Eq. [3-19] in Eq. [3-18] yields

$$\int_{z_{i,j-1}}^{z_{i,j}} \int_{y}^{y+\Delta y} \int_{x_{i-1,j}}^{x_{i,j}} \int_{t}^{t+\Delta t} -\frac{\partial\theta}{\partial t}\, dt\, dx\, dy\, dz = -\left(C_{I,J}^{k}\left[h_{I,J}^{k+1} - h_{I,J}^{k}\right] + \left[\theta_{I,J}^{k} - \theta_{I,J}^{0}\right]\right)\Delta x_{I}\,\Delta y\,\Delta z_{J}.$$ [3-20]

The right-hand side of Eq. [3-20] resembles the numerically approximated left-hand side of the h-based Richards equation (Eq. [2-5]), i.e.

$$C^{k}\left(h^{k+1} - h^{0}\right).$$

[3-21]

Numerical solutions of the h-based Richards equation are accompanied with mass balance errors due to the a priori unknown value of C (e.g. Milly, 1985; Celia *et al.*, 1990; Rathfelder and Abriola, 1994). In particular, problems occur with C values close to or equal to zero. Thus why is the Celia *et al.* (1990) approach better than the 'standard' h approach? This can be easily seen, since the first term on the right-hand side of Eq. [3-20] vanishes when the iteration process progresses towards the final solution. Thus the magnitude of C has no longer influence on the computations. Moreover, the second term on the right-hand side of Eq. [3-20] takes care of mass conservation in the numerical computation. Of course, the Taylor expansion in Eq. [3-19] can be used in the numerical approximation of the h-based Richards equation, as was done by Rathfelder and Abriola (1994), in which case the same approximated equation is obtained as in the mixed θ-h approach.

Taking together the results of Eqs. [3-8]+[3-9], [3-12]+[3-13], [3-16], [3-17] and [3-20], *the numerically approximated form of Eq. [3-1]* after rearrangement of terms is

$$A\,h_{I,J}^{k+1} = A_{W}\,h_{I-1,J}^{k+1} + A_{E}\,h_{I+1,J}^{k+1} + A_{N}\,h_{I,J-1}^{k+1} + A_{S}\,h_{I,J+1}^{k+1} + b,$$

[3-22]

with

$$A_{W(est)} = \frac{K_{x,i-1,j}^{k} \Delta y \, \Delta z_J}{\Delta x_{i-1}}, \quad A_{E(ast)} = \frac{K_{x,i,j}^{k} \Delta y \, \Delta z_J}{\Delta x_i},$$

[3-23]

$$A_{N(orth)} = \frac{K_{z,i,j-1}^{k} \Delta x_I \, \Delta y}{\Delta z_{j-1}}, \quad A_{S(outh)} = \frac{K_{z,i,j}^{k} \Delta x_I \, \Delta y}{\Delta z_j},$$

and

$$b = A_C h_{I,J}^{k} + \left[\theta_{I,J}^{k} - \theta_{I,J}^{0}\right] \frac{\Delta x_I \Delta y \, \Delta z_J}{\Delta t} - \left[K_{z,i,j}^{k} - K_{z,i,j-1}^{k}\right] \Delta x_I \, \Delta y - S_{w,I,J} \Delta x_I \, \Delta y \, \Delta z_J,$$
[3-24]

where

$$A_C = C_{I,J}^{k} \frac{\Delta x_I \Delta y \, \Delta z_J}{\Delta t}.$$

[3-25]

Finally, A is defined as

$$A = A_E + A_W + A_N + A_S + A_C.$$

[3-26]

The coefficients A_E, A_W, A_N and A_S (L^2T^{-1}) refer to the hydraulic conductivity at the interfaces between the CV under consideration and its four respective neighbors and CV geometry, and, hence, are always positive. Coefficient A_C refers to the differential moisture capacity, CV geometry and time step (L^2T^{-1}), and b contains known quantities (L^3T^{-1}). For each node the coefficients A, A_C, A_E, A_W, A_N, A_S and b have to be computed. But, when a face is common to two adjacent CV's, the flux across it must be represented by the same expression in the numerical equations for both CV's. This means that A_W and A_E are related as

$$A_{W,I,J} = A_{E,I-1,J},$$

[3-27]

and A_S and A_N are related as

$$A_{N,I,J} = A_{S,I,J-1}.$$

[3-28]

At the beginning of the first iteration level, when $k = 0$, the values from the last time step are used as the initial guesses.

3.2.4 Handling of boundary conditions

For the nodes lying on the boundaries, the boundary conditions must be taken into account when integrating Richards equation. For *Neumann* conditions, i.e. prescribed flux boundary conditions, this is very simple, since they come in naturally during the numerical approximation procedure. Consider the prescribed flux conditions at the top and bottom of the flow domain (Eqs. [2-12], [2-13] or [2-15]). The term on the right-hand side of Eq. [3-12] represents the difference in vertical Darcy flux density across the horizontal interfaces of the control volume. For a control volume at the top or bottom

boundary, one of these two fluxes is the prescribed flux condition, and can thus be used there. In general, the solution for these boundary nodes is equal to Eqs. [3-22]-[3-26], with only one or two coefficients differing. For the *Neumann or flux boundary condition at the top*, e.g. Eq. [2-12], one finds that

$$A_N = 0 ,$$

[3-29]

and

$$b = A_C h_{I,1}^k + \left[\theta_{I,1}^k - \theta_{I,1}^0 \right] \frac{\Delta x_I \Delta y \Delta z_1}{\Delta t} - \left[K_{z,i,1}^k - q_0 \right] \Delta x_I \Delta y - S_{w,I,1} \Delta x_I \Delta y \Delta z_1 .$$

[3-30]

For the *Neumann or flux boundary condition at the bottom*, e.g. Eqs. [2-13] or [2-15], one finds analogously that

$$A_S = 0 ,$$

[3-31]

and

$$b = A_C h_{I,M}^k + \left[\theta_{I,M}^k - \theta_{I,M}^0 \right] \frac{\Delta x_I \Delta y \Delta z_M}{\Delta t} - \left[q_Z - K_{z,i,M-1}^k \right] \Delta x_I \Delta y +$$

$$- S_{w,I,M} \Delta x_I \Delta y \Delta z_M .$$

[3-32]

For *the Neumann no-flow boundary conditions at x = 0 or x = X*, Eqs. [2-16] and [2-17], the solution is given by Eqs. [3-22]-[3-26] with only

$$A_W = 0 ,$$

[3-33]

or

$$A_E = 0 ,$$

[3-34]

respectively.

The *Dirichlet or pressure head boundary condition*, i.e. Eq. [2-14], is treated as follows. One could set $A_E = A_W = A_N = A_S = 0$, $A = 1$, and $b = h_Z$, where h_Z is the prescribed pressure head. However, for one of the solution procedures used in Section 3.3 this would yield a non-symmetric coefficient matrix. Therefore, a numerical trick is used as an alternative (Wang and Anderson, 1982; Larabi and de Smedt, 1994). The Eqs. [3-22], [3-23], [3-25] and [3-26] are used, and *b* is given as

$$b = h_Z .$$

[3-35]

The coefficients *A* and *b* are multiplied by a large number, e.g. 10^{25}. In that way the other terms in Eq. [3-22] are insignificant during the computations and the newly calculated pressure head is forced to the desired value. One should be aware of possible overflow problems as a result of this; however, they did not occur in my computations.

3.2.5 Root water uptake

The root water uptake model as described in Section 2.3 considers a single layer of porous medium with uniform root length density. For a root system distributed over several control volumes, it is assumed that within each control volume the roots are regularly distributed, so that for each control volume the model described in Section 2.3 can be applied. The *sink strength for each control volume* is then given by (combining Eqs. [2-21] and [2-24])

$$S_{w,I,J} = L_{rv,I,J} K_1 \left(h_{rs,I,J} - h_r \right) =$$

$$= \pi L_{rv,I,J} \frac{\rho_{I,J}^2 - 1}{G_0(\rho_{I,J})} \left(\overline{\phi_{I,J}} - \phi_{rs,I,J} \right). \tag{3-36}$$

The sum of all sink strengths then equals the actual transpiration rate T (cf. Eq. [2-19])

$$T = \sum_{I=1}^{N} \sum_{J=1}^{M} S_{w,I,J}. \tag{3-37}$$

T is a function of the root pressure head h_r and the potential transpiration rate T_p as described by Eqs. [2-27] and [2-28]. K_1, h_{rs} and R_0 are assumed to be constant for the whole root system, and h of the bulk soil in the CV is assumed to be known. This results in a set of (NxM+1) equations with (NxM+1) unknowns: NxM values of h_{rs} and h_r. However, due to the non-linear relationship between h and ϕ on the one hand and h_r and T on the other hand, the solution has to be found iteratively. The procedure consists of two steps. In the first step two estimates for h_r are obtained for which the sum of all root water uptake is less than and more than T, respectively. Secondly, the true value for h_r is computed in the range bounded by these two estimates. ϕ is evaluated according to the procedure described in Appendix 7. Although $\overline{\phi}$ is defined by Eq. [2-25] I approximate it from h in the bulk substrate in the CV.

In short the procedure is as follows. In the first step one starts with $T = T_p$, and h_r is computed according to Eq. [2-30]. Equation [3-36] is solved for h_{rs} using e.g. the method of false position (Press *et al.*, 1986). The sum of all computed root water uptakes is compared with T, cf. Eq. [3-37]. If total uptake is smaller (larger) than T, then current h_r is the lower (upper) limit. The upper (lower) limit is found by - repeatedly - increasing the current estimate of h_r with a certain factor, e.g. 5; T is adapted as well. In the second step the true value of h_r is obtained using the method of false position within the lower and upper limit range obtained in the first step. Convergence is reached when

$$\frac{\sum_{I}^{N} \sum_{J}^{M} S_{w,I,J} - T}{T} \leq \epsilon_t, \tag{3-38}$$

where ϵ_t is some small number, e.g. $\epsilon_t = 0.01$. The corresponding sink strengths can then be used in Eq. [3-24]. Thus root water uptake is considered explicitly.

3.3 Solution of the matrix equation for water movement

For each node Eq. [3-22] holds, and *the total problem can be presented in matrix notation as*

$$\mathbf{A}\, \mathbf{h} = \mathbf{b},\qquad\qquad\qquad [3\text{-}39]$$

where $\mathbf{A}$ is a coefficient matrix of (NxM) by (NxM), and the vectors $\mathbf{h}$ and $\mathbf{b}$ of length (NxM) contain the unknown values of h and the known values of b, respectively. For the CV method the coefficient matrix $\mathbf{A}$ contains the coefficients A, A_E, A_W, A_S and A_N stored in 5 bands (Figure 3-3). Matrix $\mathbf{A}$ is symmetric due to Eqs. [3-27] and [3-28], sparse since most elements are zero, positive definite, and all elements outside the main diagonal are less than or equal to zero, $\mathbf{A}$ is non-singular and $\mathbf{A}^{-1} \geq 0$, i.e. $\mathbf{A}$ is a so-called M-matrix (Meijerink and van der Vorst, 1977; Larabi and de Smedt, 1994). Due to the simple sparsity pattern, storage is easy.
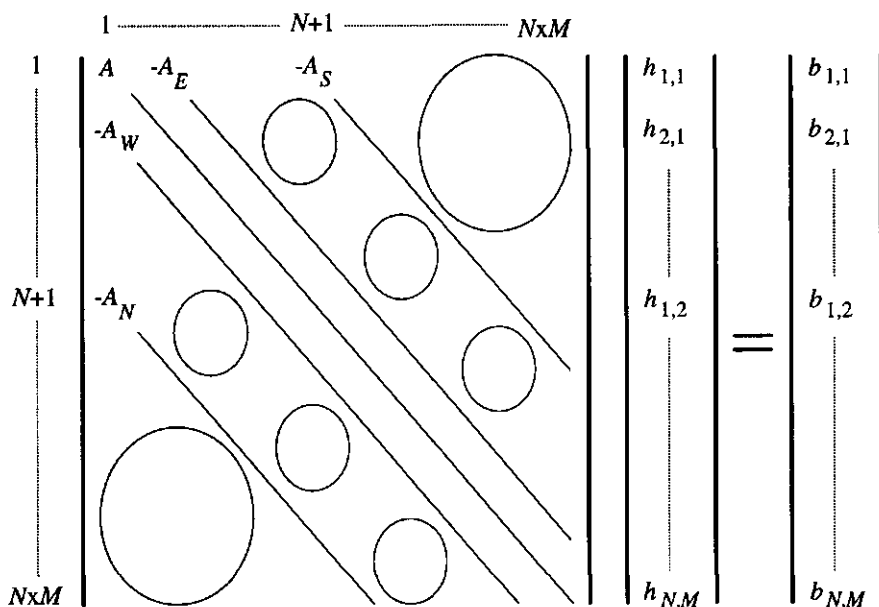
Figure 3-3 Schematic representation of the matrix notation of Eq. [3-39] showing the 5 banded sparsity pattern of coefficient matric $\mathbf{A}$ with corresponding arrangement of (un)knowns h and b in vectors $\mathbf{h}$ and $\mathbf{b}$, respectively.

The solution of Eq. [3-39] is

$$\mathbf{h} = \mathbf{A}^{-1}\mathbf{b}.$$ [3-40]

However, it is often time-consuming to find the inverse matrix of $\mathbf{A}$. A direct method of solving the problem is by the Gauss-Seidel elimination method. This method is known to be time consuming, especially for a large number of CV's. In the literature some alternative methods have been proposed. A very simple and fast method is the Alternating Direction Implicit (ADI) method, first proposed for multi-dimensional parabolic and elliptic (linear) partial differential equations by Peaceman and Rachford (1955). The ADI method functions well for unsaturated problems (Heinen and de Willigen, 1992). But when regions partly saturated and partly unsaturated were considered, the ADI method failed. An alternative method is the Incomplete Cholesky Conjugate Gradient (ICCG) method (Meijerink and van der Vorst, 1977; Kershaw, 1978; Kuiper, 1981; Golub and van Loan, 1989), which recently is used frequently in partly saturated regions (e.g. Kuiper, 1981; Kirkland *et al.*, 1992; Larabi and de Smedt, 1994). These methods were originally developed for linear problems, but they can be used in the iteration step since within the iteration the problem is linear. The ADI method is described in Subsection 3.3.1 and the ICCG method in Subsection 3.3.2. In what follows reference is made to internal nodes. The same reasoning holds, however, for boundary nodes.

3.3.1 Alternating Direction Implicit (ADI) method

The ADI method for a two-dimensional case consists of two steps. In the first step the equations are written implicitly in one direction (e.g. x) and explicitly in the other direction (e.g. z). In step two the opposite procedure is followed: explicitly in the first direction and implicitly in the second direction. For each step the resulting matrix equation is solved, with the solution of the first step used in the second step. Solution of the equations obtained in the second step then completes one iteration step.

Step 1
Assume that all values are known at iteration level k, writing Eq. [3-22] implicitly in the x-direction yields

$$A h_{I,J}^{k+1/2} = A_W h_{I-1,J}^{k+1/2} + A_E h_{I+1,J}^{k+1/2} + b.$$ [3-41]

The coefficients A_E, A_W, A_S, A_N and A_C are the same as given in Eqs. [3-23] and [3-25], but A and b are

$$A = A_E + A_W + A_C,$$ [3-42]

and

$$b = A_C h_{I,J}^k + \left[\theta_{I,J}^k - \theta_{I,J}^0\right]\frac{\Delta x_I \Delta y \Delta z_J}{\Delta t} - A_S\left[h_{I,J}^k - h_{I,J+1}^k\right] - A_N\left[h_{I,J}^k - h_{I,J-1}^k\right] +$$

[3-43]

$$- \left[K_{z,i,j}^k - K_{z,i,j-1}^k\right]\Delta x_I \Delta y - S_{w,I,J}\Delta x_I \Delta y \Delta z_J,$$

respectively. This procedure thus yields a system of M equations for each of the N rows in the z-direction. The equations can be presented in a form analogously to Eq. [3-39], but now $\mathbf{A}$ has only the three main bands filled with non-zero values, i.e. the main diagonal plus the bands directly above and directly below the main diagonal, and vector $\mathbf{b}$ contains also the explicit terms. This set of equations can be solved efficiently and quickly by a special form of the Gauss-Seidel elimination method known as the *Thomas algorithm* (e.g. Press *et al.*, 1986).

Step 2
So the values of $h_{I,J}^{k+1/2}$ are obtained and from these $K_{I,J}^{k+1/2}$ and $\theta_{I,J}^{k+1/2}$. After calculation of the average values of the conductivity at the faces of the CV's the equations are written implicitly in the z-direction

$$A h_{I,J}^{k+1} = A_N h_{I,J-1}^{k+1} + A_S h_{I,J+1}^{k+1} + b.$$

[3-44]

The coefficients A_E, A_W, A_S, A_N and A_C are as given in Eqs. [3-23] and [3-25] with all hydraulic properties evaluated at iteration level $k+1/2$, whereas A and b now are given by

$$A = A_N + A_S + A_C,$$

[3-45]

and

$$b = A_C h_{I,J}^{k+1/2} + \left[\theta_{I,J}^{k+1/2} - \theta_{I,J}^0\right]\frac{\Delta x_I \Delta y \Delta z_J}{\Delta t} - A_E\left[h_{I,J}^{k+1/2} - h_{I+1,J}^{k+1/2}\right]$$

[3-46]

$$- A_W\left[h_{I,J}^{k+1/2} - h_{I-1,J}^{k+1/2}\right] - \left[K_{z,i,j}^{k+1/2} - K_{z,i,j-1}^{k+1/2}\right]\Delta x_I \Delta y - S_{w,I,J}\Delta x_I \Delta y \Delta z_J,$$

respectively. Solution of the N equations at the M columns in the x-direction yields the values of $h_{I,J}^{k+1}$ at the iteration level $k+1$.

The ADI method can be used either for parabolic and for elliptic partial differential equations (Peaceman and Rachford, 1955; Rosenberg, 1969). However, according to the literature, for parabolic problems the complete time step should be used in both ADI steps, while for elliptic problems half the time step should be used in each of the two ADI steps. When variably saturated conditions exist in the flow domain, part of the problem is parabolic (unsaturated zone) and the rest is elliptic (saturated zone). In that case it is not known what time step is to be used. Peaceman and Rachford (1955) and Douglas *et al.* (1959) used an iteration parameter to speed up convergence for elliptic problems. This concept was successfully used by Rubin (1968) in partly saturated porous media, but our attempt failed. Another attempt to solve the mixed parabolic-elliptic problem is to force

the Richards equation in the saturated part of the porous medium to stay parabolic by introducing a compressibility coefficient as was done by e.g. Russo *et al.* (1994).

3.3.2 Incomplete Cholesky Conjugate Gradient (ICCG) method

The M-type coefficient matrix **A** (see Section 3.3) is generated by numerical approximation of the elliptic equation, as is the Laplace equation in the saturated zone, and the parabolic differential equation, as is the Richards equation for the unsaturated zone. In that case, a promising method to solve Eq. [3-39] is the ICCG method (Meijerink and van der Vorst, 1977). The ICCG method works as follows.

Matrix **A** in Eq. [3-39] is replaced by a preconditioning matrix **C**, so that the system can be solved easier. Here matrix **C** is defined as the Cholesky decomposition matrix

$$\mathbf{C} = \mathbf{L}\mathbf{L}^T, \tag{3-47}$$

where **L** is the Cholesky lower triangular matrix, and $\mathbf{L}^T$ is its transpose matrix and thus upper triangular. The elements of **L** are computed as

$$\text{for } \mathbf{A}_{\gamma\iota} \neq 0 \quad \mathbf{L}_{\gamma\iota} = \frac{1}{\mathbf{L}_{\iota\iota}} \left(\mathbf{A}_{\gamma\iota} - \sum_{\kappa=1}^{\iota-1} \mathbf{L}_{\iota\kappa} \mathbf{L}_{\gamma\kappa} \right),$$

$$\text{for } \mathbf{A}_{\gamma\iota} = 0 \quad \mathbf{L}_{\gamma\iota} = 0, \tag{3-48}$$

$$\gamma = \iota,(\iota+1),(\iota+2),...,(N+M).$$

The first and second indices refer to the column and row numbers of the matrix, respectively. For the special case of the five-banded matrix **A** in this study, the product of $\mathbf{L}_{\iota\kappa}\mathbf{L}_{\gamma\kappa}$ in the first part of Eq. [3-48] is always zero, and thus the summation term disappears. The procedure is called *incomplete* Cholesky decomposition, since *the same sparsity pattern as for* **A** *is forced on* **C**, as is stated in the second part of Eq. [3-48]. Thus storage of the elements of **C** can be done in the same way as for **A**. The discarded entries are generally small, and the incomplete construction is at least as stable as the complete construction (Meijerink and van der Vorst, 1977; Gustafsson, 1984). The benefit of the ICCG method is that the solution of the matrix equation

$$\mathbf{C}\,\mathbf{h} = \mathbf{b}, \tag{3-49}$$

is obtained in two simple steps: first, by forward substitution of

$$\mathbf{L}\,\mathbf{y} = \mathbf{b}, \tag{3-50}$$

followed by backward substitution of

$$\mathbf{L}^T\mathbf{h} = \mathbf{y}, \tag{3-51}$$

to obtain the solution **h**, where vector **y** is an intermediate dummy vector.

Since $\mathbf{C}$ is not equal to $\mathbf{A}$, the solution cannot be found directly, and iterations are needed. Here I use the conjugate gradient iterative solution (Hestenes and Stiefel, 1952; Meijerink and van der Vorst, 1977; Kershaw, 1978; Golub and van Loan, 1989; Larabi and de Smedt, 1994). The conjugate gradient method is simpler to code and requires less storage space than the standard Gaussian elimination method.

For any arbitrary initial estimate $\mathbf{h}^0$, the initial values for the residual vector $\mathbf{r}$ (being the difference between the current estimated solution and the exact solution) and direction vector $\mathbf{p}$ (being the vector pointing from the current estimated solution to the exact solution) are computed from (Kershaw, 1978)

$$\mathbf{r}^0 = \mathbf{b} - \mathbf{A}\,\mathbf{h}^0,$$

$$\mathbf{p}^0 = \left(\mathbf{L}\,\mathbf{L}^{T}\right)^{-1}\mathbf{r}^0. \qquad [3\text{-}52]$$

The solution is computed according to (Kershaw, 1978)

$$a_1^{\lambda} = \frac{\left\{\mathbf{r}^{\lambda},\ \left(\mathbf{L}\,\mathbf{L}^{T}\right)^{-1}\mathbf{r}^{\lambda}\right\}}{\left\{\mathbf{p}^{\lambda},\ \mathbf{A}\,\mathbf{p}^{\lambda}\right\}},$$

$$\mathbf{h}^{\lambda+1} = \mathbf{h}^{\lambda} + a_1^{\lambda}\,\mathbf{p}^{\lambda},$$

$$\mathbf{r}^{\lambda+1} = \mathbf{r}^{\lambda} - a_1^{\lambda}\,\mathbf{A}\,\mathbf{p}^{\lambda},$$

$$a_2^{\lambda} = \frac{\left\{\mathbf{r}^{\lambda+1},\ \left(\mathbf{L}\,\mathbf{L}^{T}\right)^{-1}\mathbf{r}^{\lambda+1}\right\}}{\left\{\mathbf{r}^{\lambda},\ \left(\mathbf{L}\,\mathbf{L}^{T}\right)^{-1}\mathbf{r}^{\lambda}\right\}}, \qquad [3\text{-}53]$$

$$\mathbf{p}^{\lambda+1} = \left(\mathbf{L}\,\mathbf{L}^{T}\right)^{-1}\mathbf{r}^{\lambda+1} + a_2^{\lambda}\,\mathbf{p}^{\lambda},$$

$$\lambda = 0, 1, 2, \ldots .$$

The scalars a_1 and a_2 are iteration parameters which are used to refine the vectors $\mathbf{r}$ and $\mathbf{p}$, respectively, the parameter λ is the local iteration counter, and the notation $\{.,.\}$ represents the in-product of two vectors, and is a scalar value. Normally, after $\lambda = MxN$ iterations the solution is obtained. However, due to rounding-off errors and since $\mathbf{L}\mathbf{L}^{T}$ is only approximately equal to $\mathbf{A}$, this may be not the case. It is obvious that the more $\mathbf{C}$ resembles $\mathbf{A}$ the less iterations are needed. Due to the simple sparsity pattern of $\mathbf{A}$ and $\mathbf{C}$, the computations can be carried out easily. Convergence is achieved as soon as for all nodes the relative difference d_I between all corresponding elements of $h^{\lambda+1}$ and h^{λ} is less than a small value ϵ_i, e.g. $\epsilon_i = 10^{-6}$, with d_I defined as

$$d_I = \frac{|\,h^{\lambda+1} - h^{\lambda}\,|}{|\,h^{\lambda+1}\,| + 100.0}. \qquad [3\text{-}54]$$

For absolute large values of h Eq. [3-54] gives approximate relative changes. In case h becomes close to zero, Eq. [3-54] gives approximate absolute changes divided by 100. For near zero values of h, relative changes would be difficult to compute, and convergence is not guaranteed; therefore, the factor 100 was introduced in Eq. [3-54].

The incomplete Cholesky conjugate gradient method was developed for linear systems. For non-linear systems this method can be used in the main iteration loop, then for each iteration the system is assumed to be linear.

3.3.3 Convergence criterion

To determine if convergence is achieved in the main iteration process, the maximum relative change in K or h is computed according to

$$d = \max\left(d_1, d_2\right),$$
[3-55]

with

$$d_1 = \frac{\mid h_{I,J}^{k+1} - h_{I,J}^{k} \mid}{\mid h_{I,J}^{k+1} \mid + 100.0},$$
[3-56]

and

$$d_2 = \frac{\mid K_{I,J}^{k+1} - K_{I,J}^{k} \mid}{K_{I,J}^{k+1} + 100.0},$$
[3-57]

where in Eq. [3-55] the operator max yields the maximum value of its arguments. Iterations are halted when for all nodes d is smaller than a small number ϵ_c, e.g. $\epsilon_c = 10^{-4}$. Equations [3-56] and [3-57] are of the same form as Eq. [3-54] (see also discussion below Eq. [3-54]).

For not too wet conditions, the largest changes will be in K rather than in h. Heinen and de Willigen (1992) determined the pressure head above which the largest changes occur in h for sand, clay, peat and loamy sand soils; they obtained values of h in the range -3 cm to -22 cm.

3.4 Explicit solution for nutrient transport

Opposite to the water movement described above, nutrient transport is considered explicitly. However, use is made of the results of the water movement computations. The nutrient flux density is described in Subsection 3.4.1. Nutrient uptake by the root system is described in Subsection 3.4.2.

3.4.1 Nutrient flux density

Solute transport is solved explicitly, i.e. the solute mass flux densities are evaluated at the control volume (CV) interfaces using the water flux densities obtained at $t+\Delta t$ and from that the dispersion-diffusion coefficients at $t+\Delta t$, and the concentrations at time t. The solute flux at a CV interface consists of a convective part and two dispersion-diffusion parts, one due to a gradient in c perpendicular to the interface, and one due to a gradient in c parallel to the interface. The three parts will be computed separately and then summed. Once all solute fluxes are known the change in total amount Q in each CV can be computed and from that the new c.

The *governing solute transport equation expressed in Q*, Eq. [2-34], is here written in two dimensions as

$$\frac{\partial Q}{\partial t} = -\frac{\partial q_x c}{\partial x} - \frac{\partial q_z c}{\partial z} + \frac{\partial}{\partial x}\left(\theta D_{xx}\frac{\partial c}{\partial x}\right) + \frac{\partial}{\partial z}\left(\theta D_{zz}\frac{\partial c}{\partial z}\right) +$$
$$+ \frac{\partial}{\partial x}\left(\theta D_{xz}\frac{\partial c}{\partial z}\right) + \frac{\partial}{\partial z}\left(\theta D_{zx}\frac{\partial c}{\partial x}\right) - S_s,$$

[3-58]

or

$$\frac{\partial Q}{\partial t} = -\frac{\partial q_{sx}^c}{\partial x} - \frac{\partial q_{sz}^c}{\partial z} - \frac{\partial q_{sxx}^d}{\partial x} - \frac{\partial q_{szz}^d}{\partial z} - \frac{\partial q_{sxz}^d}{\partial x} - \frac{\partial q_{szx}^d}{\partial z} - S_s,$$

[3-59]

where

$$q_{sx}^c = q_x c,$$
$$q_{sz}^c = q_z c,$$

[3-60]

and

$$q_{sxx}^d = -\theta D_{xx}\frac{\partial c}{\partial x}, \qquad q_{szz}^d = -\theta D_{zz}\frac{\partial c}{\partial z},$$
$$q_{sxz}^d = -\theta D_{xz}\frac{\partial c}{\partial z}, \qquad q_{szx}^d = -\theta D_{zx}\frac{\partial c}{\partial x},$$

[3-61]

Superscripts d and c refer to dispersion-diffusion and convection, respectively. Eq. [3-59] can be reduced to

$$\frac{\partial Q}{\partial t} = -\frac{\partial q_{sx}}{\partial x} - \frac{\partial q_{sz}}{\partial z} - S_s,$$

[3-62]

where

$$q_{sx} = q_{sx}^c + q_{sxx}^d + q_{sxz}^d,$$

$$q_{sz} = q_{sz}^c + q_{szz}^d + q_{szx}^d.$$

[3-63]

The expressions between the brackets of the fifth and sixth terms on the right-hand side of Eq. [3-58], i.e. q_{sxz}^d and q_{szx}^d (Eq. [3-61]), represent the solute fluxes in the x and z direction caused by gradients of c in the z and x directions, respectively. S_s is assumed to be explicitly known. *The new distribution of the solutes* follows from Eq. [3-62]. The total mass Q_m (M) of a CV is defined as (Eq. [2-46])

$$Q_{m,I,J} = Q_{I,J} \Delta x_I \Delta y \Delta z_J.$$

[3-64]

Using Eq. [3-64], Eq. [3-62] is now rewritten as

$$\frac{\partial Q_{m,I,J}}{\partial t} = \left(-\frac{\partial q_{sx,I,J}}{\partial x} - \frac{\partial q_{sz,I,J}}{\partial z} - S_{s,I,J} \right) \Delta x_I \Delta y \Delta z_J.$$

[3-65]

Equation. [3-65] is numerically solved as

$$\frac{Q_{m,I,J}^{t+\Delta t} - Q_{m,I,J}^t}{\Delta t} = \frac{q_{sx,i-1,j}^{t+\Delta t} - q_{sx,i,j}^{t+\Delta t}}{\Delta x_I} \Delta x_I \Delta y \Delta z_J + \frac{q_{sz,i,j-1}^{t+\Delta t} - q_{sz,i,j}^{t+\Delta t}}{\Delta z_J} \Delta x_I \Delta y \Delta z_J +$$

$$- S_{s,I,J}^t \Delta x_I \Delta y \Delta z_J,$$

[3-66]

so that

$$Q_{m,I,J}^{t+\Delta t} = Q_{m,I,J}^t + \left(q_{sx,i-1,j}^{t+\Delta t} - q_{sx,i,j}^{t+\Delta t} \right) \Delta y \Delta z_J \Delta t + \left(q_{sz,i,j-1}^{t+\Delta t} - q_{sz,i,j}^{t+\Delta t} \right) \Delta x_I \Delta y \Delta t +$$

$$- S_{s,I,J}^t \Delta x_I \Delta y \Delta z_J \Delta t,$$

[3-67]

The *concentration c* in CV (I,J) can be computed from (cf. Eq. [2-32])

$$c_{I,J}^{t+\Delta t} = \frac{Q_{m,I,J}^{t+\Delta t}}{\theta_{I,J}^{t+\Delta t} \Delta x_I \Delta y \Delta z_J}.$$

[3-68]

The total solute flux densities at the CV interfaces appearing in Eq. [3-67] are evaluated by Eq. [3-63] plus Eqs. [3-60] and [3-61]. The convective and dispersive-diffusive solute flux densities are obtained in the following two sections.

Convection
The *convective parts of* $\mathbf{q}_s$, Eq. [3-60], at the CV interfaces are obtained using the *method of upstream weighing* (e.g. Patankar, 1980):

$$\text{if } q_{x,i,j}^{t+\Delta t} \geq 0 \qquad q_{sx,i,j}^{c,t+\Delta t} = q_{x,i,j}^{t+\Delta t} c_{I,J}^{t}, \qquad\qquad [3\text{-}69]$$

$$\text{if } q_{x,i,j}^{t+\Delta t} < 0 \qquad q_{sx,i,j}^{c,t+\Delta t} = q_{x,i,j}^{t+\Delta t} c_{I+1,J}^{t}, \qquad\qquad [3\text{-}70]$$

and

$$\text{if } q_{z,i,j}^{t+\Delta t} \geq 0 \qquad q_{sz,i,j}^{c,t+\Delta t} = q_{z,i,j}^{t+\Delta t} c_{I,J}^{t}, \qquad\qquad [3\text{-}71]$$

$$\text{if } q_{z,i,j}^{t+\Delta t} < 0 \qquad q_{sz,i,j}^{c,t+\Delta t} = q_{z,i,j}^{t+\Delta t} c_{I,J+1}^{t}. \qquad\qquad [3\text{-}72]$$

Thus, if the Darcy water flux density is from node A to node B, the nutrient flux density is the water flux density times c at node A. Using the upstream weighing method numerical oscillations are minimized. But still small oscillations and numerical dispersion may exist, especially in explicit schemes. Daus *et al.* (1985) concluded that, for a one-dimensional problem, stability is achieved when at all positions in the flow domain the Fourier number is smaller than 0.5. The Fourier number (Fo) is defined as the ratio of the Courant (Co) and Peclet (Pe) numbers. The Pe, Co and Fo numbers (1) are defined as (e.g. Daus *et al.*, 1985; El-Kadi and Ling, 1993)

$$Pe_{I,J} = \frac{\mid q_{I,J}^{n} \mid \Delta s_{I,J}}{\theta_{I,J} D_{I,J}}, \qquad\qquad [3\text{-}73]$$

$$Co_{I,J} = \frac{\mid q_{I,J}^{n} \mid \Delta t}{\theta_{I,J} \Delta s_{I,J}}, \qquad\qquad [3\text{-}74]$$

and

$$Fo_{I,J} = \frac{Co_{I,J}}{Pe_{I,J}} = \frac{D_{I,J} \Delta t}{\left(\Delta s_{I,J}\right)^2}, \qquad\qquad [3\text{-}75]$$

where $\Delta s_{I,J}$ is the characteristic length of control volume (I,J) (L), here chosen to be the minimum of Δx_I and Δz_J of that CV, and $q_{I,J}^{n}$ is the magnitude of net flux density into CV (I,J). Simunek *et al.* (1994) advised that for all CV's $Pe < 5$, or at least < 10, and that $Co \leq 1$. This is in agreement with the Fourier number being less than 0.5 as suggested by Daus *et al.* (1985). As long as for all nodes these requirements are met, it is believed that numerical dispersion and oscillations are small. No procedure is known to me to completely remove numerical dispersion for two-dimensional models. For implicit, one-dimensional simulations Moldrup *et al.* (1992, 1994) gave procedures for removing numerical dispersion.

Dispersion-diffusion

The *dispersive-diffusive parts of* $\mathbf{q}_s$, Eq. [3-61], at the CV interfaces can be obtained from

$$q_{sxx,i,j}^{d,t+\Delta t} = -\theta^{t+\Delta t} D_{xx,i,j}^{t+\Delta t} \frac{c_{I+1,J}^{t} - c_{I,J}^{t}}{\Delta x_i}, \tag{3-76}$$

$$q_{szz,i,j}^{d,t+\Delta t} = -\theta^{t+\Delta t} D_{zz,i,j}^{t+\Delta t} \frac{c_{I,J+1}^{t} - c_{I,J}^{t}}{\Delta z_j}, \tag{3-77}$$

$$q_{sxz,i,j}^{d,t+\Delta t} = -\theta^{t+\Delta t} D_{xz,i,j}^{t+\Delta t} \frac{c_{i,j-1}^{t} - c_{i,j}^{t}}{\Delta z_J}, \tag{3-78}$$

and

$$q_{szx,i,j}^{d,t+\Delta t} = -\theta^{t+\Delta t} D_{zx,i,j}^{t+\Delta t} \frac{c_{i-1,j}^{t} - c_{i,j}^{t}}{\Delta x_I}. \tag{3-79}$$

Note that c at the nodes from the previous time step are used, while all other quantities refer to the new situation at $t+\Delta t$. In Eqs. [3-76] and [3-77] c at a node is used, while in Eqs. [3-78] and [3-79] c at an interface between nodes is used. The different components appearing in Eqs. [3-76]-[3-79] are given below.

The *dispersion-diffusion coefficients* at the CV interfaces are computed according to Eq. [2-35], which for two dimensions are given by ($\mathbf{q} > 0$)

$$\theta D_{xx} = a_L \frac{q_x^2}{|\mathbf{q}|} + a_T \frac{q_z^2}{|\mathbf{q}|} + \theta D_0 \tau(\theta), \tag{3-80}$$

$$\theta D_{zz} = a_L \frac{q_z^2}{|\mathbf{q}|} + a_T \frac{q_x^2}{|\mathbf{q}|} + \theta D_0 \tau(\theta), \tag{3-81}$$

$$\theta D_{xz} = \theta D_{zx} = \left(a_L - a_T\right) \frac{q_x q_z}{|\mathbf{q}|}. \tag{3-82}$$

If $\mathbf{q} = 0$, then

$$\theta D_{xx} = \theta D_{zz} = \theta D_0 \tau(\theta), \tag{3-83}$$

$$\theta D_{xz} = \theta D_{zx} = 0 . \qquad [3\text{-}84]$$

The water fluxes q_x and q_z needed to compute these coefficients are obtained as follows. The water fluxes perpendicular to the interfaces are known from the water solution procedure, but the water fluxes parallel to the interfaces are computed as the averages of the four nearest available water flux densities in the desired direction. Thus, for a vertical CV interface q_x and q_z are

$$q_x = q_{x,i,j}^{t+\Delta t} , \qquad [3\text{-}85]$$

$$q_z = \frac{q_{z,i,j-1}^{t+\Delta t} + q_{z,i,j}^{t+\Delta t} + q_{z,i+1,j-1}^{t+\Delta t} + q_{z,i+1,j}^{t+\Delta t}}{4} . \qquad [3\text{-}86]$$

For a vertical CV interface q_x and q_z are

$$q_x = \frac{q_{x,i-1,j}^{t+\Delta t} + q_{x,i,j}^{t+\Delta t} + q_{x,i-1,j+1}^{t+\Delta t} + q_{x,i,j+1}^{t+\Delta t}}{4} , \qquad [3\text{-}87]$$

$$q_z = q_{z,i,j}^{t+\Delta t} . \qquad [3\text{-}88]$$

The absolute value of the water flux is computed as

$$| \mathbf{q} | = \sqrt{q_x^2 + q_z^2} . \qquad [3\text{-}89]$$

In order to *evaluate the dispersive flux in the one direction induced by a gradient in c in the other direction* at a CV interface, the gradient in c along this interface must be estimated (see Eqs. [3-78] and [3-79]). The c at the edges of the interfaces, i.e. at the cross points of four CV's, are computed as the averages of the c's at the four neighbouring CV's, for example,

$$c_{i,j}^{t} = \frac{c_{I,J}^{t} + c_{I+1,J}^{t} + c_{I,J+1}^{t} + c_{I+1,J+1}^{t}}{4} . \qquad [3\text{-}90]$$

The gradient is the difference in c divided by the length of the interface, with the latter being the width of column or layer.

At the boundaries, the procedure is principly the same. Dispersive-diffusive components normal to the boundaries are set equal to zero, so that only convective fluxes are present, if any. At a boundary, Eq. [3-90] reduces to the average of the two nodes at this boundary.

3.4.2 Root nutrient uptake

In analogy with root water uptake, the root nutrient uptake as described in Chapter 2 (Section 2.6) can be used for each control volume. The solution procedure is, however, much easier than for water uptake. I assume that the root length at each position in the flow domain is known and that all roots take up at the same rate. Then it is worthwhile to express the total required uptake rate by the crop, S_{sr}, from the total root zone with volume $V (= XZ\Delta y)$ as the required uptake rate per cm root length $S_{sr,c}$ ($ML^{-1}T^{-1}$)

$$S_{sr,c} = \frac{V S_{sr}}{\Delta y \sum_{I=1}^{N} \sum_{J=1}^{M} L_{rv,I,J} \Delta x_I \Delta z_J} .$$

[3-91]

Then, according to Eq. [2-51], the uptake strength for CV (I,J) is

$$S_{s,I,J} = \min\left(S_{sr,c} L_{rv,I,J} , \frac{S_{sm,I,J}}{\Delta z_J} \right) ,$$

[3-92]

where the operator min yields the minimum value of its arguments. It is known that roots in favourable position can compensate for roots in less favourable position (e.g. de Jager, 1985). So if in some CV's nutrient uptake is limited by the maximum possible uptake, then the solution procedure is iteratively continued for the remaining CV's to determine if they can compensate for roots in less favourable conditions.

3.5 Time stepping

Computations are carried out for each time step. The time step does not necessarily have to be constant. At times when the changes are relatively small larger time steps can be used. In principle, there is no limit for the time step in fully implicit schemes. There is, however, a maximum possible time step in fully explicit schemes. Due to the implicit-explicit character of the ADI method care should be taken in choosing the time step. In general, one could require that within a time step the change in volumetric water content is restricted. For example, following Vauclin *et al.* (1979) and Vellidis and Smajstrla (1992) one could choose a new Δt which satisfies the condition

$$\Delta t \leq \frac{\zeta \Delta s_{min}}{| q_{max} |} ,$$

[3-93]

where ζ represents the maximum permissible change in water content during a time step, e.g. $\zeta = 0.01$, Δs_{min} is the minimum grid spacing, and q_{max} is the magnitude of the maximum net flux into any CV. Note that the net flux of the previous time step is used. Problems may thus occur when boundary conditions change abruptly. Equation [3-93] is

related to the Courant number defined in Eq. [3-74].

When nutrient transport is included, the time step should also be restricted according to the Courant or Fourier numbers as defined in Eqs. [3-74] and [3-75], respectively. According to Daus *et al.* (1985) *Fo* should be ≤ 0.5, so that the time step should meet the restriction

$$\Delta t \le \frac{(\Delta s_{min})^2}{2 D_{max}},$$ [3-94]

where D_{max} is the maximum observed diffusion/dispersion coefficient in any CV during the current time step.

In summary the time stepping procedure is as follows. The simulation starts with an initial time step Δt_i. Each new time step is computed according to

$$\Delta t = \min\left(\Delta t_p, \ t_m \Delta t, \ \Delta t_{max}, \ \Delta t_C, \ \Delta t_F\right),$$ [3-95]

where Δt_p is the time difference between current time and next printing time, t_m is a multiplication factor ($t_m > 1$), Δt_{max} is a maximum allowable Δt, Δt_C is the required time step based on *Co* (Eq. [3-74]), and Δt_F is the required time step based on *Fo* (Eqs. [3-75] and [3-94]). If no solute transport is considered Δt_C and Δt_F are set larger than Δt_{max}. During the solution procedure, when no convergence is reached within a maximum number of iterations, Δt is reduced by a factor 10. When Δt becomes lower than a minimum value Δt_{min} the simulation is halted. Simulations are carried out until *t* reaches the final time t_f.

3.6 The simulation model

The numerical model presented in Section 3.2 - 3.5 was programmed in Fortran 77. An early version of the code (Fussim2) was described by Heinen and de Willigen (1992), in which only the ADI method was used and in which no solute transport and root uptake was considered. The simulation runs were carried out on an Alpha 2000 main frame computer. A simplified flow scheme of the sequential computations is given in Figure 3-4. In the main program (Figure 3-4A) the respective computations are carried out in a time-loop until the final time t_f is reached. The equations that are used are given between square brackets in Figure 3-4. By setting switches in a control file, root water uptake, solute transport and root nutrient uptake can be included or excluded. It is assumed that when solute transport is considered water movement is considered as well, and that when root nutrient uptake is considered, root water uptake is also considered. The core of the simulation model is the module that solves the Richards equation (Figure 3-4B). In a iteration loop the solution is obtained either through the ADI method or the ICCG method. If convergence problems arise (maximum number of iterations exceeded, or d_l

(A)

Initialization →Change BC's→Change Δt [3-95]→Root water uptake [3-37]

Solve Richards —→ Solute fluxes [3-63]—→Root nutrient uptake [3-92]
equation [3-26,39]

New solute distribution [3-67,68] —→ $t = t + \Delta t$ —→ $t < t_f$ | no

yes

Stop

(B) | Solution of Richards equation |

Store h^t etc.

Store h^k etc.

Adapt bottom BC ?

Compute K at CV interfaces [3-11,14]

unsaturated / \ saturated

ADI
$A_E, A_W, A_S, A_N, A_C, A,$ B, [3-23,25,42,43]
Solve for $k+1/2$ [3-39]
Status at $k+1/2$ (Ch. 4)
K at CV interfaces [3-11,14]
$A_E, A_W, A_S, A_N, A_C, A,$ B, [3-23,25,45,46]
Solve for $k+1$ [3-39]

ICCG
$A_E, A_W, A_S, A_N, A_C, A,$ B, [3-23,24,25,26]
Compute L [3-48]
Solve [3-50,51,52,53,54]

Hysteresis ? (Ch. 4)

New status at $k+1$ (Ch. 4)

Convergence ? [3-55] ——————— Adapt Δt ?
                                        no
yes

Compute flux densities

Figure 3-4 (A) Flow scheme indicating sequence of main computations in simulation model and (B) detail of sequence of computations for solving the Richards equation. Reference to equation numbers in the text are given between square brackets.

Table 3-1 Lists of input parameters required by the simulation model (see also Appendix
6), and list of (possible) output variables which are given at user-supplied print
times.

Input parameters
Water
$N, M, \Delta x_I, \Delta z_J$
For all (I,J): $\theta_r, \theta_s, n, \alpha_d, \alpha_w, K_s, \lambda$
Top boundary conditions
Per $(I,1)$ type of condition
Per time unit: rain/irrigation rate, E_p, T_p (only for root water uptake)
Bottom boundary conditions
Per (I,M) type of condition plus corresponding prescribed h or q
$h_0(I,J)$
$\Delta t_i, \Delta t_{max}, \Delta t_{min}, t_f, \zeta, t_m$
ϵ_c, ϵ_f, maximum number of iterations
Initial $\kappa_h, \epsilon_\kappa$ (see Chapter 4)
Root water uptake
$K_1, R_0, a, h_{r,1/2}$
$L_{rv}(I,J)$ (if root growth give also k_L, $t*$ and start time, and $L_{rvf}(I,J) = L_{rv}(I,J)$,
see Chapter 7)
Solute transport
$c_f, a_T, a_L, D_0, f_1(I,J), f_2(I,J), \theta_f(I,J)$
$c_0(I,J)$
Root nutrient uptake
S_{sr}

Output variables
Water
$\theta(I,J), h(I,J), K(I,J), C(I,J), H(I,J), q_x(i,j), q_z(i,j)$, total water storage, total change in water storage since $t = 0$, water mass balance error, total amount of water that passed top and bottom boundaries
Root water uptake
$S_w(I,J)$ (actual rate and cumulative since $t = 0$), h_r, T, total water uptake by plant roots
Nutrient transport
$c(I,J), Q_m(I,J), q_{sx}(i,j), q_{sz}(i,j)$, total nutrient storage, total change in nutrient storage since $t = 0$, water mass balance error, total amount of nutrient that passed top and bottom boundaries
Root nutrient uptake
$S_s(I,J)$ (actual rate and cumulative since $t = 0$), total nutrient uptake by plant roots

becomes too large) the time step is decreased and the iterations are started again beginning with the values of h^t, θ^t, K^t, and C^t. The computations of the new status variables (θ^{k+1}, K^{k+1}, and C^{k+1}; for ADI also $\theta^{k+1/2}$, $K^{k+1/2}$, and $C^{k+1/2}$) including hysteresis are done according to the models presented in the next chapter (Chapter 4). When convergence is reached the Darcian flux densities across the CV interfaces in x- and z-directions are computed according to Eq. [2-2]. They can be used to generate flux density distribution plots (see Chapters 7 and 8), and they are used in the solute transport module. There are also routines for writing output to files and for computing integral properties, such as net amounts of input into flow domain (not shown in Figure 3-4).

In Table 3-1 (previous page) lists are presented of the input parameters required by the simulation model, and of the (possible) output variables. Values for the input parameters are obtained from laboratory and greenhouse experiments as described in Chapters 4-6, and some parameters are obtained from literature (Chapter 5). The simulation model is used in Chapters 7 and 8.

3.7 Conclusions

In this chapter I have presented a numerical solution for the water movement and nutrient transport equations, including root uptake. The Richards equation is solved implicitly, while root uptake and nutrient transport are treated explicitly. Due to the partly explicit character of the model, the choice of the time step is motivated.

This chapter gives rise to the following conclusions.

- The Richards equation expressed in the mixed θ-h form can be solved numerically without mass-conservation problems, when the control volume finite element method (or any other finite element method) is used in combination with the fully implicit time approximation of the storage term according to Celia *et al.* (1990).
- For the control volume method applied in this study, the set of numerical equations expressed in matrix notation results in a five-banded coefficient matrix. Solution of this system is achieved by either the Alternating Direction Implicit (ADI) method or by the Incomplete Cholesky Conjugate Gradient (ICCG) method.
- As long as the system is unsaturated the faster ADI method can be used. For partially saturated conditions the ADI method fails to solve the problem.
- During periods of partial saturation the slower ICCG method must be used. In the ICCG method the five-banded coefficient matrix obtained with the rectangular control volume method results in simple computations, since in the computation of the Cholesky matrix less computations are needed.

Chapter 4

Hysteretic hydraulic properties of the

coarse sand substrate

To solve the Richards equation, Eq. [2-4], for a specific case the hydraulic properties are needed, i.e. the relationships between K, θ and h. Several mathematical models have been proposed in the literature. The water retention characteristic is sometimes written as an empirical polynomial or as a nonlinear relationship. In some cases the hydraulic conductivity function is calculated from the water retention characteristic, using assumptions about the pore structure. Many of the commonly used nonlinear water retention characteristics belong to a single family of functions, as was shown in the "superclass of soils" article by Raats (1992). In soil science the most commonly used models for the hydraulic properties are the models of van Genuchten (1980) and Mualem (1976). Recently, also the hydraulic properties of some horticultural substrates have been described by these models (e.g. Milks *et al.*, 1989; Wallach *et al.*, 1992a,b; Otten, 1994; Otten *et al.*, 1996). I will use these models as well, further referred to as the van Genuchten-Mualem model (Section 4.1). The $\theta(h)$ and $K(h)$ relationships are known to be hysteretic (Miller and Miller, 1956). In Section 4.2 the modified dependent domain model of Mualem (1984) for describing hysteresis is presented. In Section 4.3 the physical properties including the K, θ and h relationships for the coarse sand substrate used in this thesis are presented. The parameters in the van Genuchten-Mualem model are determined from an equilibrium method (Subsection 4.3.2), and from a transient multi-step outflow method (Subsection 4.3.3). In Section 4.4 the parameters obtained in Section 4.3 are compared and combined to one set.

4.1 The van Genuchten-Mualem relationships for $\theta(h)$ and $K(\theta)$

The *water retention function* $\theta(h)$ given by van Genuchten (1980) reads as

$$S_e(h) = \frac{\theta(h) - \theta_r}{\theta_s - \theta_r} = \begin{cases} \dfrac{1}{\left(1 + |\alpha h|^n\right)^m} & h \leq 0 \\ \\ 1 & h > 0 \end{cases}, \qquad [4\text{-}1]$$

where S_e is the reduced volumetric water content (-) or effective saturation ($0 \leq S_e \leq 1$), θ_r and θ_s are the residual and saturated volumetric water contents ($L^3 L^{-3}$), respectively, α (L^{-1}), n ($n > 1$; (1)) and m (1) are curve shape parameters. The steepness of the water

retention characteristic is determined by n, whereas m determines the value for S_e when $h = -1/\alpha$. For given constant parameters, an increase in α causes a shift of the water retention characteristic to lower volumetric water contents.

The *hydraulic conductivity function* $K(\theta)$ given by Mualem (1976) reads as

$$K_r(S_e) = \frac{K(S_e)}{K_s} = S_e^\lambda \left[\frac{\int_0^{S_e} h^{-1}(\eta)\,d\eta}{\int_0^1 h^{-1}(\eta)\,d\eta} \right]^2 , \qquad [4\text{-}2]$$

where K_r is the relative hydraulic conductivity (1), K_s is the hydraulic conductivity (LT^{-1}) at saturation, and λ is a curve shape parameter (1) representing a pore-size distribution index, which is sometimes assumed to be equal to 0.5 as suggested by Mualem (1976). For saturated conditions, i.e. $h \geq 0$, $S_e = 1$ (Eq. [4-1]), Eq. [4-2] reduces to $K_r(1) = 1$. Substituting Eq. [4-1] in Eq. [4-2] one obtains (Leij *et al.*, 1992)

$$K_r(S_e) = S_e^\lambda \left[I_{S_e^{1/m}}(m+1/n,\,1-1/n) \right]^2 , \qquad [4\text{-}3]$$

where I_η is the incomplete beta function of order η. In case the parameters m and n are related according to

$$m = 1 - \frac{1}{n}, \quad n > 1 , \qquad [4\text{-}4]$$

a simple expression for K_r is obtained

$$K_r(S_e) = S_e^\lambda \left[1 - \left(1 - S_e^{1/m} \right)^m \right]^2 . \qquad [4\text{-}5]$$

The corresponding expression for $K_r(h)$ follows from substitution of Eq. [4-1] in Eq. [4-5]:

$$K_r(h) = \begin{cases} \dfrac{\left[\left(1 + |\alpha h|^n \right)^m - |\alpha h|^{n-1} \right]^2}{\left(1 + |\alpha h|^n \right)^{(\lambda + 2)m}} & h \leq 0 \\[4mm] 1 & h > 0 \end{cases} . \qquad [4\text{-}6]$$

Finally, substituting Eq. [4-1] in Eq. [2-6], an expression for the differential moisture capacity $C(h)$ can be obtained:

$$C(h) = \begin{cases} \left(\theta_s - \theta_r \right) n\, m\, \alpha^n\, |h|^{n-1} \left(1 + |\alpha h|^n \right)^{-1-m} & h \leq 0 \\[3mm] 0 & h > 0 \end{cases} . \qquad [4\text{-}7]$$

In Section 4.3 methods are presented and used to determine the parameters in the van Genuchten-Mualem model.

4.2 Modified dependent domain hysteresis model of Mualem

The relationships $\theta(h)$ and $K(h)$ are known to be hysteretic (Miller and Miller, 1956), which means that different relationships exist for drying and wetting processes. It is assumed that $K(\theta)$ is not hysteretic. Topp (1969) showed experimentally that $\theta(h)$ is hysteretic and that $K(\theta)$ has negligible hysteresis. Any porous medium has hysteretic hydraulic properties. Since in closed horticultural cropping systems frequent cycles of drying and wetting occur, it is important to account for hysteresis. Following Kool and Parker (1987b), in this thesis I use the following hysteresis model.

The main drying and wetting water retention curves
The *main drying water retention characteristic* can be expressed by Eq. [4-1], with the parameters:

$$\theta_{s,d}, \quad \theta_{r,d}, \quad \alpha_d, \quad n_d, \quad m_d,$$

and the *main wetting water retention characteristic* can also be expressed by Eq. [4-1], with the following parameters:

$$\theta_{s,w}, \quad \theta_{r,w}, \quad \alpha_w, \quad n_w, \quad m_w.$$

The subscripts d and w refer to main drying and main wetting, respectively. In order to reduce the number of parameters, following Kool and Parker (1987b), it is assumed that

$$\theta_{s,d} = \theta_{s,w} = \theta_s, \quad \theta_{r,d} = \theta_{r,w} = \theta_r, \quad n_d = n_w = n, \quad \text{and} \quad m_d = m_w = m.$$

This implies that the main wetting characteristic and the main drying characteristic only differ in the parameter α. For $\alpha_w > \alpha_d$ the wetting curve lies to the left of the drying curve. The two main curves are closed at the end-points θ_r and θ_s. Note that the main wetting characteristic also ends at θ_s, implying that air entrapment, at $h = 0$, is not taken into account.

In case the drying process along the main drying curve is reversed into a wetting process somewhere in the flow domain, then a scanning wetting curve is followed. Similarly, scanning drying curves exist. Between the main wetting characteristic and the main drying characteristic there are an infinite number of *scanning curves*. It is time-consuming to determine a large number of scanning curves in the laboratory, so that mathematical models are very useful. With these models the scanning curves can be computed. It is important that such a model considers scanning curves as closed loops, otherwise the so-called pumping effect (Jaynes, 1984) occurs. Comparisons of several hysteresis models were carried out by Jaynes (1984) and Viaene *et al.* (1994). In this thesis the *modified dependent domain model of Mualem* (1984), having closed scanning loops, is used. In a comparative, statistical study by Viaene *et al.* (1994), this model performs best of the so-called two-branch models. Two-branch hysteresis models require as input both the main drying and the main wetting characteristics. The expressions for the scanning curves are given below using the notation used by Kool and Parker (1987b).

Modified dependent domain model of Mualem (1984)
Mualem's (1984) model accounts for the pore water blockage against air in drying
processes, but blockage of access to water during wetting processes is considered
negligible. Thus the dependence of the domains refers to the drying process, and in the
wetting process the pores are assumed to be independent. This results in a complicated
expression for drying and a simpler one for wetting. The *scanning drying curve* is defined
as (Figure 4-1)

$$\theta_{sd}(h) = \theta_{\Delta} - P(\theta)\left[\theta_s - \theta_w(h)\right]\left[\theta_w(h_{\Delta}) - \theta_w(h)\right],$$ [4-8]

and the *scanning wetting curve* is defined as (Figure 4-1)

$$\theta_{sw}(h) = \theta_{\Delta} + P(\theta_{\Delta})\left[\theta_s - \theta_w(h_{\Delta})\right]\left[\theta_w(h) - \theta_w(h_{\Delta})\right],$$ [4-9]

where subscripts *sw* and *sd* refer to the scanning wetting and scanning drying curves,
respectively, and subscript Δ refers to the reversal point. The different components of
Eqs. [4-8] and [4-9] are shown in Figure 4-1.

The function $P(\theta)$ is given by

$$P(\theta) = \frac{\theta_s - \theta}{\left[\theta_s - \theta_w(h^+)\right]^2},$$ [4-10]

where h^+ is the pressure head at which

$$\theta_d(h^+) = \theta.$$ [4-11]

Using Eq. [4-1] h^+ can be computed as follows[1]

$$h^+ = -\frac{1}{\alpha_d}\left[\left(\frac{\theta - \theta_r}{\theta_s - \theta_r}\right)^{-1/m} - 1\right]^{1/n}.$$ [4-12]

For drying processes P is a function of the unknown θ, while for wetting processes P is
a function of the known θ_{Δ}. Therefore, Eq. [4-8] must be solved iteratively, while Eq.
[4-9] can be computed directly. A short discussion on the function P is presented in the
Appendix 1. For a further discussion on the function P the reader is referred to Mualem
(1984).

The Mualem model fails to converge to the correct θ_r or θ_s. Therefore, an additional
constraint is needed to prevent θ falling outside the main wetting curve and main drying
curve:

$$\theta_w(h) \le \theta(h) \le \theta_d(h).$$ [4-13]

[1] Note that in Eq. (11) of Kool and Parker (1987b) the minus sign is missing.

Absolute pressure head $|h|$ (cm)
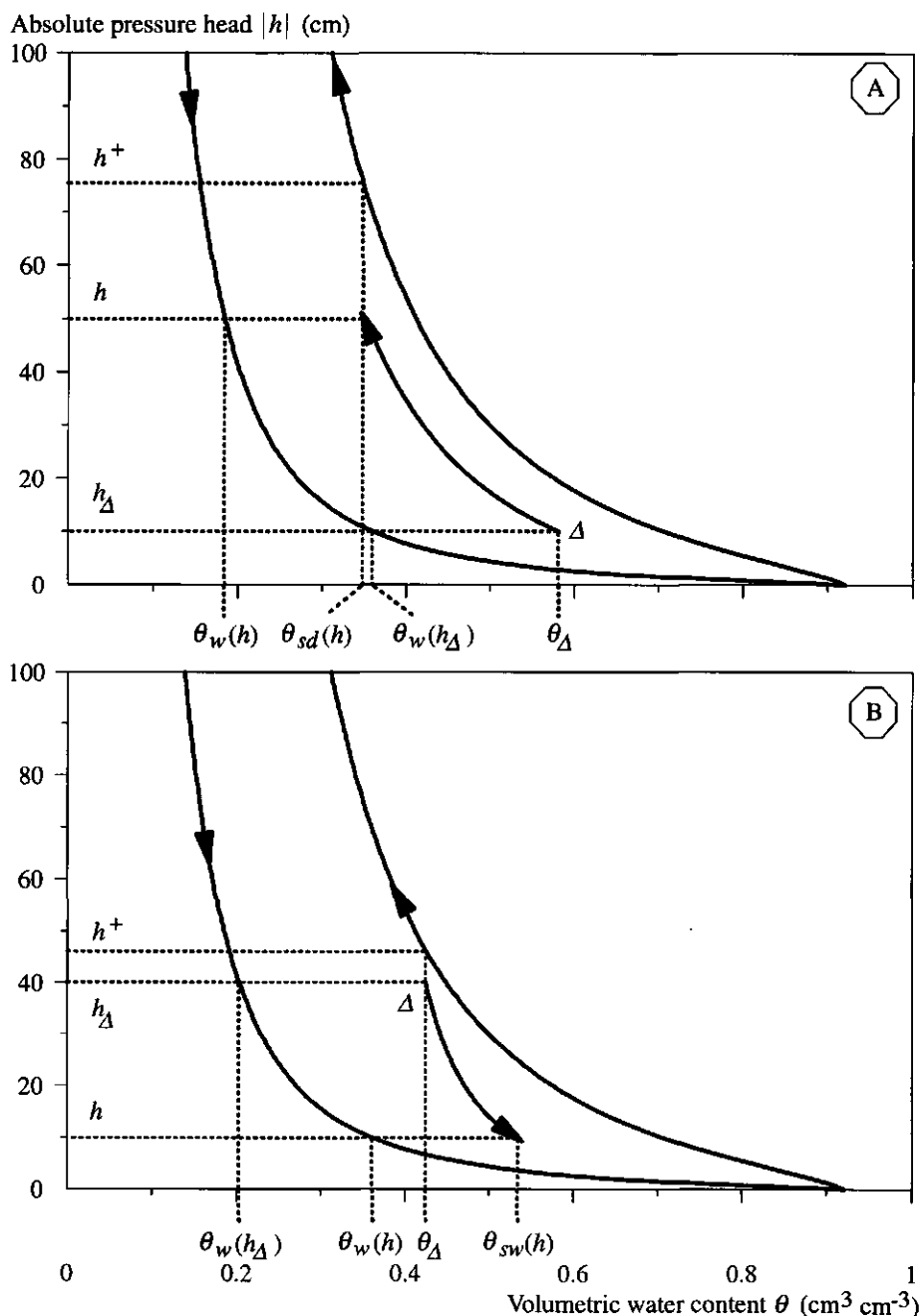
Figure 4-1 Main drying, main wetting, and examples of scanning drying (A) and scanning wetting (B) curves according to Eqs. [4-8] and [4-9]. Parameter values apply to a mixture of 75% peat and 25% perlite (hydraulic properties from Otten, 1994).

The *differential moisture capacity belonging to the drying scanning curve* follows from differentiating Eq. [4-8] with respect to h^2:

$$C_{sd}(h) = \left(T_1 + T_2\right) P(\theta) \left[1 + T_1 T_2 T_3\right]^{-1} C_w(h),$$ [4-14]

with

$$T_1 = \theta_s - \theta_w(h),$$ [4-15]

$$T_2 = \theta_w(h_\Delta) - \theta_w(h),$$ [4-16]

and

$$T_3 = -\left[\theta_s - \theta_w(h^+)\right]^{-2} + 2\left(\theta_s - \theta\right)\left[\theta_s - \theta_w(h^+)\right]^{-3} T_4 C_w(h^+),$$ [4-17]

with

$$T_4 = \left[\alpha_d(n-1)(\theta - \theta_r)\right]^{-1} \left[\left\{\frac{\theta - \theta_r}{\theta_s - \theta_r}\right\}^{-1/m} - 1\right]^{-m} \left\{\frac{\theta - \theta_r}{\theta_s - \theta_r}\right\}^{-1/m}.$$ [4-18]

The *differential moisture capacity belonging to the wetting scanning curve* follows from differentiating Eq. [4-9] with respect to h:

$$C_{sw}(h) = P(\theta_\Delta)\left[\theta_s - \theta_w(h_\Delta)\right] C_w(h).$$ [4-19]

A complicated expression for the drying differential moisture capacity, i.e. Eq. [4-14], is obtained due to differentiating P with respect to h, while for the wetting process the derivative $\partial P/\partial h$ is zero, and thus a simple expression for C_{sw}, i.e. Eq. [4-19], is obtained.

For each grid point in the control volume model (see Chapter 3) the hysteresis model must be used. Thus for each node the *status of drying or wetting* must be known and adapted if necessary. The status of the node is stored as κ_h and can have four values:

  - 2: drying along main drying curve,
  - 1: drying along scanning drying curve,
  +1: wetting along scanning wetting curve, and
  +2: wetting along main wetting curve.

A change of κ_h occurs when h at a node at time $t+\Delta t$ meets the criterion (Kool and Parker, 1987b)

$$\frac{h^t - h^{t+\Delta t}}{\kappa^*} \geq \epsilon_\kappa,$$ [4-20]

---

[2] Eq. (14) of Kool and Parker (1987b) is wrong. They gave a minus-sign in front of $T_1 T_2 T_3$ instead of a plus-sign. In the expression for T_4 they raised the term between square brackets to the power $+m$ instead of $-m$. The parameter α was not specified as α_d. Note that they used $-T_4$ in the expression for T_3 and that in T_4 the term $(1-n)$ was used. This is the same as $+T_4$ with in the expression for T_4 the term $(n-1)$ as is given here.

where ϵ_κ (L) is set to some small positive number, e.g. $\epsilon_\kappa = 0.01$, to ignore the effect of small local oscillations in the calculated pressure head, and κ^* is defined as

$$\begin{cases} \kappa^* = -1 & \text{if } \kappa_h < 0 \\ \\ \kappa^* = +1 & \text{if } \kappa_h > 0 \end{cases} \qquad [4\text{-}21]$$

Possible reversals of κ_h are from -2 or -1 to $+1$, from $+2$ or $+1$ to -1, from -1 to -2, and from $+1$ to $+2$. The change from -1 to -2 or from $+1$ to $+2$ occurs when the constraint of Eq. [4-13] is not met. As soon as the status of a node becomes $+2$ or -2 the van Genuchten-Mualem model (Section 4.1) can be used.

Note that, after returning at a reversal point, the Mualem hysteresis model stays on the current scanning loop. Other models (Dirksen *et al.*, 1993; Otten, 1994) step over on the previous scanning loop. A comparison between the hysteresis module described here and that of Dirksen *et al.*, (1993) yielded similar results for some one-dimensional flow problems (Koorevaar, 1995, personal communication).

4.3 Characterization of the coarse sand substrate

The parameters occurring in the equations describing the hydraulic properties given above can be obtained from water retention data and hydraulic conductivity data with the help of the parameter optimization program RETC (van Genuchten *et al.*, 1991; Leij *et al.*, 1992). Alternatively, data from one-step or multi-step outflow experiments can be used with the help of the parameter optimization program SFIT (Kool and Parker, 1987a), or with the programs MULSTP (van Dam *et al.*, 1994) or MLSTPM (Eching *et al.*, 1994).

In Subsection 4.3.1 the particle weight fraction distribution, the porosity, and the hydraulic conductivity at saturation of the coarse sand substrate are given. The main drying and wetting characteristics determined with a standard laboratory equilibrium method are presented in Subsection 4.3.2. The hydraulic properties obtained from multi-step outflow experiments are presented in Subsection 4.3.3.

4.3.1 Particle weight fraction distribution, porosity, and
hydraulic conductivity at saturation

In this thesis a coarse sand was used as a substrate in the greenhouse experiments as described in Chapter 5. From the *particle weight fraction distribution* (Figure 4-2) of the coarse sand substrate, it follows that the median diameter is 0.6 mm.

Weight fraction (g g^{-1})
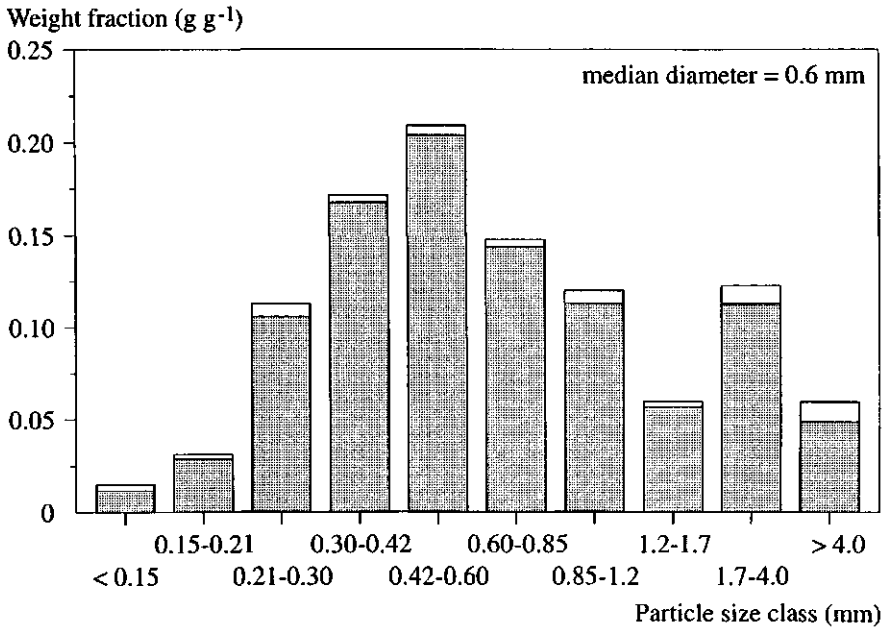
Figure 4-2 Particle weight fraction distribution of the coarse sand used as substrate in the sand bed growth system. The open bars at the top represent the standard deviation of four samples.

The average *dry bulk density* ρ_d (M L^{-3}) of the coarse sand at the experimental site described in Chapter 5 increased in time (Figure 4-3). In January and February 1992, the sand beds were completely inundated in order to settle the sand, resulting in an increase in ρ_d. This thesis mainly focuses on experiments carried out in May-July 1993 and in August-December 1993. It is assumed that during this period ρ_d was constant, and equal to the values obtained in July 1993. The ρ_d was determined at three 5 cm depth intervals one week after the harvest of the May-July 1993 experiment. During that week the sand bed system was irrigated regularly, so that the loosened top layer could settle again. Statistical analysis of variance (Genstat 5 Committee, 1993) of the 100 cm^3 core samples showed that ρ_d was 1680 kg m^{-3} at depth 0-5 cm and 1720 kg m^{-3} at depths 5-10 cm and 10-15 cm. The *porosity* ϕ_p (L^{3}L^{-3}) can be computed from ρ_d according to

$$\phi_p = 1 - \frac{\rho_d}{\rho_s}, \qquad [4\text{-}22]$$

where ρ_s is the particle density (L^{3}L^{-3}) of the coarse sand, here taken as 2650 kg m^{-3} (e.g. Blake and Hartge, 1986). The porosity ϕ_s is 0.366 m^3 m^{-3} at depth 0-5 cm and 0.351 m^3 m^{-3} at depth 5-15 cm.
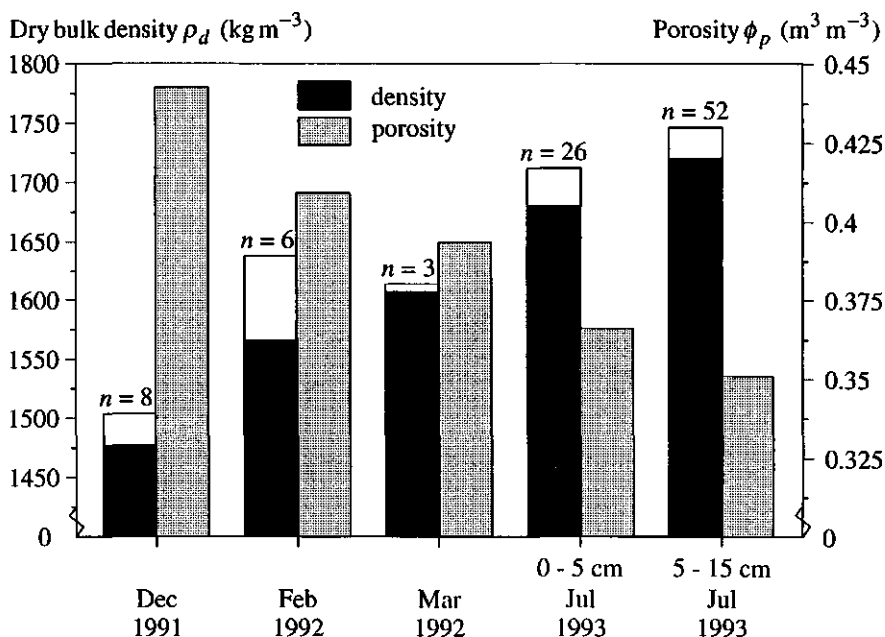
Figure 4-3 Average dry bulk density ρ_d and porosity ϕ_p at four sampling dates during the experimental period. The number of samples at each sampling date are given as *n*; the standard deviation is given by the white bars. In July 1993 samples were taken at three five cm depth intervals, but only the top 0-5 cm was significantly different from the other samples. See text for further explanation.

The *hydraulic conductivity at saturation* K_s (L T^{-1}) was determined according to the Dutch standard procedure NEN 5789 (NEN 5789, 1991) using artificially filled cores of 2865 cm^3 at a density of 1700 kg m^{-3}, being the average of ρ_d in the sand beds. K_s decreased from 1256 cm d^{-1} at day 1 to 85 cm d^{-1} at day 3 (Figure 4-4). Possible reasons are: 1) physical breakdown of the structure when fine particles are transported to the bottom of the column causing a barrier to outflow, and 2) clogging of the pore system caused by bacterial and/or algae growth (cf. Vandevivere and Baveye, 1992). Biological growth can be expected since non-sterile substrate and tap water were used. The experiment was repeated in a second column using a 39% (by weight) ethanol solution instead of tap water. Principally, the intrinsic permeability is the same for all fluids, so that K_s can be computed from the conductivity of ethanol K_e according to

$$K_s = K_e \frac{\eta_e}{\eta_l} \frac{\rho_l}{\rho_e} ,$$

[4-23]

Hydraulic conductivity at saturation K_s (m d^{-1})
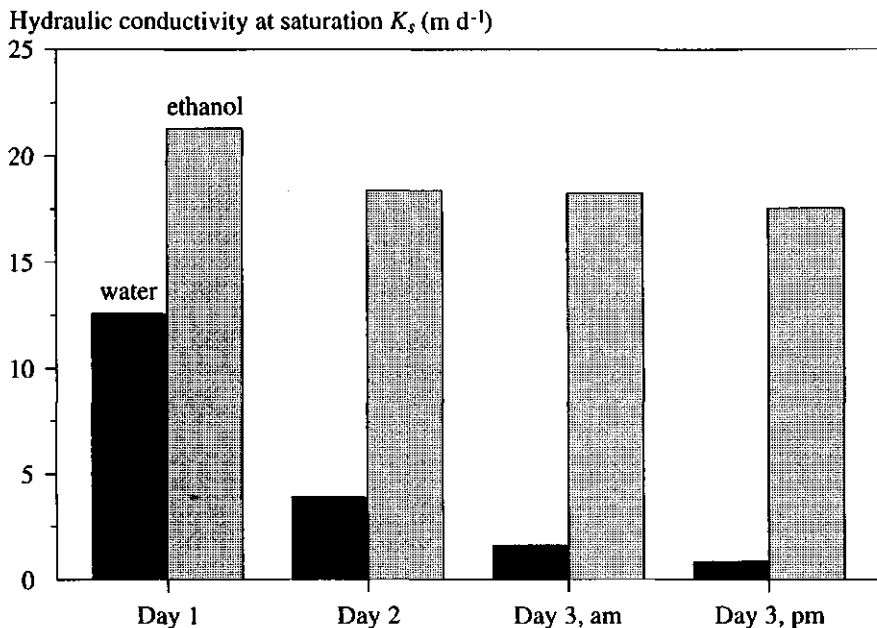
Figure 4-4 Conductivity at saturation determined with tap water and ethanol during three consecutive days.

where η_e is the viscosity of ethanol (= 2.836 10^{-2} g s^{-1} cm^{-1} at 20 °C; 39% ethanol), η_l is the viscosity of water (= 1.002 10^{-2} g s^{-1} cm^{-1} at 20 °C), ρ_e is the density of ethanol (= 0.937 g cm^{-3} at 20 °C; 39% ethanol), and ρ_l is the density of water (= 0.998 g cm^{-3} at 20 °C) (constants obtained from Weast, 1975). After a small decrease during day 1 the conductivity remained constant during days 2 and 3 (Figure 4-4). Ideally, this computed conductivity for water from the ethanol measurements should yield a good value for K_s, but this is not the case here. For some natural soils this phenomenon is sometimes observed as well. Usually this is attributed to an interaction between the percolating fluid and the soil matrix (Klute and Dirksen, 1986), presumably with clay particles and/or adsorbed ions. This argument may not be the reason for the difference observed in this study, but no other causes are known. More important is the fact that the conductivity for ethanol remained constant in time. Ethanol prevents growth of bacteria and algae, so that it is unlikely that physical breakdown of the pore system is the main cause for the observed decrease in conductivity for water.

Algae growth at the sand bed surface was visible during the greenhouse experiments reported in Chapter 5. Since it is difficult to achieve the same conditions in the laboratory with respect to the density of algae, type of solution, temperature and light, I decided to

use the hydraulic conductivity for water obtained at day 1, i.e. K_s = 12.56 m d^{-1}, in the remainder of this thesis.

4.3.2 The equilibrium water retention method

Four representative core samples, used to determine the dry bulk density in Subsection 4.3.1, were used to determine the *water retention characteristic*: two samples from the 0-5 cm layer and two samples from the 5-15 cm layer. The method used was the *equilibrium hanging water column method* (NEN 5786, 1991), adapted in such a way that outflow occurred in a horizontal tube. The first cycle consisted of the initial main drying characteristic from saturation to a pressure head of h = -100 cm, followed by a primary wetting characteristic up to h = -3 cm, thus not to complete saturation; the second cycle consisted of a drying curve and a wetting curve (Figure 4-5). The initial drying curve differs markedly from the second one, while the wetting curves are close to each other. This behaviour is not uncommon (e.g. Klute, 1986) and is attributed to entrapped air. For three of the four samples, the second drying process yielded at h = -100 cm a higher θ than the first drying process: for the 0-5 cm samples this was 0.014 cm^{3}cm^{-3}, and for the 5-10 cm or 10-15 cm samples 0.005 cm^{3}cm^{-3}. This unexpected behaviour might be caused by an increase of biological mass in the samples during the experiment, which increased the water holding capacity. However, this minor effect is disregarded in the remainder of this section.

The RETC code (van Genuchten *et al.*, 1991) was used to determine the parameters of the hydraulic properties (Table 4-1). For this purpose θ at h = -1000 cm and θ at h = -5000 cm were used as additional input as well: 0.0139 cm^3 cm^{-3} and 0.0124 cm^3 cm^{-3}, respectively. The observations were statistically compared to each other with applied pressure head and location of the samples as factors. Only for the first drying cycle θ of the top layer was significantly lower than for the bottom layer. The parameters for all data of the second cycle were determined as well (Table 4-1). Note that the parameters obtained for all data of the second cycle are close to the averaged parameters of the top and bottom layers of the second cycle; graphically no differences are noticeable. This aspect will be used in Subsection 4.3.3. There are two subjects that need further discussion. Firstly, the volumetric water content θ_s, and secondly, the description of the wetting data.

In all cases the estimated θ_s for the first cycle data is 0.05 cm^{3}cm^{-3} to 0.06 cm^{3}cm^{-3} smaller than ϕ_p = 0.366 or 0.351, as obtained in Subsection 4.3.1. Apparently, the samples were not completely saturated at the beginning of the experiment. For the second cycle θ_s is more than 0.1 cm^{3}cm^{-3} smaller than ϕ_p. Anticipating on results of Chapters 5 and 7, it appeared that conditions close to saturation occur in the greenhouse experiments. Thus with the current water retention curves of the second cycle it will not be possible to describe the experimental data in the substrate. The water retention curves will be adapted based on the following reasoning. The core samples used in the laboratory

Absolute pressure head $|h|$ (cm)
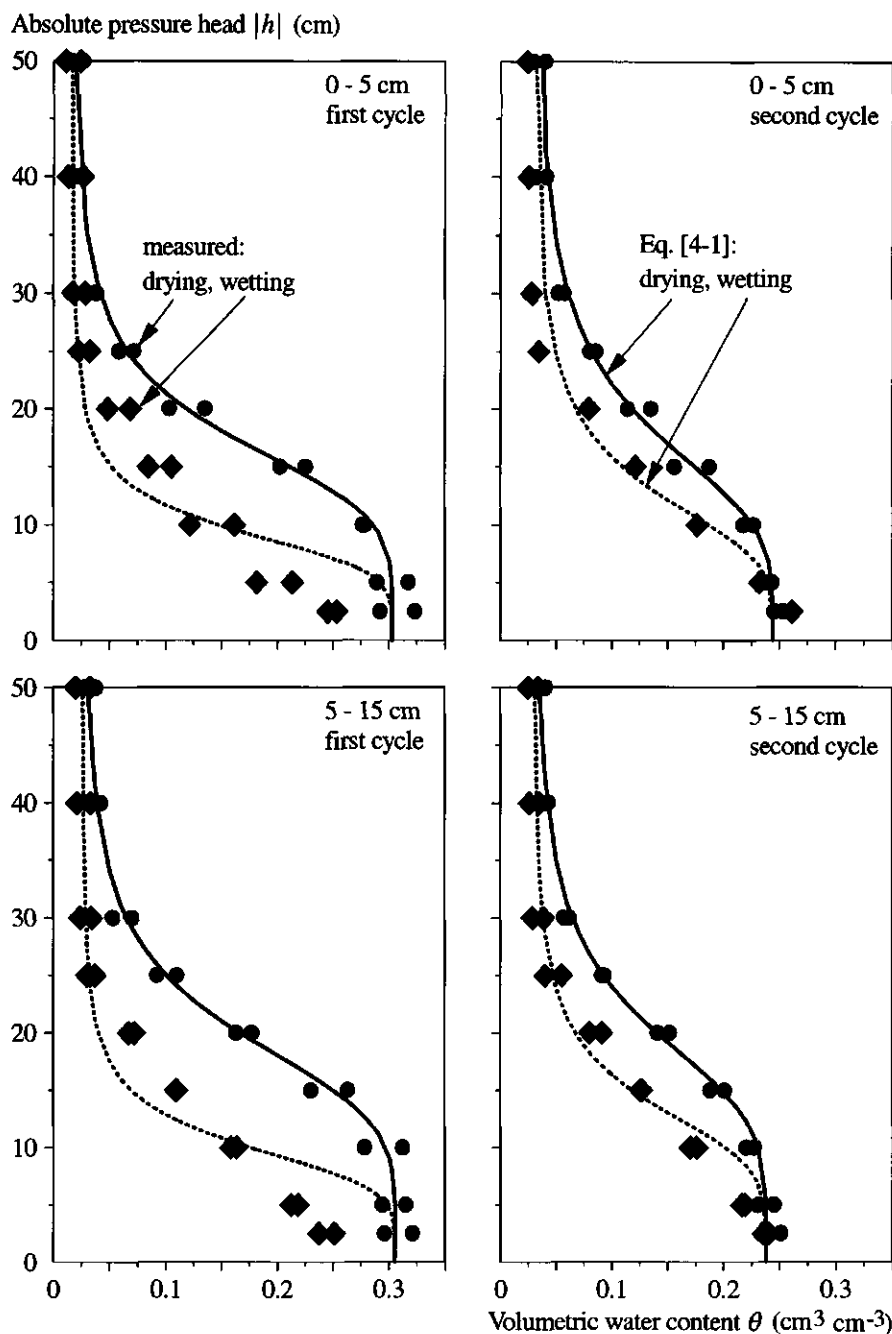
Figure 4-5 Two cycles of drying and wetting characteristics determined on two samples of the top layer (0-5 cm; upper two graphs) and two samples of the bottom layer (5-15 cm; bottom two graphs) of the sand bed cropping system.

Table 4-1 Parameter estimates (RETC, van Genuchten *et al.*, 1991) of the hydraulic properties θ_r (-), θ_s (-), n (-), α_d (cm^{-1}), and α_w (cm^{-1}), of the coarse sand substrate obtained from the equilibrium method for the two cycles of drying plus wetting for the top (0- 5 cm; data of two samples used) and bottom (5- 15 cm; data of two samples used) of the sand bed system, and for the second cycle for top and bottom together. Parameter estimates are given for the drying, the wetting, and for the restricted wetting characteristics for which the drying parameters (given between brackets) are used except for the α_w parameter. In all cases it is assumed *a priori* that $m = 1 - 1/n$ (-). The goodness of fit is given as r^2.

	Drying	Wetting-restricted	Wetting	Drying	Wetting-restricted	Wetting
Cycle 1	Top			Bottom		
θ_r	0.01573	(0.01573)	0.00910	0.02311	(0.02311)	0.01888
θ_s	0.30276	(0.30276)	0.24246	0.30584	(0.30584)	0.23592
n	4.98171	(4.98171)	2.82246	4.90919	(4.90919)	3.37394
α_d	0.06069			0.05312		
α_w		0.11074	0.11745		0.09466	0.09301
r^2	0.9933	0.9272	0.9723	0.9919	0.9602	0.9867
Cycle 2	Top			Bottom		
θ_r	0.02398	(0.02398)	0.01576	0.02565	(0.02565)	0.02099
θ_s	0.24512	(0.24512)	0.25198	0.23835	(0.23835)	0.23034
n	3.85485	(3.85485)	3.39879	4.53626	(4.53626)	3.43214
α_d	0.06098			0.05216		
α_w		0.08514	0.08854		0.07654	0.08095
r^2	0.9906	0.9896	0.9911	0.9928	0.9815	0.9886
Cycle 2	All					
θ_r	0.02633	(0.02633)	0.02007			
θ_s	0.24117	(0.24117)	0.23724			
n	4.21992	(4.21992)	3.45511			
α_d	0.05622					
α_w		0.08035	0.08343			
r^2	0.9889	0.9806	0.9861			

were (de)watered from below. In the greenhouse experimental set-up watering was from the top and water removal occurred throughout the profile and at the drain when the sand at this position was saturated. Due to hysteresis, a soil sample which is watered from below (absorption, wetting curve) will be drier than a soil sample which is watered from above (desorption, drying curve). For comparison, Otten (1994) did not have the difference in water supply/removal between his laboratory method and his experimental method; in both cases (de)watering was from below. The best solution to overcome the problem for the present situation is to determine $\theta(h)$ using a laboratory experimental set-up at which water is applied/removed from the top. Unfortunately, such a set-up was not available. There are other possibilities to come to a better estimate of the water retention characteristic.

- Firstly, the optimization program RETC can be used with the measured retention data and with the restriction of $\theta_s = \phi_p$, or with additional input data $\theta = \phi_p$ at $h = 0$ cm. However, then the data near saturation, which are of importance in this study, will not be described well.
- Secondly, the obtained laboratory retention characteristics can be scaled so that $\theta_s = \phi_p$, or with the inclusion of air blockage.

This last method is adopted here, taking $\theta_s = \phi_p - 0.04$, where the factor 0.04 was arbitrarily chosen. It was assumed that the effective saturation (Eq. [4-1]) and θ_r of the unscaled and scaled retention curves are the same. From Eq. [4-1] it follows immediately that except for θ_s all parameters remain the same. The *main drying curves of the first cycle were used in the scaling procedure*, and the resulting sets of parameters and curves are given in Table 4-2 and Figure 4-6, respectively.

Table 4-2   Scaled set of hydraulic parameters θ_r (-), θ_s (-), n (-), α_d (cm^{-1}), and α_w (cm^{-1}), as obtained for the layers 0-5 cm and 5-15 cm using the equilibrium method; it is assumed *a priori* that $m = 1 - 1/n$ (-). See text for explanation.

Depth	θ_r	θ_s	n	α_d	α_w
0-5 cm	0.01573	0.326	4.98171	0.06069	0.11074
5-15 cm	0.02311	0.311	4.90919	0.53120	0.09466

The restricted parameter optimization for the wetting data, i.e. with the exception of α_w all parameters are the same as for the drying process, works well for the second cycle data but unsatisfactorily for the first cycle data. As discussed above, I will use the first cycle data, but then the hysteresis model of Section 4.2 fails to describe the wetting data. Alternatives to represent the wetting data are discussed below.

- Use Eq. [4-1] for drying and wetting data with more than one pair of parameters differing from each other, e.g. have also n different besides α. This method has the

Absolute pressure head $|h|$ (cm)
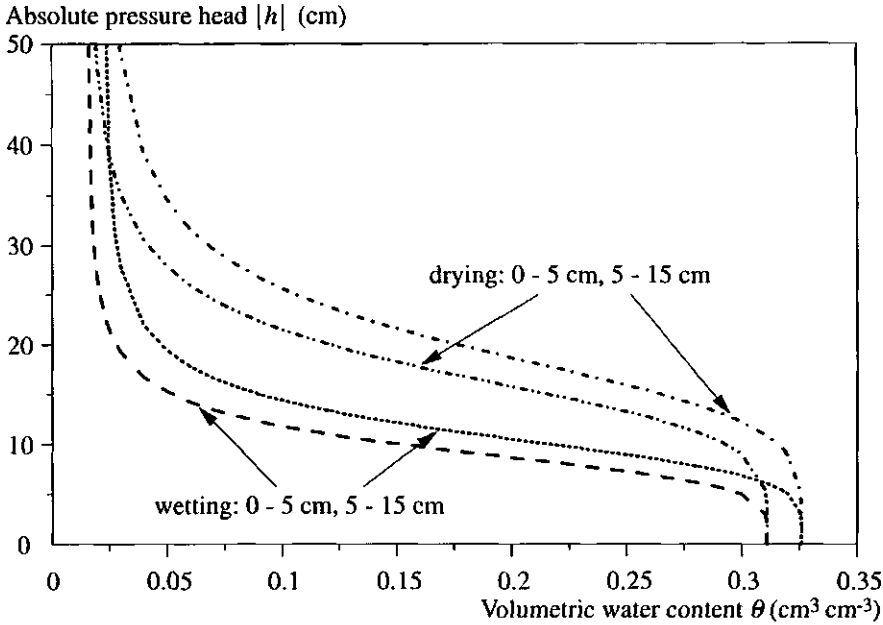
Figure 4-6 Scaled main drying and main wetting characteristics for the top (0-5 cm) and bottom (5-15 cm) layers of the sand bed system as obtained from the equilibrium retention data. Hysteretic parameters are given in Table 4-2. See text for further explanation.

disadvantage that the wetting and drying curves will cross, which is physically unrealistic. This can be demonstrated by setting up Eq. [4-1] for the drying and wetting cases and by setting the two equations equal to each other, yielding

$$| h | = \alpha_w^{-1} \left(\left(1 + | \alpha_d h |^{n_d} \right)^{m_d / m_w} - 1 \right)^{1/n_w} . \qquad [4\text{-}24]$$

The solution for h can be obtained iteratively. By approximation, when $|\alpha h|^n \gg 1$ and $m = 1 - 1/n$, the value of h where the curves cross can be computed from

$$| h | = \left(\frac{\alpha_w^{n_w - 1}}{\alpha_d^{n_d - 1}} \right)^{(n_d - n_w)^{-1}} . \qquad [4\text{-}25]$$

For example, for $n_d = 4.9$, $n_w = 2.2$, $\alpha_d = 0.06$ cm^{-1} and $\alpha_w = 0.19$ cm^{-1} the value for h where the two curves cross according to Eq. [4-24] is 27.27 cm, while the approximation according to Eq. [4-25] yields 27.82 cm. When $\alpha_w = \alpha_d$, Eq. [4-25] reduces to $|h| = \alpha^{-1}$. Since crossing of the wetting and drying curves is physically unrealistic, I will not use this alternative. Moreover, for the case when also n is

different, the $K(\theta)$ characteristic becomes hysteretic, as can be seen from Eq. [4-5]. This was also recognized by Kool and Parker (1987a), but they did not mention the crossing of the drying and wetting curves.

■ The wetting data can also be represented by cubic splines with an exact fit through the data, or by smoothed cubic splines with a least squares fit through the data. The cubic spline method yielded for the top and bottom cases of the wetting data negative slopes, i.e. $C < 0$ and hence $D < 0$, for the lower h's, thus being unrealistic. With the smoothed cubic splines method this was mostly the case as well, which makes this method very difficult to implement. Therefore, I did not use the (smoothed) cubic splines representation of the wetting data.

■ The data were fit with the van Genuchten model, Eq. [4-1]: first the drying data were fit and then, independently, the wetting data. This does not result in the best least squares fit of both sets of data. It is not possible to carry out a simultaneous fit with RETC. Instead, I used the mathematical software package Mathematica (Wolfram, 1991) to do the simultaneous fit (see Appendix 2 for Mathematica codes and resulting parameters). The sum of squares of differences between fitted values and observations was $2.30 \cdot 10^{-2}$ for the layer 0-5 cm; for comparison, the sum of squares of differences for the independent fit (Table 4-1) was $3.38 \cdot 10^{-2}$, i.e. $2.32 \cdot 10^{-3}$ for the drying data plus $3.15 \cdot 10^{-2}$ for the wetting data. The simultaneous fit improved the total sum of squares compared to individual fit. However, the observed laboratory wetting data near saturation were still not well described. The simultaneous fit resulted in lower estimates for θ_s and a much lower estimate for n; the other estimates were close to the results from individual fits.

■ The simplest alternative is using the original data set in tabulated form and use linear interpolation for intermediate values. The slope C can be determined easily as well.

When comparing simulation results and field measurements in Chapter 7, I will present results for two methods of representing the main drying and wetting curves. In both cases the main drying curve is represented by the van Genuchten function, Eq. [4-1], with α_d. In the first method the wetting curve is represented by the van Genuchten function with α_w and the other parameters equal to those of the drying curve, which will be referred to as the 'α_d-α_w-method' (Section 4.2). In the second method the wetting curve is represented in tabulated form, which will be referred to as the 'α_d-data interpolation method'.

Kool and Parker (1987b) stated that, if no information on the wetting curve is available, for natural soils $\alpha_w = 2\,\alpha_d$. The coarse sand substrate used here has a ratio α_w / α_d in the range 1.78-1.93; for the second cycle this ratio was in the range 1.4-1.5. Surprisingly, Otten (1994) obtained $\alpha_w / \alpha_d = 6.9$ for a mixture of 75% peat + 25% perlite.

4.3.3 The transient multi-step outflow method

The *transient outflow* method has long been used *to determine the hydraulic properties of porous media* (e.g. Gardner, 1956; Doering, 1965; Passioura, 1976; Kool *et al.* 1985;

Parker *et al.* 1985). Kool and Parker (1987a) developed a computer program (SFIT) with which, amongst others, the outflow data can be used to obtain estimates of the different parameters occurring in the van Genuchten-Mualem model. In the SFIT program the one-dimensional form of the Richards equation, together with the van Genuchten-Mualem model, is solved. The resulting estimates are often not unique (e.g. Kool *et al.*, 1985; Mous, 1993). Recently, some authors have improved the method. Van Dam *et al.* (1994), supported theoretically by Mous (1993), used the multi-step outflow method. This method was further improved by Eching *et al.* (1994), supported by Toorman *et al.* (1992), to obtain not only outflow data but *h* data in the sample as well. In this thesis I used multi-step outflow data with additionally measured *h*'s in combination with the SFIT program, which is also able to deal with multi-step experiments and additional *h* data.

The experimental set-up was similar to that of van Dam *et al.*, (1994), except that outflow entered the burette at its top. A tensiometer was installed at the top of the sample approximately 0.25 cm below the surface. Both the tensiometer and the burette were connected to pressure transducers, which were recorded automatically. Instead of applying air pressures to the top of the sample, suctions were applied at the bottom of the porous plate with a hanging water column. After the samples were saturated, the initial condition was applied by setting the outflow position 10 cm below the bottom of the sample. An initial unsaturated condition is required by the optimization program. Earlier attempts to start with an initial pressure head at the bottom of 5 cm yielded estimated water retention characteristics, which were not comparable to the ones obtained in Subsection 4.3.2. The respective bottom boundary conditions were: -15 cm, -20 cm, and -30 cm or -40 cm. Eight representative core samples, used to determine dry bulk density in Subsection 4.3.1, were used. Samples 1-4 were subject first to the boundary conditions -15 cm, -20 cm and -40 cm. Secondly, the same samples were subject to the boundary conditions -15 cm, -20 cm and -30 cm, denoted by samples 1a-4a. Samples 5-8 were subject to the boundary conditions -15 cm, -20 cm and -30 cm and the final average θ was determined by oven-drying the core sample. This θ was assigned to the centre of the core sample where the final *h* was -32.5 cm, and this $\theta(h)$ was input for the program SFIT (samples 5, 7, 8; sample 6 was not oven-dried), or not (samples 5a-8a). For samples 4a and 6 no data from the tensiometer were available.

The estimates plus standard errors of the van Genuchten-Mualem model parameters as obtained with the SFIT program are given in Table 4-3. Ranges to which the parameters were restricted and the initial estimates of the parameters are given in Table 4-4. The ranges are mostly arbitrarily chosen, except the minimum value for *n* which must be larger than 1 (see below Eq. [4-1]), but is advised to be 1.1 by Kool and Parker (1987a); the maxima of the ranges for K_s and θ_s are somewhat larger than the measured K_s and ϕ_p of Subsection 4.3.1. Optimization was carried out three times, with the second and third time based on randomly chosen initial estimates by SFIT (all within the given ranges). The best results, i.e. those with the highest r^2 value, are presented in Table 4-3, except

Table 4-3 Parameter estimates (SFIT, Kool and Parker, 1987a) of the hydraulic properties θ_r(-), θ_s (-), n (-), α_d (cm^{-1}), K_s (cm d^{-1}), and λ (-) of the coarse sand substrate obtained from the multi-step outflow method for eight core samples and their averages (avg); below the estimates of each sample the standard errors are given between parentheses, and for the averages this is the standard deviation (std). In total 77 to 80 measured outflows and 77 to 80 measured h's were used for each sample. For samples 1-4 the applied h's at the bottom were -15, -20 and -40 cm, and -15, -20 and -30 cm (denoted by 1a-4a); for samples 5-8 these were -15, -20 and -30 cm; for samples 5-8 the final θ was measured and used as input in the SFIT model, i.e. this final θ was assigned to the centre of the sample, while for samples 5a-8a this information was not used. Samples 1, 4 and 7 are from the top (0-5 cm) layer, samples 2, 3, 5, 6 and 8 are from the bottom (5-15 cm) layer. The number of digits is as given by the program SFIT.

Sample	θ_r	θ_s	n	α_d	K_s	λ	r^2
1	0.001	0.27998	4.50186	0.06524	814.142	0.71963	0.9994
	(0.0003)	(0.0148)	(0.2727)	(0.0021)	(287.07)	(0.1746)	
1a	0.00559	0.28836	4.99099	0.06107	245.043	-0.08052	0.9984
	(0.0142)	(0.0283)	(0.5321)	(0.0028)	(116.73)	(0.1586)	
2	0.01772	0.28062	4.62611	0.0583	696.811	0.66902	0.9995
	(0.0060)	(0.0087)	(0.1944)	(0.0008)	(93.96)	(0.0772)	
2a	0.00973	0.26205	4.14418	0.05862	605.245	0.58953	0.9996
	(0.0028)	(0.0191)	(0.3551)	(0.0023)	(115.55)	(0.1364)	
3	0.00111	0.27832	4.71514	0.05419	562.498	0.58319	0.9977
	(0.0009)	(0.0115)	(0.3062)	(0.0013)	(227.35)	(0.2235)	
3a	0.01107	0.29307	4.29801	0.04501	777.388	0.53478	0.9985
	(0.0032)	(0.0257)	(0.5176)	(0.0008)	(423.59)	(0.1393)	
4	0.0444	0.28078	4.13958	0.06674	1291.334	1.11475	0.999
	(0.0230)	(0.0301)	(0.1918)	(0.0022)	(493.16)	(0.1891)	
4a	0.00027	0.32033	6.46139	0.06503	1300.665	0.31696	0.887
	(0.0019)	(0.2119)	(3.9800)	(0.0237)	(5614.38)	(2.0855)	
5	0.04048	0.28000	6.19107	0.05119	402.157	-0.04942	0.9999
	(0.0013)	(0.0015)	(0.1384)	(0.0002)	(42.98)	(0.0049)	
5a	0.00059	0.24326	6.07241	0.05143	1439.982	0.64787	0.9999
	(0.0000)	(0.0023)	(0.1297)	(0.0002)	(49.79)	(0.0176)	
6	0.01091	0.29858	4.78356	0.05471	980.304	0.92454	0.9989
	(0.0036)	(0.0145)	(0.4430)	(0.0015)	(272.35)	(0.1608)	
7	0.04484	0.30899	6.56756	0.05623	422.733	0.04449	0.9998
	(0.0009)	(0.0023)	(0.1406)	(0.0003)	(34.39)	(0.0037)	
7a	0.00012	0.27127	6.23987	0.0568	1166.410	0.45979	0.9998
	(0.0000)	(0.0036)	(0.1705)	(0.003)	(45.19)	(0.0336)	
8	0.03941	0.27201	6.66351	0.04946	1421.406	0.87204	0.9996
	(0.0012)	(0.0017)	(0.1439)	(0.0002)	(59.83)	(0.0496)	
8a	0.01638	0.26091	5.70976	0.04977	964.762	0.54051	0.9993
	(0.0014)	(0.0064)	(0.3038)	(0.0003)	(106.11)	(0.0687)	
avg	0.01624	0.28124	5.34033	0.05625	872.725	0.52581	
std	0.0167	0.0186	0.9207	0.0062	375.65	0.3351	

Table 4-4 Minimum and maximum allowable values and initial estimates for the van Genuchten-Mualem model parameters θ_r (-), θ_s (-), n (-), α_d (cm^{-1}), K_s (cm d^{-1}) and λ (-) used in the parameter optimization program SFIT.

	θ_r	θ_s	n	α_d	K_s	λ
Minimum	0.0	0.25	0.0	1.1	0.0	-5.0
Maximum	0.1	0.37	0.1	10	1440.0	5.0
Initial	0.01	0.30	0.05	4.5	1200.0	0.0

for samples 1a, 3, 3a, 4, 4a, and 8a for which the second highest r^2 value was used; some of the parameters at the case with the highest r^2 value were at or very near the boundaries of the allowable ranges given in Table 4-4, and for sample 4a the case with the highest r^2 value did not converge normally.

In all cases the resistance of the porous plate was estimated by SFIT, and this result was close to the initially measured resistance. The estimated resistance instead of the measured resistance was used, since then the actual resistance at the bottom boundary of the sample, i.e. resistance of porous plate plus contact resistance between substrate and porous plate, is obtained. The initial h at the tensiometer position was set equal to the equilibrium starting condition, and the changes of h in time were as measured.

Large differences between the three sets of estimated parameters per sample were obtained. In most cases two of the optimizations resulted in high r^2 values, but with different parameter sets. However, graphically the differences between the two water retention characteristics are negligible. One of the three optimizations mostly resulted in low values of r^2, in three cases even negative (*sic* !) values were obtained. It can be concluded that it is difficult to obtain unique estimates. In all cases the outflow was predicted very well with the obtained parameters, and time course of h was also well predicted (Figure 4-7).

All obtained *main drying water retention characteristics* are presented in Figure 4-8A. The differences between the curves are large, and even the two curves determined on the same sample sometimes differ markedly. Differences between samples from the top 0-5 cm and samples from the bottom 5-15 cm of the sand bed are not observed. It is recalled here that the initial status of the samples was -10 cm at the bottom of the samples and thus -15 cm at the top. Thus there was no information available near saturation. At the end of the experiment the bottom conditions were -40 cm (samples 1-4) or -30 cm (all other samples). The optimized van Genuchten-Mualem parameters are based only on data in the range -10 cm to -35 cm or -45 cm. The part of the curves outside this range must be regarded as an extrapolation.

Normalized cumulative outflow (cm^3 cm^{-2})

Pressure head h (cm)

Time t (h)
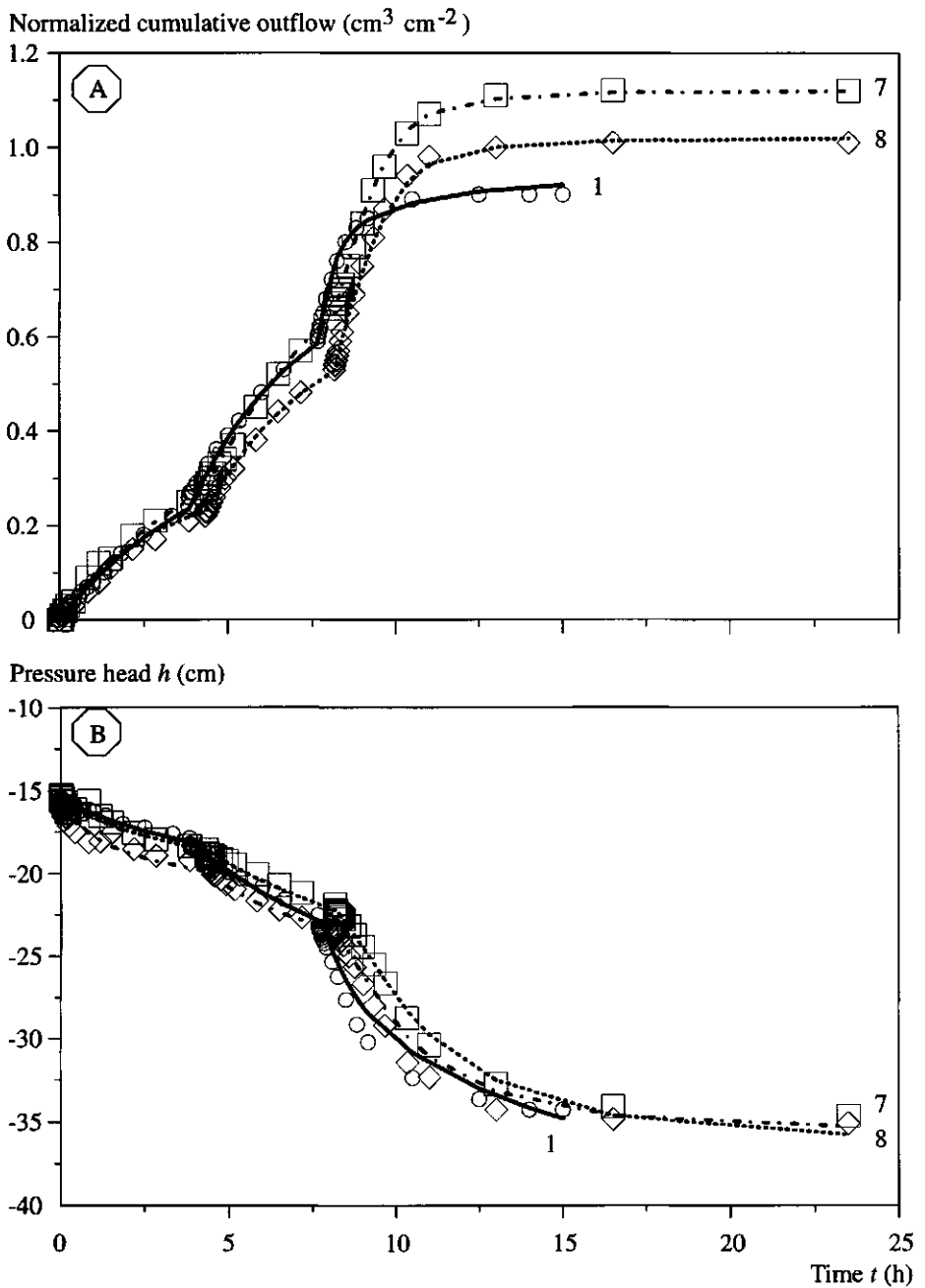
Figure 4-7 Examples of predicted (lines) and measured (symbols) normalized outflow and pressure heads for the coarse sand obtained with the multi-step outflow method and SFIT (Kool and Parker, 1987a) optimization program for samples 1, 7 and 8.

Absolute pressure head $|h|$ (cm)
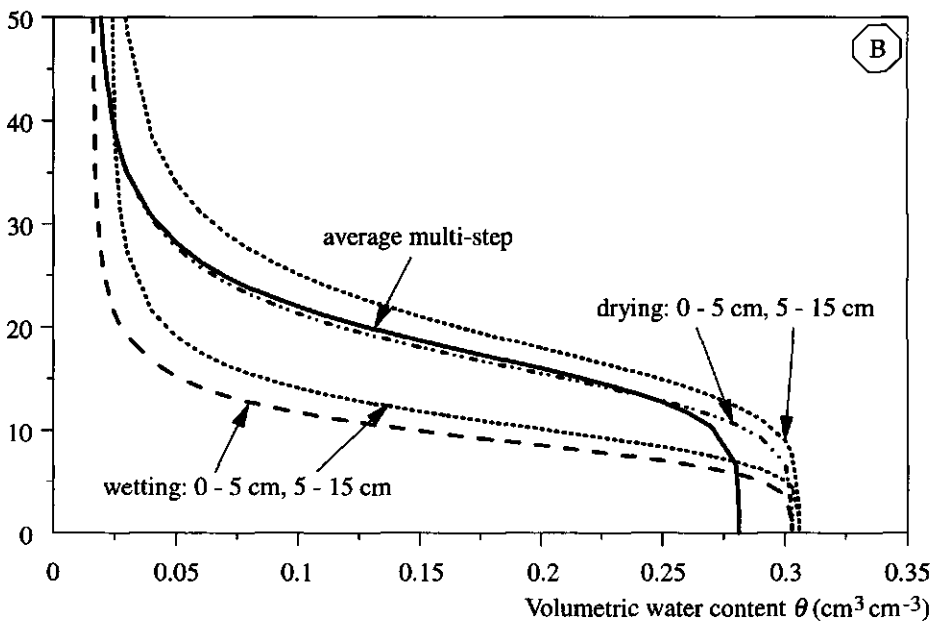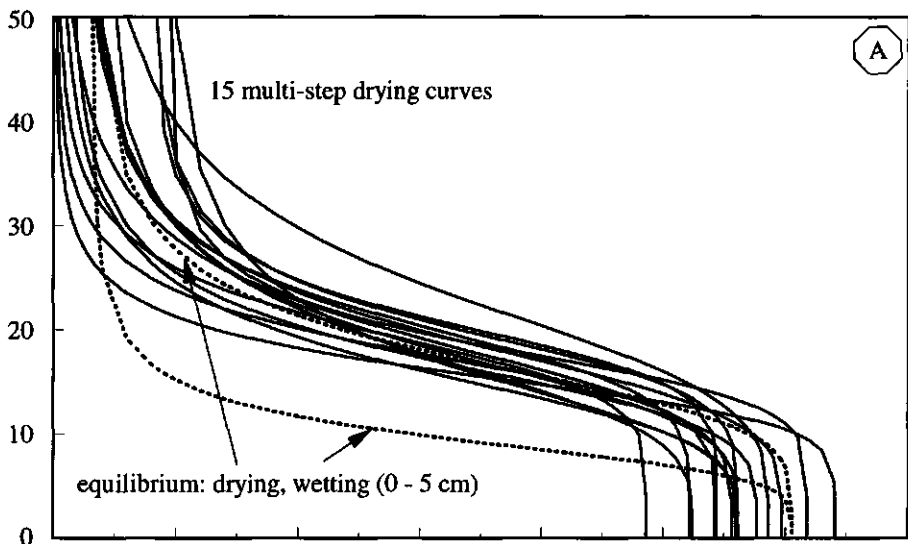
Figure 4-8 (A) The fifteen multi-step main drying water retention characteristics according to the parameters given in Table 4-3, and (B) the main drying water retention characteristic based on the averaged parameters of the multi-step outflow samples compared with the main drying and main wetting curves as obtained with the equilibrium method of Subsection 4.3.2.

For the equilibrium method it was observed that averaging the parameters of individual fitted water retention curves yielded the same parameters as when all data were used in the fitting procedure (Subsection 4.3.2). Therefore, instead of determining the parameters for the 15 multi-step outflow cases (approximately 2400 data points), the parameters are computed as the averages of the 15 individual cases (Table 4-3). Except near saturation, the main drying curve obtained from these averaged parameters agrees closely with the main drying curves obtained during the first cycle of the equilibrium method in Subsection 4.3.2 (Figure 4-8B). The reason why there may be a difference near saturation follows from what is said above: there was no information of the outflow behaviour of the samples for $h > -10$ cm. Following the reasoning of Subsection 4.3.2, the average parameters can be scaled, so that $\theta_s = \phi_p - 0.04$, and the remainder of the parameters remain unchanged.

The *hydraulic conductivity characteristics* of the fifteen samples are presented in Figure 4-9A, and the average $K(\theta)$ characteristic is presented in Figure 4-9B. They are compared with the first cycle $K(\theta)$ characteristics obtained with the van Genuchten-Mualem parameters from the equilibrium method plus the measured K_s of Subsection 4.3.1, i.e. K_s = 1256 cm d^{-1}, and with an assumed (see below Eq. [4-2]) $\lambda = 0.5$. The individual curves differ markedly from each other. However, the average $K(\theta)$ curve obtained with the multi-step outflow method is in close agreement with the one obtained from the equilibrium method, except that K_s differs. The multi-step outflow method yielded K_s in the range of 245 cm d^{-1} to 1440 cm d^{-1}, with an average value of 873 cm d^{-1}. This average value is 0.70 times the measured value of 1256 cm d^{-1} (Subsection 4.3.1). The lower obtained K_s may be due to the lower estimate for θ_s, which, as said above, may be caused by the fact that no outflow information for $h > -10$ cm was available.

It is concluded that the multi-step outflow method may not be the most accurate method to obtain the hydraulic properties for coarse substrates, unless one is satisfied by averaging the results of a large number of samples. A better approach could be to determine the water retention characteristic with an equilibrium method (which should not take too much time, since equilibrium is expected to occur fast for coarse substrates), combined with a steady state flux-controlled method, e.g. the drip infiltrometer method used by Stolte *et al.* (1994), to obtain the hydraulic conductivity characteristic. Moreover, care must be taken when using the results for conditions outside the range of the experimental conditions. For example, it was observed in this study that near saturation the outflow results deviated from the equilibrium results.

Hydraulic conductivity K (cm d^{-1})
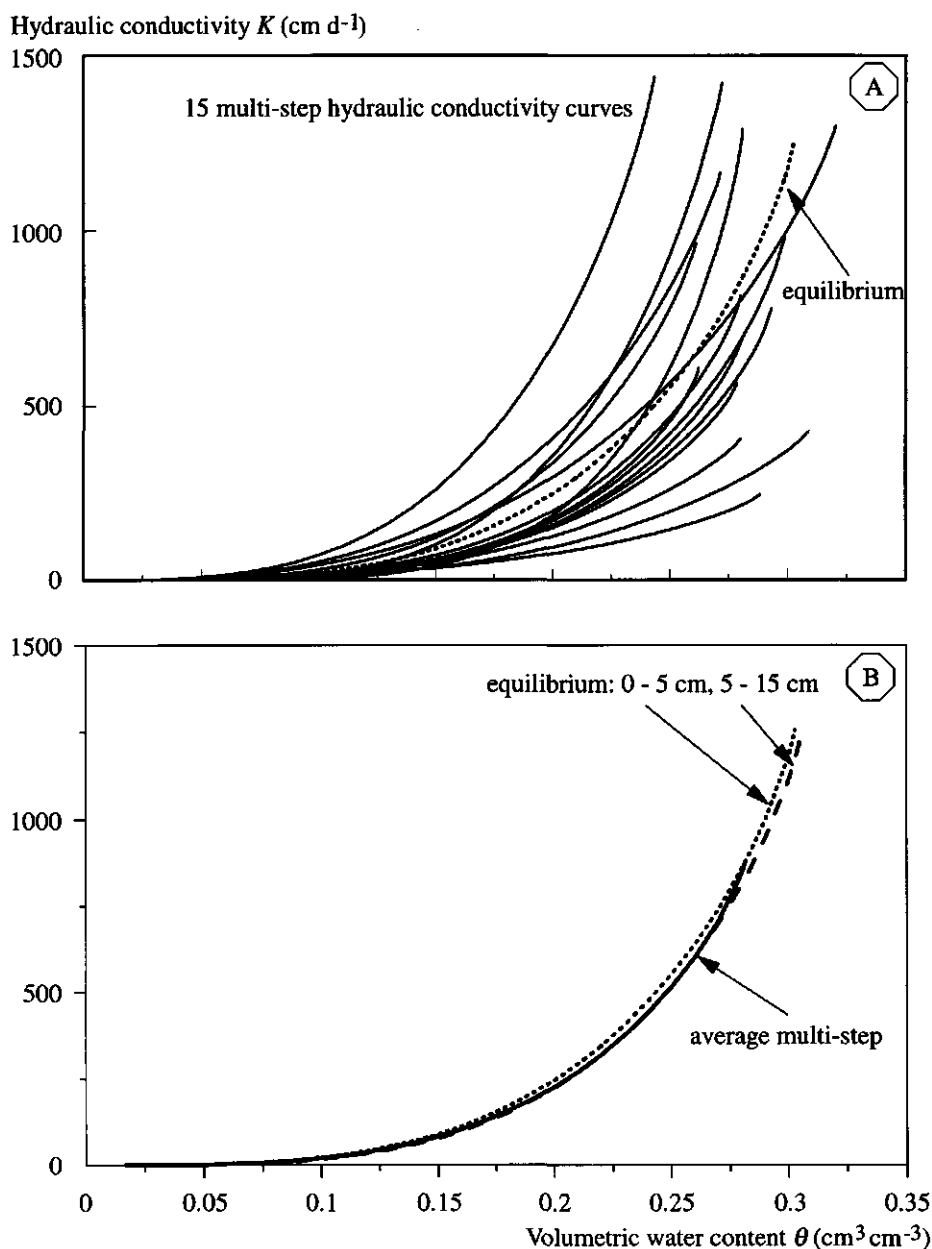
Figure 4-9 (A) The fifteen multi-step hydraulic conductivity characteristics according to parameters given in Table 4-3, and (B) the hydraulic conductivity characteristic based on the averaged parameters of the multi-step outflow samples compared with that obtained with the parameters of the equilibrium method (Subsection 4.3.2) and measured hydraulic conductivity at saturation and assumed value for $\lambda = 0.5$.

4.4 The final set of hydraulic properties

In Subsections 4.3.2 and 4.3.3 two methods were used to determine the hydraulic properties of the coarse sand substrate. The results of the two methods were not always equal to each other, and either method yielded only part of the total set of hydraulic parameters. So, the results of the two methods must be combined. On average, the main drying curves obtained during the first drying procedure of the equilibrium method, and the average drying curve obtained from the transient multi-step outflow method are similar (Figure 4-8B; Tables 4-1 and 4-3). In Subsection 4.3.2 it was also discussed that the methods used here, with (de)watering from below, do not reflect what is actually happening in the coarse substrate. It was proposed to scale the obtained $\theta(h)$ curves so that $\theta_s = \phi_p$-0.04. This was also done for the multi-step results, and the scaled multi-step $\theta(h)$ curve is similar to the ones obtained with the equilibrium method (Figure 4-8B), and typically with the one for the top layer (0-5 cm). I will use the $\theta(h)$ curves from the equilibrium method in the remainder of this thesis. The scaling procedure has an effect on the $K(\theta)$ characteristic. It is assumed that K_r given by Eq. [4-5] is the same for the non-scaled and the scaled cases. This is true when λ is unaffected by the scaling. If λ is strongly correlated to the adapted parameters θ_s or K_s this is most likely not the case. The program SFIT gives estimates of the correlation coefficients between the parameters. On average for the 15 cases in Table 4-2, the correlation coefficient between λ and θ_s was 0.211 (±0.442) and that between λ and K_s was 0.134 (±0.692). Since these are small I will neglect these correlations, and thus assume λ remains unaffected by the scaling procedure. As K_s I use the measured value of Subsection 4.3.1: $K_s = 1256$ cm d^{-1}. The resulting $K(\theta)$ relationship is presented in Figure (4-10). *The final set of scaled parameters are given in Table 4-5.* As mentioned at the end of Subsection 4.3.2, I will use two methods for representing the wetting curve: the 'α_d-α_w-method', with α_w given in Table 4-5, and the 'α_d-data interpolation method' using the experimental wetting data.

Table 4-5 Final set of scaled parameters of the hydraulic properties θ_r (-), θ_s (-), n (-), α_d (cm^{-1}), α_w (cm^{-1}) K_s (cm d^{-1}), and λ (-) for two depth intervals of the coarse sand substrate obtained from the equilibrium and multi-step outflow methods.

Depth	θ_r	θ_s	n	α_d	α_w	K_s	λ
0-5 cm	0.01573	0.326	4.98171	0.06069	0.11745	1256	0.52581
5-15 cm	0.02311	0.311	4.90919	0.05312	0.09466	1256	0.52581

Absolute pressure head $|h|$ (cm)

Hydraulic conductivity K (cm d $^{-1}$)

Volumetric water content θ (cm^3 cm^{-3})
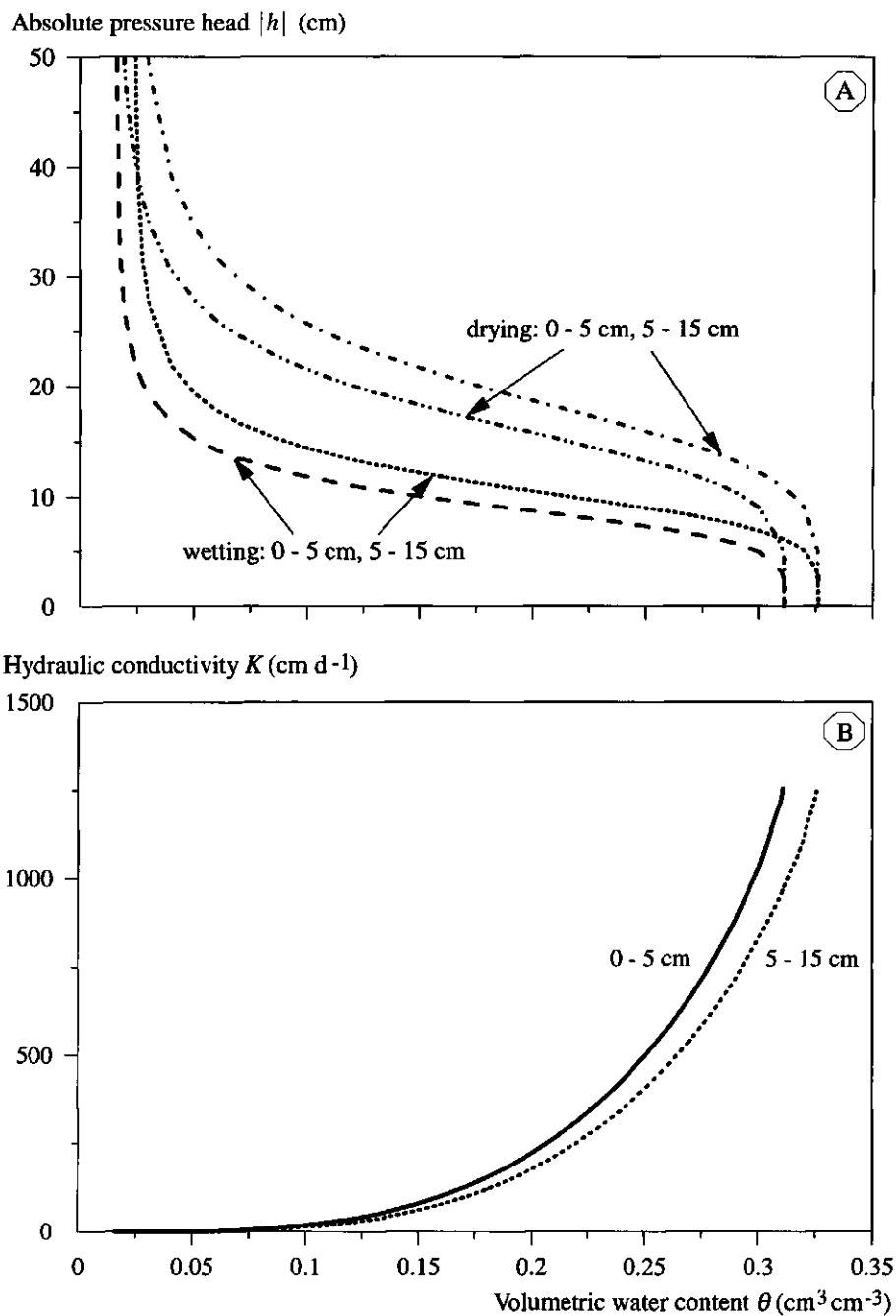
Figure 4-10   Final (A) drying and wetting $\theta(h)$ curves and (B) $K(\theta)$ curves for the two depth intervals of the coarse sand substrate.

4.5 Conclusions

In this chapter I have presented models for describing hysteretic water retention and hydraulic conductivity data, and a model for describing scanning curves. I have presented results of the physical characterization of the coarse sand substrate that is used in this thesis: particle weight fraction distribution, dry bulk density, porosity, hydraulic conductivity at saturation, and water retention and hydraulic conductivity characteristics. The following conclusions are drawn.

- Determination of the water retention characteristic $\theta(h)$ in a standard laboratory set-up, where (de)watering occurs at the bottom of the sample, results in drier conditions compared to conditions obtained in horticultural practice where watering occurs at the top and dewatering occurs everywhere in the substrate. This feature can be explained by hysteresis. For subsequent cycles of drying and wetting in the laboratory set-up, $\theta(h)$ becomes even more drier. The resulting estimate of θ_s at saturation thus becomes smaller than the porosity, and in this thesis also smaller than measured θ. It is possible to upscale the laboratory obtained $\theta(h)$ curves to expected values of θ_s. Assuming that the degree of saturation remains unchanged, the new $\theta(h)$ curve is described by the same set of parameters, except for θ_s.
- The van Genuchten (1980) model for water retention curves describes well the main drying curve for the coarse sand substrate.
- Contrary to a proposal by Kool and Parker (1987), the wetting data obtained from the first cycle of drying and wetting could not be described by the same set of parameters, exclusive the α parameter, obtained for the main drying curve. If, additionally, for the wetting curve another parameter is also assumed to be different from that for the drying curve, it is shown that the drying and wetting curves will always cross, which is physically impossible and thus cannot be used.
- Small differences in dry bulk density of the sand resulted in significantly different $\theta(h)$ relationships.
- Measurements of hydraulic conductivity at saturation on non-sterile samples resulted in a decreasing K_s with time, which was not observed when ethanol was used as percolating fluid. Ethanol prevents microbial activity. Thus, microbial activity influences K_s, and makes it difficult to determine an operational value for K_s. The effect of different values for K_s has not been taken into account further in this thesis.
- Using samples of equal dry bulk density, the transient multi-step outflow method resulted in large variability in obtained physical characteristics. The multi-step outflow method may not be the most accurate method to obtain the hydraulic properties for coarse substrates, unless one is satisfied by averaging the results of a large number of samples. A better approach could be
  1) to determine the water retention characteristic with an equilibrium method, which is not too time consuming, since equilibrium is expected to be reached fast for coarse substrates, and
  2) to determine the hydraulic conductivity characteristic with a steady state flux-

controlled method, e.g. the drip infiltrometer method described by Stolte *et al.* (1994).

■ Care must be taken when using the results obtained with the multi-step outflow method for conditions outside the experimental range of conditions. For example, it was observed in this study that near saturation the outflow results deviated from the equilibrium results.

■ The average $\theta(h)$ relationship obtained with the multi-step outflow method was in agreement with the main drying $\theta(h)$ relationship obtained with the hanging water column method.

Chapter 5

Description of sand bed system and experiments

In this first chapter the experimental layout of the greenhouse compartment (Section 5.1), including the measurement equipment (Section 5.2), will be presented. Next in Section 5.3 the water supply control system is described. Finally, the experiments carried out are discussed (Section 5.4).

5.1 Experimental layout of greenhouse compartment

5.1.1 Greenhouse compartment with sand beds

At the Glasshouse Crops Research Station (GCRS) at Naaldwijk, The Netherlands, a greenhouse compartment of 250 m^2 was used as the experimental site. In this compartment four sand beds were constructed (Figure 5-1), two of which have a surface area of 42.5 m^2 and the other two of 50.3 m^2. Due to the presence of 30 cm wide concrete tiles, the effective growth areas are 40.7 and 48.1 m^2, respectively. The greenhouse floor is made of concrete and is sloping approximately 1% towards the supply and drainage tanks. The construction of the sand bed growth system is schematically presented in Figure 5-2. The borders of the sand beds were made of concrete walls of 25 cm height and 12 cm width. Polystyrene foam plates of 78 cm width and 4 cm height were placed over the total length of the bed, 4 cm apart. Above the foam plates and in the gaps between them, an impermeable plastic sheet, 0.5 mm thickness, was placed. In the gaps between the plates perforated drain tubes (Subsection 5.1.3) were situated, which ended in a common non-perforated PVC collecting drain at the end of the bed. The drains have the same slope as the concrete floor. In order to prevent root growth and substrate washing into the drain, an anti-rooting mat was placed over the drains plus plastic sheet. The remainder of the bed was filled with a coarse sand, for which the physical characteristics were given in Chapter 4, to a thickness of approximately 15 cm. Each of the four systems can be operated individually, since each has its own supply and drainage system, as described below.

5.1.2 Nutrient solution supply system

The nutrient solution supply system or fertigation system consisted of a supply tank and a choice between an overhead sprinkling system or a surface drip system. The supply tank had a volume of 1.3 m^3. A pump[1#] delivered the nutrient solution from the bottom of the

---

[#] The superscripts 1 through 19 appearing in this chapter refer to specifications of the equipment as given in Appendix 3.
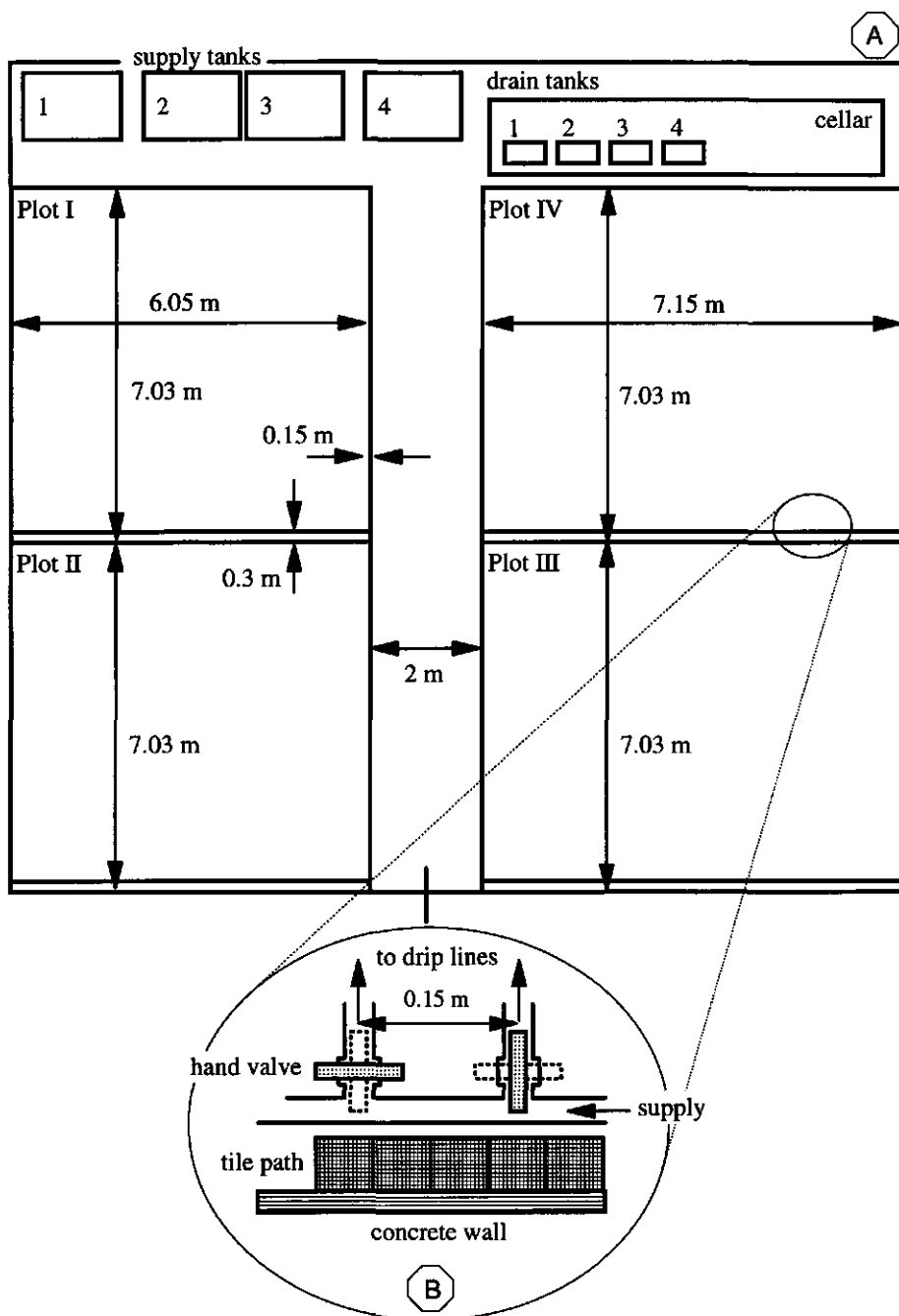
Figure 5-1 (A) Layout of greenhouse compartment with four sand bed growth systems, four supply tanks, and four drainage tanks, and (B) a detail of the drip line connection.

crop

15 cm

substrate

ø 4 cm

25 cm

4 cm

~ 80 cm

1
2
3
4
5
6
7
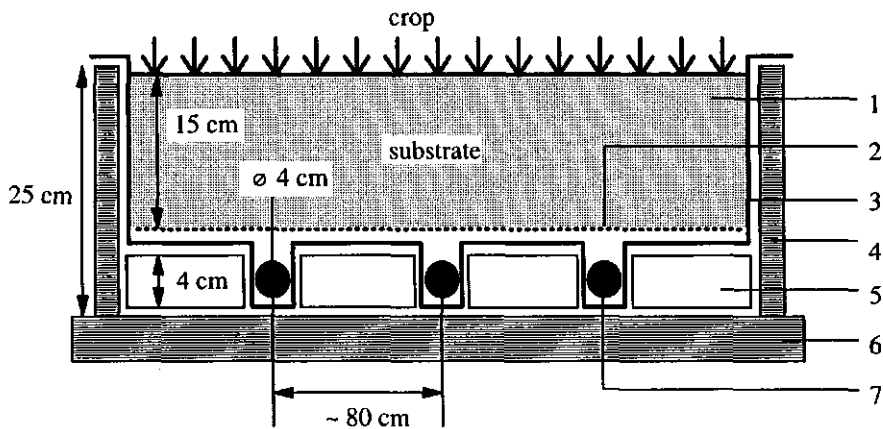
1: coarse sand   5: extended polystyrene foam

2: anti rooting mat   6: concrete floor

3: impermeable plastic sheet   7: plastic corrugated drain

4: concrete wall

Figure 5-2 Schematic cross sectional view of the sand bed growth system, indicating some dimensions (not at scale).

supply tank to the sprinkling or drip system. By means of a hand valve in the pump's return flow pipe line, the supply pressure could be adapted to the desired operating pressure of the chosen way of supply. The overhead sprinkling system consisted of three pipe lines with evenly spaced sprinklers[2]. The two small beds had 14 sprinklers, the two large beds 17 sprinklers. The overhead sprinkling system was used during the first days of growth, in order to assure good supply of nutrient solution to the small root system. As plants grew older the surface fertigation system was used. The supply pipeline for surface drip fertigation had evenly spaced junctions at 15 cm intervals where drip lines[3] could be installed (Figure 5-1B). The junctions could be opened or closed by hand valves. The dripper distance was 30 cm. The water level in the supply tank was measured regularly with an in-situ calibrated pressure transducer[4]. In this way the total amount of nutrient solution supplied, and the amount of drain water that returned from the drainage tanks could be followed in time. The voltage output of the pressure transducer was connected with an analog input-card in a personal computer.

5.1.3 Drainage system with control system

Plastic corrugated, perforated drain tubes[5] were used. The drains were open at the upper end and at the lower end they ended in a closed PVC collecting drain. The collecting drain transported the drain water to a drainage tank. The drainage tank had a volume of 140 dm^3 and was located below the bottom of the substrate bed in a cellar. The water level in the drainage tank was measured and controlled by a drain control system.

The drain control system consisted of an immersed pump, high and low level sensors, an immersed pressure transducer[4], a temporary drain outflow collector, and a control box connected to a personal computer (Figure 5-3). The pump[6] was activated whenever the water level reached one of the two high level sensors. Pumping was stopped as soon as the water level dropped below one of the two low level sensors. The low level was necessary in order to prevent the pump to fall dry. The difference between high and low level was set as large as needed for accurate measurements of differences in water level, but was kept as small as possible in order to keep the buffer of drain water in the tank small. On average the water level difference corresponded to 20 dm^3. The water level could be measured at any desired time with the in-situ calibrated pressure transducer. The level sensors and pressure transducer were positioned in a perforated plastic tube to dampen the oscillations of the water level. In most cases the high level will be reached during drainage. In order to prevent the drain outflow that occurs during pumping to be routed to the supply tank as well, a temporary drain collector was installed, with a volume of 8 dm^3. As soon as the high level is reached, the temporary drain collector is closed with
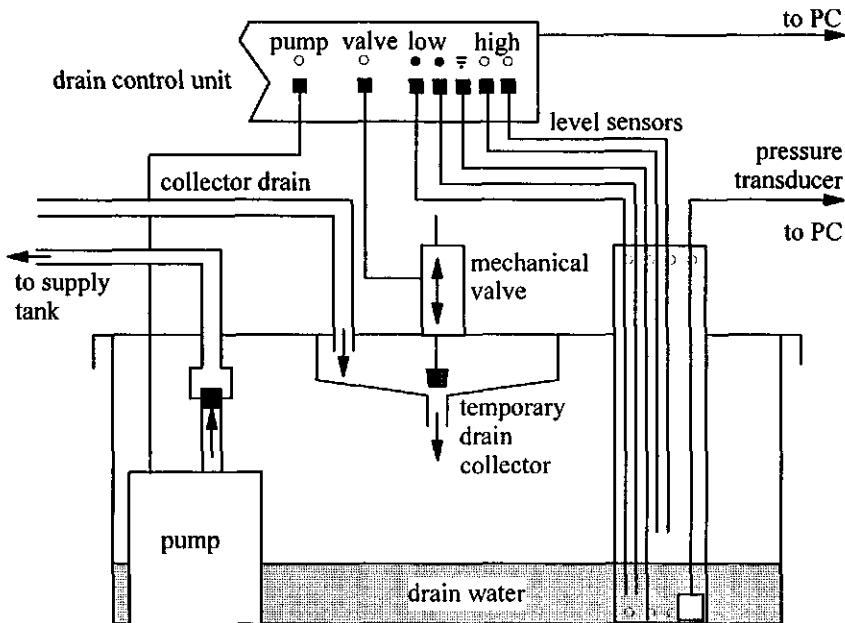
Figure 5-3 Schematic view of the drainage tank control system; PC: personal computer.

a mechanical valve. After the pump stopped the mechanical valve was opened. The control box could handle the four drainage tank systems, and was controlled by a computer program on a personal computer. The voltage output of the pressure transducers was transferred to an analog input-card on the personal computer. The software program continuously scanned the high and low level sensors, and measured the water level at regular times. Just before the pump started and after it stopped water levels were measured as well.

5.2 Measurement equipment

Besides the water level registrations in the supply and drainage tanks to measure total water use, measurements were carried out in the root zone and in the greenhouse atmosphere as well. Measurements in the root zone consisted of the volumetric water content and electrical conductivity of the bulk substrate using time domain reflectometry, soil water pressure head using tensiometry and soil temperature using sensors equipped with thermistors. To monitor the signals a data acquisition system was used. All the equipment will be discussed briefly in the forthcoming sections. A record of the greenhouse atmospheric conditions was available from the local (GCRS) climate computer.

5.2.1 Data acquisition system

A Workhorse Data Acquisition System[7] (Keithley, 1991) coupled via a RS232 serial interface cable with a personal computer[8] was used to monitor the signals of the sensors (Figure 5-4). One 16-channel analog input board plus five 16-channel expansion multiplexer analog input boards gave 96 analog input channels. Measurements were carried out with 12 bits resolution at a preselected voltage input range, depending on the expected magnitude of the analog signal. There was one 16 channel digital isolated output board present, which was used for channel selection for the time domain reflectometry switch box.
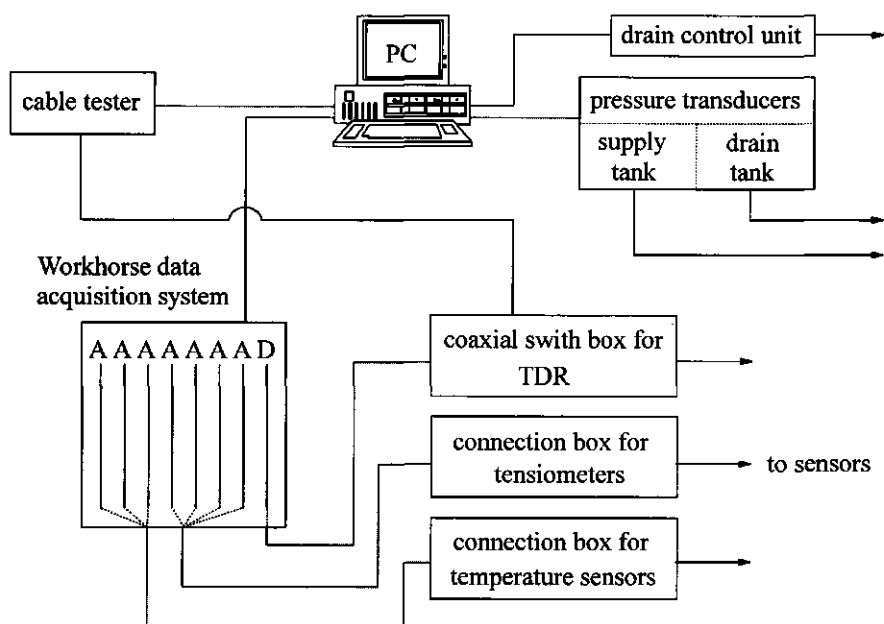
Figure 5-4 Schematic representation of the data acquisition system; PC: personal computer.

5.2.2 Time Domain Reflectometry (TDR)

Time Domain Reflectometry (TDR) is a rather new and sensitive technique to measure the volumetric water content of a porous medium (Topp *et al.*, 1980; Whalley 1993). It offers good possibilities for automatic measurement systems (e.g. Baker and Allmaras, 1990; Heimovaara and Bouten, 1990; Herkelrath *et al.*, 1991; Heimovaara, 1993). For this study an automatic TDR system was constructed (Figure 5-5). It consisted of one cable tester[9] and a switch box consisting of seven six-way coaxial switches[10]. The seven switches were connected in a tree structure (cf. Heimovaara and Bouten, 1990) hence up to thirty-six TDR sensors could be connected using coaxial SMA connectors[11]. The TDR sensors were of the three-rod type, since these have been shown to be practically the best with a small measurement volume around the probe (Zegelin *et al.*, 1989). Stainless steel rods were used with rod diameter of 2 mm, rod spacing of 12 mm, and rod length outside the probe head of 150 mm. The design of the probe dimensions was based on minimal disturbance of the substrate during installation, probe impedance properties, measurement volume, and possibilities to measure the electrical conductivity of the porous medium (Appendix 4). The probe head was made of epoxy. The coaxial cable was of type RG 400 ST[12], with an extra black polyurethane outer sleeve to prevent water to enter the cable. This high quality cable with low damping properties was chosen since long cables were used. The
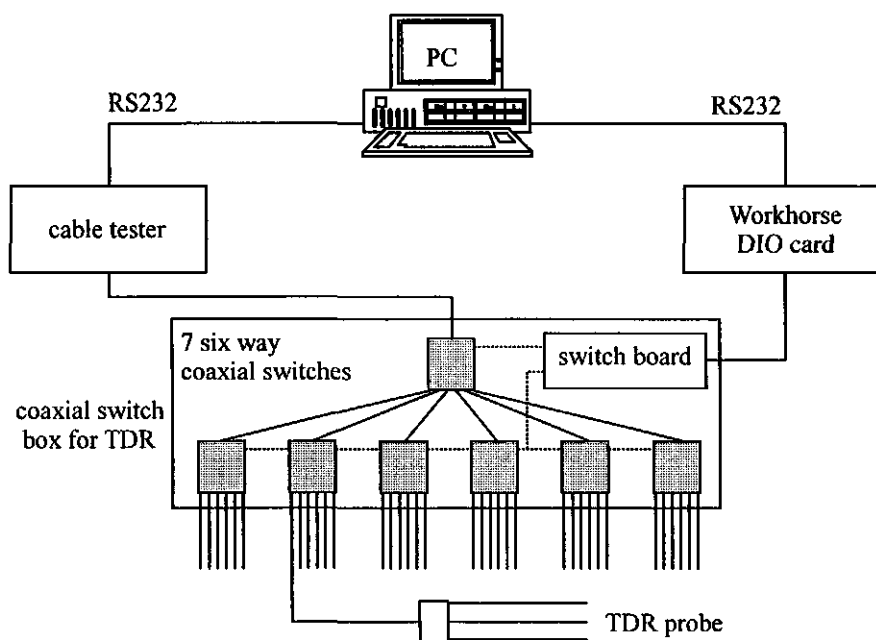
Figure 5-5 Schematic representation of the TDR measurement system with 36 TDR probes; PC: personal computer.

outside diameter and length of the cable were 5 mm and 14 m, respectively. The cable length between the coaxial switches to the mother-coaxial switch was 1 m, and the cable length between mother-coaxial switch to the cable tester 4 m. Thus the total length of the coaxial cable between a TDR probe and cable tester was 19 m. The cable tester was connected to a RS232 interface of a personal computer. Measurements of the TDR sensors were controlled by a Turbo Pascal software program based on programs written by Heimovaara and Bouten (1990) and Heimovaara (1993). Each TDR sensor was calibrated for exact sensor length and cable length by taking measurements in air and water. This information is needed for proper use of the registration and analysis software programs. The TDR sensors were installed horizontally with the rods parallel to the drains at three depths, 2.5, 7.5 and 12.5 cm above bottom of the sand bed, and at positions above a drain or midway between two drains.

A *calibration curve* for the coarse sand was determined in the laboratory, using one of the sensors with cable length of 14 m. The procedure of Dirksen and Dasberg (1993) was used. PVC columns of inner diameter 9.8 cm and length 20 cm were filled with coarse sand at different water contents and an average dry bulk density ρ_d of 1750 kg m^{-3}. The filling procedure was found to be quite reproducible, and the dry bulk density was very

close to the dry bulk densities present in the sand beds. The sensor was pushed in the centre of the column, with the middle rod along the central axis. The columns were placed horizontally to ensure even water content distribution along the sensor. After the TDR readings were taken, the actual water content was determined gravimetrically, w_g (kg kg^{-1}); the volumetric water content θ was computed according to

$$\theta = \frac{\rho_d}{\rho_l} w_g ,$$
[5-1]

where ρ_l is the density of water (= 1000 kg m^{-3}). The measurements were carried out at approximately constant temperature of 20 °C.

Several *functional relationships between volumetric water content θ and apparent dielectric permittivity* K_a (1) have been reported in literature (e.g. Topp *et al.*, 1980; Ledieu *et al.*, 1986; Herkelrath *et al.*, 1991; Dirksen and Dasberg, 1993). In this study the following functional relationship appeared to describe the data well ($r^2 = 0.9928$) (Figure 5-6A)

$$\theta = \alpha_1 + \alpha_2 K_a^{0.5} + \alpha_3 K_a + \alpha_4 K_a^{1.5} ,$$
[5-2]

with the dimensionless parameters $\alpha_1 = -0.62792$, $\alpha_2 = 0.544535$, $\alpha_3 = -0.11528$, and $\alpha_4 = 0.009101$. In many studies the calibration function of Topp *et al.*, (1980) is used. However, in this study this third order polynome failed to describe the observations well (Figure 5-6A). Ledieu *et al.* (1986) and Herkelrath *et al.* (1991) used a linear functional relationship between θ and $K_a^{0.5}$, i.e. Eq. [5-2] with $\alpha_3 = \alpha_4 = 0$. In the present study such relationship was not satisfactory, and the best fit was obtained with $\alpha_1 = -0.10764$ and $\alpha_2 = 0.09677$ with $r^2 = 0.9455$ (Figure 5-6A). The validity of the new calibration function was tested by carrying out an in-situ calibration. TDR measurements were taken in the sand beds prior to taking core samples next to the probes. The volumetric water contents in the core samples were determined and plotted against the TDR measured dielectric permittivity data (Figure 5-6B). At high dielectric permittivity, i.e. in the wet range, the calibration functions differed markedly from the field data. A possible reason might be that when taking the wet soil samples water was pushed out of the sample during removing the core.

The *dielectric permittivity of a medium is temperature dependent*. It is assumed that only the dielectric permittivity of water in the porous medium is temperature dependent (e.g. Heimovaara, 1993). The dielectric permittivity at a certain temperature $K_a(T)$ follows from

$$K_a^{0.5}(T) = K_a^{0.5}(20) f_K(T) ,$$
[5-3]

where $K_a(20)$ is the dielectric permittivity at 20 °C, T is the temperature (°C), and the temperature correction function $f_K(T)$ is given as

Dielectric permittivity K_a (-)
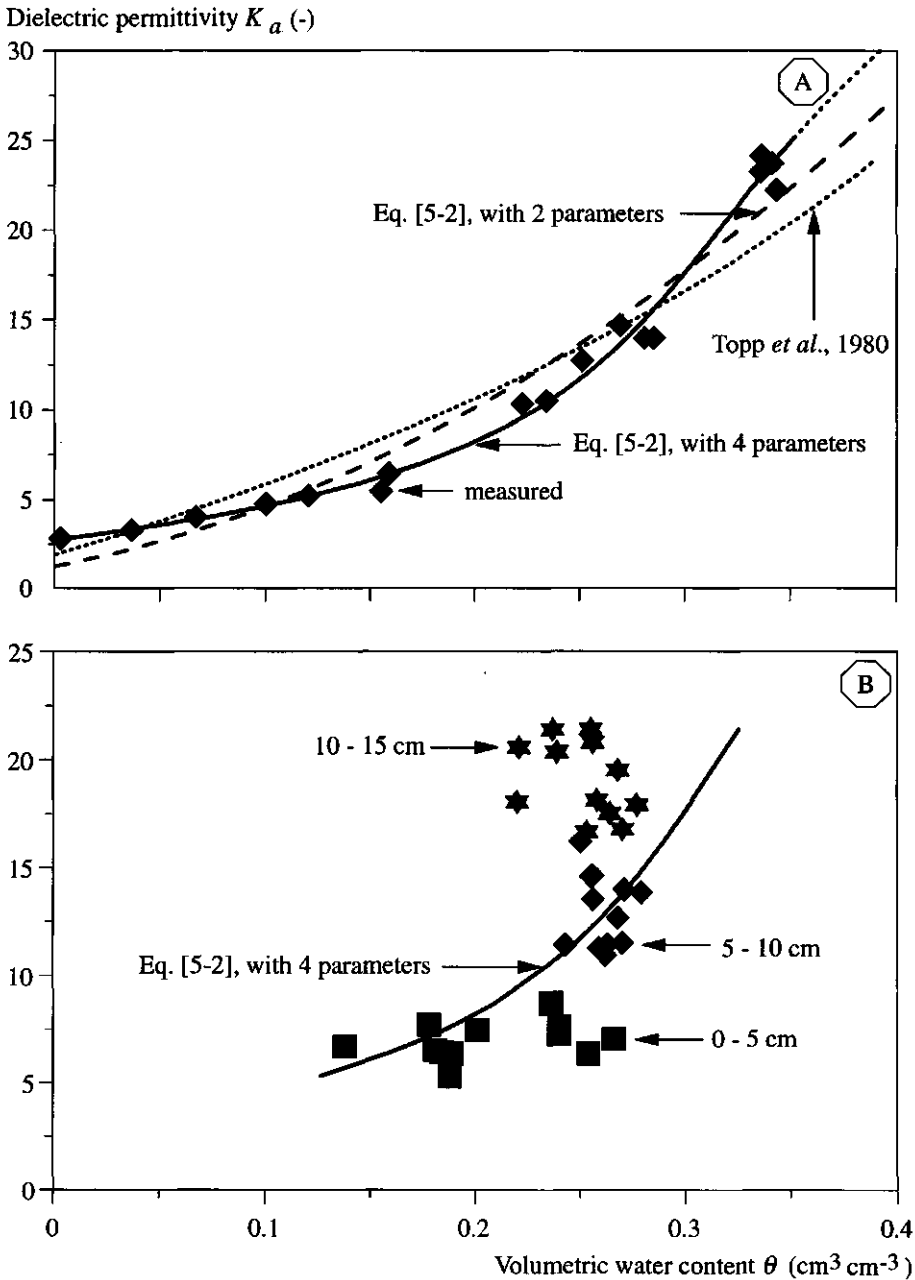
Figure 5-6 (A) Time domain reflectometry calibration curve for the coarse sand substrate described by the calibration function Eq. [5-2] using two of four parameters and by the Topp *et al.* (1980) calibration function, and (B) in-situ calibration of time domain reflectometry: comparison between measured water contents and predictions according to Eq. [5-2] with 4 parameters.

$$f_K(T) = \left[1 - 0.45687 \cdot 10^{-2} \, (T - 20) + 0.10791 \cdot 10^{-4} \, (T - 20)^2 + \right.$$
$$\left. - 0.17809 \cdot 10^{-7} \, (T - 20)^3 \right]^{0.5}. \qquad [5\text{-}4]$$

The temperature correction function is valid for the 0 to 1 GHz frequency range for bulk water (Hasted, 1973) and can be obtained from the dielectric permittivity - temperature table of e.g. Weast (1975; page E-61). Substrate temperatures were measured using thermistors as described in Subsection 5.2.4. The temperature correction function in the range of 0 °C to 50 °C can be very well approximated by the a linear relationship ($r^2 = 0.9997$)

$$f_K(T) = 1 - 2.258 \cdot 10^{-3} \, (T - 20). \qquad [5\text{-}5]$$

A temperature of 0 °C or 50 °C thus causes a correction of approximately -5% or +5%, respectively, on the measured water content. Equation [5-5] was used in this thesis.

Additional to volumetric water content determination it is also possible to determine *bulk soil electrical conductivity* with TDR (e.g. Dalton and van Genuchten, 1986; Zegelin *et al.*, 1989). The TDR system was calibrated in bulk KCl solutions with electrical conductivities, EC (S m^{-1}), ranging from 0.1 S m^{-1} to 2 S m^{-1} at three temperatures, i.e. 10 °C, 20 °C and 30 °C. The actual EC was measured with a calibrated electrode[13]. The TDR wave forms were analysed by obtaining the wave form amplitudes of the incoming signal and the final amplitude (Heimovaara, 1993). The EC according to TDR is given by

$$EC = \frac{K_p}{R_t - R_c}, \qquad [5\text{-}6]$$

where K_p is the TDR 'cell' constant (m^{-1}) of the sensor, R_c is the combined series resistance of the cable tester, connectors and cable (Ω), and R_t is the total resistance of the TDR system and follows from

$$R_t = Z_c \frac{1 + \rho_\infty}{1 - \rho_\infty}, \qquad [5\text{-}7]$$

where Z_c is the characteristic impedance of the cable tester system including the coaxial cable (50 Ω), and ρ_∞ is the reflection coefficient at long times defined as

$$\rho_\infty = \frac{V_\infty - V_A}{V_A}, \qquad [5\text{-}8]$$

where V_a and V_∞ are the wave form amplitudes (V) of the incoming signal and the final amplitude, respectively. Using the EC values measured by the electrode and the R_t values

by TDR, the unknowns K_p and R_c were obtained by linear regression: $K_p = 3.224$ m^{-1} and $R_c = 1.242 \, \Omega$, with regression coefficient $r^2 = 0.996$. The comparison between TDR and electrode is very good (Figure 5-7). The electrical conductivity is commonly expressed at a certain reference temperature, e.g. at 25 °C. The measured EC can be transformed to EC_{25} according to

$$EC_{25} = EC_T (1 + f_T (25 - T)) , \qquad [5\text{-}9]$$

where T is the temperature (°C) and f_T is a temperature coefficient (°C)$^{-1}$ of the medium, which depends on the medium itself and on T. Heimovaara (1993) obtained an average value for soil samples of $f_T = 0.0216$ (°C)$^{-1}$.

TDR yields a bulk EC of the substrate. In literature several models have been proposed to *relate bulk substrate electrical conductivity* at current volumetric water content, $EC_b(\theta)$, *to that of bulk aqueous solution*, EC_w. Here I use the model of Mualem and Friedman (1991) given by

$$EC_w = EC_b(\theta) \frac{\theta_s}{\theta^{\lambda+2}} , \qquad [5\text{-}10]$$

where λ is the same pore size distribution index which is also present in the hydraulic conductivity expression of Mualem (1976) (Section 4.1, Eq. [4-2] or [4-5]). Equation
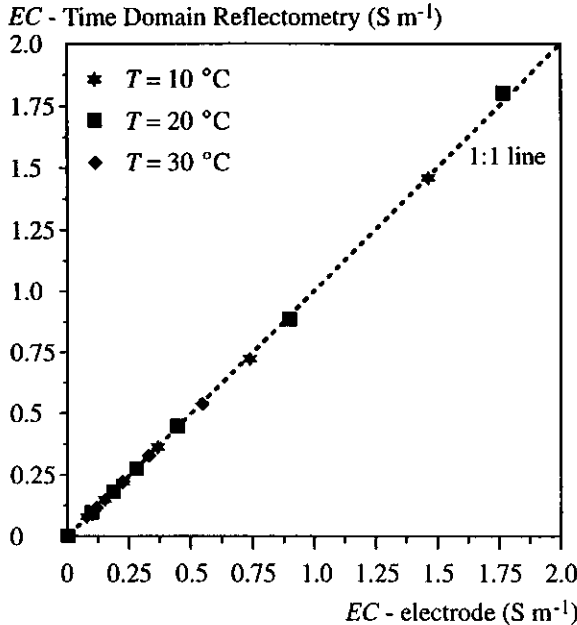
Figure 5-7 Electrical conductivity EC obtained with TDR compared with EC obtained with an electrode at three different temperatures. The 'cell' constant of TDR is $K_p = 3.224$ m^{-1}.

[5-10] holds for coarse, chemically inert substrates with a small surface area, such as the coarse sand used in this thesis.

Mualem (1976) concluded that λ can be considered constant with magnitude 0.5. Several authors (e.g. Leij *et al.*, 1992; Wösten *et al.*, 1994), however, experienced that λ varies from soil to soil. For the Dutch soils ('Staringreeks'), Wösten *et al.* (1994) gave values ranging from -8.823 to 0.912, while Otten (1994) obtained a value of 2.35 for a substrate consisting of 75% peat plus 25% perlite. In all cases λ was obtained from hydraulic conductivity data. The effect of changing λ is demonstrated by a simple example. If λ for a certain soil ('sand-b1' of Wösten *et al.*, 1994) is changed from -0.14 to 0.5, the hydraulic conductivity is underestimated at $\theta = 0.1$, 0.2, 0.3 and 0.4 by 0.373, 0.602, 0.789 and 0.954, respectively. However, the ratio $EC_w/(EC_b\,\theta_s)$ (Figure 5-8) is overestimated by 4.37, 2.80, 2.16 and 1.80, respectively. Thus, changes in λ have a larger impact on the computation of EC_w from obtained EC_b values, than on K.
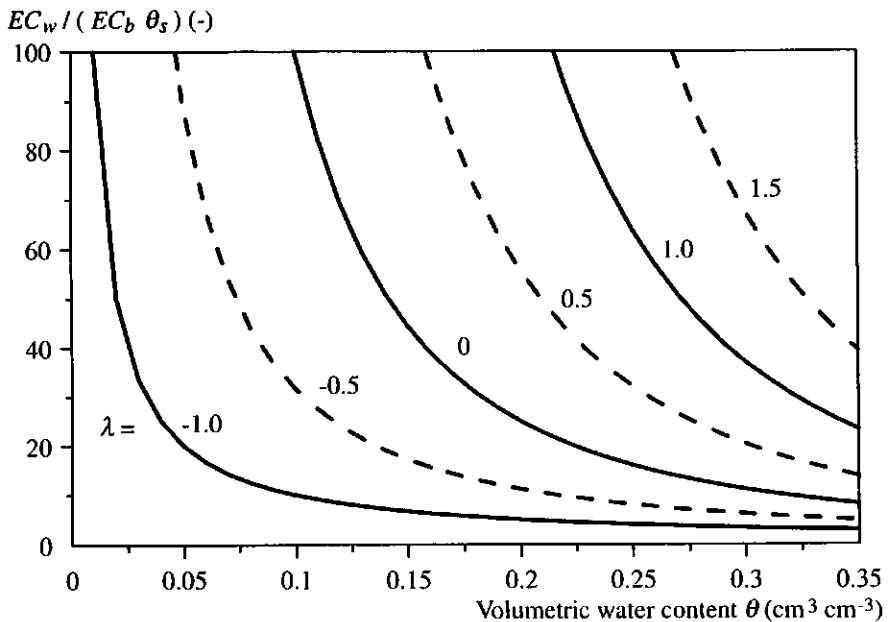
Figure 5-8 The effect of the magnitude of the pore size distribution index λ on the computation of the electrical conductivity of the bulk aqueous solution EC_w based on the bulk electrical conductivity EC_b and volumetric water content at saturation θ_s as a function of the volumetric water content θ according to Eq. [5-10].

5.2.3 Tensiometry

Tensiometry is a well-known technique to determine the pressure head h of a porous medium (e.g. Cassell and Klute, 1986). It offers possibilities for automatic measurements using pressure transducers (e.g. Nyhan and Drennon, 1990; van den Elsen and Bakker, 1992). In this study thirty-six water-filled tensiometers with temperature compensated pressure transducers[14] (Micro Switch, 1986) were used. The tensiometer system was based on an early prototype of van den Elsen and Bakker (1992). High flow porous ceramic round top tensiometer cups[15] (Eijkelkamp, 1987) were used. A copper tube connected the cups with the pressure transducer (Figure 5-9): length 7 m, inner diameter 1 mm, outer diameter 2 mm. The copper tube inside the ceramic cup ended at the round top of the cup. A second copper tube, ending at the open end of the ceramic cup, could be used as outlet for flushing purposes, so that air inside the tensiometers could be removed in-situ. The connection between copper tube and transducer was realized via a three-way valve with luer lock ends[16]. This offered possibilities for in-situ calibration of the pressure transducer or flushing of the tensiometer, without having to disconnect the two. The copper tube was surrounded by a plastic sleeve to prevent copper being released to the root zone. The tensiometers were horizontally installed with the cups parallel to the drains at three depths, 2.5, 7.5 and 12.5 cm above the bottom of the sand bed, and at positions above a drain or between two drains. The pressure transducers were located about 40 cm above the concrete greenhouse floor, or approximately 36 cm above the bottom of the sand beds. Thus negative pressures were recorded by the transducers, since
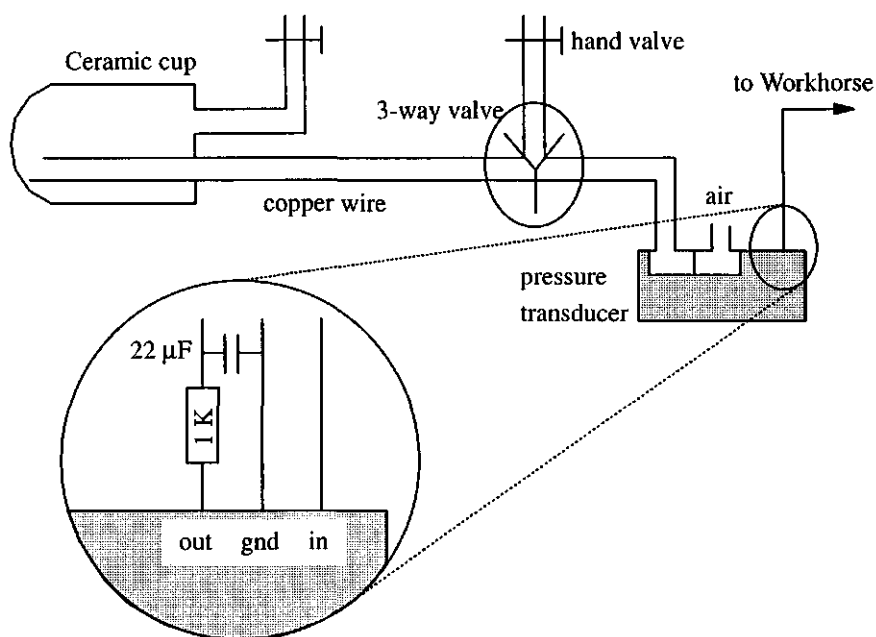
Figure 5-9 Schematic representation of the tensiometer measuring system.

the tensiometer cups were below the pressure transducers, i.e. at 33.5, 28.5 and 23.5 cm, respectively. All pressure transducers were supplied with an excitation of 8 V, and the output signals were connected to the Workhorse.

Calibration of the pressure transducers was carried out using a calibration kit[17]. In total three calibrations were carried out: at the start and at the end of the experimental period, and prior to the main experiment (see Section 5.4). The linear calibration line is given by

$$h = \alpha_1 + \alpha_2 V_v, \qquad\qquad [5\text{-}11]$$

where h is the pressure head (m), V_v is the measured voltage (V), α_1 is the intercept (m) and α_2 is the sensitivity (m V^{-1}). The results differed between the three calibrations, with the results of the first and final calibration being nearly equal (Table 5-1). For all three cases the calibration lines differ from the theoretical line, when the pressure transducers obtained 8 V excitation (Table 5-1). At high matric pressure heads, say between 0 and -50 cm, the first and last calibration lines are between the theoretical lines at excitations 7.75 and 8 V, the intermediate calibration is between 7.5 and 7.75 V. In principle, a precisely adjustable, temperature independent excitation source was used. It is, therefore, unclear why the second calibration results differ so much from the other two and the expected calibration line. The final calibration line was used in this thesis.

Table 5-1 Average results of the calibration lines of all sensors given as α_1 and α_2 occurring in Eq. [5-11], with standard deviations given between brackets. The theoretical calibration lines at different excitation are given in the bottom part of this table.

Calibration	α_1 (10^{-2} m)	α_2 (10^{-2} m V^{-1})
Before	214.77 (1.28)	-218.98 (0.65)
Halfway	215.28 (2.95)	-224.33 (0.66)
After	219.42 (4.69)	-220.41 (1.12)

Excitation V_v (V)	α_1 (10^{-2} m)	α_2 (10^{-2} m V^{-1})
7.25	200	-220.69
7.5	200	-213.33
7.75	200	-206.45
8	200	-200.00
8.25	200	-193.94

5.2.4 Substrate temperature

The temperature of the substrate bed was measured as well. It was used to make corrections on the TDR readings (see Subsection 5.2.2). The temperature was measured using thirty-six sensors with thermistors[18]. The two wires at the end of the sensor cable were connected to an analog input channel of the Workhorse system. At the analog input channel the Workhorse internal voltage supply was used to convert resistance to voltage, using a precision resistance and a capacitance (Figure 5-10). In this way the temperature between 5 °C and 50 °C could be measured on the Workhorse 0-1 V range. The temperature sensors were horizontally installed at three depths, 2.5, 7.5 and 12.5 cm above the bottom of the sand bed, and at positions above a drain or between two drains. *Calibration* of the sensors connected to the Workhorse was carried out using a water bath[19]. The calibration lines per sensor were approximately the same and did not change in time. There was no difference in average actual calibration line and the theoretical calibration line. The theoretical calibration line was obtained from the known resistance-temperature tabular data that belongs to the thermistors. In order to measure a resistance on the analog input board of the Workhorse system, the following electrical adaption on the input board was carried out. The resistance was converted to a voltage by applying the internal Workhorse excitation S (14.76 V) over a precision resistance R_v (10^5 Ω). The measured voltage V_v (V) and the thermistor resistance R_{th} (Ω) are related through the second law of Kirchhoff:
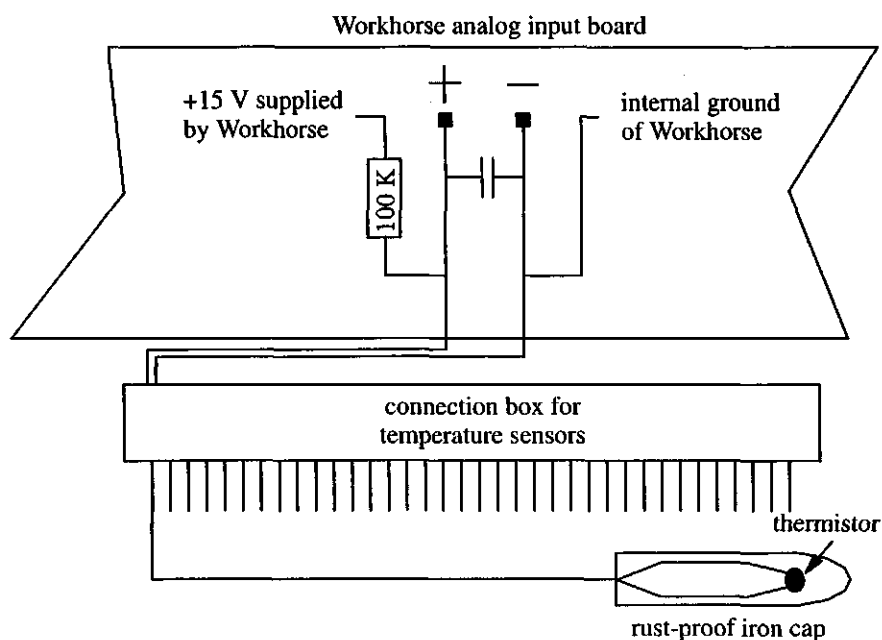
Figure 5-10 Schematic representation of the temperature measuring system; WH: Workhorse.

$$V_v = \frac{S R_{th}}{R_v + R_{th}}.$$

[5-12]

A sum of two exponential relationships between voltage and temperature could describe the theoretical and calibration data very well:

$$T = -13.081 + 44.869\, e^{-7.79643\, V_v} + 59.771\, e^{-1.148222\, V_v}.$$

[5-13]

Percentage of variance accounted for was more than 0.999 in all cases.

5.3 Water supply control system

At the Glasshouse Crops Research Station (GCRS) a water supply control system was developed for tomatoes grown on rockwool (de Graaf and Spaans, 1989). The basis of this system is a simple equation which computes the actual transpiration integrated over time T (mm) according to

$$T = \left(\alpha_T R + \beta_T DM \right) s,$$

[5-14]

where R is the global radiation measured outside the greenhouse integrated over time ($J\, cm^{-2}$), DM is called 'degree-minutes' defined as the difference between heating pipeline temperature and greenhouse air temperature of one degree during a time span of one minute integrated over time ($K\, min^{-1}$), s is a plant size factor defined as the actual plant length divided by the length of the mature plant, and α_T ($mm\, cm^2\, J^{-1}$) and β_T ($mm\, min\, K^{-1}$) are empirical crop factors, which may be different for different crops. For tomato $\alpha_T = 1.78 \cdot 10^{-3}\, mm\, cm^2\, J^{-1}$ and $\beta_T = 2.2 \cdot 10^{-5}\, mm\, min\, K^{-1}$. In this research lettuce (*Lactuca sativa*) was grown. Since Eq. [5-14] was never used in relation to lettuce production, it was decided to use the same α_T and β_T values as for tomato. In pilot experiments this system was working satisfactory. The transpiration model, Eq. [5-14], was obtained in the absence of evaporation from the substrate. In this study the computed actual transpiration was considered to be actual evapotranspiration. Heinen and van Moolenbroek (1995) presented a calibration of an extended version of this model. Since lettuce expands laterally instead of vertically, it was decided to interpret the factor s as the fractional substrate cover. It was assumed that s increased linearly in time from planting date to expected harvest date from 0 to 1.

At a central location at the GCRS the incoming radiation is measured. Inside the greenhouse the wet and dry bulb temperatures are measured at 1 m above the floor as well as the temperature of the heating pipes. This information is stored on the central climate computer of the GCRS and used in Eq. [5-14] to compute the cumulative (evapo)transpiration from the last water supply on. After a certain threshold value for the cumulative evapotranspiration is reached, nutrient solution is supplied during a preset

time, and cumulation is restarted at zero. The duration of supply depends on the delivery rate of the dripper/sprinkler system and on the desired leaching fraction, and was kept constant during the experiment.

It is common practice in horticulture to supply 40 to 70% more nutrient solution than needed to refill the substrate with an amount of water equal to that lost by evapotranspiration (de Willigen and van Noordwijk, 1987). This is done in order to remove excess of salts. Salt accumulates in the root zone since the nutrient uptake concentration is lower than the concentration of the supply solution. This difference is purposely maintained in order to prevent nutrient depletion in the root zone. These statements hold for both open, non-circulating and closed, recirculating growing systems. In the present study the amount of nutrient solution supplied equalled the computed evapotranspiration plus a desired amount of leaching. It is stated here that leaching in open growing systems means loss of water and nutrient to the subsoil, while in closed systems the drain water is collected and reused. Therefore, in closed systems large leaching fractions can be used.

5.4 Description of the specific experiments

Four experiments were carried out to parameterize and validate the simulation model described in Chapters 2 to 4. Some details including the goal of these experiments are explained in Table 5-2. Each of the four experiments has been given an unique name to which they will be referred to in the remainder of this thesis: 'Rooting', 'Growth & Uptake', 'Water Use', and 'Breakthrough' experiments, respectively.

In the 'Rooting' and 'Growth & Uptake' experiments the four plots were treated differently. The total amount of fertigation water added each fertigation was 1.3 (plots I and III) or 2.0 (plots II and IV) times the estimated evapotranspiration. Thus, the *excess EX* (1) *of water application* was 0.3 or 1.0 times the estimated evapotranspiration. *EX* corresponds to the *leaching fraction LF* (1) according to

$$LF = \frac{EX}{1 + EX}.$$ [5-15]

Leaching fraction is the ratio of the amount of drainage water and the amount of irrigation water (US Salinity Laboratory Staff, 1954; Rhoades and Loveday, 1990), and is commonly used in salinity control situations. With $EX = 0.3$ or 1.0, $LF = 0.23$ or 0.5.

In the 'Rooting' and 'Growth & Uptake' experiments the planting density was chosen such that one plant row was located above a drain, another plant row was located precisely between two drains, and a third row was located between these two rows.

Table 5-2 Summary of the important features of the four experiments carried out with lettuce (*Lactuca sativa*). In the bottom part the different treatments that were applied are explained.

Name	Cultivar	Plant density (plants m^{-1})	Growth period	Goal
Rooting	Cortina	16.67	31-07 to 14-09 1992	To determine final root length density, L_{rv}, and root radius, R_0, (Schwarz *et al.*, 1995).
Growth & Uptake	Flora	16.67	25-05 to 06-07 1993	To determine fresh and dry weights, total water use, nutrient uptake, and substrate physical condition in the root zone to be used as input data or validation data for the simulation model of Chapters 2, 3, and 4.
Water use	Karlo	20.0	29-09 to 07-12 1993	To determine total water use or evapotranspiration, *ET*, and its partitioning into transpiration, *T*, and bare substrate evaporation, *E*; one plot was used to measure denitrification (Postma *et al.*, 1995).
Break-through	-	-	-	To determine breakthrough of KNO_3 in a laboratory sand bed system at steady state drip application; data are used to calibrate the longitudinal, a_L, and transversal, a_T, dispersivities.

Name	Plot	Number of drip lines per crop row	Excess *EX* (*LF*)	Comment
Rooting	I	1:2	0.23 (0.23)	)
	II	1:2	1.0 (0.5)	) Schwarz *et al.* (1995).
	III	1:1	0.23 (0.23)	)
	IV	1:1	1.0 (0.5)	)
Growth & Uptake	I	1:2	0.23 (0.23)	
	II	1:2	1.0 (0.5)	
	III	1:1	0.23 (0.23)	
	IV	1:1	1.0 (0.5)	
Water use	I	1:1	1.0 (0.5)	Covered.
	II	1:1	1.0 (0.5)	Uncovered.
	III	1:1		Not used.
	IV	1:1	0.5 (0.23)	Denitrification measurements (Postma *et al.*, 1995).

In plots III and IV drip lines were positioned between all crop rows, while in plots I and II drip lines were only present between the two rows farthest from the drain.

Parameters that were not measured in the experiments are: the root hydraulic conductance K_1, the diffusion of a nutrient in free water D_0, actual relationship between tortuosity factor and volumetric water content $\tau(\theta)$ expressed by the parameters θ_l, f_1 and f_2 in Eq. [2-36], and the parameters $h_{r,1/2}$ and a occurring in the transpiration reduction function, Eq. [2-28]. Values for these parameters as obtained or estimated from the literature are given in Table 5-3. Unfortunately, no data for lettuce for K_1, a and $h_{r,1/2}$ could be found. They are estimated as follows. De Willigen *et al. (in prep.)* listed for several crops data from the literature for K_1, from which the average value $K_1 = 3.6 \ 10^{-6}$ cm d^{-1} was used. Campbell (1985, 1991) suggested that $a = 10$ is a good average value, which I will adopt here. Taylor and Ashcroft (1972; their Table 14.3) stated that lettuce grows optimally when h in the root zone never becomes less than -400 to -600 cm. Assuming that for these relatively wet conditions the resistance to water movement in the soil is much lower than that across the root surface (e.g. de Willigen *et al., in prep.*), h_r can be estimated from Eq. [2-30]. For $h = -400$ cm, $K_1 = 3.6 \cdot 10^{-6}$ cm d^{-1}, $T_a = 0.6$ cm d^{-1}, $L_{rv} = 2$ cm cm^{-3}, and $\Delta z = 15$ cm, one obtains $h_r \approx -6000$ cm. Then from Eqs. [2-27] and [2-28] it follows that for $T_a = 0.99\,T_p$, $h_{r,1/2} \approx -9500$ cm. For sand the parameters θ_l, f_1 and f_2 were given in Table 2-1. The diffusion coefficient D_0 depends on the type of nutrient. For an ideal solution it can be computed from the ionic mobility μ (L^{2}T^{-1}V^{-1}) according to (Atkins, 1978)

Table 5-3 List of parameter values not obtained from experiments, but taken from literature or estimated otherwise.

Parameter	Magnitude	Unit	Comment
K_1	3.6 10^{-6}	cm d^{-1}	No data for lettuce found in literature; average of values listed by de Willigen *et al., in prep.*
a	10	-	Campbell (1985, 1991); see text for explanation.
$h_{r,1/2}$	-9500	cm	Based on Taylor and Ashcroft, 1972; see text for explanation.
D_0	1.6	cm^2 d^{-1}	For NO_3 as computed with Eq. [5-16]; see text for explanation.
θ_l	0.12	-	) Derived from sand/loam data of
f_1	1.58	-	) Barraclough and Tinker (1981); see Table 2-1.
f_2	-0.17	-	)

$$D_0 = \frac{\mu_m k_B T}{n_v e},$$ [5-16]

where k_B is the Boltzmann constant ($= 1.381 \; 10^{-23}$ J K^{-1}), T is the absolute temperature (K), n_v is the valence of the ion (1), and e is the electron charge ($= 1.6022 \; 10^{-19}$ C). For several ions values for μ_m are listed in Appendix 8. In this thesis I will focus on the inert nutrient that is most dominantly present in glasshouse cropping systems, i.e. NO_3, for which D_0 is computed as 1.6 cm^2 d^{-1}.

5.5 Conclusions

In this chapter I have described the experimental system and the experiments. The following conclusions are drawn

- The TDR calibration curve as obtained in the laboratory for the coarse sand differed from the so-called 'universal' curve of Topp *et al.* (1980). The calibration curve was a third order polynome in $K_a^{0.5}$. *In-situ* obtained calibration data showed a large scatter, which may be due to the difficulties in taking core samples in the wet coarse sand. Thus, *in-situ* determination of the TDR calibration function in wet coarse substrates is not advisable.

- If the Mualem (1976) $K(\theta)$ and the Mualem and Friedman (1991) EC_w-EC_b relationships are valid, then the common parameter λ appearing in both equations has most effect on the EC_w-EC_b relationship. The parameter λ can be determined more accurately from a EC_w-EC_b calibration procedure.

Chapter 6

Growth, rooting characteristics, and water and nutrient balances of lettuce grown in irrigated sand beds

In this chapter results of measurements carried out on the greenhouse sand bed production system are described. The following data were collected: lettuce production (Section 6.1), root length density distribution and root radius (Section 6.2), water use and its partitioning into transpiration and evaporation (Section 6.3), relationships between dry weight, evapotranspiration or transpiration and radiation (Section 6.4), nutrient uptake (Section 6.5), and nutrient balance (Section 6.6). In Chapter 7 these data are used as input or boundary conditions for the validation of the simulation model. The hypothesis was that lettuce production and nutrient uptake are independent of the growth system. When this is true, it is possible to develop a model based on root zone characteristics only (i.e. the model of Chapter 2) without having to deal with differences in crop reaction. To determine whether this hypothesis is valid, in some sections the results of the sand beds will be compared with data obtained for lettuce grown on a Nutrient Film Technique (NFT) system (Heinen *et al.*, 1991, denoted as NFT1; Heinen, 1994, denoted as NFT2). For convenience, these references are mentioned here only once. Although comparison concerns lettuce grown in the same period of the year, the actual glasshouse climatic conditions were different, and in the NFT experiments a different cultivar, *i.e. Sitonia*, was used. Thus, a true comparison is not possible. The sand bed data presented in this chapter refer to the 'Rooting', 'Growth & Uptake', and 'Water Use' experiments as described in Chapter 5 (Section 5.4; Table 5-2). At the end of this chapter temperature patterns (Section 6.7) and electrical conductivity patterns (Section 6.8) observed in the root zone are presented.

6.1 Lettuce production

6.1.1 Final fresh and dry weights and dry matter content

The *fresh and dry weights* of lettuce heads grown on irrigated sand beds were determined in three experiments (Table 6-1). The harvest for the 'Rooting' experiment was carried out before the crop was fully grown, due to a preset time schedule; it was estimated that the crop would have been fully grown one week later. The dry matter contents ranged from 3.3% to 4.9%. The average dry matter content of 4.2% is normal for lettuce grown in glasshouses. For example, Roorda van Eysinga and Smilde (1971) reported 3.5% - 5.5%.

Table 6-1 Fresh (f) and dry (d) weights (g) and dry matter content (dm, %), including standard deviations, of lettuce heads grown on irrigated sand beds for three experiments; data are presented for the four sand beds I through IV. The number of lettuce heads used per harvest were 30, 36 and 5 per plot for the three respective experiments.

Experiment		Sand bed			
		I	II	III	IV
'Rooting'	f	237.0±33.3	227.8±28.8	222.0±31.3	224.5±32.4
	d	10.7±1.5	10.6±1.3	9.9±1.2	10.8±1.5
	dm	4.5±0.2	4.7±0.3	4.5±0.2	4.9±0.6
'Growth & Uptake'	f	326.7±52.9	322.2±49.5	336.3±35.3	354.9±34.2
	d	14.0±2.2	13.9±2.0	14.3±1.3	15.5±2.3
	dm	4.3±0.2	4.3±0.2	4.3±0.2	4.4±0.4
'Water use'	f	183.9±25.5	197.0±27.4	204.4±28.9	239.9±13.5
	d	6.1±0.8	6.6±0.9	8.1±1.3	10.0±0.9
	dm	3.3±0.1	3.4±0.1	4.0±0.3	4.2±0.5

In the two NFT experiments comparable dry matter contents of 3.9% and 5.5% were obtained.

The treatments (Section 5.4, Table 5-2) in the 'Rooting' and 'Growth & Uptake' experiments offered possibilities to carry out an analysis of variance (Genstat 5 Committee, 1993) to determine whether the treatments affected fresh or dry weights or dry matter content. For convenience the description of the treatments is repeated here. Either one (plots I and II) or two (plots III and IV) drip lines were used in half the region between two drains, combined with an excess *EX* (*LF*) of fertigation water of 0.3 (0.23) (plots I and III) or 1.0 (0.5) (plots II and IV) times the estimated evapotranspiration. Half the region between two drains contained three rows of crops: row 1 above the drain, row 3 between two drains, and row 2 between rows 1 and 3.

For the *'Rooting' experiment* the fresh weights of the four plots and of the three different rows were equal. There was a significant row effect on dry weight, with the row above a drain yielding the lowest dry weight: 9.9 g versus 10.8 g for the other two rows. For the dry matter content there was a significant plot effect: plots I and III, which had a low *EX*, had lower dry matter contents than plots II and IV, which had a high *EX*.

In the *'Growth & Uptake' experiment* significant plot, row and plot-row interaction effects were encountered. Plot IV yielded the highest fresh weight of 354.9 g per head, while the other three plots yielded an average fresh weight of 328.4 g. Averaged over the four plots, the row above the drain yielded the lowest fresh weight (314.0 g) and the row between two drains yielded the highest fresh weight (354.5 g). The increase of fresh weight with distance between the crop row and drain positions was present in plots I and II, but was not significant in plots III and IV. Similar effects were observed for the dry weights: plot IV yielded a dry weight of 15.5 g and plots I, II and III yielded on average a dry weight of 14.1 g; the row above the drain had a dry weight of 13.6 g and the row between two drains had a dry weight of 15.1 g. The row effect on dry weight was obvious in plots I and II, but not in the other two plots. There was no significant effect of any kind for the dry matter content data of the 'Growth & Uptake' experiment.

Especially for summer growth periods, the restricted supply of fertigation water had a negative effect on crop production. When the dripper density is equal to the planting density - with drip lines between all crop rows as was the case in plots III and IV - no row effects were observed. Highest production was obtained in plot IV, i.e. when the surplus of fertigation water added was 2 times the estimated evapotranspiration; production was larger than in plot III, which had a surplus of 1.3.

6.1.2 Lettuce growth as a function of time

The fresh and dry weight production of lettuce grown on pure nutrient solution as a function of time can be well described by a logistic function (Heinen *et al.*, 1991; Heinen, 1990a, 1994). A logistic model is obtained as the product of an exponential and a monomolecular or Mitscherlich model. The growth rate is given by

$$\frac{dW}{dt} = k_L W \left(1 - \frac{W}{W_f} \right) , \qquad [6-1]$$

where W is the weight (M), t is the time (T), W_f is the (asymptotic) final weight, and k_L is an inverse time constant (T^{-1}). Integrating Eq. [6-1] yields an expression for W as a function of t:

$$W(t) = \frac{W_i W_f}{W_i + \left(W_f - W_i \right) e^{-k_L t}} , \qquad [6-2]$$

where W_i is the (asymptotic) initial weight. The logistic growth model has an inflection point where the weight W^* is defined as

$$W^* = 0.5 W_f , \qquad [6-3]$$

and the time t^* as

$$t^* = \frac{1}{k_L} \ln \left(\frac{W_f - W_i}{W_i} \right) . \qquad [6-4]$$

The inverse time constant k_L is given by

$$k_L = \frac{4}{W_f} \left(\frac{d W}{d t} \right)^*,$$

$$k_L = 2 \left(\frac{1}{W} \frac{d W}{d t} \right)^*, \qquad\qquad [6\text{-}5]$$

$$k_L = \lim_{W \to 0} \frac{1}{W} \frac{d W}{d t},$$

where the superscript * refers to the value at the inflection point.

During the *'Growth & Uptake' experiment* several intermediate harvests in the four plots were carried out. Statistical analysis of variance yielded a significant row effect on growth, but no plot effect. In Subsection 6.1.1 a plot effect on final weights was observed, but apparently when intermediate data are considered as well, this effect disappears. Thus only the average results for all plots are presented. With Genstat 5 (Genstat 5 Committee, 1993; Appendix 5) the parameters in Eq. [6-2] were optimized (Table 6-2), and the resulting logistic function is shown in Figure 6-1A. In all cases the regression coefficient was larger than 0.999, so that also for lettuce grown in irrigated sand beds a logistic function can be used.

Table 6-2 Optimized parameters of the logistic growth function Eq. [6-2]: W_i and W_f are the initial and final weights (g) of the heads, respectively, k_L is the inverse time constant (d^{-1}), and t^* is the time of inflection (d).

	W_i	W_f	k_L	t^*
Dry weight	0.011	16.9	0.2157	34.0

The *dry weight production of lettuce grown in sand beds was compared to that obtained in the two NFT experiments* (Figure 6-1B). In al three cases the plants were pre-grown outside the experimental set-up. However, the initial weights of the plants differed between the three cases. The data of the two experiments with the lowest initial weights were shifted backwards in time so that the same initial weight resulted (Figure 6-1B). The time shift was determined by assuming exponential growth in the early stages of growth, i.e. an exponential curve was fitted through the first four data points and the time when the weight according to this exponential curve was equal to 0.06 g, i.e. the initial weight for NFT1, was determined. For NFT2 and SAND the time shifts were 10.34 d and 9.34 d, respectively. Although differences in cultivars, planting density and pattern, and growth

Dry weight *W* (g)

Time *t* (d)
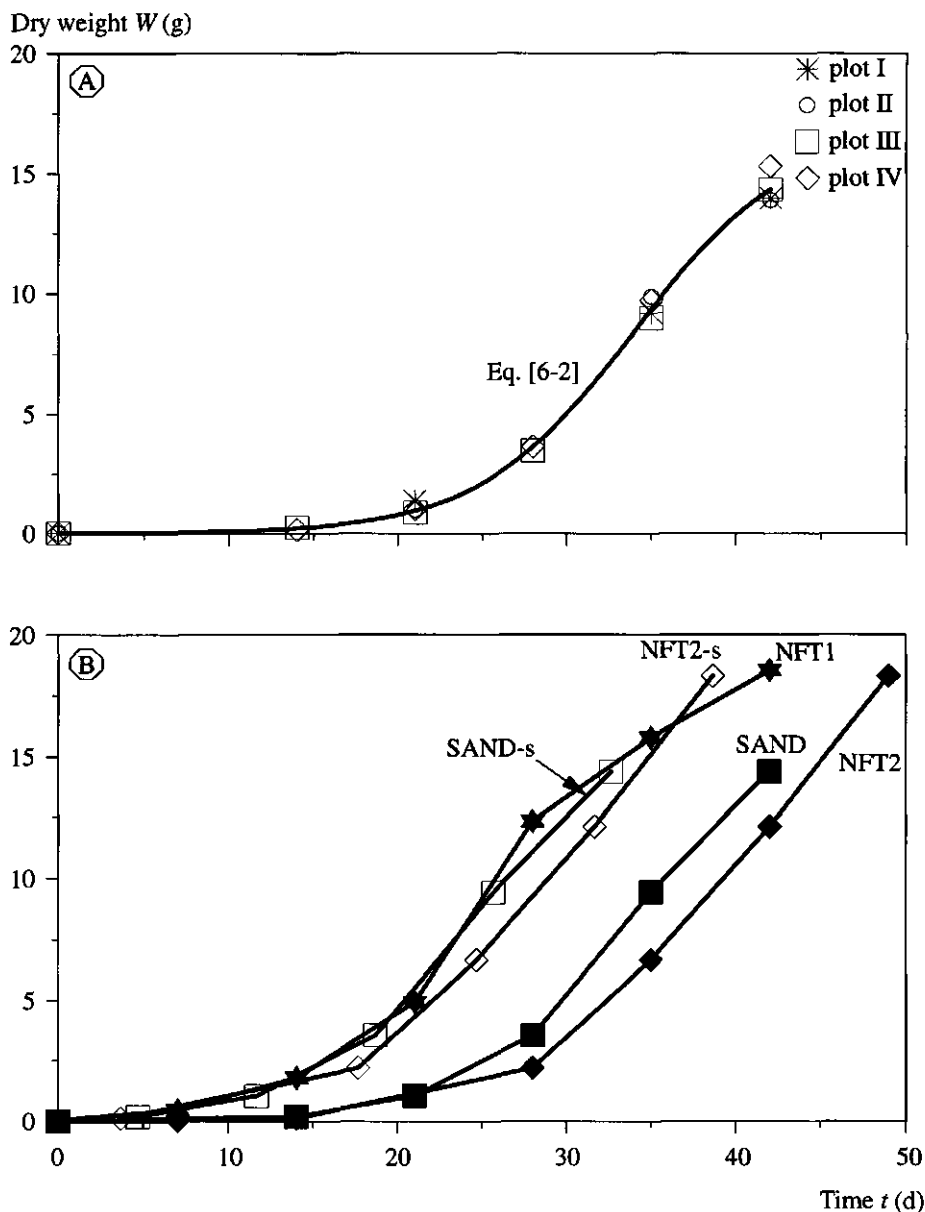
Figure 6-1 (A) Average logistic growth function, Eq. [6-2], for dry matter *W* production of lettuce grown in plots I through IV and the actually measured dry weights; parameters are given in Table 6-2. (B) Comparison of measured *W* of lettuce grown on two nutrient film technique (NFT) experiments (Heinen *et al.*, 1991: NFT1; Heinen, 1994: NFT2) and grown in sand beds (SAND). Data of NFT2 and SAND are also shifted backwards in time: NFT2-s and SAND-s (see text for explanation).

system existed, there is almost no difference in the time course of dry matter production. For example, the slopes of the curves near the inflection points are about the same.

Crop growth is mainly determined by two environmental factors, i.e. *temperature* and *radiation* (see e.g. Charles-Edwards, 1986; Bierhuizen, 1960; Bierhuizen and Feddes (1963). The latter concluded that for many crops grown in greenhouses, including lettuce, radiation is the dominant factor with respect to the final dry weight of the crop. Their data for lettuce suggest a linear relationship between final dry weight and cumulative radiation *R* (Figure 6-2). Figure 6-2 also shows data obtained in the 'Growth & Uptake' and 'Water Use' experiments. The result from the 'Water Use' experiment is in close agreement with the autumn data of Bierhuizen and Feddes (1963), but the result of the 'Growth & Uptake' experiment falls below their summer data. The following aspects must be considered when an explanation is sought for this deviation.
- During the 'Growth & Uptake' experiment very high root zone temperatures (see Section 6.7) were measured, which may have negatively influenced growth.
- The 'Growth & Uptake' experiment was carried out during a very warm spring, so that the heat sum may have had more influence on growth than for the data of Bierhuizen and Feddes (1963).
- Different in cultivars may result in different growth.
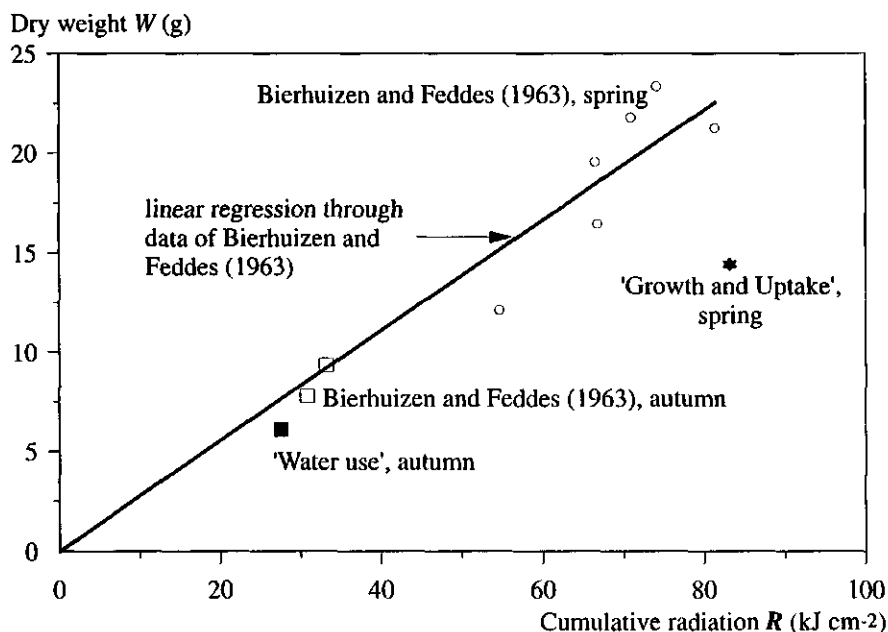
Figure 6-2 Dry weight *W* of lettuce as a function of cumulative radiation *R* for lettuce grown in spring ('Growth & Uptake') and autumn ('Water Use') experiments, compared with spring and autumn data from Bierhuizen and Feddes (1963). The line is the linear regression through the Bierhuizen and Feddes (1963) data.

The *relationships between dry weight and cumulative radiation **R** in the course of time* for the sand bed and NFT experiments is presented in Figure 6-3A. The original data for the NFT2 and sand bed experiments are also shifted backwards in time using the same time lag as given above. Even after this time shift, the results between the three experiments differ from each other. However, it would probably have been better to apply a shift in radiation, so that the initially experienced radiation during pre-growing is equal. These data are, however, not available. The *dry weights as a function of heat sum* T_h resulted in a close agreement between the three experiments, i.e. after the time shift (Figure 6-3B). The heat sum is here defined as $T_h = \sum \overline{T} t$ (°Cd) with $\overline{T}$ the average temperature at day t. The product of radiation and temperature, as suggested by Day (1986), did not result in a close agreement (data not shown).

The relationships between dry weight and radiation on the one hand and evapotranspiration and transpiration on the other hand for the experiments 'Growth & Uptake' and 'Water Use' are presented in Section 6.4.
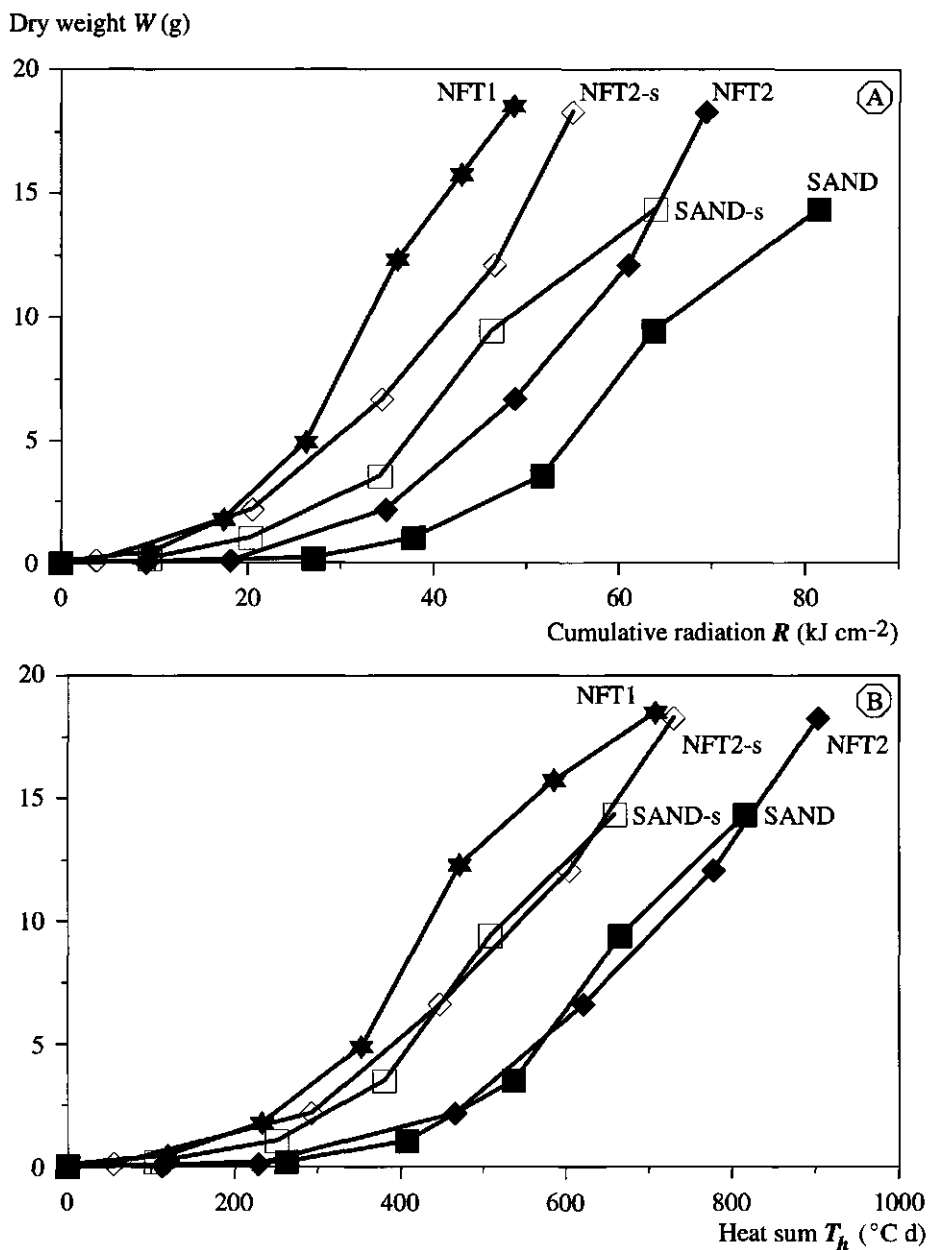
Dry weight W (g)

Figure 6-3 Dry weight as a function of (A) cumulative radiation and (B) heat sum for lettuce grown on two nutrient film technique (NFT) experiments (Heinen et al., 1991: NFT1; Heinen, 1994: NFT2) and grown in sand beds (SAND). Data of NFT2 and SAND are also shifted backwards in time: NFT2-shifted and SAND-shifted (see text for explanation).

6.2 Root length density distribution and root radius

6.2.1 Introduction

Root length density, L_{rv}, and *root radius*, R_0, are important parameters in both the root water uptake and the root nutrient uptake modules (Sections 2.3 and 2.6, respectively. Root length density can be determined non-destructively in-situ using minirhizotrons (e.g. Gijsman *et al.*, 1991), or destructively by taking substrate samples of known volume in which the total root length is measured. In the small root zones of the sand bed system described above, minirhizotrons are not very suitable, so it was decided to use the destructive sampling method. This method is time-consuming, especially the counting of the root length. Therefore, only one detailed sampling was carried out for a mature crop. The method and results are described in detail by Schwarz *et al.* (1995). They determined root data in a rectangular soil monolith (Figure 6-4) in all plots. They presented data for plots II and IV only, since these data were taken in twofold and thus could be statistically analysed. In this thesis results for all plots are presented. Since most of the roots were found in the shaded area of Figure 6-4C, the results refer to this area only.

6.2.2 Root length density

The patterns of *root length density distribution* in plots I and II were similar, as well as those of plots III and IV. Therefore, only the averages of plots I and II and of plots III and IV are presented (Figure 6-5). Of course roots were concentrated near the plant positions, i.e. at horizontal distances of 0 cm, 20 cm, and 40 cm. In plots I and II the plant at horizontal position 0 cm has less roots than the plants at horizontal positions 20 cm and 40 cm. This is related to the fact that in plots I and II no dripper was present at horizontal distance 10 cm, as was the case in plots III and IV. Higher salt concentrations developed at that location (Schwarz *et al.*, 1995; their Figure 2), evidently causing less root formation (Schwarz *et al.*, 1995; their Figure 7c). The root length densities in plots III and IV gradually decreased with depth independent of the horizontal position, except near the plant position. Averaged over the four beds, about 50% of the roots were found in the upper 5 cm layer, 40% in the layer 5-10 cm, and only 10% in the lower 5 cm. Although lettuce grown on sandy soils can reach a rooting depth of 50 cm to 70 cm (Schuurman and Schäffner, 1974), this small rooting depth of 15 cm in the sand beds was enough for a normal production (see Section 6.1). This indicates that if there is enough nutrient solution available, the crop does not need to have a large root system. Then the root length density may not be an important factor. The small amount of roots found in the bottom 5 cm is due to the high volumetric water content that existed permanently in this layer (see Section 7.3) and possibly restricted aeration (see Subsection 6.2.3) in the bottom layer.
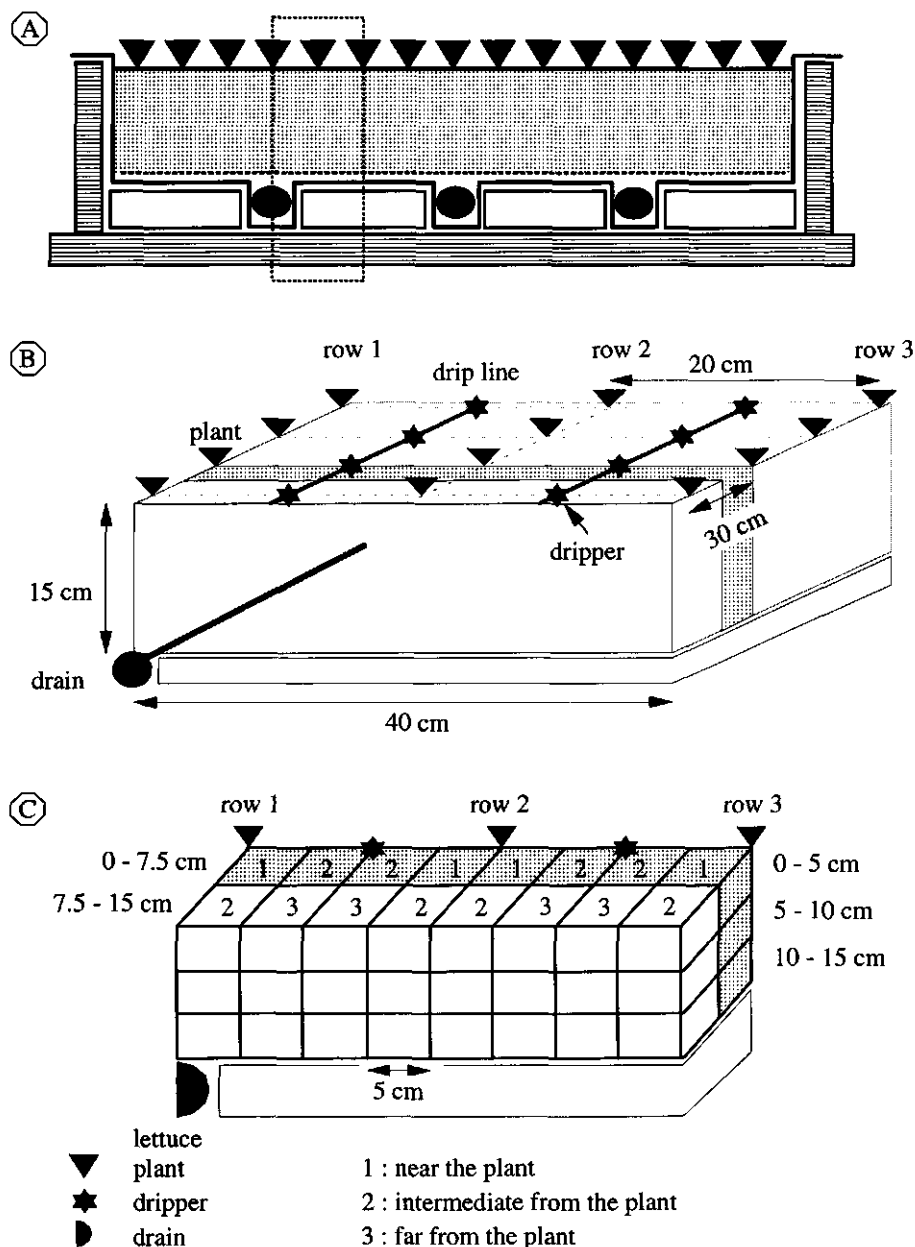
Figure 6-4 (A) Schematic cross sectional view of the sand bed system; in (B) a three-dimensional view of half the area between two drains (dotted rectangle in A) is given, and in (C) a detail of the volume of the root zone that was sampled (shaded area in B) is given (after Schwarz *et al.*, 1995). Only data from the shaded area in (C) are presented in this thesis.

Depth z (cm)
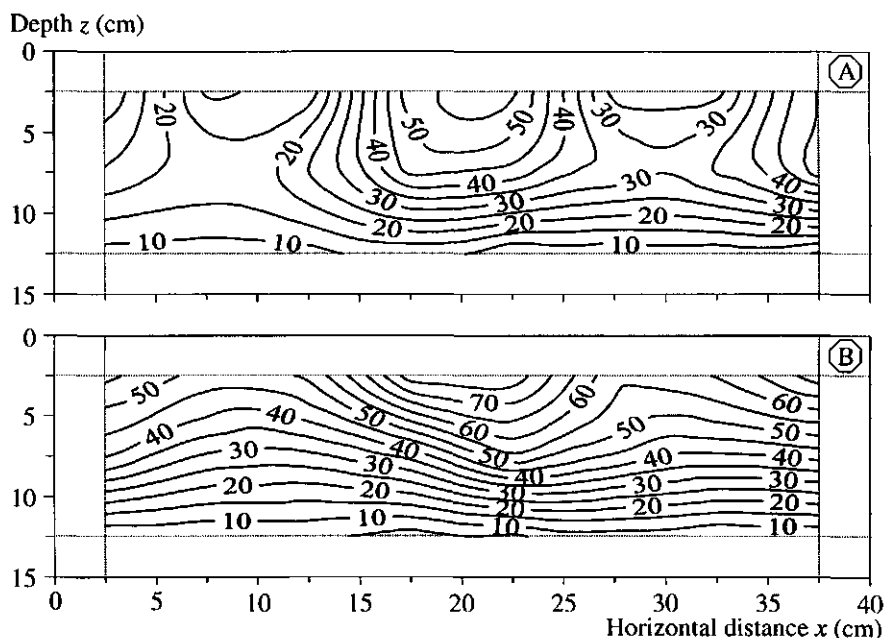
Figure 6-5 Root length density, L_{rv} (mm cm^{-3}) distribution, (A) averaged for plots I and II, and (B) averaged for plots III and IV.

6.2.3 Root radius

The frequency distributions of *root radii* in plots II and IV were skewed and showed two peaks (Schwarz *et al.*, 1995; their Figure 6), a small one for radii of 0.35-0.40 mm and a larger one for radii of 0.1-0.15 mm. The coefficient of variation for the radius was 17.0% for plot II and 14.9% for plot IV. The average root radius for all samples was R_0 = 0.17 mm. Root radius did not differ between the plots or with distance from the plant. It increased with depth and decreased with increasing EC. However, these effects are minor and the average root radius is used in the remainder of this thesis. For comparison, de Willigen and van Noordwijk (1987) reported a root radius of 0.185 mm for lettuce grown in a water culture. The increased root radius in the bottom layer of the sand beds was related to increased aerenchyma formation in the cortex (qualitatively confirmed only), which is normally an adaptation to reduced aeration (van Noordwijk and Brouwer, 1993). Lettuce roots can have a gas-filled root porosity of 5% to 6% (de Willigen and van Noordwijk, 1989). Average gas-filled porosities of other species are, e.g., carnation 0.3%, tomato 3.2%, sweet pepper 3.7%, rose 5.8%, and rice approximately 20% (van Noordwijk and Brouwer, 1993).

6.3 Partitioning water use into transpiration and evaporation

The 'Water Use' experiment was carried out to determine the partitioning of the total amount of water use into transpiration and evaporation. Heinen and van Moolenbroek (1995) used these data together with incoming global radiation and greenhouse heating to obtain the parameters of an extended version of the water supply control model presented in Section 5.3. It appeared that the experimental data could be described quite well by this model. However, the crop size factor or fractional coverage needed to increase linear in time and extrapolation to other experiments was not possible. Measurements of fractional coverage (de Graaf, 1980; unpublished data) suggest, however, a S-shape of coverage with time. Therefore, I decided to present a different analysis of the data in this thesis (Subsections 6.3.1 and Section 6.4).

6.3.1 Method

The water use i.e. evapotranspiration of a closed sand bed system was determined by monitoring the water levels in the supply and drainage tanks using in-situ calibrated pressure transducers (see Subsections 5.1.2 and 5.1.3). To determine whether the storage of water in the sand bed changed in the course of time, the volumetric water content was determined at three depths at several locations in the sand beds, using the time domain reflectometry technique (see Subsection 5.2.2).

The *water use represents the evapotranspiration rate ET* (mm d^{-1}) and consists of the *evaporation rate from the substrate E* (mm d^{-1}) plus the *transpiration rate T* (mm d^{-1}),

$$ET = E + T.$$ [6-6]

In order to get an impression of the partitioning of ET into its two components, one of the plots was covered with plastic. In this way evaporation from the substrate was prevented. It was assumed that T of the crop in the covered plot I is equal to T of the uncovered plot II. Thus the water use for the *covered plot ET_c* is

$$ET_c = T,$$ [6-7]

and for the *uncovered plot ET_u* is (using Eq. [6-6])

$$ET_u = E + T.$$ [6-8]

Substituting Eq. [6-7] in Eq. [6-8] yields

$$ET_u = E + ET_c.$$ [6-9]

Each day enough water was supplied to all plots so that drainage occurred. The daily water use was thus equal to the total amount supplied minus the amount that had drained. The data are represented as the time integrated quantities ET (mm), E (mm) and T (mm). Due to the frequent fertigations the sand was wet all the time, so that potential evapotranspiration, potential evaporation and potential transpiration presumably occurred.

In the remainder of this chapter I will assume that these processes occurred at a potential rate.

It is recognized that the moisture and temperature conditions in the covered plot may differ from those in the uncovered plot, and that the crop in the covered plot also got reflected light from the plastic cover. Thus the climatic conditions for the covered and uncovered plots will be different. However, in a pilot experiment (van Moolenbroek en Heinen, 1994), where this method was tested, no visual differences in crop development were observed. To determine if differences in growth existed between the covered and uncovered plots two harvests were carried out, three weeks before and at the end of the growth period. Per plot five plants were harvested at each time. Fresh and dry weights and dry matter content were determined and analysed statistically, using the analysis of variance procedure of Genstat 5 (Genstat 5 Committee, 1993).

6.3.2 Results

In this subsection first the partitioning data are presented. At the end the total amounts of water that were used in the 'Water Use' and 'Growth & Uptake' experiments are presented.

Partitioning
Statistical analysis of the fresh and dry weights and dry matter content of the lettuce heads (see Table 6-1, plot I versus plot II) showed no significant coverage effect. The time domain reflectometry results showed no changes in water storage on a daily basis. Thus, the measured did not have to be corrected for changes in storage in the root zone.

In Figure 6-6 the *time coursers of ET, E and T* are presented. The total water use of the uncovered plot at the end of the growth period was 46.6 mm (Figure 6-6). The contribution of E to ET_u was large at the beginning, during the first day approximately 90% evaporated. At the end of the growth period ET_u is mainly determined by T. From day 309 onwards, the average daily E was less than 0.1 mm d^{-1}; at that time the fractional substrate coverage by the crop (see below) was more than 0.8. In total 21.1 mm evaporated from the sand surface and 25.4 mm transpired, or 45% of ET_u was evaporation from the substrate and 55% was transpiration. The large contribution of E to ET may be explained by the fact that the lettuce crop canopy becomes closed at a very slow rate in winter periods. For commercial growers this aspect may be important, since water is costly.

De Graaf (1980) also determined E as a difference in water use from uncovered and covered small weighing lysimeters and reported for lettuce E contributions of 40% in autumn, 62% in winter and 30% in spring. Losses due to E have been reported for other crops as well. For example, Otten (1994) obtained E contributions between 19% in spring period up to 41% in winter period with *Ficus benjamina* grown in pots on flooded benches.

Dynamics of water and nutrients in sand beds

Cumulative evapotranspiration *ET*, evaporation *E*, transpiration *T* (mm)
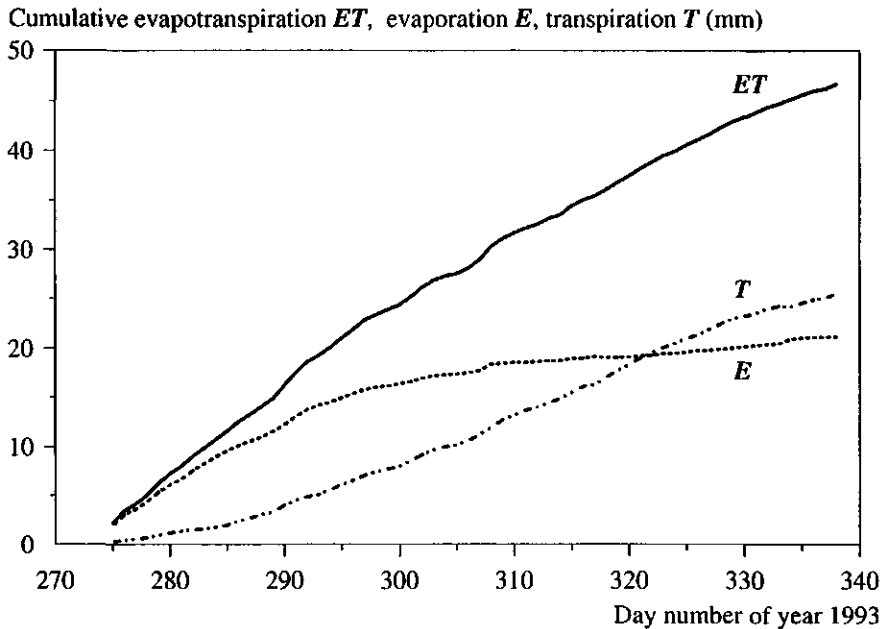
Figure 6-6 Cumulative evapotranspiration *ET* (mm), cumulative evaporation from the substrate *E* (mm) and cumulative transpiration *T* (mm) as a function of time for the 'Water Use' experiment.

For several arable crops growing in the open, i.e. potatoes and sugar beets (Feddes, 1987), and cotton and sorghum (Ritchie, 1983), consistent relationships were obtained between the *contribution of potential transpiration* T_p *to potential evapotranspiration* ET_p, as a function of leaf area index *LAI* (L^2L^{-2}). They distinguished two relationships, one for wet and one for dry soil surfaces. For a crop like lettuce, which forms a compact head, *LAI* is not a good measure. Since for some crops, e.g. potatoes (van der Schans *et al.*, 1984), empirical relationships between *LAI* and fractional substrate coverage S_c (L^2L^{-2}) exist, it is likely that there exists also a relationship between T_p/ET_p and S_c. Since S_c was not measured during the 'Water Use' experiment, I used data obtained by de Graaf (1980; unpublished data) for lettuce grown in a greenhouse during the same period of the year (Figure 6-7). The measured S_c data could be well described by the following logistic function

$$S_c = \frac{1}{1 + e^{-k_S(t - t^*)}},$$ [6-10]

with the inverse time constant $k_S = 0.1186$ d^{-1}, and t^* representing the time corresponding to the inflection point, $t^* = 23.29$ d. The measured contribution of T_p to ET_p

Fractional substrate cover S_c (-)
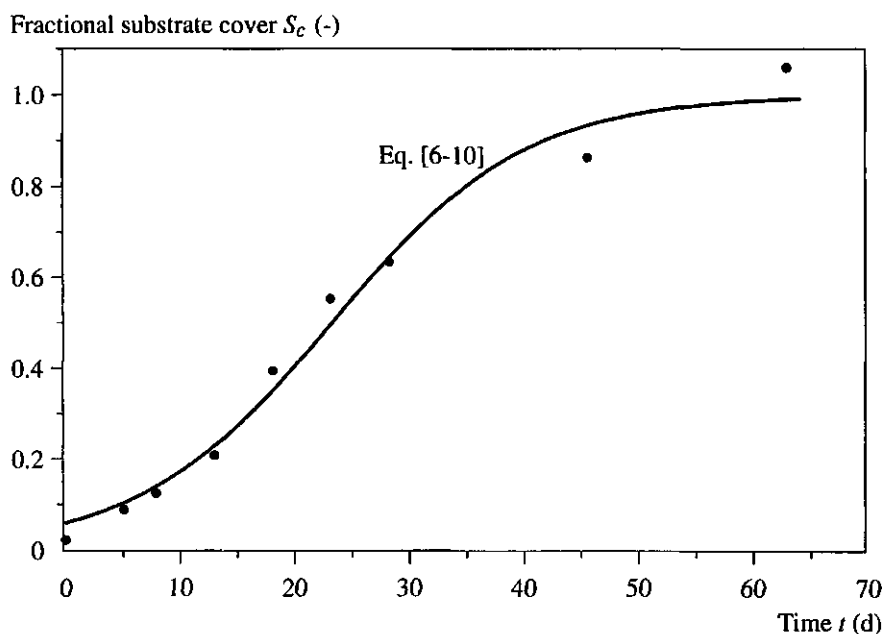
Figure 6-7 Fractional substrate cover S_c as a function of time for lettuce grown in a greenhouse (de Graaf, 1980; unpublished data), and fitted logistic description, Eq. [6-10], of the data.

as a function of S_c is presented in Figure 6-8. In Figure 6-8 curves based on data of T_p/ET_p versus S_c for wet soil surfaces from Feddes (1987) and Ritchie (1983) are also presented. The S_c values for these curves were obtained by using the inverted S_c - *LAI* relationship for potatoes from van der Schans *et al.* (1984). The curves in Figure 6-8 must be regarded as an illustration, since three of the four crops were not potatoes, and thus the conversion from *LAI* to S_c is not quite appropriate. The measured data are scattered, but the increasing trend of the T_p/ET_p data with increasing S_c follows the relationships of Feddes (1987) and Ritchie (1983). The measured data and the data from the literature could be well described by the following exponential relationship

$$\frac{T_p}{ET_p} = 1 - e^{-k_T S_c},$$
[6-11]

where k_T is a dimensionless rate constant. For the measured data k_T was determined as 1.995 ($r^2 = 0.53$), and for the data of Feddes (1987) and Ritchie (1983) k_T was determined as 2.566 ($r^2 = 0.99$) and 1.889 ($r^2 = 1.00$), respectively. Although different crops are involved and the data of Feddes (1987) and Ritchie (1983) were transformed using a relationship which was determined for potatoes in another study, it is remarkable

Transpiration contribution to total water use T/ET (-)
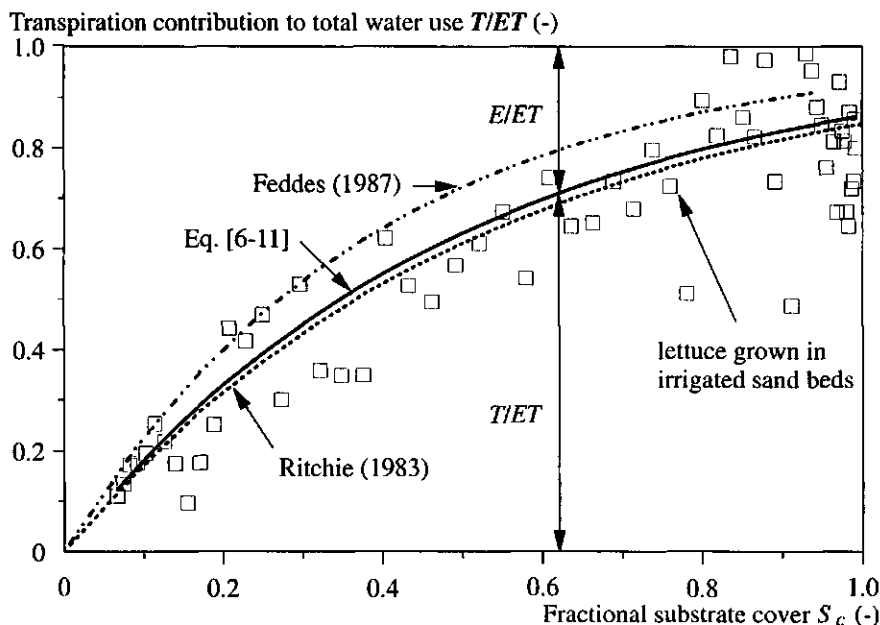
Figure 6-8 Contribution of lettuce transpiration T to evapotranspiration ET as a function of fractional substrate cover S_c. Also presented are T_p/ET_p data from Feddes (1987) and Ritchie (1983) for wet soil surfaces (see text for explanation).

to see that the measured and fitted data for lettuce grown in irrigated sand beds are in close agreement with the derived relationships from the literature.

Total water use
During the 'Water Use' and 'Growth & Uptake' experiments the *total water use or evapotranspiration ET* for the whole growth period was determined (Table 6-3). During the 'Water Use' experiment the total water use in the uncovered plot II amounted to 46.6 mm, while in the covered plot I this was 21.1 mm. The average ET for the four sand beds during the 'Growth & Uptake' experiment was 92.0 mm. The differences between the plots were small, indicating that the treatments used in this experiment - either one or two drip lines used in half the region between two drains, with an excess of fertigation water of 1.3 or 2.0 times the estimated evapotranspiration - did not result in different evapotranspiration amounts. Expressed per plant the average total water use during the 'Water Use' experiment was 2.33 l plant^{-1} (plot II) and for the 'Growth & Uptake' experiment this was 6.36 ($\pm$0.52) l plant^{-1}.

Table 6-3 Total water use *ET* per plot (mm) for the 'Water Use' and 'Growth & Uptake' experiments (nd = not determined). The *ET* per plant of plot II of the 'Water Use' experiment and the averaged *ET* expressed per plot (mm) or per plant (1 plant^{-1}) for the 'Growth & Uptake' experiment are also presented.

Experiment	Sand bed				Averaged	
	I	II	III	IV	(mm)	(1 plant^{-1})
'Water Use'	21.1	46.6	nd	nd	-	2.33
'Growth & Uptake'	92.4	89.9	88.0	97.9	92.0	6.36

6.4 Relationships between dry weight, evapotranspiration or transpiration and radiation

During the 'Growth & Uptake' and 'Water Use' experiments *ET*, *T* (only 'Water Use' experiment), and global radiation *R* (kJ cm^{-2}) were daily measured. Moreover, the dry weight increase of lettuce in time could be well described by logistic functions (Eq. [6-2]), so that also daily dry weights are available. The *relationships among the cumulative R, ET, T and W* are presented in a so-called three-quadrants figure (Figure 6-9). The patterns of the spring ('Growth & Uptake') and autumn ('Water Use') data are similar, but the magnitudes differ. The estimates of W_i in the logistic function were 0.011 g and 0.083 g for the 'Growth & Uptake' and 'Water Use' experiments, respectively. Thus the initial plant size differed between the two experiments and hence the initial contribution of *T* to *ET* differed also. This difference is not accounted for in this section.

In Figure 6-9 also the *transpiration for the 'Growth & Uptake' experiment* is given. This quantity was not measured, but it was derived according to the procedure described below. This procedure is meant to illustrate how the relationship between *T/ET* and S_c can be used to determined *T* based on measured *ET* and S_c. It is assumed that the relationship between *T/ET* and S_c is independent of the season. Since S_c was not measured, it was estimated by assuming that the ratio between S_c and W/W_f is a function of the growth stage, i.e. t/t_h, where t_h is the time of harvest. For the 'Water Use' experiment this ratio is known and thus for known W/W_f of the 'Growth & Uptake' experiment S_c for this experiment could be computed. These data could also be described with Eq. [6-10] with $k_S = 0.1970$ d^{-1} and $t^* = 27.77$ d. Now daily values for S_c and *ET* are known, and the daily *T* could be computed (Figure 6-9). Note that the time t^* at the inflection point of the curve in the 'Growth & Uptake' experiment is larger than that in the 'Water Use' experiment, although the total growth period was smaller. This is due to the fact that the relative growth, W/W_f, as a function of growth stage, i.e. t/t_h, lagged behind
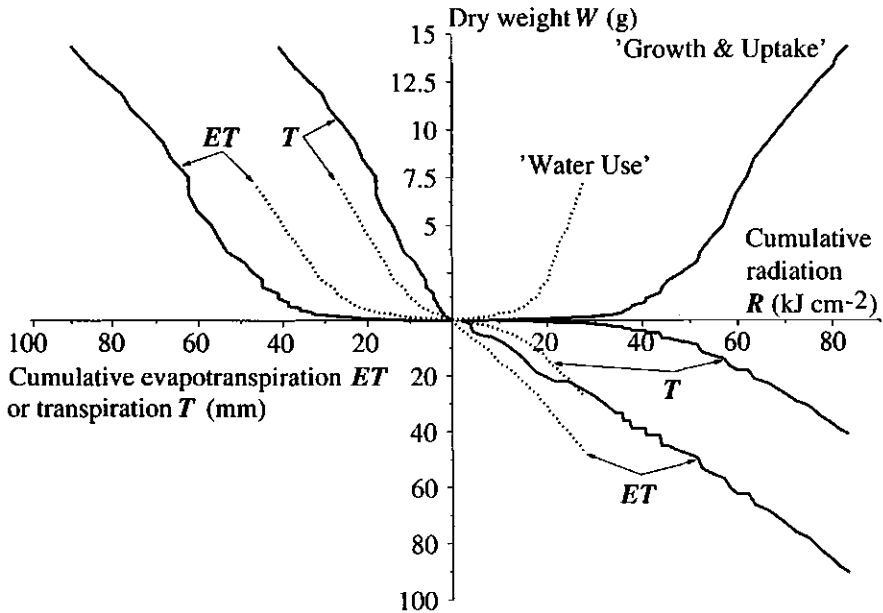
Figure 6-9 Relationships between dry weight of lettuce *W*, cumulative water use *ET* or cumulative transpiration *T* and cumulative radiation *R* for the two experiments 'Growth & Uptake' (solid lines) and 'Water Use' (dotted lines).

that of the 'Water Use' experiment, which might be an indication that growth was not optimal.

An alternative way to relate *R*, *ET* and *W* is by presenting them *on a relative basis*, i.e. relative to their maximum measured values (Figure 6-10). For both experiments, i.e. 'Growth & Uptake' and 'Water Use', there existed an almost linear 1:1 relationship between relative radiation R/R_f and relative total water use ET/ET_f, where subscript *f* refers to time of harvest. Up to half of the total received radiation, the relative dry weight W/W_f in the 'Water Use' experiment was slightly larger than in the 'Growth & Uptake' experiment. This is caused by the higher initial weight of the plants. From that period on the increase in relative dry weight W/W_f for the 'Growth & Uptake' experiment is larger than that for the 'Water Use' experiment, but at the end the two lines approach each other.
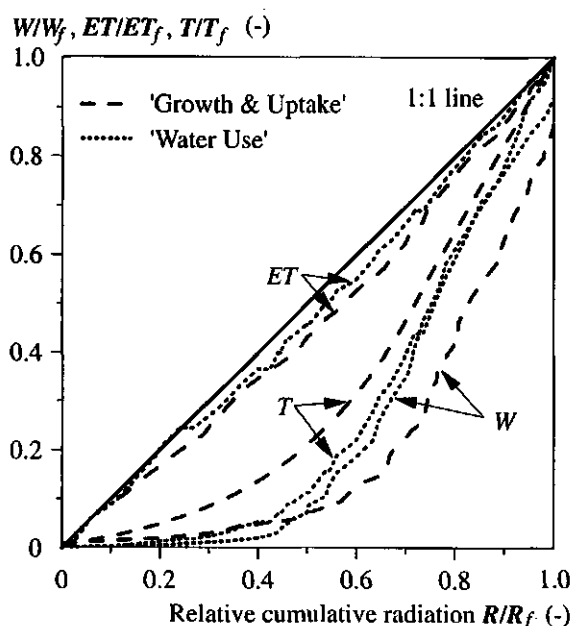
Figure 6-10 Relative dry weight W/W_f, water use ET/ET_f and transpiration T/T_f as a function of relative cumulative radiation R/R_f.

6.5 Nutrient uptake

Uptake data of nutrients by lettuce grown in sand beds ('Growth & Uptake' experiment) are presented in several ways: cumulative uptake as a function of time described by a logistic function (Subsection 6.5.1), cumulative uptake of N, K and P versus time or cumulative daily radiation (Subsection 6.5.2), and as observed constant uptake ratios between nutrients (Subsection 6.5.3). The data will be presented on total plant basis and compared to data obtained in the two NFT experiments. No root content data for the sand bed experiment were available. Total plant content was determined by assuming the same ratio of shoot/root contents as observed in the NFT experiment of Heinen (1994).

6.5.1 Nutrient uptake

Uptake of nutrients by a crop can be determined by following the accumulation of the nutrients in the crop or by following the depletion in the cropping system, i.e. supply and drainage tanks and root zone. Even for well controlled experiments with water cultures, depletion generally exceeds accumulation (e.g. Willumsen, 1980, 1984; Heinen *et al.*, 1991, 1995; Voogt, 1993; Heinen, 1994). In this section I present only the accumulation

data, which can be regarded as uptake. In a later section (Section 6.6) the depletion data
are presented as well. During the 'Growth & Uptake' experiment regularly some plants
were harvested and analysed for contents of macro-nutrients plus Na and Cl. As for
lettuce grown in NFT, *cumulative nutrient uptake* by the crop could be well described by
a logistic function equivalent to Eq. [6-2], with W then representing cumulative nutrient
uptake (mmol per plant) (Table 6-4). Moreover, the *relative cumulative uptake* for some
nutrients was in close agreement with the relative dry matter production (Figure 6-11).
Especially the cumulative uptake of N and K follows exactly the dry matter production,
thus the contents of these elements remain constant in time. The uptake of P, Ca, Mg, S
and Na was relatively smaller as plants grew older, while for Cl the uptake was relatively
larger, except at the end of the growing period. In NFT experiments slightly different
patterns were observed; however, in all cases N and K showed close agreement with dry
matter production, so that uptake of these elements can be estimated from dry matter
production data.

Table 6-4 Optimized parameters of the logistic cumulative nutrient uptake for all macro-
nutrients plus Na and Cl, Eq. [6-2]: W_i and W_f are the initial and final uptakes (mmol
per plant), respectively, k_L is the inverse time constant (d^{-1}), and t^* is the time (d) of
inflection.

Nutrient	W_i	W_f	k_L	t^*
N	0.065	74.763	0.2137	33.0
K	0.042	44.501	0.2085	33.4
P	0.004	5.084	0.1979	36.1
Ca	0.007	5.800	0.1894	35.5
Mg	0.003	2.958	0.2015	34.2
S	0.003	1.714	0.1823	34.8
Na	0.003	1.473	0.1743	35.5
Cl	0.003	1.529	0.1971	31.6

Relative cumulative uptake or dry weight W/W_f (-)
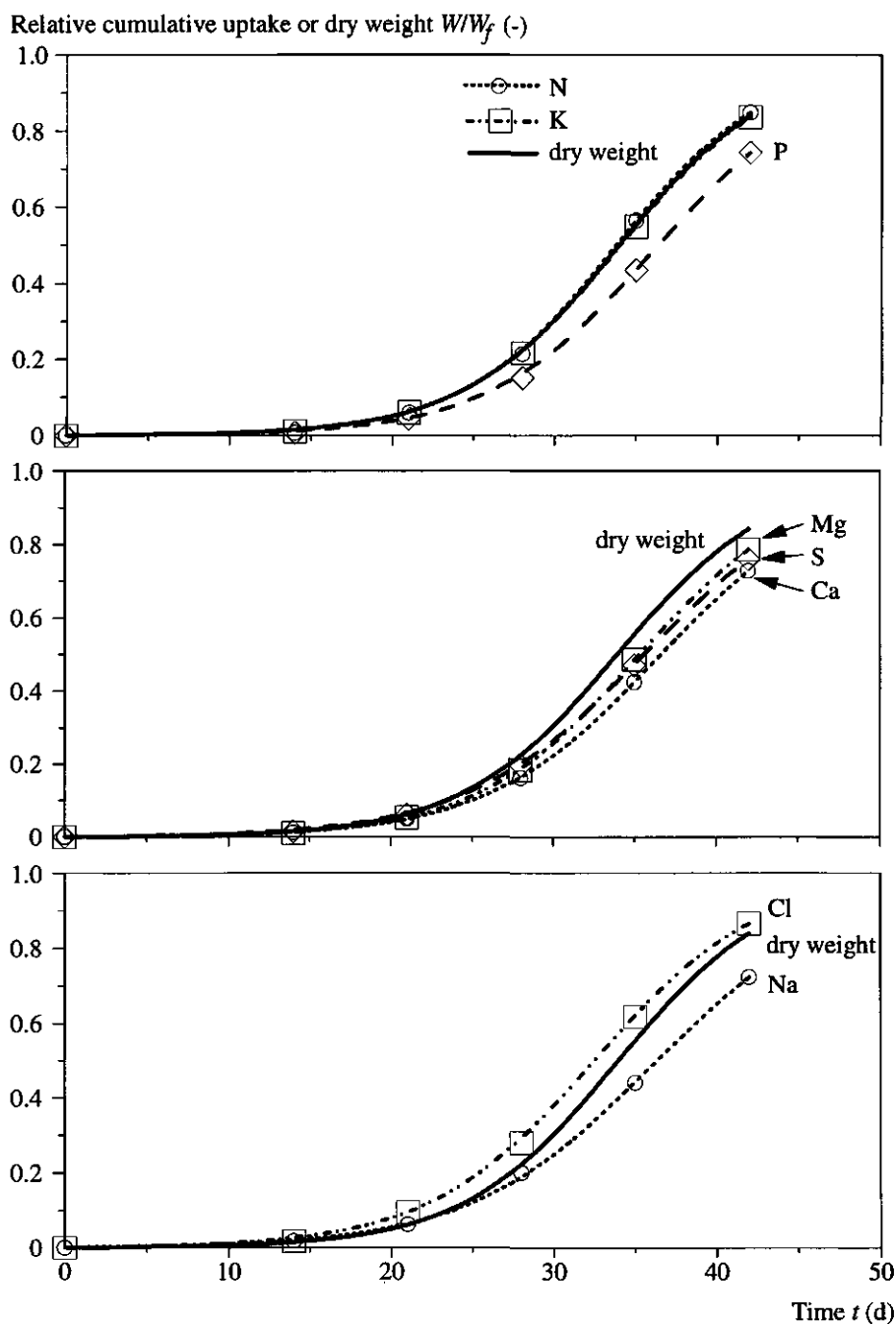
Figure 6-11 Relative cumulative uptake of all macro-nutrients as well as Na and Cl and relative dry matter production as a function of time.

Nitrate content of shoot (g kg^{-1})
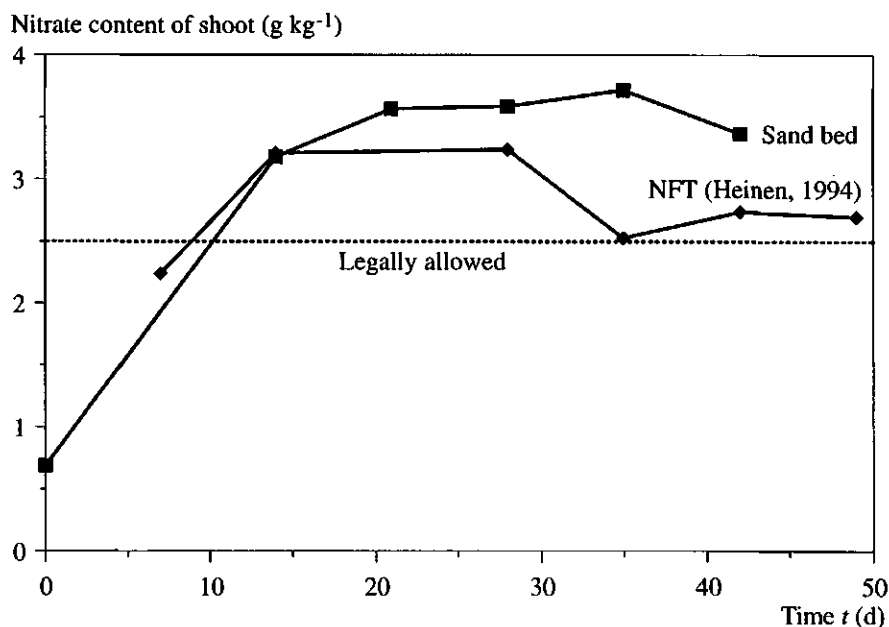
Figure 6-12   Nitrate content per kg fresh weight of lettuce heads grown in sand beds and in NFT (data from Heinen, 1994) as a function of time compared to the legally allowed content of marketable lettuce heads.

The *nitrate content of the shoot* was measured as well (Figure 6-12), since it is an important measure of the quality of lettuce heads. The nitrate content increased in time during the first three weeks, and remained more or less constant afterwards. However, the final content was much larger than the legally allowed content in The Netherlands of 2500 mg kg^{-1} (fresh). For comparison, the nitrate content data of lettuce grown in NFT (Heinen, 1994) is shown in Figure 6-12 as well.

6.5.2 Comparison of uptake of N, K and P by lettuce grown in

sand beds and in NFT

The *cumulative uptake of N, K and P* in lettuce grown in sand beds and on two NFT experiments *as a function of time or as a function of heat sum* is presented in Figure 6-13. In Section 6.1 a similar comparison was done for dry matter production. There a time shift for the second NFT (NFT2) and the sand bed experiments was introduced, so that

Cumulative uptake N (mmol)

Cumulative uptake K (mmol)

Cumulative uptake P (mmol)
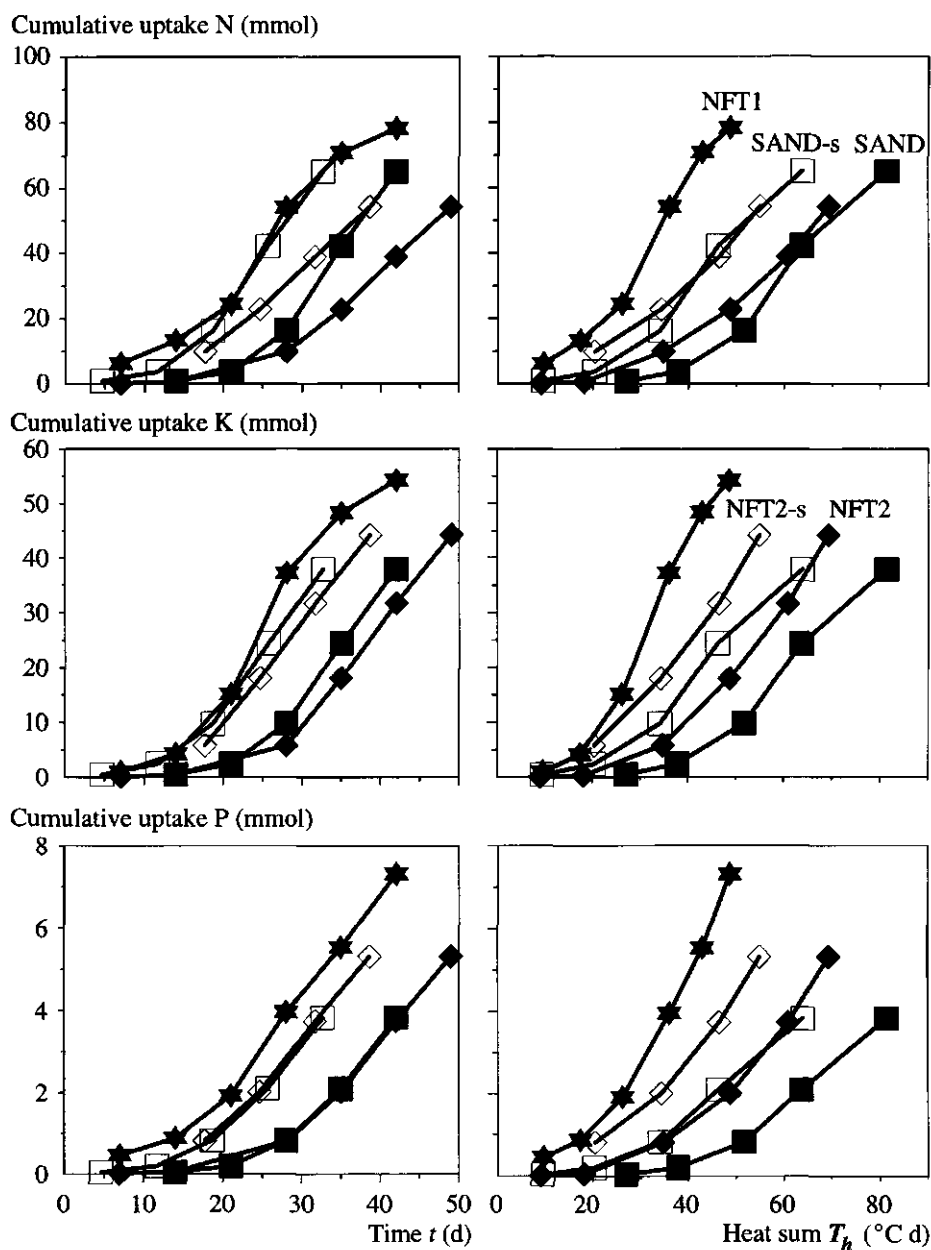
Figure 6-13 Comparison of uptake of N, K and P as a function of time or heat sum for lettuce grown in nutrient film technique (NFT) experiments (Heinen et al., 1991: NFT1; Heinen, 1994: NFT2) and grown in sand beds (SAND). Data of NFT2 and Sand are also shifted backwards in time: NFT2-s and SAND-s (see text for explanation).

at time zero the initial weights were the same. The same time shifts were used for the data in Figure 6-13. The actual uptake differed between the three experiments, but in most cases the time shift did not result in close agreement. This is due to the non-equal initial contents of the nutrients, even after the time shift, however, the average contents differed also between the three. For example, the initial contents for N, K and P of lettuce grown in sand beds would have been the same as those of lettuce grown in NFT1 at time shifts of 9.85 d, 8.52 d and 12.21 d, respectively. Compared to the time shift based on initial dry weight, i.e. 9.34 d, only for P the sand bed data would come closer to those of NFT1. The average contents of N, K_2O and P_2O_5 for lettuce grown in sand beds were 51.2 mg g^{-1} dry matter (dm), 102.2 mg g^{-1} dm, and 12.8 mg g^{-1} dm, respectively; for NFT1 these were 61.1 mg g^{-1} dm, 63.9 mg g^{-1} dm and 10.5 mg g^{-1} dm, respectively, and for NFT2 these were 54.2 mg g^{-1} dm, 63.0 mg g^{-1} dm and 10.6 mg g^{-1} dm, respectively. There was no close agreement between the three experiments for uptake as a function of the heat sum, but the slopes of the curves are similar (Figure 6-13). There was also no agreement for uptake as a function of cumulative daily radiation (data not shown). Although there is no exact agreement in accumulation data, the average slopes of the last part of the curves, e.g. the last four data points, in Figure 6-13 are in most cases similar, with the exception of accumulation of N in the NFT2 experiment. Thus, final uptake differed between the three experiments and thus between the NFT and sand bed systems, but on average the final uptake rate was the same.

All N and K_2O contents presented in this section fall in the ranges given by Roorda van Eysinga and Smilde (1971), but the P_2O_5 contents are lower than the range given by these authors.

6.5.3 Constant nutrient uptake ratios

The cumulative uptake in the crop can also be used to determine if there are *constant uptake ratios between the nutrients*. When constant uptake ratios exist between several nutrients, then dosage of nutrients can be based on the determination of uptake of only a few nutrients. For all possible combinations between nutrients the uptake ratios in each of the last three weeks were determined. The three obtained ratios were considered as constant when the difference between the maximum and the minimum values divided by their mean was less than 0.2 (arbitrarily chosen). The data are based on whole plant uptake and on shoot uptake (Table 6-5). For several combinations of nutrients constant uptake ratios were obtained in both the sand bed experiment as in the NFT2 (Heinen, 1994) experiment. However, the magnitude of the ratios differed between the two experiments (Figure 6-14). Only the uptake ratios Ca/K and S/K were comparable.

The high uptake of Ca and Mg in the sand bed system might be explained by the large amounts of Ca and Mg present in the calcareous sand.

Table 6-5 Uptake ratios between macro-nutrients and Na and Cl (mmol)for lettuce grown in sand beds, with less than 20% difference between maximum and minimum observed ratios (in relation to their mean) during the last three weeks. If the difference was less than 10% the ratio is underlined. Two cases are considered: whole plant uptake and shoot uptake data.

Whole plant uptake

	K	P	Ca	Mg	S	Na	Cl
N	0.590	0.055	0.061	0.035	0.020	0.017	0.023
K	1	0.093	0.103	0.058	0.034	0.028	0.038
P		1	1.112	0.638	0.386		
Ca			1	0.569			
Mg				1	0.611		
S					1	0.824	1.106
Na						1	1.364

Shoot uptake

	K	P	Ca	Mg	S	Na
N	0.599	0.052	0.065	0.034	0.017	0.017
K	1	0.086	0.108	0.057	0.029	0.028
P		1	1.251	0.664	0.341	0.330
Ca			1	0.531	0.272	0.264
Mg				1	0.512	0.491
S					1	0.955
Na						1

Ratio of constant uptake ratios, sand bed / NFT (-)
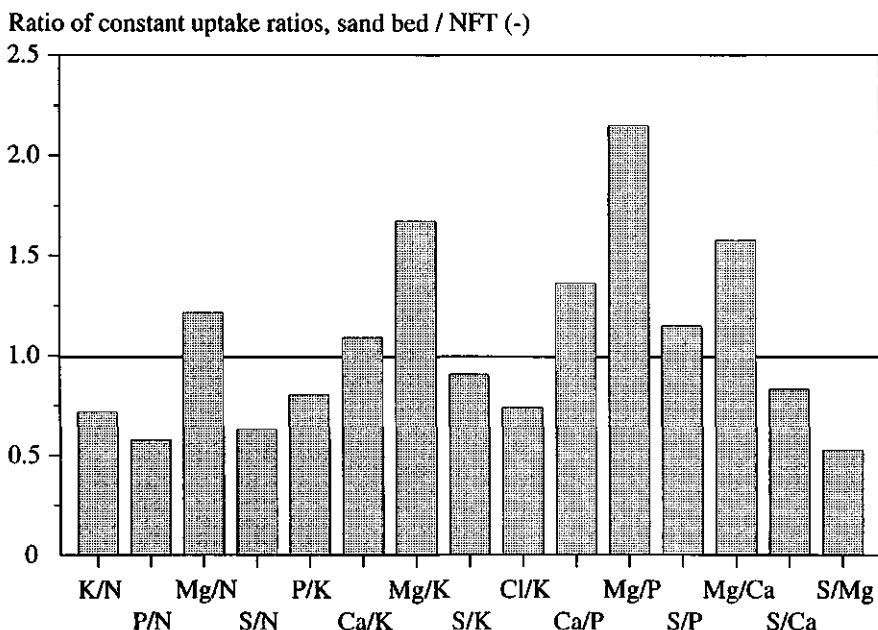
Figure 6-14   Comparison of observed constant nutrient uptake ratios determined for lettuce
grown in sand beds and lettuce grown in NFT (Heinen, 1994). Equal constant
uptake ratios are obtained when their ratio equals one.

6.6 Nutrient balance

6.6.1 The mass balance

Introduction
Ideally, *the nutrient uptake by a crop determined as accumulation in the crop*, U_a (M),
is equal to *the uptake determined from the depletion from the growth system*, U_d (M):

$$U_a = U_d,$$ [6-12]

with

$$U_a = \left(A_{cf} - A_{ci}\right)N_p,$$ [6-13]

and

$$U_d = D_A - \left(A_{sf} - A_{si}\right) - \left(A_{df} - A_{di}\right) - \left(A_{bf} - A_{bi}\right),$$ [6-14]

where A is the amount (M) of a nutrient in the crop A_c, in the supply tank A_s, in the
drainage tank A_d or in the sand bed buffer A_b, N_p is the number of plants in the growth

system, D_A is the amount (M) added to the system as dosage, and subscripts i and f refer to the initial and final amounts, respectively.

The deviation from a perfect mass balance is expressed as the dimensionless quantity L

$$L = \frac{U_d - U_a}{U_a}.$$ [6-15]

The mass balance is perfect when $L = 0$. When $L > 0$ the depletion from the system is larger than the accumulation in the crop, and when $L < 0$ the depletion from the system is smaller than the accumulation in the crop.

In order to indicate *the effect of the buffer of the sand bed* on the mass balance, the depletion will be given either with or without the buffer data. For this purpose *the depletion without the sand bed buffer data*, U_{d-}, is given by

$$U_{d-} = D_A - \left(A_{sf} - A_{si}\right) - \left(A_{df} - A_{di}\right),$$ [6-16]

so that from Eqs. [6-14] and [6-16]

$$U_d = U_{d-} - \left(A_{bf} - A_{bi}\right).$$ [6-17]

The *deviation from a perfect mass balance without considering the sand bed buffer* data, L_-, is given by

$$L_- = \frac{U_{d-} - U_a}{U_a}.$$ [6-18]

The changes in the buffer of the sand bed were determined by analysing sand samples, taken at several locations at three depths, on total content of the different nutrients. Some sand samples were also used to determine the nitrogen and potassium content in a 1:2-by-volume extract, which is considered as an alternative for the buffer content. The measured concentration in the extract solution is transformed into an actual substrate solution concentration by multiplying it with a dilution factor F_d. The dilution factor F_d is obtained as follows. The procedure of the 1:2-by-volume extraction method is to add so much substrate sample at given volumetric water content θ ($L^3 L^{-3}$) to a known volume V_w (L^3) of water, such that the final volume of the mixture equals $1.5V_w$. The substrate sample contains also air, but this does not increase the total volume of the wet mixture. Thus more than $0.5V_w$ volume of the substrate sample has to be added to the water, i.e. $0.5\theta V_w/(1-\phi_a)$, where ϕ_a is the air-filled porosity ($L^3 L^{-3}$). The total amount of water in the mixture is equal to $V_w + 0.5\theta V_w/(1-\phi_a)$, and F_d is given by

$$F_d = \frac{\dfrac{0.5\,\theta V_w}{1 - \phi_a} + V_w}{\dfrac{0.5\,\theta V_w}{1 - \phi_a}} = 1 + \frac{2\left(1 - \phi_a\right)}{\theta}. \qquad\qquad [6\text{-}19]$$

The 1:2 by volume extraction data are only relevant when all N and K are present in the substrate solution and not adsorbed or incorporated in organic matter. At the end of the 'Growth & Uptake' experiment the organic matter of the four plots was on average 0.065%, which is low compared to typical agricultural soils which can have organic matter contents of a few percent. The average cation exchange capacity (CEC) of the sand at the end of this experiment was 0.733 cmol+ kg^{-1}. This CEC is low compared to typical agricultural soils (see e.g. Bolt *et al.*, 1978). For comparison, the total desired cation concentration in the root zone for lettuce is 23 mmol+ l^{-1} (Sonneveld and Straver, 1988). Assuming an average volumetric water content of 0.25 cm^3 cm^{-3} and an average dry bulk density of 1700 kg m^{-3}, this amount of cations corresponds to 0.338 cmol+ kg $^{-1}$ of the adsorption complex. Thus the small CEC may be important in the present context. The total amount of Ca and Mg present in the coarse sand was large. I assume that these naturally present di-valent ions occupy the adsorption complex, so that adsorption of the nutrients in solution does not occur.

Results
In general, for all nutrients, the treatments applied in the 'Growth & Uptake' experiment had no effect on the mass balance and its several components. Two exceptions are the depletion U_d for K and Mg. The depletion for K and Mg in plots I and II, with fertigation only between the rows far from the drain, was larger than in plots III and IV. I have no explanation for this. I decided to give only averages for the four plots for all nutrients (Tables 6-6, 6-7).

   The variation in nutrient uptake, U_a, was less than 8% for all nutrients, except for Cl (16.5%). The depletion of nutrients from the system, U_d, showed much more variation between the four plots, with the variation coefficient ranging from -166% for Na to +95% for P. For N the total content of the sand before and after the experiment was very low, i.e. near the detection limit. Since these data are accompanied with a large uncertainty, I set the change in buffer content for N equal to zero, so that $U_d = U_{d^-}$. For nutrients N, K, P, and Mg, U_d was larger than U_a. For Ca, S and Na U_d was negative and U_{d^-} was positive. This indicates that the change in buffer content was extremely large, and more than the total amount added D_A. Thus there was an unexplainable gain of Ca, S and Na. The laboratory techniques used to determine S and Na in soil samples are accompanied with a large uncertainty, which might explain the S and Na data. Ca can be determined accurately. However, the sand was rich in CaCO$_3$. If CaCO$_3$ was heterogeneously present in the sand, sampling errors may have caused the large differences in buffer content between the start and end of the experiment. For all nutrients the change in buffer content had a large impact on the depletion results. The effect differed per plot, resulting in large

standard deviations for U_d. The change in buffer content was negative for K, P, and Mg, and positive for Ca, S, Na, and Cl. A smaller content at the end is unexpected. Prior to the experiment, the sand beds were flushed with water, so that the initial content was small. At the end, the substrate is filled with a nutrient solution and with biomass, so that the final buffer content is expected to be larger than the initial content. No good explanation can be given for the observed decrease in buffer content.

Based on the 1:2-by-volume extraction method, the N and K content had increased. The U_d based on these results, however, then became smaller than U_a.

Table 6-6 Average uptake by lettuce grown on four irrigated sand beds U_a (mmol m^{-2}), average amounts of nutrients supplied to the system, D_A (mmol m^{-2}), and the average depletion from the sand bed systems with, U_d (mmol m^{-2}), and without, U_{d-} (mmol m^{-2}), considering the changes in the sand bed buffer. Standard deviations are given as ±.

Element	U_a	D_A	U_d	U_{d-}
N[1]	756.5±54.2	1035.5±111.4	1282.1±90.3	1282.1±90.3
N 1:2			357.5±96.5	
K[2]	392.6±31.2	571.6±62.4	2594.5±530.2	673.9±56.4
K 1:2			288.0±61.1	
P[3]	36.1±2.1	267.9±35.3	431.1±56.9	308.7±33.4
Ca	44.9±1.7	222.7±24.2	-4427.8±806.3	294.7±25.1
Mg[4]	23.0±1.4	45.7±4.9	1172.2±794.2	59.8±3.7
S	11.4±0.8	67.3±7.2	-31.9±38.3	86.2±7.4
Na[5]	11.2±0.8	27.5±3.0	-244.2±347.3	49.5±3.0
Cl	15.1±2.5	0.8±0.1	0.2±3.1	10.3±1.8

[1] The total content in the sand bed initially and at the end was near the detection limit, so it was decided to set the change in buffer content equal to zero.

[2] The average depletion in plots I and II was 3052 mmol m^{-2}, in plots III and IV it was 2137 mmol m^{-2}.

[3] U_d based on data of three plots only; fourth analysis was more than 20 times larger (-5103).

[4] The average depletion in plots I and II was 1822 mmol m^{-2}, and in plots III and IV it was 523 mmol m^{-2}.

[5] U_d based on data of three plots only; fourth analysis was negative (-69).

The deviations from a perfect mass balance are extremely large, with a large variation between the plots. For N and K, using the 1:2-by-volume extraction data, the deviations were relatively small but negative. Under very well controlled conditions, e.g. in NFT

systems, it is generally observed that depletion from the system exceeds accumulation in the crop. For the NFT2 experiment the deviations from perfect mass balance are rather small (Table 6-7). In the NFT1 experiment, where the plants grew in small peat press pots and where some leaks occurred during the experiment, the deviations were much larger (Table 6-7). The deviations observed in the sand bed system were much larger than the those observed in the NFT experiments.

Table 6-7 Average deviations from a perfect mass balance L (Eq. [6-15], %) or $L_{\cdot}$ (Eq [6-18], %) (± standard deviation) for lettuce grown in sand beds during the 'Growth & Uptake' experiment compared to values obtained for lettuce grown in Nutrient Film Technique (Heinen *et al.*, 1991: NFT1; Heinen, 1994: NFT2). L for N and K with the change in buffer content based on changes in the 1:2 by volume extraction method are given by N 1:2 and K 1:2, respectively.

Element	Sand bed		NFT1	NFT2
	L	$L_{\cdot}$	L	L
N[1]	69.9±13.5	69.9±13.5	73.8	16.7
N 1:2	-53.0±11.3			
K	565.9±153.8	72.1±16.1	62.7	13.0
K 1:2	-26.9±13.3			
P[2]	1081.1±139.3	755.6±101.0	0.3	21.4
Ca	-9939.8±1480.3	557.5±52.2	222.9	28.4
Mg	5017.2±3544.7	160.7±12.4	230.4	21.4
S	-373.7±335.7	659.4±74.7	555.1	-7.3
Na[3]	-2201.2±3084.8	344.5±29.1	1600.0	-44.1
Cl	-101.1±24.1	-31.3±10.2	-16.8	1.4

[1]　See comment [1] in Table 6-6.

[2]　See comment [3] in Table 6-6; L of fourth sample was -296.

[3]　See comment [5] in Table 6-6; L of fourth sample was -42748.

Possible reasons why, even under well controlled conditions, depletion exceeds accumulation in the crop are: net immobilization, precipitation, adsorption to organic matter and root exudates, system leaks, removal of bad plant material, differences in analyses techniques for solutions, crops and substrate, and in particular for N denitrification and ammonia volatilization. However, net immobilization, precipitation and adsorption should be accounted for when analysing the sand on total content. Thus

it is not very well possible to give a cast-iron explanation why depletion exceeds uptake. Processes which indeed mean an extra loss of N from the system are denitrification and ammonia volatilization. Some measurements to quantify these fluxes were carried out by Postma *et al.* (1994), and the results are summarized in the next section (Subsection 6.6.2).

6.6.2 Gaseous nitrogen losses and denitrification rate

As mentioned above in Subsection 6.6.1, even for well controlled experiments with water cultures, depletion generally exceeds uptake. In this section the results of *in-situ measurements of gaseous nitrogen (N) losses and denitrification rate*, carried out by Postma *et al.* (1994), are summarized (Table 6-8). I determined whether these losses can explain the mass balance error for N as found in the previous section. Measurements were done in plot IV of the 'Water Use' experiment. There was no ammonia volatilization and nitrous oxide emission was negligible. The average denitrification rate was 0.114 mmol m $^{-2}$ d $^{-1}$, ranging from 0.057 mmol m $^{-2}$ d $^{-1}$ to 0.343 mmol m $^{-2}$ d $^{-1}$. High nitrous oxide concentrations in the nutrient solution at the bottom of the sand bed were measured. Apparently, the nitrous oxide is transported downwards with the fertigation water. The estimated average net discharge of N with the draining water was 0.054 mmol m $^{-2}$ d $^{-1}$. On average total N losses were 0.168 mmol m $^{-2}$ d $^{-1}$. The experiment lasted 64 d, hence the total nitrogen loss was 10.75 mmol m $^{-2}$. Compared to the total N uptake of 778.0 mmol m $^{-2}$ in the crop, this total N loss is only 1.4%, which is much smaller than the mass balance error presented in Table 6-7.

Table 6-8 Summary of the gaseous nitrogen losses and denitrification rate measured *in-situ* by Postma *et al.* (1994). Quantities expressed in mol refer to nitrogen N.

NH_3 volatilization	≈ 0	
Denitrification rate	0.114	mmol m^{-2} d^{-1}
N_2O emission	<0.014	μmol m^{-2} d^{-1}
N_2O concentration at depth 1 cm and 7 cm	<1.0	ml m^{-3}
N_2O concentration at 15 cm	100.0	ml m^{-3}
Net discharge N_2O with drained water	0.054	mmol m^{-2} d^{-1}

6.7 Substrate temperature

The measured *substrate temperatures* T at the different plots were alike, and thus only averages over the plots per depth are given (Figure 6-15). The pattern of T changes in the sand bed is, apart from a time lag, directly related to the changes in air temperature (Figure 6-15). As expected, with increasing depth the amplitude of the T fluctuation decreases and the maximum of the amplitude is reached later. During the 'Growth & Uptake' experiment high T in the root zone were recorded. During 14 days of the 42 days the experiment lasted, the maximum T in the root zone exceeded 30 °C, of which during 3 days the maximum T was higher than 35 °C. With respect to growth of lettuce, in the literature different optimum T 's of the nutrient solution were reported. For example, according to van der Boon *et al.* (1990), Ikeda and Osawa (1984), Morgan *et al.* (1980) and Mongeau and Stewart (1984) optimum T 's were 13 °C, 24 °C, 25 °C and 30 °C, respectively. These differences in optimum T 's may be due to differences in climatic conditions and cultivars. In all cases the optimum T is lower than the T 's observed in this summer experiment. Thus crop growth may have been negatively affected by the high temperatures in the root zone.
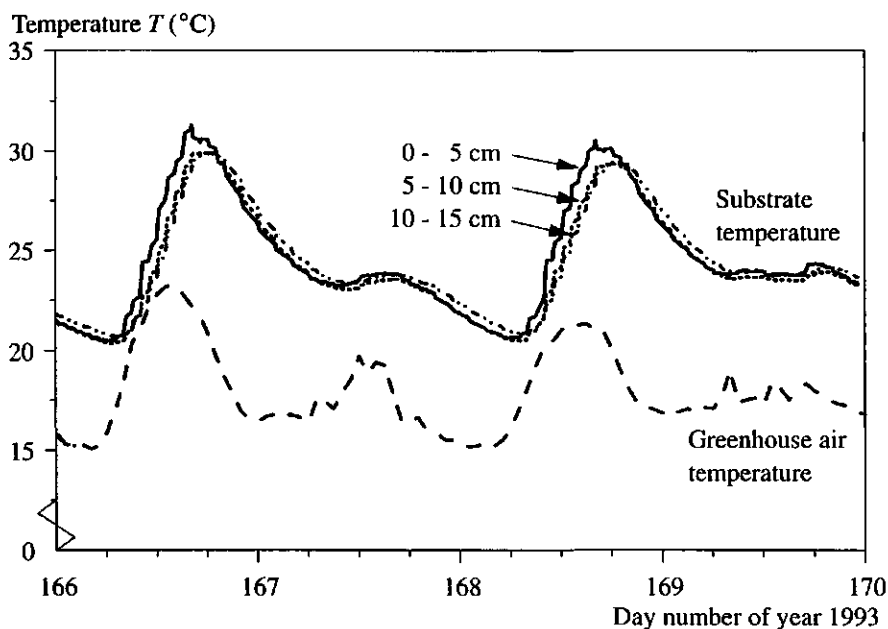
Figure 6-15   Substrate temperature measured at three depths and air temperature inside the greenhouse at approximately 1 m above the sand bed surface as a function of time.

6.8 Measured electrical conductivity

Electrical conductivity (*EC*) measurements according to the method described in Subsection 5.2.2 were carried out only during the 'Water Use' experiment. However, during this experiment in autumn ample nutrient solution was supplied twice per day between all rows of the plants. In this way salt accumulation is not likely to occur. Accordingly, *the measured bulk electrical conductivity EC_b and computed water electrical conductivity EC_w* show a gradual decrease in time (Figure 6-16). The average EC_w lies in the range of 1.3 to 1.8 dS m^{-1}. This range will be compared to available data of the *EC* of the nutrient solution. On days 291, 308 and 334, the *EC*'s of the nutrient solution in the supply vessel prior to addition of fresh nutrient solution was 1.7, 1.9 and 1.8 dS m^{-1}, respectively. On day 291 the *EC* of the drainage water in the drain vessel was 1.7 dS m^{-1}. After resupplying fresh solution to the supply vessel, the *EC* of the nutrient solution in the supply vessel was 2.3 dS m^{-1}. Thus, EC_w in the root zone was lower than the *EC* of the nutrient solution. The resupply of fresh nutrient solution on day 308 caused a small increase in EC_b and EC_w (Figure 6-16). The increase is only small due to the large buffer of nutrient solution in the sand bed.

The EC_b increased with depth. From the computed EC_w data it follows that the middle layer had the highest EC_w while the top layer had the lowest EC_w. Based on the primarily upward movement of nutrient solution in the root zone, evaporation occurring at the sand bed surface, and uptake occurring at a lower concentration than that of the fresh nutrient solution, it is expected that the concentration of nutrient solution increases towards the sand bed surface. The data, however, do not indicate that. The data refer to a depth of 2.5 cm, so that the surface EC_w is not known. Moreover, it has not been verified whether the Mualem-Friedman (1991) model, Eq. [5-10], is valid for this substrate. The large deviations of EC_w which were not observed in EC_b are due to the scatter in measured θ.

The *EC* data must be considered with care. At the end of the experiment the exact location of the TDR probes was determined by carefully digging them out. It appeared that the rods of almost all probes did not run parallel to each other. This means that the cell constant k_p (Eq. [5-2]) is no longer valid for the probe, and, therefore, the measured *EC* data are wrong.

The effect of diverging or converging rods of the TDR probe on measured dielectric permittivity K_a is negligible as was determined in the laboratory on both air and water measurement.

Bulk electrical conductivity EC_b (dS m⁻¹)
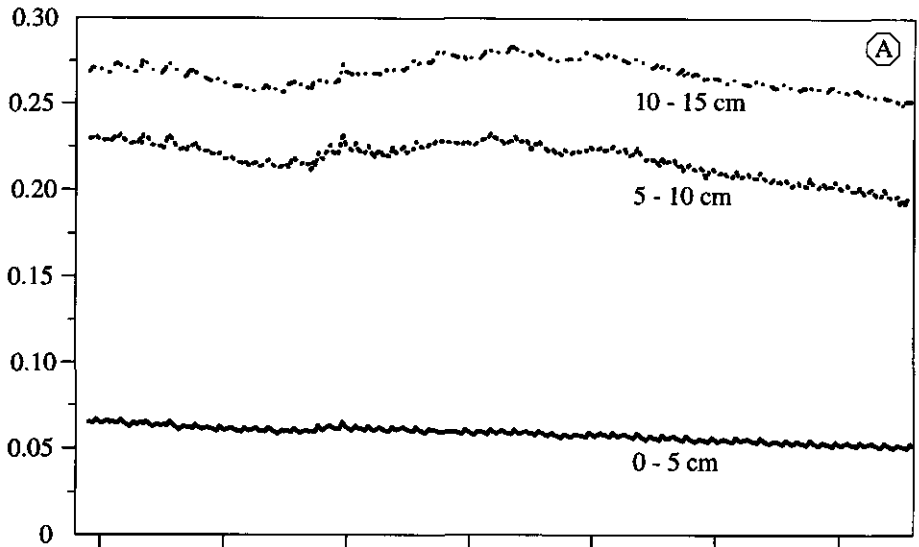
Water electrical conductivity EC_w (dS m⁻¹)

Day number of year 1993
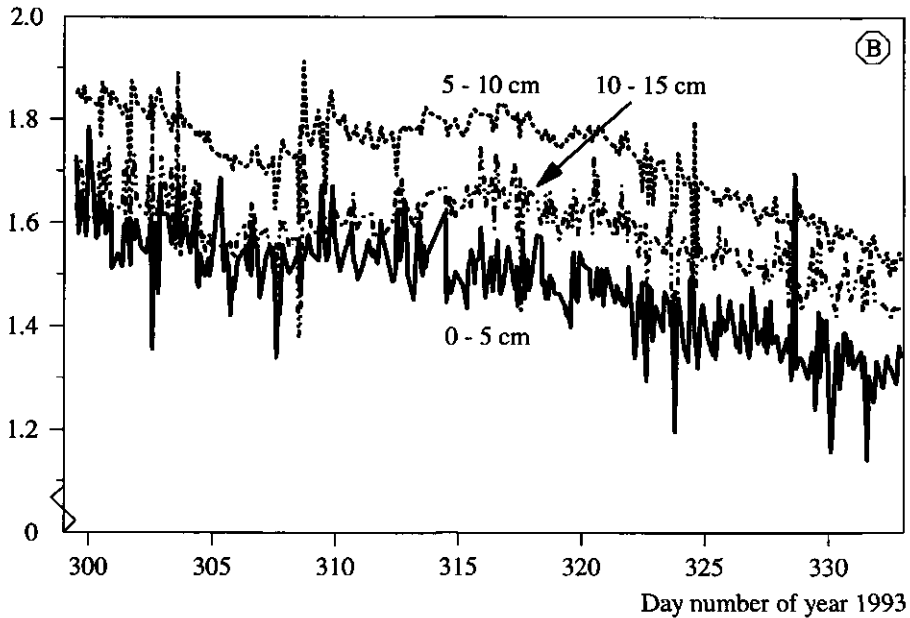
Figure 6-16   (A) Substrate bulk electrical conductivity EC_b as measured by TDR, and (B)
substrate solution electrical conductivity EC_w calculated according to Eq. [5-11]
at depths of 0-5 cm, 5-10 cm and 10-15 cm as a function of time. EC_w data are
smoothed data, i.e. averages of each data point and its two neighbors in time.

6.9 Conclusions

In this chapter I have presented growth, rooting characteristics, and water and nutrient balances for lettuce grown in irrigated sand beds.
The following conclusions are drawn.

- Dry matter production of lettuce grown in irrigated sand beds can be well described by a logistic growth function.
- Dry matter production as a function of time was equal to that obtained for lettuce in nutrient film technique experiments of Heinen *et al.* (1991) and Heinen (1994), when the initial weights of the crops were set equal. However, nutrient uptakes in the two systems were different. This may be caused by differences in lettuce cultivar used in the two growth systems. So, no definitive conclusions can be drawn about the hypothesis that growth and uptake by a crop is system independent.
- Especially for summer growth periods, restricted supply of fertigation water had a negative effect on crop production. When the dripper density is equal to the planting density - with drip lines between all crop rows - no row effects were observed. Highest production was obtained when the surplus of fertigation water added was 2 times the estimated evapotranspiration.
- Dry matter production as a function of cumulative radiation showed less correspondence between the sand bed and NFT data. A better agreement was obtained when expressed as a function of heat sum.
- The low final dry weight of lettuce observed in the sand bed system, as compared to literature data, may be due to the high root zone temperatures.
- The cumulative uptake of nutrients can be well described by a logistic function. The relative cumulative uptake of N and K is equal to the relative dry matter production, i.e. the contents of these elements in the crop remain constant in time. Thus dry matter production can be used to estimate N and K uptake.
- The high final nitrate content of the lettuce head was already observed after one third of the total growth period.
- Determination of root length density (Schwarz *et al.*, 1995) showed that a homogeneous supply of water resulted in a more even horizontal distribution of roots, than when water was given less evenly distributed. Most roots were present in the top 10 cm.
- Bedding systems result in a large contribution of substrate surface evaporation to the total amount of water used during the growth period, especially in the beginning of the growth period. This affects the spatial distribution of water and nutrients in the early stages of growth. It may result in fast increases in concentration near the root surface and consequently may be harmful to the small root system present there.
- A good exponential relationship was obtained between the contribution of potential transpiration to potential evapotranspiration as a function of fractional substrate coverage. This relationship makes it possible to estimate potential transpiration based on easily measured total water use and fractional substrate coverage.

■ It was not possible to set up a perfect mass balance for all nutrients. An uncertain factor in the mass balance is the large buffer in the substrate.

■ Denitrification measurements by Postma *et al.* (1995) yielded only small losses of nitrogen from the cropping system, which could not explain the gap in the mass balance of nitrogen.

■ Covering the sand bed with plastic to prevent evaporation from the sand surface did not result in different dry matter production compared with production in uncovered sand.

Chapter 7

Root zone conditions : measurements and simulation

In this chapter I will compare simulated data using the water movement and solute transport model of Chapters 2 and 3 with experimental data. In Section 7.1 a short overview is given of the input parameters used in the simulation model, most of these data coming from Chapters 4 and 6. The *in-situ* water retention characteristics (Section 7.2), and some typical observed time courses in volumetric water content θ (Section 7.3), and pressure head h (Section 7.4) will be shown. In Section 7.5 a parameterization of the solute module is presented based on a breakthrough experiment. The measured θ and h originate from the 'Growth & Uptake' experiment. Simulations were carried out for half the region between two drains (see Figures 1-1B and 2-1). A period of twelve days during the 'Growth & Uptake' experiment was chosen for which simulations were carried out, of which the first two days were assumed to be the starting period. The choice of the initial status is discussed at the end of Section 7.2. If not indicated else, the simulation results refer to the ' α_d-*data interpolation method*' hysteresis model (Chapter 4). Where amounts are given, they refer to a vertical slab of the sand bed with x, y, z dimensions of 40 cm, 1 cm and 15 cm, respectively, i.e. to a volume of 600 cm^3. In order to reduce the amount of information, I decided to use data from plot II only, i.e. the treatment with only drip lines far from the drain and with a leaching fraction of $LF = 0.5$.

7.1 Short description of input parameters used

in the simulation model

All input parameters used by the simulation model are listed in Appendix 6. Some specific parameters are discussed in the following.
Top boundary conditions
Drip irrigation at $(x,z) = (30$ cm, 0 cm) is simulated as known flux density across a 5 cm^2 area represented by two control volumes in layer 1. At the remaining top control volumes evaporation occurs. Irrigation and evaporation are discussed in some more detail below.
Irrigation
The times, duration and exact amounts of water given per irrigation are known. The average dripper rate is 23 ml min^{-1}. The drippers are separated 30 cm in the y-direction. Since the y-direction is excluded in the simulation model, the drip lines are assumed to consist of equally spaced drippers at 1 cm interval, each with a dripper rate of 1/30th of the actual dripper rate. With the dripper area being 5 cm^2, the irrigation rate is 23/(5*30) $= 0.153$ cm min^{-1}. The duration of irrigation in plot II was 31 min.

Transpiration and evaporation
The daily potential transpiration data obtained in Chapter 6 are used as input. I assume that transpiration occurs during day-time only. For the spring season I assume this to be from 6:00 h until 20:00 h. Since no daily pattern in time is known, it is kept constant during this 14 h period. The rate is total potential transpiration divided by length of day time. Transpiration also occurs during the fertigation period. Evaporation occurs at all control volumes of the top layer, also during the fertigation period.

Bottom boundary condition
From earlier simulation runs it appeared that there was almost no difference in predicted phreatic level when the seepage drain was represented as 2 or 10 nodes; using 1 node to represent the seepage drain resulted in a different position of the phreatic level. Therefore, I use 2 nodes to represent the seepage drain, i.e. the nodes of the first and second control volume at the left of the bottom layer. The remaining control volumes of the bottom layer are regarded as no-flow boundaries.

Initial condition
I assume the substrate to be in equilibrium with the bottom nodes, with no horizontal gradients in pressure head h. The choice of the initial level of h will be discussed in Section 7.2.

Solution procedure
The ADI method is used when the system is completely unsaturated, and the ICCG method is used when partial saturated conditions occur. For safety reasons, the switch between the two solution methods occurs not when somewhere in the flow domain h becomes ≥ 0 cm, but when $h \geq -0.5$ cm.

Root length density
The final root length density $L_{rv,f}$ of lettuce grown in spring was published by Schwarz *et al.* (1995). I account for root growth by assuming a logistic growth function (cf. Eq. [6-2]) with these measured values as the maximum W_f. Equation [6-2] combined with Eq. [6-4] is here written as

$$L_{rv}(t) = \frac{L_{rv,f}}{1 + e^{-k_L(t - t^*)}}, \qquad [4\text{-}1]$$

where t is the time since the start of root growth in the sand bed. The inverse time constant is set equal to that for shoot growth: $k_L = 1.498$ min^{-1} (Table 6-2), and the time of inflection is set equal to halfway the total growth period: $t^* = 30240$ min. Note that in Eq. [7-1] the initial L_{rv} is not present, as it is embedded in t^*.

7.2 *In-situ* water retention data

I start with presenting the *in-situ water retention characteristics* as obtained from the 'Growth & Uptake' experiment in the sand beds. Both volumetric water content θ and pressure head h were measured at comparable positions, at depths of 2.5 cm, 7.5 cm, and
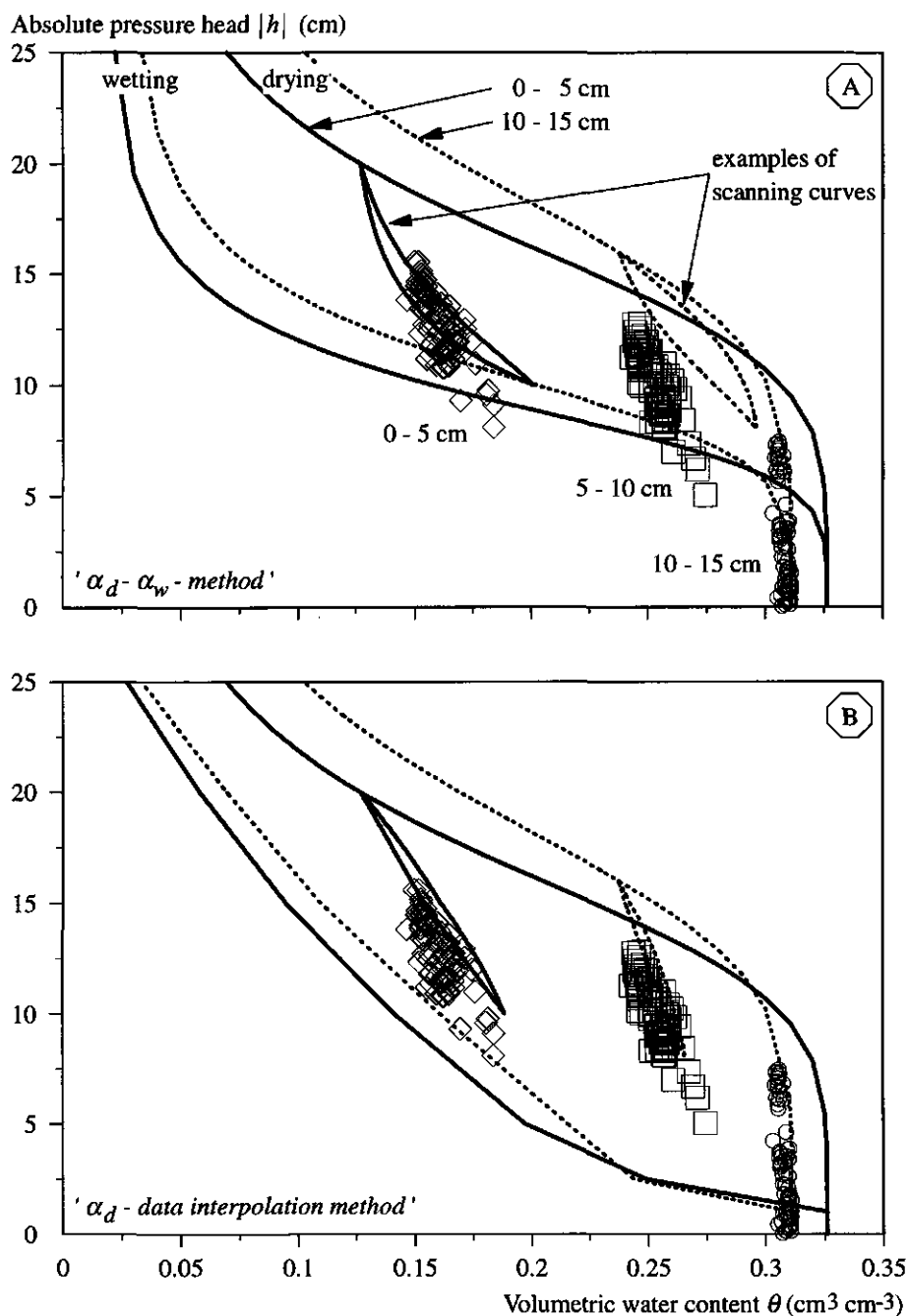
Figure 7-1 *In-situ* water retention characteristic measured at depths of 2.5, 7.5 and 12.5 cm compared to the water retention characteristics obtained in Chapter 4: (A) ' α_d-α_w-method', and (B) ' α_d-data interpolation method'.

12.5 cm. All data from two consecutive days, both with fertigation, are presented in Figure 7-1. The data at each of the three measurement depths are clustered. Since frequent fertigations took place, at each depth the ranges of h and θ are small. These data should be compared with the water retention characteristics as obtained in the laboratory (Chapter 4). Later in this chapter, the measured time courses of θ and h will be compared with simulated data. The simulated data are mainly determined by the water retention characteristics used as input. The main drying and wetting curves of the 'α_d-α_w-*method*' hysteresis model presented in Chapter 4 do not enclose entirely the experimental data (Figure 7-1A). The two examples of scanning curves are given for demonstration purposes only. In Chapter 4 it was also mentioned that the 'α_d-α_w-*method*' model was not doing well in describing the laboratory obtained wetting data. The 'α_d-*data interpolation method*' hysteresis model, proposed as the alternative method in describing the wetting curve, results in a much better description of the observed *in-situ* $\theta(h)$ characteristics (Figure 7-1B): all experimental data are enclosed by the main drying and main wetting curves. From Figure 7-1 it is clear that the results obtained with the 'α_d-α_w-*method*' model will not describe the observations very well, and that it will result in too wet conditions.

Note that the experimental data at depth 0-5 cm should be compared with the solid lines, and the data at depths 5-10 cm and 10-15 cm with the dotted lines. The given scanning curves are not optimized curves based on observations, but are chosen such that they more or less are close to them. They originate at the main drying curves at $h = -20$ cm or -16 cm, and return there after a reversal at $h = -10$ cm, or -8 cm, respectively.

The experimental $\theta(h)$ data are used to obtain a reasonable initial condition in h, used as input for the simulation model. The restriction of the simulation model is that only initial conditions on either the main drying or on the main wetting curve can be considered. Initial conditions somewhere inside the $\theta(h)$ domain are not possible, since then the history should be known and input as well. It is expected that, due to the wet conditions during the experiment, near unit h-gradient conditions exist (verified in Subsection 7.4.2). Thus a choice of initial h-condition could be a h-profile in equilibrium with $h = 0$ cm at the bottom. However, from Figure 7-1 it becomes clear that when $h = -15$ cm at the top of the sand bed, it will be impossible to describe the observed data at $z = 2.5$ cm. I decided to chose initial conditions on the main drying curve, so that expected scanning wetting curves originating at these points go through the *in-situ* $\theta(h)$ data. The initial h-distribution was in equilibrium with $h = -8.5$ cm at the bottom of the sand bed. In one case, simulation results for an initial condition with $h = -1$ cm at the bottom will be given as well (Subsection 7.3.2).

This choice of initial condition biases the simulation outcome. An unique initial condition can only be obtained by starting the simulation when the sand beds were filled with air-dry sand. The simulation must then take care of the total history of water supply and withdrawal, inundations, drying out between experiments, changing hydraulic properties due to changing in bulk density etc., which can practically not be done.

7.3 Water content

7.3.1 Measured

During fertigation *the volumetric water content θ measured by TDR* increased up to 0.05 cm^3cm^{-3} in the top layer, in the bottom layer there was almost no change (Figure 7-2). Fertigation was controlled automatically (Section 5.3); fertigation was initiated whenever water loss by evapotranspiration *ET* was approximately 1.5 mm. In all cases 30% or 100% more water was applied than this estimated *ET*, hence drainage occurred following each fertigation. Even under these wet conditions the top 5 to 10 cm did not become water saturated. The bottom 5 cm, however, was always very wet; with a porosity $\phi_p = 0.351$ cm^3cm^{-3} (Subsection 4.3.1), air-filled porosity was about 0.05 $cm^3 cm^{-3}$. Under these conditions aeration problems may exist. With respect to nitrogen this may cause denitrification. However, Postma *et al.* (1994) observed only small gaseous losses of nitrous oxide at the soil surface in an autumn period (Subsection 6.6.2). At the bottom of the sand bed high nitrous oxide concentrations were measured, and nitrous oxide leached from the sand bed with the draining water.
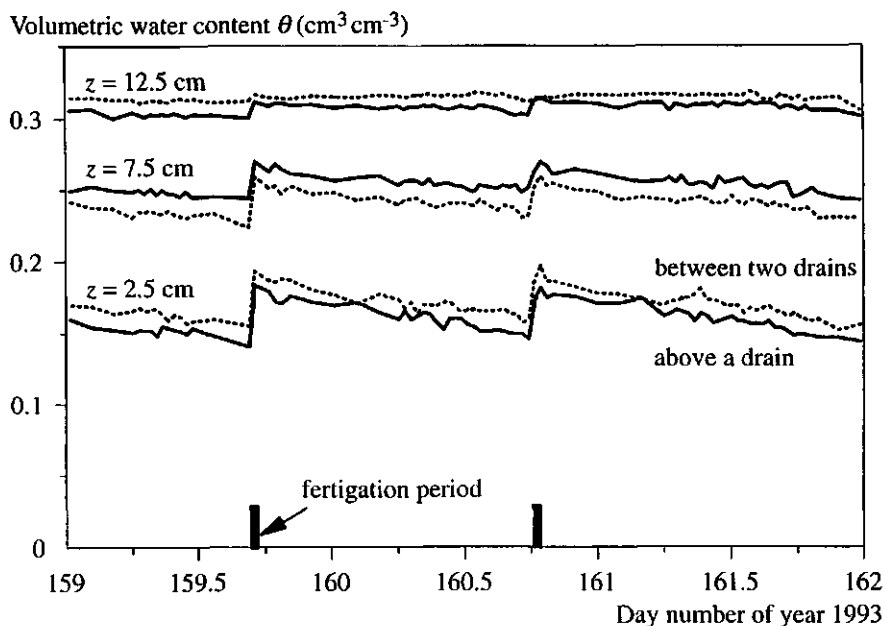
Figure 7-2 Volumetric water content measured with TDR at three depths of 2.5, 7.5 and 12.5 cm at positions above a drain and between two drains as a function of time. Each line represents the average of two sensors in plot II. The vertical bars indicate the duration of the fertigation period.

The *differences in* θ *between positions above a drain and between drains* are small. At a given depth the time courses above a drain or between the drains are similar. The differences of θ between and above a drain at comparable depths remain more or less constant in time. One would expect the positions between drains to be wetter than positions above a drain, since during drainage a phreatic surface develops which is highest midway between the drains, and because also at that position water is applied. However, in the middle layer it is wetter above the drain. Differences may be due to local differences in bulk density, differences in installation depth of the TDR probes, differences in history of changes in volumetric water content causing the water contents at different points to arise from different scanning curves. Differences in average installation depth alone could not explain the observed differences for the middle layer.

7.3.2 Simulated

Simulated time courses of θ for the same period as in Figure 7-2 are given in Figure 7-3, for the cases ' $\alpha_d - \alpha_w$ *-method*' and ' α_d *-data interpolation method*'. The simulated profiles based on the ' $\alpha_d - \alpha_w$ *-method*' do not agree with the measured profiles. The volumetric water content θ is underestimated in the upper layer, and overestimated in the middle layer. The latter can be attributed to the shape and position of the scanning curve. This can be seen in Figure 7-1A, where the dotted scanning curve points towards the wet side and as a result the corresponding value of $d\theta/dh$ is too large. The ' α_d *-data interpolation method*' case, on the other hand, describes the observed $\theta(t)$ profiles rather well. It slightly overestimates θ in the middle layer. The observed rises in θ during fertigation are predicted well, and the decrease in θ during the day due to *ET* is predicted well too. Thus, with respect to θ, the ' α_d *-data interpolation method*' must be preferred over the ' $\alpha_d - \alpha_w$ *-method*'. In the bottom layer there is almost no temporal variation in θ, not even during a fertigation period. This is due to the steepness of the $\theta(h)$ characteristic near saturation: for a large range of h, θ hardly changes. For example, when θ decreases 0.01 $cm^3 cm^{-3}$ beginning at θ_s, h decreases according to the main drying curve from 0 to -8.7 cm (0-5 cm) or -10.0 cm (5-15 cm). Assuming near unit h-gradient conditions (see Subsection 7.4.2) then $h = -2.5$ cm in the middle of the bottom layer, provided $h = 0$ cm at the bottom, and thus near saturated conditions exist there.

The *difference in* $\theta(t)$ *for positions above a drain or between two drains* obtained with the simulation model using the ' α_d *-data interpolation method*' is demonstrated in Figure 7-3B. As expected, at all times it is wetter at positions between two drains than above a drain. However, the differences are small as was also indicated by the measurements (Figure 7-2). In this particular example, the difference increases during a fertigation-drainage period in the top two layers, but decreases at the bottom layer. Whether this difference increases or decreases depends on differences in C, K, and ∇h at the two positions.

Volumetric water content θ (cm^3 cm^{-3})
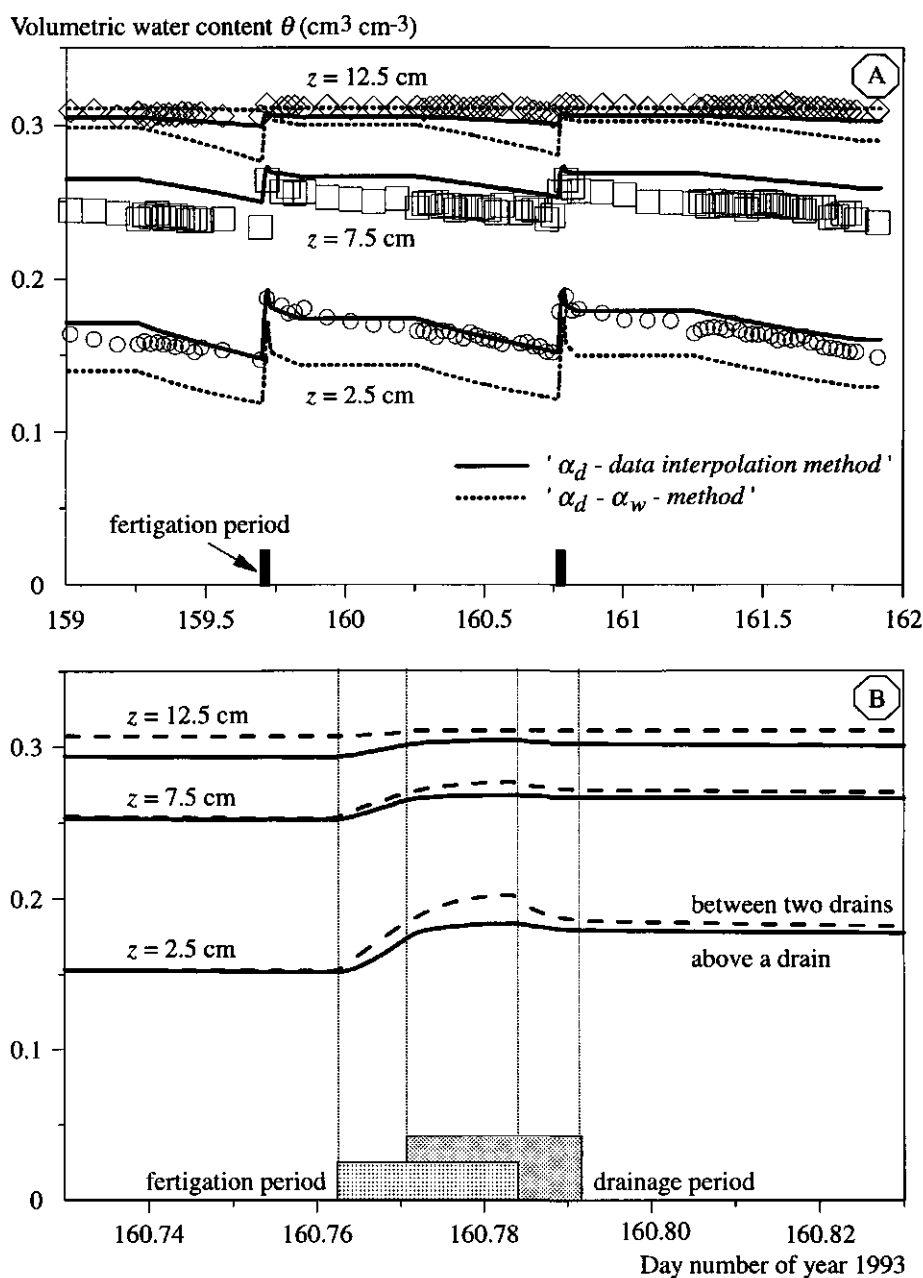
Figure 7-3 (A) Simulated volumetric water contents, using either the 'α_d-*data interpolation method*' or 'α_d-α_w *method*' hysteresis models, compared to experimental data at depths 2.5, 7.5 and 12.5 cm for plot II. The bottom part (B) shows a detail of the time course of volumetric water content during a fertigation-drainage event showing the differences for positions above a drain or between two drains.

The *simulated spatial distribution of θ* in the sand bed is shown in Figure 7-4 prior to the
start of a fertigation (Figure 7-4A) and at some time during the period of fertigation and
drainage (Figure 7-4B). Prior to the start of fertigation, $θ(x)$ at given z is about constant,
except deeper in the sand bed, where above the drain $θ$ decreases. This is due to
differences in history of the flow process (hysteresis). It cannot be concluded from Figure
7-4A that there is horizontal flow from right to left, since water does not flow due to a
gradient in $θ$. In fact, there is no horizontal movement at that time as will be seen from
the h distribution in Subsection 7.4.2. During fertigation $θ$ increased below the dripper.

With the simulation model additional information about the root zone conditions can be
obtained. The *total amount of water stored in the root zone* of the simulated profile
(40x15x1=600 cm^3) is presented for four cases: the ' $α_d$-*data interpolation method*', the
' $α_d$-$α_w$-*method*' for two initial conditions with h = -8.5 cm (1) or h = -1 cm (2) at the
bottom, and for the case when hysteresis is not included (Figure 7-5). The non-hysteretic
case results in much wetter conditions. The maximum water storage after a fertigation is
close to the maximum storage based on $θ_s$ (= $φ_p$-0.04). The wet initial condition
(' $α_d$-$α_w$-*method*', 2; results only for first three days) resulted in a wetter profile than the
drier initial conditions. After each fertigation the final amount of water storage is
approximately the same (Figure 7-5A). The rapid increase in water storage during
fertigation is followed by a rapid decrease mainly caused by drainage, which in turn is
followed by a slower decrease caused by evapotranspiration. In detail (Figure 7-4B), four
stages can be considered: a period with evapotranspiration ET only, a period with
irrigation I and ET, a period with I, ET and drainage D, and a period with ET and D.
Drainage occurs in a short period after the start of irrigation (see later in this section). Just
before the start of fertigation the total amount of water differs between the several
occasions, because the method of estimating *ET* was not calibrated for lettuce grown on
sand beds. *ET* was, however, never underestimated too much, and at all times drainage
(see later in this section) occurred. The results of the simulations where hysteresis is
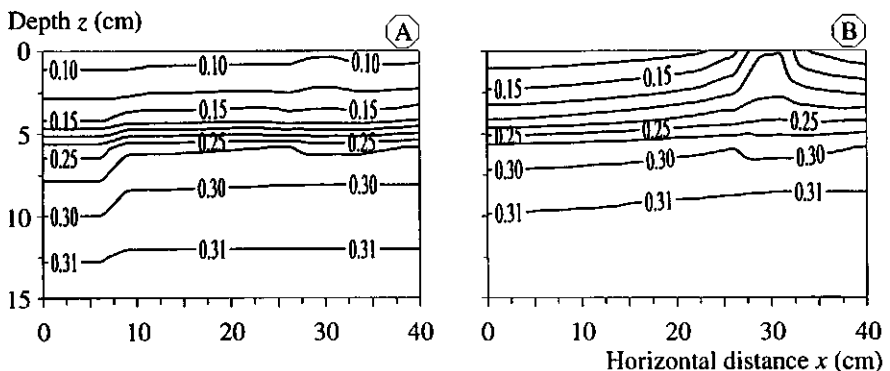
Figure 7-4 (A) Simulated distribution of volumetric water content $θ$ for two times: just before
the start of a fertigation period, and (B) some time during the combined fertigation-
drainage event.
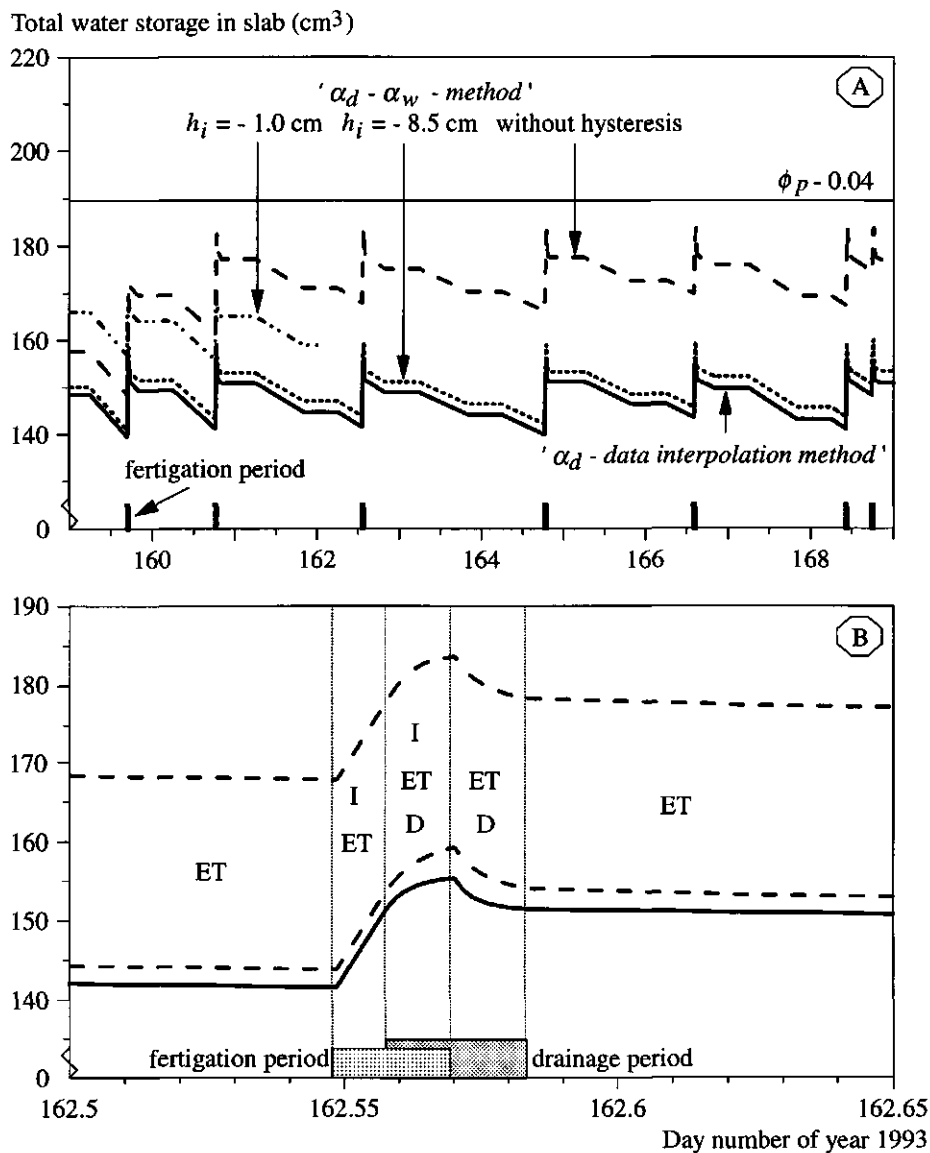
Figure 7-5 (A) Simulated time course of total water storage in the region between two drains for four cases: 'α_d-*data interpolation method*', 'α_d- α_w-*method*' with initial equilibrium *h* distribution with *h* = -8.5 cm (1) or *h* = -1.0 cm (2) at the bottom, and for the case when hysteresis is not included. The maximum storage based on ϕ_p-0.04 is given as a horizontal line. In (B) a detail is given of the time course of change of total storage around a fertigation-drainage period, showing four stages: 1) with evapotranspiration ET, 2) with irrigation I and ET, 3) with I, ET and drainage D, and 4) with ET and D.

included indicate that during the ten day period total water storage is on average constant, so that a starting period of the simulations of two days is sufficient. For the non-hysteretic case, the total water storage still increases during days 159 and 160, indicating that the starting period of two days is not enough. In general, *hysteresis resulted in drier conditions* in comparison with simulations using only the main drying curve, not just for the total water storage, but at all positions in the flow domain. This is, with respect to aeration, a benefit of hysteresis for the use of coarse substrates, even when frequent fertigation occurs.

The simulated *cumulative amount of drainage water* compares well with measured amounts (Figures 7-6). For the non-hysteretic case, due to the wetting up during days 159 and 160 (see Figure 7-5), the outflow starts later, but the difference in predicted outflow stays approximately the same from day 161 onwards. On average, the simulations with hysteresis included fits measured outflow well (Figure 7-6A), but not during each drainage period (Figure 7-6B). Simulated outflow occurs somewhat earlier in time. The decreasing rate of outflow in course of time, as observed in the experimental data, is not simulated. That the actual drainage occurred later in time than the simulated drainage is due to the facts that the water leaving the substrate had to travel from the bottom of the plot to the drain tank through the collecting drain pipe, and that the anti-rooting mat between the substrate and the drains (Chapter 5) has a resistance to flow, which was not considered in the model.

There are several other reasons why simulated and measured drainage differ. Since measurements of the water level in the drainage vessels were carried out at regular time intervals, the true maxima and minima of the levels just before and after pumping the excess drainage water to the supply vessel were not known[1]. The data of Figure 7-6A were obtained from the supply vessel. Drainage in that case is equal to the assumed amount of irrigation, i.e. delivery rate as determined at the start of the experiment times irrigation time, minus the differences in water level in supply and drainage vessels before the start of irrigation and end of drainage. Equipment errors of pumps, valves and clogging of drippers have influence on this method. The true irrigation amount could not be measured, since the lowest water level in the supply vessel could not always be determined due to the discrete times of measurements and to the fact that during irrigation also excess drainage water could be added to the supply vessel, so that a wrong minimum would have been used. Besides these experimental problems, also the model input has errors. In Chapter 6 (Sections 6.3 and 6.4) a method was proposed to obtain T out of the measured ET. The actual T, and thus E, may have been different, and thus the exact distribution of removal of water from the sand bed may have been different for the simulated and actual cases. For example, if at day 159 the actual E was greater, and thus T was less, than was used in the model, the sand bed surface was drier just before the start

---

[1] The method was improved at the beginning of the 'Water Use' experiment, so that the results from that experiment, Section 6.3, are more reliable.

Cumulative outflow from drain (cm^3)
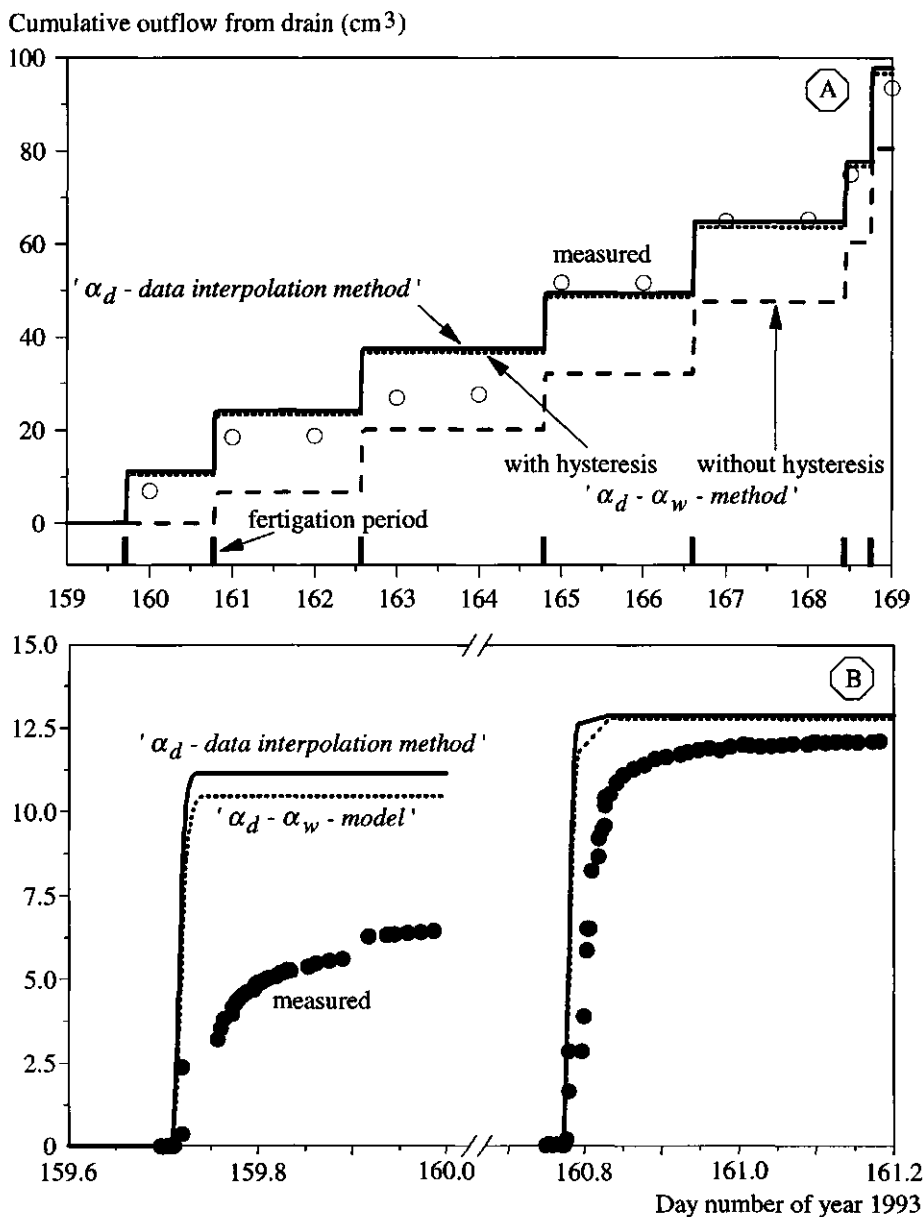
Figure 7-6 (A) Time course of cumulative outflow from half the region between two drains for the hysteretic, both the 'α_d-*data interpolation method*' and 'α_d- α_w *method*' cases, and non-hysteretic simulations compared to experimental data. The vertical bars indicate the duration of the fertigation period. In (B) a detail of simulated and measured outflow from half the region between two drains, for days 159 and 160 is given.

of irrigation. Then, during irrigation and just after it, more water would flow more towards the sand bed surface, and less drainage would occur.

With the simulation model, the flux densities across the control volume interfaces can be easily computed, and from that at each node the net flux density can be calculated. The *net flux density distribution*, with hysteresis included for the ' α_d-*data interpolation method*', at four times around the fertigation period at day 162 is presented in Figure 7-7[2]; note that the length scale of the arrows in parts A and D are different from that in B and C. Just before the start of fertigation when only evapotranspiration occurs (Figure 7-7A), there is upward movement of water. There are horizontal components in the fluxes which are due to a distributed root water uptake, since water movement is towards regions with high root length density. When there is irrigation, but not yet drainage (Figure 7-7B), there is downward movement of water below the dripper and water moves away from this region, causing upward movement at the left. A *saturated zone* develops quickly and drainage starts and water movement is towards the drain (Figure 7-7C). The saturated zone reaches its maximum at $(x, z) = (40.0$ cm, 11.32 cm) at the time when irrigation stops. The height of the phreatic level is computed by linear interpolation of h between two neighbouring nodes, one with $h < 0$ cm and the other with $h > 0$ cm. After irrigation stops (Figure 7-7D), the saturated zone decreases quickly. Even with a small saturated zone, there is a large region where water movement is towards the drain. The saturated zone vanishes in the time interval $t = 840$-900 min, and a similar situation as in Figure 7-7A develops again. Relatively stagnant regions are located at the upper left, upper right, and lower right corners of the sand bed system. However, it is remarkable to see that there is significant water movement towards the upper corners during the stage of irrigation only (Figure 7-7B). How this affects the nutrient distribution will be shown in Chapter 8.

---

[2]   The flux density distribution graphs were constructed from x, y, F_x, and F_z data with the help of the graphical program XY of van Heerden en Tiktak (1994).
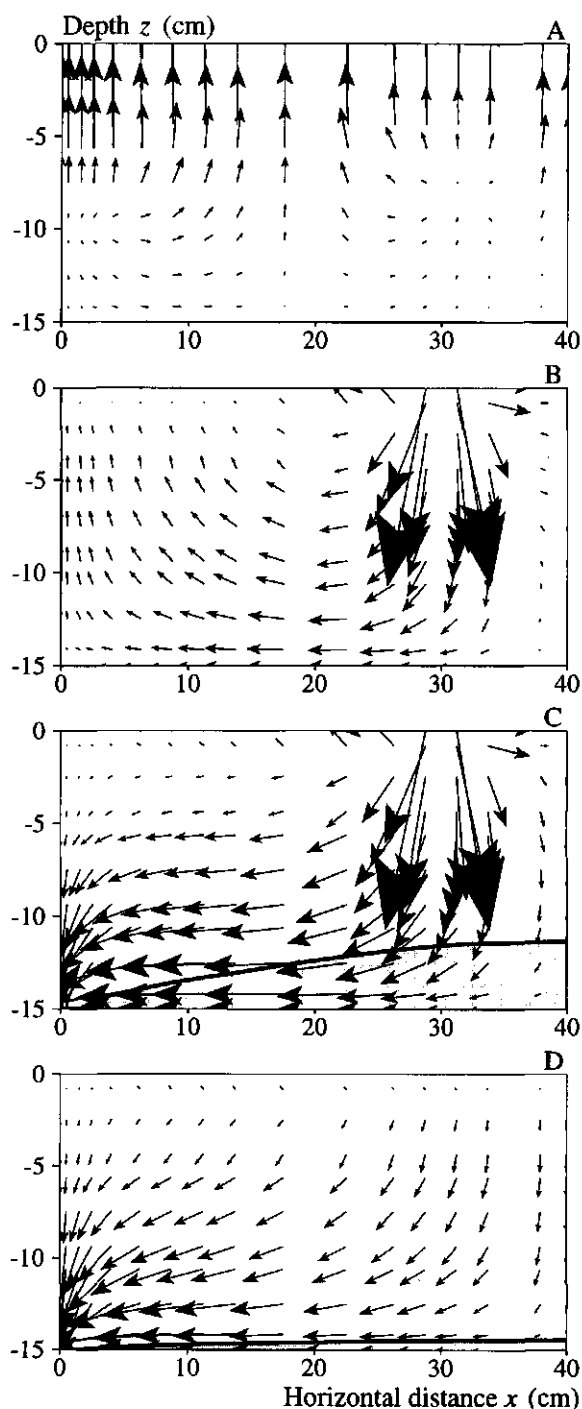
Figure 7-7
Simulated net flux density distribution at four times at day 162: (A) before the start of a fertigation period with evapotranspiration ET only ($t = 660$ min), (B) just before start of drainage, i.e. with irrigation I and ET ($t = 802$ min), (C) just before the end of fertigation, i.e. with I, drainage D, and ET ($t = 820$ min), and (D) just before end of drainage, i.e. with D and ET ($t = 830$ min). The size of the arrows represents the relative magnitude of the flux density; the parts of the arrows outside the sand bed system are not drawn for practical reasons. In (B) and (C) an arrow with length of 10 x-axis units corresponds with 0.2 cm min^{-1}; the arrows in (A) and (D) are enlarged 500 and 5 times, respectively. The shaded area in (C) and (D) is the saturated zone.

7.4 Pressure head

7.4.1 Measured

Measurements of the pressure head h at three depths at locations above a drain and between two drains in all four plots yielded large differences. These appear to be mainly due to differences in installation depths of the tensiometers. On average, there were no significant differences between positions above a drain or between two drains. In view of the large differences between tensiometers installed at nominally the same depth, I decided to present only the averaged pressure heads at the three depths (Figure 7-8A). Thus, there seemed to be no effect of the treatments used in that particular experiment (as described in Table 5-2). The averages of all standard deviations per line are shown by the vertical bars at the left side of Figure 7-8A. After the start of fertigation there is a rapid increase of *h* followed by a slow decrease in time. On average the difference in *h* between two successive measurement depths amounted to 5 cm. At the beginning of days 166 and 168, *h* increased, while one would expect a decrease due to evapotranspiration. An increase can be expected due to a change in surface tension at the water-air interface with increasing temperature.

For one set of three sensors installed at three depths above each other, the $h(z)$ *profile at different times* was determined using *h* from positions between two drains (Figure 7-8B). At all times these data indicate a unit gradient in *h*, which could also be seen in Figure 7-8A. After each fertigation, *h* at depth 11.45 cm was positive, thus saturated conditions occurred at that depth.

7.4.2 Simulated

The *simulated time courses of h* are shown in Figure 7-9. The order of magnitude of simulated *h* corresponds to that measured, but there are some specific differences between simulations and measurements. In the simulation model no temperature effects are included, so that the rise of *h* in the beginning of the days 166 and 168 can never be simulated (see the remark at the end of Subsection 7.4.1). A second difference is that in the simulations the boundary conditions at night are all of no-flow type (if drainage had stopped), which resulted in *h* to remain constant. The measurements indicated, however, that even during night *h* changed. The drop of *h* during a drainage event is fast according to the simulations, but much slower in reality. This difference may be partly due to the differences in actual and model $\theta(h)$ characteristics. Another reason is that actually the drainage rate is lower than the simulated drainage rate (Figure 7-6) most likely caused by the resistance of the anti-rooting mat. The decrease may also be dampened due to the increase caused by increasing temperatures, as mentioned in Subsection 7.4.1. During the periods of *ET* only, the change of *h* in time is larger in the simulations than in the measurements, e.g. during day 167. This is also due to the non-perfectness of the hysteretic properties used in the model. Sometimes the changes are comparable, such as
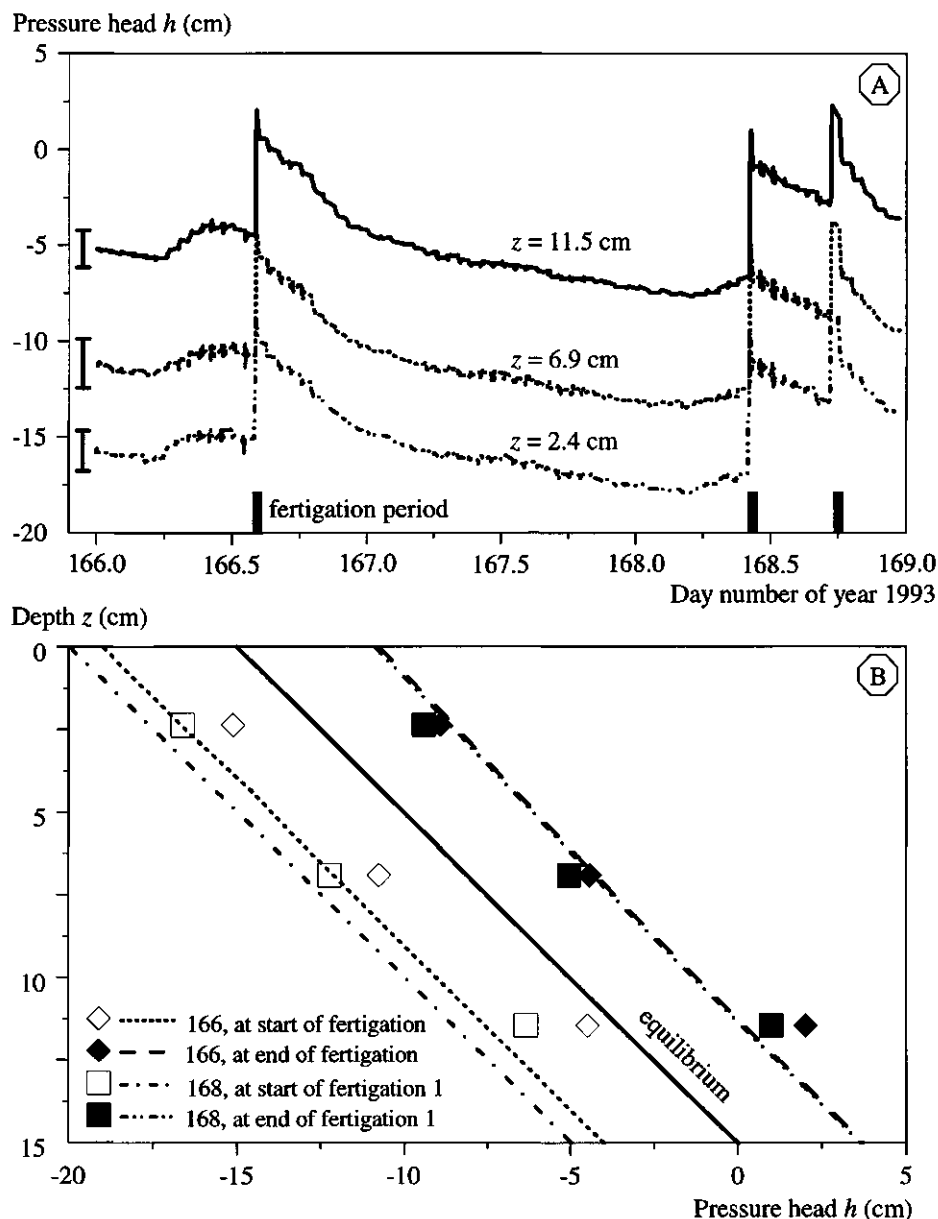
Figure 7-8 (A) Averaged measured pressure heads at three depths in the sand bed. The averages
of the standard deviations of all standard deviations per line are shown by the vertical
bars. The average installation depths were 2.4 cm, 6.9 cm, and 11.5 cm. (B) Pressure
head - depth profile (points) of a set of three tensiometers at several times. The solid
line refers to unit gradient with $h = 0$ at the bottom. The simulated results are given
as broken lines.

Pressure head h (cm)
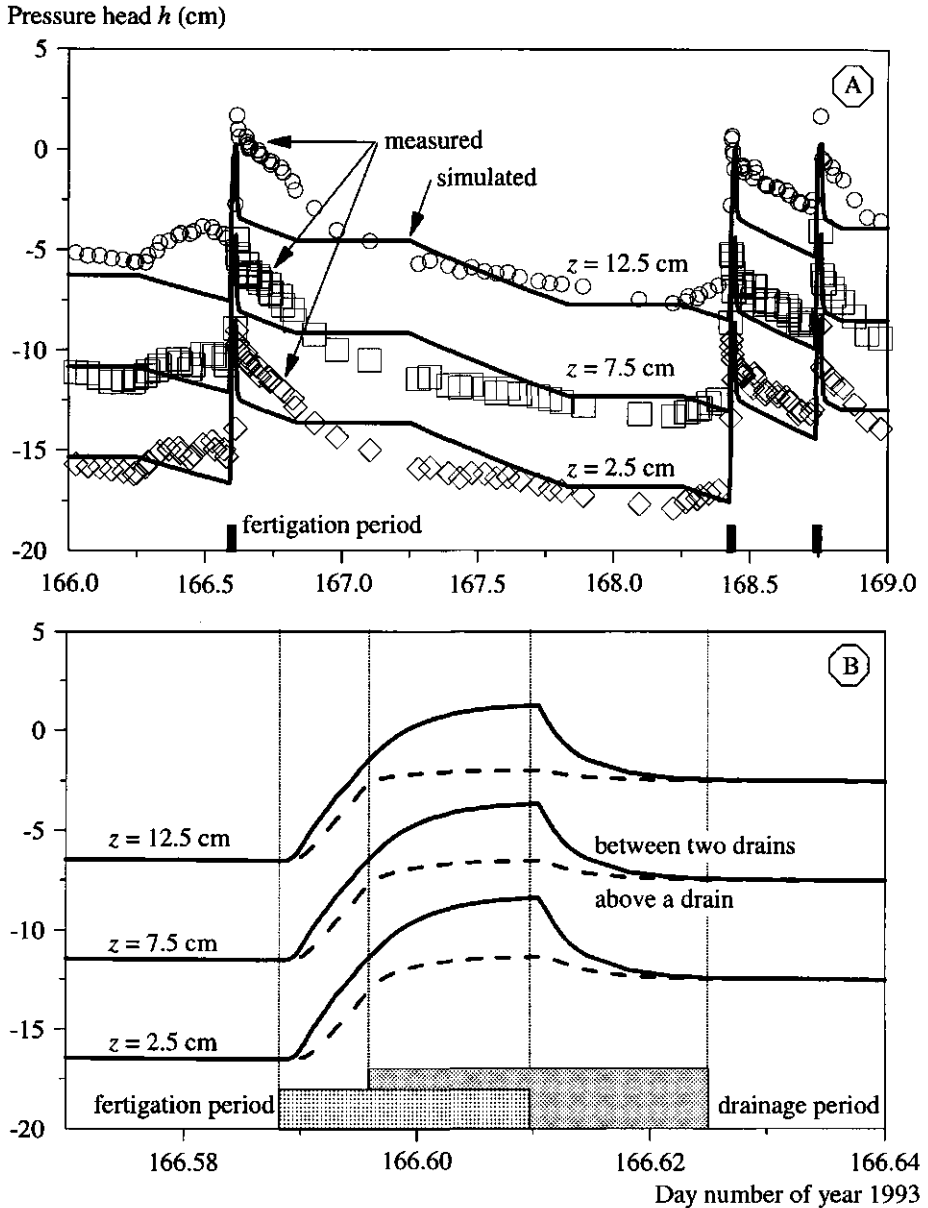
Figure 7-9 (A) Simulated time course of h during days 166-168 compared to the experimental data from Figure 7-8. There is a small difference in depth for simulated and experimental data: measured at $z = 2.4$, 6.9, and 11.5 cm, simulated at $z = 2.5$, 7.5, 12.5 cm. In (B) the simulated results during a fertigation-drainage event for two x positions, one between two drains and the other above a drain, are shown.

during the period between the two fertigations at day 168.

The simulations indicate that h at a given depth was independent of distance to the drain, except during a fertigation-drainage event (Figure 7-9B). Then, h is larger between two drains than at comparable depth above a drain. Soon after drainage stops, the values of h at the two locations are similar again. The times when fertigation starts, drainage starts, fertigation stops, and drainage stops, are clear in the simulation results, especially for the positions above a drain.

The *simulated h(z) profiles* (Figure 7-8B) indicate that the $h(z)$ distribution is, under these wet conditions, always at equilibrium, i.e. there exists a unit-gradient in h. At the end of a fertigation period the simulated results compare well with the experimental data. Just before the start of a fertigation, the simulations resulted in lower h than measured. This is due to the rise of h just before the fertigation events at days 166 and 168, as shown in Figure 7-7.

The *simulated distribution of h* in the sand bed is shown in Figure 7-10 prior to the start of a fertigation (Figure 7-10A) and some time during the period of fertigation and drainage (Figure 7-10B). Before the start of fertigation the h distribution in the x direction is uniform, thus no horizontal flow occurs, but only vertical flow. During fertigation, h rises at the dripper location. When drainage occurs, there is a saturated zone at the bottom indicated by the $h = 0$ cm contour line. This figure can be compared with the flux density distribution given in Figure 7-7C.
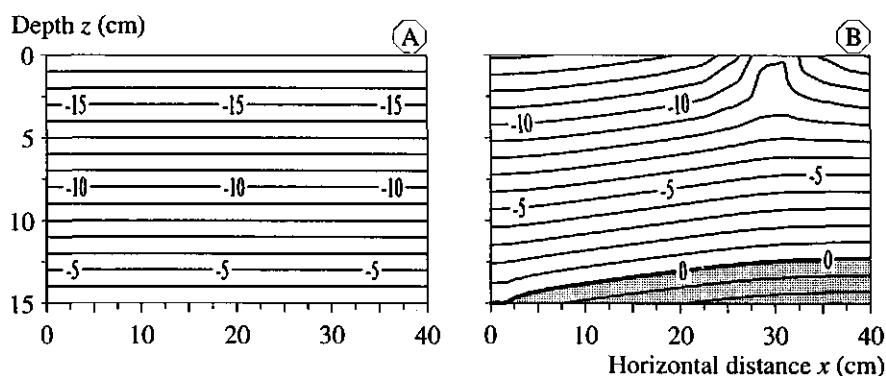
Figure 7-10 (A) Simulated distribution of pressure head h just before the start of a fertigation period, and (B) some time during the combined fertigation-drainage event.

At all times during the simulations, the simulated actual transpiration is equal to the measured transpiration. Thus, no crop water stress occurs in the simulations. The differences between required root water pressure heads in simulations with and without hysteresis were negligible. The *time course of root water pressure head* h_r (Figure 7-11) shows an increase of h_r during the day. This is caused by the fact that roots grew during the day, and the increase in root surface area is so large that the energy required by the root system to withdraw water from a nevertheless drying substrate decreases in time. A second feature observed is the decrease in h_r just after the start of irrigation. This is explained by the fact that part of the root zone becomes saturated, in which case roots present in the saturated zone are assumed not to function. Thus a smaller total root surface area has to withdraw more water per unit root surface, which can be achieved by decreasing h_r. As the extent of the saturated zone decreases, h_r increases again. In reality transpiration shows a diurnal course, which was not introduced in the simulation model. As a result of this, water stress can occur in reality and not in the simulations; a diurnal course of the transpiration would reflect in the h_r time course as well. Of course, in view of root growth, the level of h_r does not say anything about the magnitude of transpiration. For example, the transpiration on day 167 is more than two times larger than that on day 160, but h_r is smaller.

Figure 7-11 Simulated time course of root water pressure head. The vertical bars at the horizontal axis indicate the duration of fertigation times. The numbers refer to the daily potential transpiration rates.

7.5 Calibration of solute transport module

No detailed measurements of solute distribution in the sand bed were carried out during the greenhouse experiments, hence no validation for the solute transport module can be carried out. Instead, calibration of this module was performed to estimate the magnitudes of the longitudinal and transversal dispersivities a_L and a_T. A small sand bed - with x, y and z dimensions of 84 cm, 120 cm and 25 cm - was filled with 15 cm of the coarse sand and two 120 cm long drain tubes were located in the bottom corners. Solution was added by eight drippers: four on each side of the line of symmetry. This sand bed was equal to two half regions between two drains as used in the greenhouse experiments. Initially water was applied by the drippers until - near - steady state was reached. Then a solution of KNO_3 was applied and the outflow from each of the two drains was collected at regular intervals. The resulting breakthrough curve (BTC) was described by the simulation model (see Appendix 6 for the description of input parameters). By trial and error, the best set of a_L and a_T values were searched. The set of values for the dispersivities were a_L, $a_T \in [0, 0.2, 0.5, 1, 2, 3, 4, 5, 10$ cm]. Only cases are considered with $a_L \geq a_T$.

For all combinations the sum of squared differences (SSQ) between observations and simulated values were obtained (Table 7-1). All BTC's were visually compared to the observed BTC's as well, and a few characteristic examples of simulated BTC's are given

Table 7-1.   Sum of squared differences between observed and simulated breakthrough data for different values of longitudinal and transversal dispersivities (cm) a_L and a_T (nd: not determined).

a_T	a_L 0	0.2	0.5	1	2	3	4	5	10
0	0.236	0.217	0.193	0.162	0.121	0.103	0.042	0.171	nd
0.2		0.184	0.148	0.106	0.061	0.105	0.046	0.054	0.134
0.5			0.142	0.102	0.059	0.045	0.041	0.053	0.131
1				0.099	0.057	0.045	0.053	0.052	0.127
2					0.057	0.044	0.043	0.050	0.123
3						0.044	0.043	0.048	0.121
4							0.042	0.047	0.117
5								0.046	0.115
10									0.107

in Figure 7-12. In general, the value of a_L dominates the shape of the simulated BTC. A small value of a_L results in a steeper BTC and a later start of breakthrough than observed. A larger value of a_L, i.e. $a_L \geq 3$ cm, results in a flatter BTC and a earlier breakthrough than observed. In all cases the tailing of the observed BTC is not predicted well, especially not with the lower values of a_L. For a given value of a_L the magnitude of a_T does not have much effect on SSQ, except for the lowest values of a_L. The lowest values of SSQ are obtained for a_L in the range 2 cm to 5 cm. I decided to use $a_L = 2$ cm since it results in a good prediction of the first part of the BTC. The magnitude of a_T is of less importance. Based on Bear and Verruijt (1987) who stated that the ratio of a_L/a_T ranges from 10 to 20, I decided to use $a_T = 0.1\,a_L$, i.e. $a_T = 0.2$ cm.

Taking into account that the true process of solute transport below the dripper is three-dimensional and the model is two-dimensional, and the fact that the true application was not completely continuous but intermittent, I conclude that the solute transport module behaves reasonably well.

Relative drain effluent concentration c/c_f (-)

Relative volume of applied solution V_s/V_i (-)
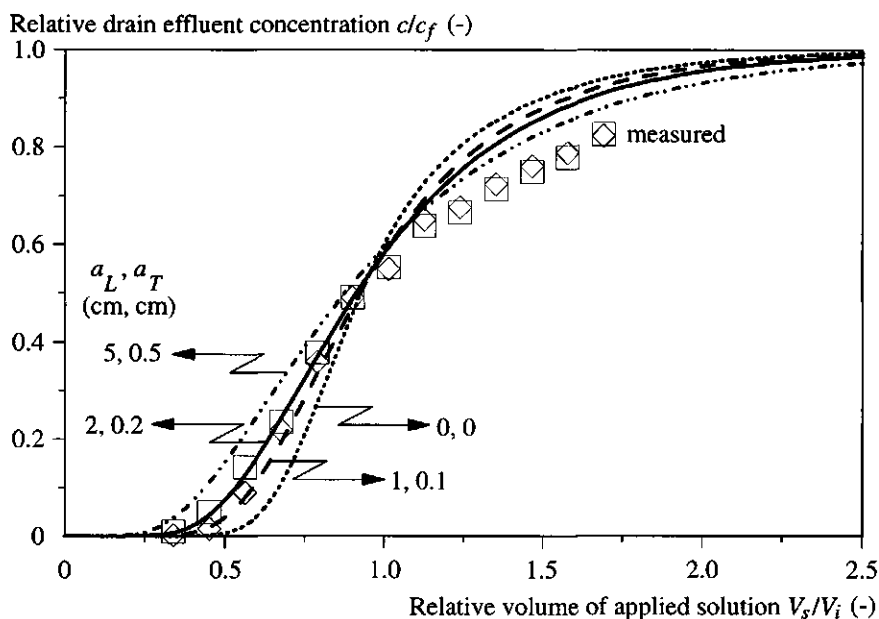
Figure 7-12 Breakthrough curve measured in a small sand bed system with drip application and predicted by the simulation model for the indicated values of the longitudinal a_L and the transversal a_T dispersivities. The x-axis represents the volume V_s of solution applied relative to the volume V_i of solution present in the sand bed, and the y-axis represents the concentration c of the effluent relative to the influent concentration c_f.

7.6 Simulated nitrogen distribution

Prediction of the *EC* of the substrate solution is not part of the simulation model, so that no comparison with measured solute distribution can be made. Therefore, I give some results of the distribution for one solute, e.g. nitrogen (N). The N computations were done for the same period as for the water computations (Sections 7.3 and 7.4). The *time course of total amount of N stored in half the region between two drains* shows a periodic pattern, with increase due to input via fertigation, and decrease due to drainage and plant N uptake (Figure 7-13), just as observed for total water storage (Figure 7-5). The initial amount everywhere in the flow domain was approximately 2.0 mmol, and $c_0 = 15$ mmol l^{-1}. As with total water storage, the simulation without hysteresis shows that after the two day starting period the total storage of N still increases for two days. Including hysteresis results in lower total N storage. With the drainage water, N is also removed from the flow domain (Figure 7-13). The difference in N storage and N outflow between the simulations with and without hysteresis remains constant in time after day 161, as is also the case for water (Figure 7-6).
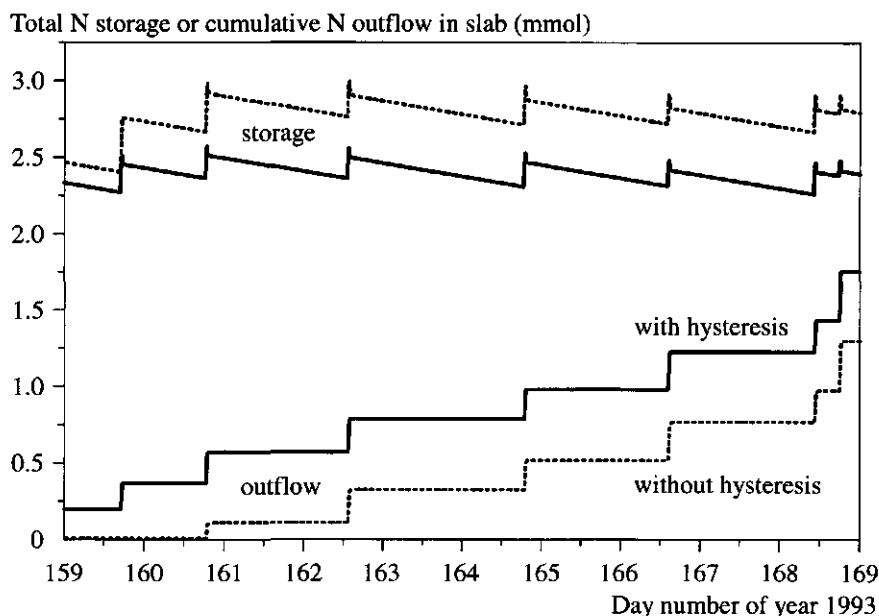
Figure 7-13   Simulated time course of total N storage (upper two lines) and cumulative N outflow from the drain (bottom two lines) for half the region between two drains for cases with and without hysteresis.
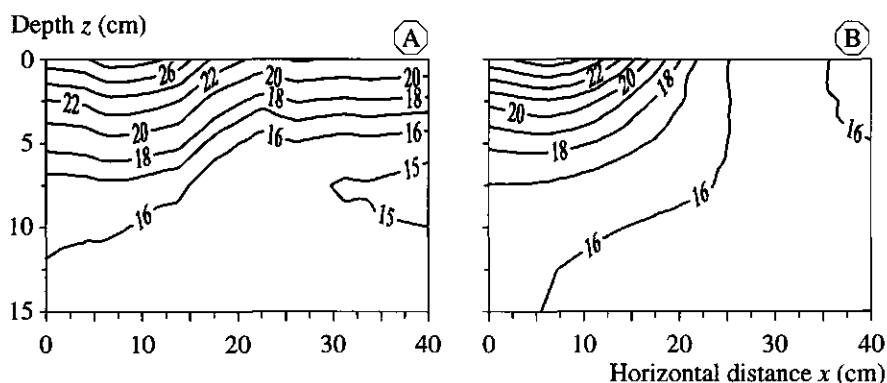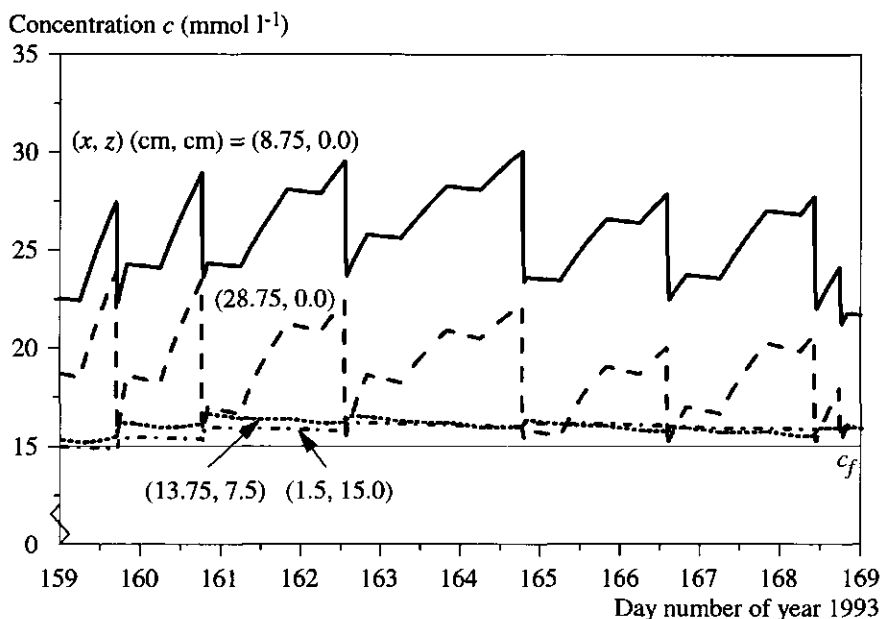
7.7 Conclusions

In this chapter I have presented a comparison between measured and simulated volumetric water content, cumulative outflow from a drain, and pressure head. Moreover, the longitudinal and transversal dispersivities are determined from a breakthrough experiment.

This chapter gives rise to the following conclusions and findings.

- *In-situ* determined $\theta(h)$ characteristics agreed with the (scaled) laboratory characteristics for the ' α_d - *data interpolation method*'.
- The choice of the initial condition in a simulation model is difficult when hysteresis is considered. If an initial condition somewhere in the hysteretic θ-h domain is chosen, the history of drying and wetting should be known and input as well.
- The measured *distributions in space and time of θ and h, and the cumulative outflow* patterns were described well by the simulation model.
- Hysteresis results in drier conditions and in larger air contents. In coarse substrate systems frequent fertigations are possible, without negative consequences for aeration.
- Breakthrough curve data were used to obtain estimates of the longitudinal and transversal dispersivities.
- Net water and solute flux density distributions are helpful in understanding the dynamics of water and nutrients in the root zone.

Chapter 8

Application of the model in case studies

In this chapter I will explore some aspects that can be studied with the simulation model. It is not a complete explorative study in designing the best cropping system with the best fertigation strategy. It is meant as a demonstration, and many more aspects can be studied. Those are left to the imagination of the reader. I will focus on some questions from practice.

- What is the maximum height of a phreatic surface and its time of disappearance during an irrigation-drainage cycle in a bedding system, and can these features be predicted by existing analytical solutions? (Section 8.1).
- What is the maximum allowable time span between two fertigation events, and what should determine that? In other words, how much water is available in the cropping system, and how are the concentrations of solutes affected when the substrate dries out? (Section 8.2).
- How much new solution must be flushed through the substrate to replace a resident solution by the new solution? (Section 8.3).
- Can the simulation model be used for other substrates and other cropping systems as well? In Section 8.1 different substrates will be used, and in Section 8.4 some simulation results for a rockwool slab cropping system will be presented.

8.1 Appearance and disappearance of a phreatic surface

as a function of drain distance

8.1.1 Introduction

When drainage occurs in a bedding system (Figure 1-1B, 2-1) it means that a saturated zone is present. The larger the distance between two drains the higher the phreatic surface will rise. After application of water stops, the saturated zone will disappear eventually. Saturated conditions are undesirable with respect to aeration of the roots. In designing bedding systems, or other types, the question is what drain distance is still tolerable so that the saturated zone does not become too large and/or remains present for too long periods. Note that even when there is no phreatic surface present, unfavourable conditions with respect to aeration may exist, but this is not considered in this section. I will study here the special case of steady, uniform application of water, because for that situation analytical solutions are available to predict the maximum height of the phreatic surface and the rate of disappearance of the saturated zone once the application of water stops. I will compare simulation results with analytical solutions, and consider the bedding

system with coarse sand (Subsection 8.1.2) or with other types of substrates (Subsection 8.1.2).

I assume that a regular grid of drippers, 16.67 drippers m^{-2}, with a drip rate of 30 ml min^{-1} (Chapter 5) can be approximated by a continuous rate of infiltration over the total surface with an intensity of $s_i = 0.05$ cm min^{-1}. For a given drain distance L_D (L), the *maximum height m_0* (L) *of the phreatic level* midway between two drains is computed, and *the time $t_{0.1}$* (T) *needed for this level to drop to a level equal to 10% of this maximum height.* Analytical expressions for m_0 and $t_{0.1}$ are obtained from the literature. However, these are only valid when water movement only occurs below the phreatic surface. Since this is actually not the case, it is likely that the analytical values will differ from numerically obtained values.

For drains on an impermeable layer and assuming horizontal movement of water, i.e. Dupuit-Forchheimer flow, Hooghoudt (1937, 1940) gave an approximate expression for m_0:

$$m_0 = \frac{L_D}{2}\sqrt{\frac{s_i}{K_s}} . \qquad [8\text{-}1]$$

The shape $m_p(x)$ (L) of the phreatic surface is that of a quarter of an ellipse with semi-major axis ($L_D/2 - x_D$) and semi-minor axis m_0 (Figure 8-1):

$$m_p(x) = m_0\sqrt{1 - \left(\frac{x - L_D/2}{L_D/2 - x_D}\right)^2} . \qquad [8\text{-}2]$$

After infiltration stops, the phreatic level will drop. The time t_{mp} when a certain height $m_p(L_D/2)$ midway between two drains occurs can be estimated from (van Schilfgaarde, 1974)

$$t_{mp} = \frac{2\,L_D^2 f}{9\,K_s}\frac{m_0 - m_p(L_D/2)}{m_0\,m_p(L_D/2)} , \qquad [8\text{-}3]$$

where f is the drainable porosity or specific yield (L^{3}L^{-3}), which will be elaborated in the next paragraph. Equation [8-3] is valid for an initial condition where $m_p(x)$ is given by an ellipse, i.e. Eq. [8-2]. The time $t_{0.1}$ when $m_p(L_D/2) = 0.1\,m_0$ follows from Eq. [8-3] as

$$t_{0.1} = \frac{2\,L_D^2 f}{K_s\,m_0} . \qquad [8\text{-}4]$$
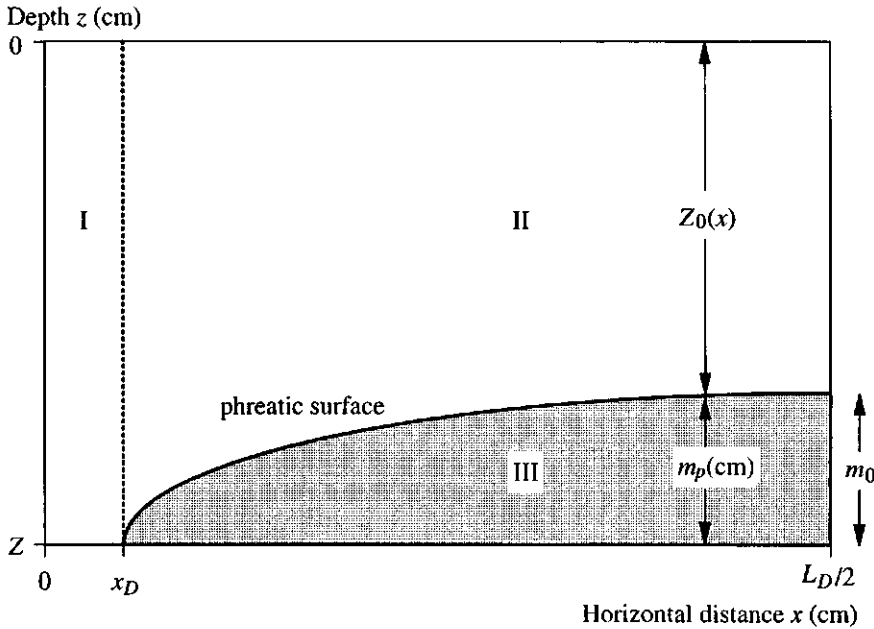
Figure 8-1 Half the region between two drains showing the quantities $m_p(x)$, m_0 and $Z_0(x)$. Also indicated are the three regions for which the water storage is evaluated in order to obtain the drainable porosity f: I: unsaturated zone above half a drain, II: unsaturated zone above the phreatic surface, and III: saturated zone below the phreatic surface.

Substitution of Eq. [8-1] in Eq. [8-4] yields

$$t_{0.1} = \frac{4\,L_D f}{\sqrt{s_i\,K_s}}.$$

[8-5]

Note that according to Eqs. [8-1] and [8-5], both m_0 and $t_{0.1}$ are proportional to L_D, and inversely proportional to the square root of K_s.

The *drainable porosity or specific yield f* in Eqs. [8-3] and [8-5] is considered as a constant, however, in reality it varies with time (Raats and Gardner, 1974; van Schilfgaarde, 1974), and thus makes evaluation of Eqs. [8-3] and [8-5] complicated. For simplicity reasons, I treat f as a constant. Based on the definition of global specific yield of Raats and Gardner (1974), f is defined as the change in volume of water V_d (L^3) between the start and end of the drainage process divided by the change in volume of the saturated zone V_{ds} (L^3) during the same time period:

$$f = \frac{V_d}{V_{ds}}. \qquad [8\text{-}6]$$

V_d is computed as the volume of water V_{d1} present in the flow domain when the phreatic surface has reached its maximum height minus the volume of water V_{d2} present when the saturated zone has just disappeared:

$$V_d = V_{d1} - V_{d2}. \qquad [8\text{-}7]$$

The amount of water present in the flow domain follows from integrating $\theta(h)$ over z for all x. For wet conditions in coarse porous media, it can be assumed that h is in equilibrium with z, i.e. $dh = dz$ (Subsection 7.4.2; Otten, 1994). The following three regions are considered (Figure 8-1): (I) the vertical region above the drain, with a radius x_D, from $x = 0$ to $x = x_D$, (II) the region above the phreatic surface from $x = x_D$ to $x = L_D/2$, and (III) the region below the phreatic surface from $x = x_D$ to $x = L_D/2$. So, V_{d1} follows from

$$V_{d1} = \int_0^{x_D} \int_y^{y+\Delta y} \int_0^{z} \theta(h)\,dh\,dy\,dx + \int_{x_D}^{L_D/2} \int_y^{y+\Delta y} \int_0^{z-m_p(x)} \theta(h)\,dh\,dy\,dx +$$

$$+ \frac{\pi}{4}\left(\frac{L_D}{2} - x_D\right) m_0 \Delta y\, \phi_p, \qquad [8\text{-}8]$$

where the three parts on the right-hand side refer to the three respective regions mentioned above. The third part of Eq. [8-8] represents a quarter of the area of an ellipse (Spiegel, 1968) with unit width in the y-direction (Δy) times the saturated water content or porosity ϕ_p. V_{d2} follows from

$$V_{d2} = \int_0^{L_D/2} \int_y^{y+\Delta y} \int_0^{z} \theta(h)\,dh\,dy\,dx. \qquad [8\text{-}9]$$

The indefinite integral $\int \theta(h)dh$ for the van Genuchten expression of $\theta(h)$, i.e. Eq. [4-1], is not available. I evaluated the integral with the Gauss-Legendre integration method, and the multiple integrals appearing in Eqs. [8-8] and [8-9] by a nested Gauss-Legendre method (Press *et al.*, 1986).

V_{ds} is defined as the change volume of the saturated zone between start and end of drainage, the latter being zero. Thus, V_{ds} is equal to a quarter of the area of an ellipse times unit thickness in the y-direction:

$$V_{ds} = \frac{\pi}{4}\left(\frac{L_d}{2} - x_D\right) m_0 \Delta y. \qquad [8\text{-}10]$$

Substituting Eqs. [8-7]-[8-10] in Eq. [8-6] yields

$$
f = \frac{\displaystyle\int_{x_D}^{L_D/2}\int_0^{Z-m_p(x)} \theta(h)\,dh\,dx - \int_{x_D}^{L_D/2}\int_0^{Z} \theta(h)\,dh\,dx}{\dfrac{\pi}{4}\left(\dfrac{L_D}{2}-x_D\right)m_0} + \phi_p .
\tag{8-11}
$$

Note that f represents some average value for the total drainage period, and that the unsaturated region above the drain has no effect on f. The first double integral in Eq. [8-11] refers to the distribution at the start of the drainage process, and the second double integral to the distribution at the end. The latter is greater than the former, and, consequently, $0 \le f \le \phi_p$. Equation [8-11] can be simplified to

$$
f = \frac{\displaystyle\int_{x_D}^{L_D/2}\int_{Z-m_p(x)}^{Z} \left(\phi_p - \theta(h)\right) dh\,dx}{4\left(\dfrac{L_D}{2}-x_D\right)m_0} .
\tag{8-12}
$$

Equation [8-12] indicates that f is equal to the volume of air that enters the substrate at the surface during the drainage process.

8.1.2 Results for coarse sand

The simulation runs (input parameters are listed in Appendix 6) for $x_D = 2$ cm and four values of L_D, i.e. 40 cm, 80 cm, 120 cm and 160 cm, resulted in lower values for m_0 and $t_{0.1}$ than predicted by Eqs. [8-1] and [8-5], respectively (Table 8-1). The simulated m_0

Table 8-1 Comparison between analytical and simulated values for m_0 (cm) and $t_{0.1}$ (min) and height of capillary fringe h_{cf} (cm) for four values of drain distance L_D.

L_D (cm)	m_0 Eq. [8-1]	m_0 simulated	h_{cf} Eq. [8-14]	$t_{0.1}$ Eq. [8-5]	$t_{0.1}$ simulated
40	4.8	2.1	1.0	47	10
80	9.6	5.8	2.7	58	20
120	14.4	11.0	6.8	60	27
160[1]	19.2	17.3		61	30

[1] Results for m_0 suggest ponding; simulation results are doubtful.

result (ICCG method) for $L_D = 160$ cm is doubtful, since it suggests ponding; the height of the sand bed was 15 cm. Thus, the boundary condition for the ponded area had to be changed from a flux condition to a pressure head condition, which feature is not included in the simulation model. Some reasons why the analytical and numerical results differ are:
- there is horizontal movement of water above the phreatic surface, which is not accounted for in the analytical solutions (see discussion in the following paragraph);
- the specific yield f is in reality not constant.

In deriving Eq. [8-1] it is assumed that water flows horizontally in the saturated zone, and that above the phreatic surface there is no horizontal movement of water. However, also above the phreatic surface there is horizontal movement of water (see, e.g., Figure 7-7). Raats and Gardner (1974) gave an estimate of horizontal flow above the phreatic surface. Their rationale was to assign this movement to an equivalent capillary fringe above the phreatic surface. At a certain position x the total horizontal flow in the region above the phreatic surface is given by (Raats and Gardner, 1974)

$$\int_{0}^{Z_0(x)} q_x \, dz = \frac{dZ_0(x)}{dx} \, \phi(h = -Z_0(x)), \qquad [8\text{-}13]$$

where q_x is the horizontal component of the water flux density (LT^{-1}), $Z_0(x) = Z - m_p(x)$ is the distance (L) between substrate surface and phreatic surface at x (Figure 8-1), $dZ_0(x)/dx$ (1) is the slope of the phreatic surface at x and ϕ is the matric flux potential (L^2T^{-1}) as defined in Eq. [2-7]. In the saturated zone ϕ in Eq. [8-13] is equal to K_s times the height of the saturated zone. The horizontal movement of water above the phreatic surface can be assigned to an equivalent saturated capillary fringe region with height h_{cf} (L) according to

$$h_{cf} = \frac{\phi(h = -Z_0(x))}{K_s}. \qquad [8\text{-}14]$$

For the cases of $L_D = 40$ cm, 80 cm and 120 cm h_{cf} at $x = L_D/2$, was computed (Table 8-1; see Appendix 7 for evaluation of ϕ). The sum of h_{cf} and simulated m_0 then comes closer to the values of m_0 as computed with Eq. [8-1]; for $L_D = 40$ cm and 80 cm the sum is still lower, and for $L_D = 120$ cm it is higher. The capillary fringe approach is valid for $s_i \ll K_s$ for which a vertical equilibrium h-distribution is a good approximation; here $K_s/s_i = 17.4$.

In conclusion, in designing sand bed systems with an optimal L_D, Eqs. [8-1] and [8-5] can only be used as a first approximation, as they overestimate m_0 and $t_{0.1}$ with respect to the simulated values. The value for m_0 can be adapted by the capillary fringe approach as discussed above. It is remarkable to see that saturated conditions in the sand occur only for very short periods. For example, under steady conditions for $L_D = 120$ cm, the phreatic

surface reaches to within 5 cm of the surface, but when infiltration stops it decreases after 30 minutes to 1 cm above the bottom. Thus, *under practical conditions, saturated conditions will not persist for too long periods, and due to the shape of $\theta(h)$, aeration problems are unlikely.*

8.1.3 Results for some other substrates

The quantities m_0 and $t_{0.1}$ were also obtained for a bedding system filled with four other types of substrates and one natural soil, for which the hydraulic properties were obtained from the literature (see Table 8-2 and Figure 8-2): *rockwool* (da Silva *et al.*,1996), a *potting medium* consisting of 75% peat and 25% perlite (Otten, 1994), *cocospeat* (Kipp and Wever, 1993), 2-4 mm *clay beads* (Kipp and Wever, 1993) and a Dutch *natural loam* top soil known as 'zavel-b8' in the Dutch 'Staringreeks' (Wösten *et al.*, 1994). I took L_D = 120 cm and s_i = 0.05 cm min^{-1}. For the loam soil these conditions could not be used, since complete saturation resulted. Therefore, for I took for this soil L_D = 12 cm and s_i = 0.001 cm min^{-1}.

Table 8-2 Hydraulic parameters according to Eqs. [4-1] and [4-5] for four different types of substrates as obtained from the literature: θ_r (-), θ_s (-), K_s (cm d^{-1}), n (-), α_d (cm^{-1}), α_w (cm^{-1}) and λ (-). The parameters for rockwool, cocospeat and clay beads were obtained from graphical or tabulated data of $\theta(h)$ and $K(h)$ using the optimization code RETC of van Genuchten *et al.* (1991).

	Rockwool (da Silva *et al.*, 1996)	Peat-perlite mixture (Otten, 1994)	Cocospeat (Kipp and Wever, 1993)	Clay beads 2-4 mm (Kipp and Wever, 1993)	Loam 'zavel-b8' (Wösten *et al.*, 1994)
θ_r	0.00673	0.0	0.40190	0.16701	0.0
θ_s	0.92402	0.92	0.92928	0.76	0.43
n	3.90471	1.42	2.84388	2.2486	1.284
α_d	0.08730	0.13	0.08181	0.80756	0.0096
α_w	1.00013	0.90	n.a.[1]	n.a.[1]	n.a.[1]
K_s	6174.0	8640.0	8640[2]	8640[2]	2.25
λ	-0.28288	2.35	0.5[3]	0.5[3]	-2.733

[1] n.a.: not available
[2] K_s not available, taken equal to that of peat-perlite mixture of Otten (1994)
[3] λ not available, taken equal to 0.5, which is a reasonable guess for soils (Mualem, 1976)

Absolute pressure head $|h|$ (cm) Hydraulic conductivity K (cm min^{-1})

Volumetric water content θ (cm^3 cm^{-3})

Effective saturation S_e (-)
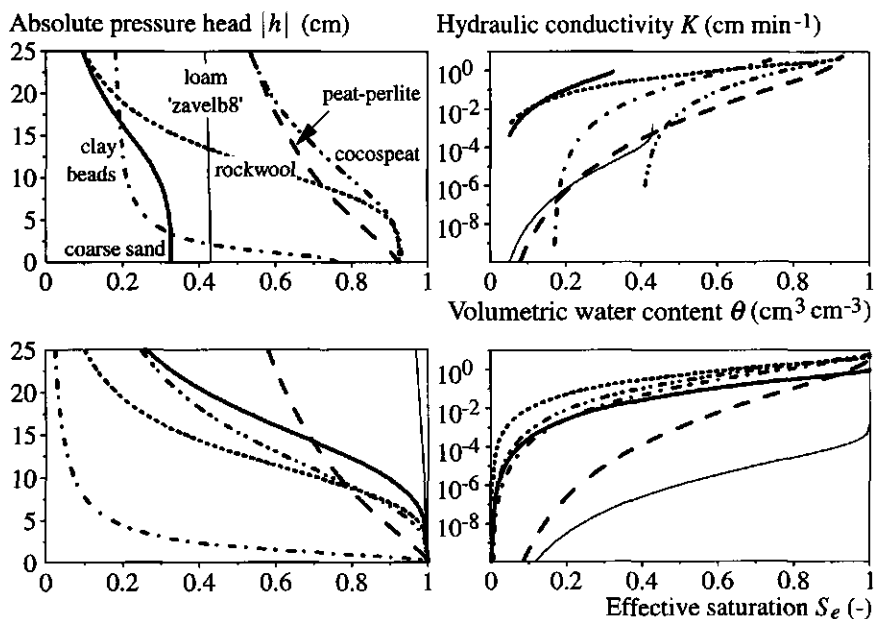
Figure 8-2 Main drying water retention curves $\theta(h)$ and $S_e(h)$ and hydraulic conductivity curves $K(\theta)$ and $K(S_e)$ (cm h^{-1}) for several substrates for which the parameters according to the van Genuchten and Mualem relationships, i.e. Eqs. [4-1] and [4-5], are given in Tables 4-5 and 8-2.

Rockwool, peat-perlite mixture, cocospeat, clay beads

The simulation results show that in the coarse substrates having high porosities lower values for m_0 occur than in the coarse sand substrate (Table 8-3). In all cases m_0 according to Eq. [8-1] is larger than the simulated values. The low values for h_{cf} indicate that there is not much horizontal water movement in the unsaturated zone in these substrates. The analytical estimates for $t_{0.1}$ (Eq. [8-5]) are much larger than the numerically obtained values (Table 8-3). This is due to an erroneous estimate of f. The numerically obtained $t_{0.1}$ for each substrate, except for cocospeat, is larger than for the coarse sand.

Loam 'zavel-b8'

For the loam soil 'zavel-b8' soil the simulated value for m_0 is larger than the computed value using Eq. [8-1] (Table 8-3). The numerically obtained $h(z)$ distributions indicated that the assumption dh = dz is not true. In that case h_{cf} cannot be computed according to Eq. [8-14], and also f and $t_{0.1}$ may may not be computed.

If the loam soil is a good representative of all fine-textured substrates (natural soils),

it is concluded that natural soils can only be used in thin layer bedding systems when L_D and s_i are very small, and thus are practically unsuitable. But even for those small values of L_D and s_i, aeration may not be sufficient, since the air-filled porosity above the phreatic surface is very low according to the water retention characteristic (Figure 8-2).

Table 8-3 Simulated and analytical values for m_0 (cm) and $t_{0.1}$ (min) for several substrates for a drain distance $L_D = 120$ cm and an irrigation intensity $s_i = 0.05$ cm min^{-1}. For loam 'zavel-b8' $L_D = 12$ cm and $s_i = 0.001$ cm min^{-1}.

	Coarse sand	Rock-wool	Peat-perlite mixture	Cocos-peat	Clay beads	Loam 'zavel-b8'
m_0, Eq. [8-1]	14.4	6.5	5.5	5.5	5.5	4.8
m_0, simulated	11.0	2.7	4.4	2.2	2.1	6.4
h_{cp} Eq. [8-14]	6.8	0.4	0.3	0.1	0.0	12.6
$t_{0.1}$, Eq. [8-5]	60	432	225	176	490	241
$t_{0.1}$, simulated	27	62	94	24	115	124

Cocospeat: effect of K_s and λ on m_0
Not all hydraulic properties were known: e.g. for cocospeat K_s and λ. A simple sensitivity analysis with the simulation model for cocospeat showed that m_0 depends on the value of K_s, but not exactly linearly with $K_s^{-0.5}$ as suggested by Eq. [8-1] (Table 8-4). The value for m_0 for $K_s = 0.5$ cm min^{-1} is doubtful, since it suggests ponding (see earlier discussion). For one particular value of K_s the effect of λ on m_0 was small (Table 8-4).

Table 8-4 Simulated values for m_0 (cm) for cocospeat for different values of K_s (cm min^{-1}) or λ (-).

K_s	λ	m_0	K_s	λ	m_0
0.5	0.5	18.6[1]	6.0	-2.5	1.9
1.0	0.5	10.0	6.0	0.5	2.2
2.0	0.5	5.7	6.0	2.5	2.4
3.0	0.5	4.1	8.0	0.5	1.7
4.0	0.5	3.2	10.0	0.5	1.4

[1] Results for m_0 suggest ponding; simulation results are doubtful.

8.2 Water storage, root water pressure head and

irrigation scheduling

In glasshouse cropping systems, frequently irrigations take place. Based on visible interpretation, the grower decides to irrigate when the top layer looks or feels dry. Here I will explore how much water is available in the substrate for different ranges of pressure head based on the water retention characteristic (Subsection 8.2.1). In addition I will assess the effect on root water pressure head using the root water uptake model of Section 2.3 (Subsection 8.2.2). Furthermore, I will evaluate with the help of the simulation model if the time of irrigation based on the need for water (Subsection 8.2.3) differs from that for control of concentration c of a nutrient or electrical conductivity EC (Subsection 8.2.4).

8.2.1 Analytical approximation of water storage

Water storage in a 15 cm layer coarse sand
I assume that h is in equilibrium in the substrate, as is observed under near saturated conditions (Subsection 7.4.2; Otten, 1994). The amount of water stored in a layer of 15 cm coarse sand for different values of h at the bottom, and thus h-15 cm at the top, can be computed by integrating $\theta(h)$, Eq. [4-1], over h (Figure 8-3A; see also Section 8.1). Since the indefinite integral $\int \theta(h)dh$ with $\theta(h)$ as given by Eq. [4-1] is not available, I evaluate it using the Gauss-Legendre routine of Press *et al.* (1986). According to the main drying curve for $h = 0$ cm at the bottom, there is in total 4.15 cm of water available. According to the main wetting curve, represented by the ' $\alpha_d - \alpha_w$ -*model*' (Chapter 4), 3.24 cm is available. Both values are corrected for the residual amount of water. With an average daily evapotranspiration of, e.g., 0.4 cm d^{-1}, this means that, with $h = 0$ cm at $t = 0$ d, there is enough water available for 8 to 10 days, depending on the exact pathway of $\theta(h)$. During most of this period, h at the bottom remains relatively high (Figure 8-3). From Figure 8-3A the effect of cumulative water withdrawal on the value of h at the bottom can be simply obtained (Figure 8-3B). It follows that the change in h at the bottom as a function of cumulative water withdrawal is near linear up to a withdrawal of 3 cm, after which h changes rapidly. If on-line irrigation control is to be used in such a system based on measurement of h, it can be seen from Figure 8-3B that h at the bottom should not exceed say -15 cm (main wetting characteristic) or -25 cm (main drying characteristic). *When for this particular situation tensiometers are used for control of water supply, it is clear that these should be very sensitive since only small changes occur. Measuring actual water contents using e.g. TDR would be better. The benefit of measuring water content instead of pressure head is that the change in actual storage of water is determined and that hysteresis does not play a role.* Note that in reality, when the substrate dries out, the condition of equilibrium will no longer hold.

Water storage (cm)
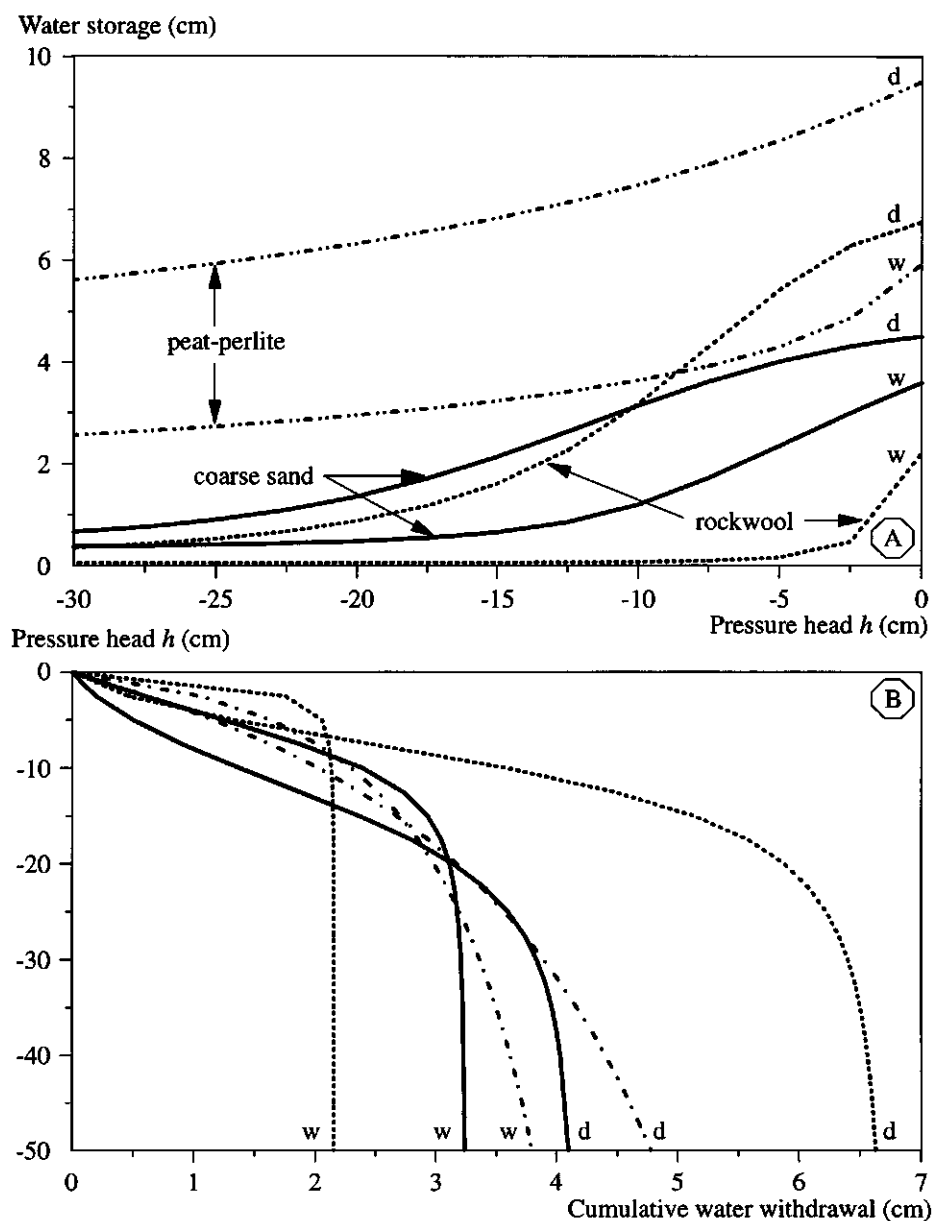
Figure 8-3 (A) The amount of water stored in 15 cm coarse sand, 7.5 cm rockwool or 12 cm peat-perlite mixture (based on physical properties of Tables 4-5 and 8-2) as a function of pressure head h at the bottom assuming equilibrium of h with height. The top lines refer to the main drying curves (d) and the bottom lines to the main wetting curves (w). In (B) h at the bottom as a function of cumulative water withdrawn is given based on the main drying (d) and wetting curves (w).

Water storage in a rockwool slab and in a pot filled with a peat-perlite mixture
For comparison, results for a 7.5 cm thick rockwool slab and for a 12 cm pot filled with
a peat-perlite mixture are given in Figure 8-3 as well. For rockwool it is obvious that the
difference in water storage based on main drying and main wetting curves differs largely.
Thus, if rockwool is allowed to dry out for a very long period, the amount of water
storage will decrease drastically from about 6.5 cm to a minimum of 2 cm. Similarly,
starting with an initially dry rockwool slab, without saturating it first, results in a system
with a small amount of water available to the crop.

8.2.2 Analytical estimate of root water pressure head

Since for not too extremely dry conditions the resistance for water flow through the root
is larger than that for water flow through the substrate (de Willigen *et al.*, *in prep.*), it is
possible to estimate h_r from Eq. [2-21] with h_{rs} equal to h (i.e. from Eq. [2-30]). With
$h = 0$ cm, $\Delta z = 15$ cm, $K_1 = 3 \; 10^{-6}$ cm d^{-1}, h_r can be computed as a function of L_{rv}
(Figure 8-4). Depending on the exact shape of the transpiration reduction function of Eq.
[2-27], it can be determined whether the plant has water stress when the substrate dries
out for longer periods. For example, for the transpiration reduction function given by Eq.
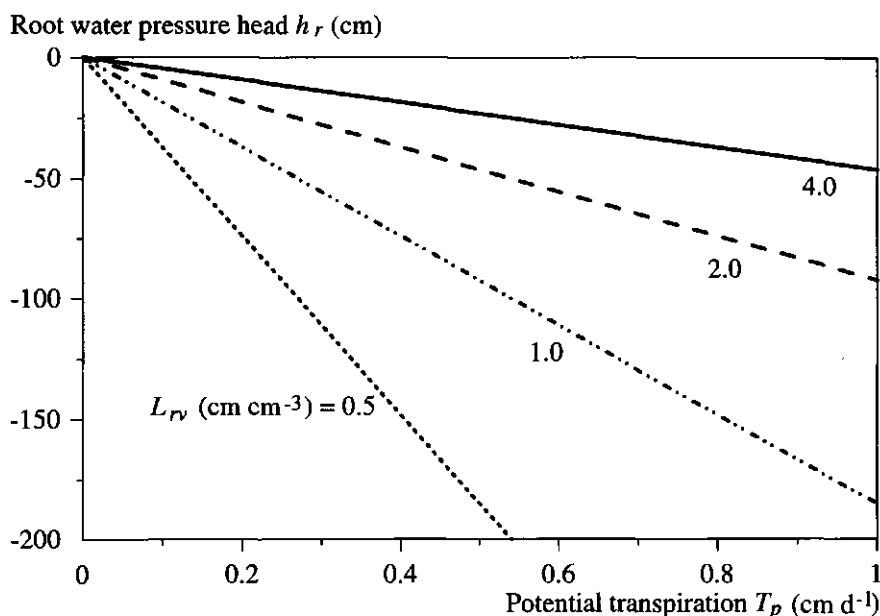
Figure 8-4 Root water pressure head h_r as a function of potential transpiration rate T_p for
different values of root length density L_{rv} assuming that there is no resistance to
water movement in the substrate surrounding the root and that the pressure head at
the root-substrate interface is equal to the bulk pressure head in the surrounding
substrate (Eq. [2-21]).

[2-28], with $h_{r,1/2} = -10^{-4}$ and $a = 10$, $T_a = 0.99\,T_p$ when $h_r = -6316$ cm. For $T_p = 0.4$ cm d^{-1} this means that no water stress occurs when $L_{rv} \geq 1.5$ cm cm^{-3}. For a mature plant this is generally the case. In the substrate h remains high: with the assumption of equilibrium (see previous paragraph), it does not become less than -45 cm during the first 8 to 10 days of water withdrawal at an assumed constant $T_p = 0.4$ cm d^{-1}, which is negligibly small with respect to h_r. *Based on water storage and root water pressure head it is concluded that it is not necessary to irrigate frequently in the sand bed system.* Based on the example used in this and the previous subsections, once a week is still possible. The maximum time span between two irrigation events depends on cumulative *ET*.

8.2.3 Simulation results: irrigation based on replenishment of evapotranspiration

With the simulation model, some runs were carried out
1) to determine whether problems with respect to water exist when the sand bed system is allowed to dry out to different limits, and
2) to show the effect on solute distribution in the sand bed.
The input parameters are listed in Appendix 6. The runs refer to the situation of Chapter 7, except that an irrigation control module was used to control the start time of irrigation. Irrigation started whenever the cumulative ET_p exceeded a threshold value. Five cases are considered, denoted by E1-E5 (Table 8-5). For cases E1-E4 measured evapotranspiration data of Chapter 7 were used. For the E5 case instead of using actual data daily evapotranspiration rate was set as 0.06 cm h^{-1}. The ET_p threshold value for case E1 results in a comparable fertigation frequency as used in the 'Growth & Uptake' experiment. Based on the initial condition of h being in equilibrium with $h = -8.5$ cm at the bottom, there was initially about 3.0 cm water available, so that only for the E5 case problems are to be expected with respect to water availability after about 85 hours (note: evapotranspiration occurred during 14 h d^{-1}).

Table 8-5 Five cases, E1-E5, for which simulations were carried out with irrigation controlled by a threshold value for ET_p (cm). Simulation results refer to the lowest h (cm) at $z = 0$ cm and $z = Z$ cm and lowest h_r (cm) at the last day of simulation. For case E5 the data refer to $t = 63$ h.

	E1	E2	E3	E4	E5
Threshold ET_p	0.15	0.5	1.0	2.0	4.0
$h\ (z = 0)$	-16.9	-20.9	-25.0	-39.2	-40.7/-53.2
$h\ (z = Z)$	-1.9	-5.9	-9.8	-22.3	-22.4
h_r	-1025	-1031	-1042	-1043	-8066

No problems were encountered with respect to root water uptake for the cases E1-E4. The differences between h_r obtained for cases E1-E4 were small with a maximum difference of about 2% (Table 8-5). At the last day prior to the irrigation event, the differences in h between the top and the bottom of the sand bed show that for cases E1-E3 near unit gradient conditions in h existed, but for case E4 this was not true anymore. The numerical solution for the E5 case ran into problems after 63 h. At that time h at the surface ranged from -41 cm to -53 cm, h at the bottom was about -22 cm (Table 8-5), and the total amount of available water present in the substrate was still 0.9 cm. Numerical difficulties were observed in determining h_r due to a rapidly decreasing h at the surface; h_r had decreased already to -8066 cm resulting in water stress (Table 8-5). Here we see that the above approach fails to predict the amount of available water under dry conditions, since then there is no equilibrium anymore.

Differences between the five cases were most pronounced with respect to concentration c (Figure 8-5). In the upper left corner c increased in all cases, exceptionally in the case E5. After a fertigation, c at the upper left corner did not come close to the input concentration $c_f = 15$ mmol l^{-1}. It remained high and after the fertigation at day 11 for the cases E1-E4 it amounted to 45 to 50 mmol l^{-1}. For the cases which were fertigated most frequently, e.g. E1-E3, c at the upper left corner shows a daily pattern of increasing

Concentration c (mmol l^{-1})
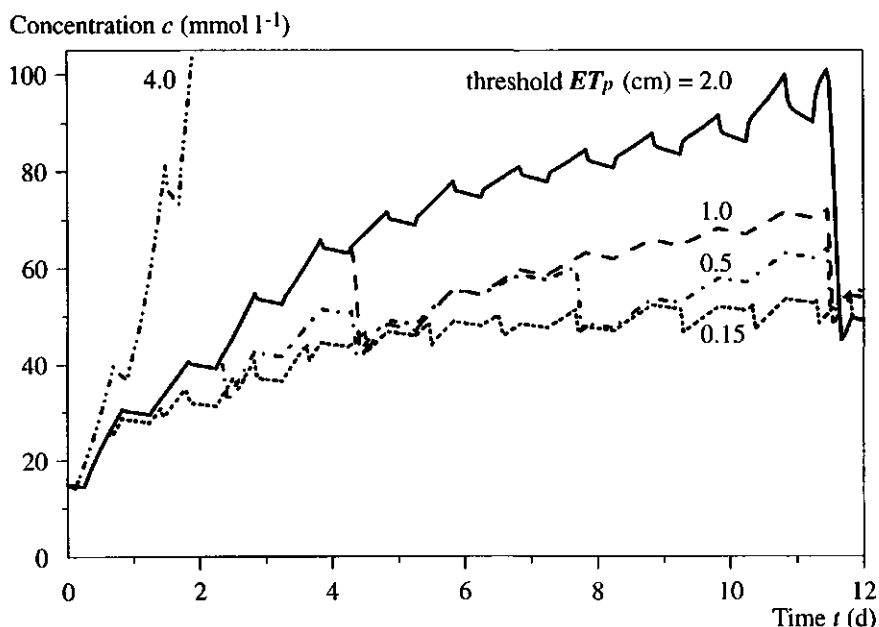
Figure 8-5 Time course of concentration at the upper left corner in a sand bed at four different fertigation frequencies: fertigation with leaching fraction of 0.5 occurred whenever the cumulative potential evapotranspiration ET_p exceeded a threshold value of 0.15 cm, 0.5 cm, 1.0 cm or 2.0 cm (cases E1-E5 of Table 8-5).

during the day due to a lower uptake concentration than the concentration in the root zone, and decreasing during the night due to nutrient uptake and diffusion away from this zone towards zones of lower c. Fertigation resulted in a sharp decrease in c. For the E4 case, where fertigation only took place at day 11, the pattern is slightly different. Besides the three stages just mentioned, there are also two other stages present. At the end of the day when water uptake ceased, a rapid decrease in c at the upper left corner is observed, which is caused by redistribution of water in the sand until equilibrium in h is reached again. The next morning, when evapotranspiration starts again, the equilibrium condition in h rapidly vanishes resulting in a sharp increase in c at the upper left corner.

The question remains whether the conditions with respect to c are harmful for crop growth. Lettuce belongs to the moderately sensitive crops with respect to EC (US Salinity Laboratory Staff, 1954; Maas and Hoffman, 1977a,b). Bernstein (1964) presented yield reductions of lettuce at different EC values in saturated extract, EC_e (Table 8-6). The simulations were done with $c_f = 15$ mmol l^{-1}, which is about the concentration of N in the nutrient solution used in the experiments. The EC of the nutrient solution for lettuce is about 2.3 dS m^{-1}. Assuming that uptake of all nutrients occurred at the same ratio at which they appear in the nutrient solution and assuming that EC is linearly related to the sum of all c's (see Appendix 8), then EC of the sand bed substrate solution can be estimated from c obtained in the simulation model according to the relationship

$$EC = 2.3 \frac{c}{15}.$$ [8-15]

Sonneveld *et al.* (1990) obtained the following empirical relationship between EC and EC_e:

$$EC_e = \frac{EC}{1.6}.$$ [8-16]

The average simulated c, and average estimated EC and EC_e at depths 2.5 cm and 5.0 cm are given in Table 8-7. At depth interval 0-2.5 cm problems are expected with respect to optimal growth conditions, since there $EC_e > 2$ dS m^{-1}, for which Bernstein (1964) gave yield reductions (Table 8-6). However, it is only part of the root zone that has this high EC_e, since at depth 5 cm $EC_e < 2$ dS m^{-1}. For case E4 the conditions of c may be undesirable, but no problems were encountered with respect to water availability.

Table 8-6 Percentage yield reduction of lettuce at different electrical conductivities in a saturation extract EC_e (dS m^{-1}) of the substrate (after Bernstein, 1964).

EC_e	2	3	5	>7
Yield reduction	10%	25%	50%	no data given; presumably 100%

Table 8-7 Average concentration c_{av} (mmol l^{-1}), and estimates of electrical conductivity of substrate solution EC_{av} (dS m^{-1}), and electrical conductivity in a saturation extract $EC_{e,av}$ (dS m^{-1}) according to the simulation results of cases E1-E4 at the end of day 10 at depths 2.5 cm and 5 cm (see text for explanation).

Case	c_{av}		EC_{av}		$EC_{e,av}$	
	2.5	5.0	2.5	5.0	2.5	5.0
E1	23.2	17.0	3.6	2.6	2.2	1.6
E2	25.5	16.8	3.9	2.6	2.5	1.6
E3	29.3	17.1	4.5	2.6	2.8	1.6
E4	41.7	20.0	6.4	3.1	4.0	1.9

In conclusion, *for this particular cropping system, frequent fertigations are needed to keep the c of the nutrients or EC below acceptable levels, and that fertigation times should be controlled by c or EC and not solely by θ.*

8.2.4 Simulation results: irrigation based on control of concentration

In this subsection I present *results of simulation runs in which fertigation was controlled by c.* Fertigation was initiated when c at one particular position in the sand bed system (e.g. a position where an on-line sensor could be present) exceeded a threshold value (the input parameters are listed in Appendix 6). Fertigation was started whenever at $(x, z) = (8.75 \text{ cm}, 2.5 \text{ cm})$ c exceeded 21 mmol l^{-1}. This value is somewhat larger than the optimal c of 19 mmol l^{-1} for N in nutrient solution of lettuce grown on NFT (Sonneveld and Straver, 1988). After fertigation stops the control mechanism is activated again. Three cases are considered: with one or two surface drippers, and with one buried dripper (Figure 8-6). The first case is the one used mostly in the previous examples. The second case was used in the experiments (no data reported): Schwarz *et al.* (1995) reported for this situation a more even root distribution than for the case with only one dripper. The third case is used to determine if buried fertigation might be an alternative for water and nutrient solution supply. The third case may result in too high solute concentrations at the surface due to the primarily upward movement of substrate solution, analogous to the situation of potted plants on flooded benches used by Otten (1994).
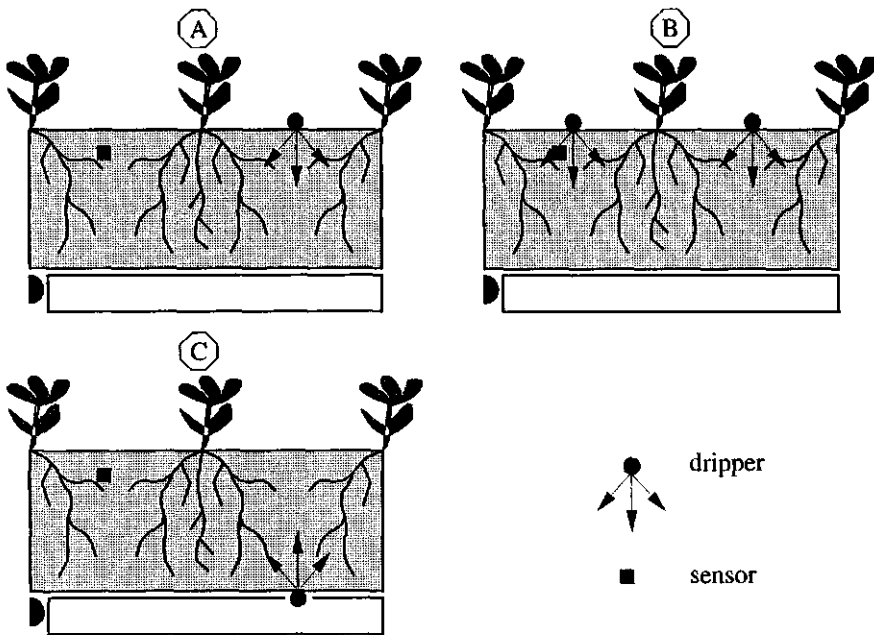
Figure 8-6 Dripper and sensor location configuration for the three cases where fertigation was controlled by a threshold concentration c at the sensor location: (A): one surface dripper; (B): two surface drippers; (C): one buried dripper.

In all three cases c at the sensor location could be kept below the set-point of 21 mmol l^{-1} (Figure 8-7). The case with two drippers at the top resulted in only three times of fertigation, while the other two cases resulted in frequent fertigation, sometimes even periods of 'continuous' fertigation existed. In all three cases water and nutrient uptakes by the crop are as required. At the surface c remains below 50 mmol l^{-1}. The mass balance results for water and N show that for this twelve day period in the second case about 15% less water and N is applied, and the outflow is about 26% less than for the other two cases (Table 8-8). About 31% and 27% of the N input leaves the substrate with the drain water for the first and second case, respectively. *Thus, to have a dense grid of drippers, i.e. drip lines between all plant rows, has the advantage that fewer fertigations occur, and that on average less water and nutrients are applied and leave the substrate through the drain.* This is due to the drier conditions in that case, leading to less drainage.

Of course, care must be taken in placing sensor and dripper in the system. For example, if a single surface dripper were placed near the sensor of Figure 8-6, the results (times of fertigation, c at sensor location) for this case would perhaps not differ much from case with two surface drippers, except that solutes would accumulate at the right part of the root zone.

Concentration c (mmol l^{-1})
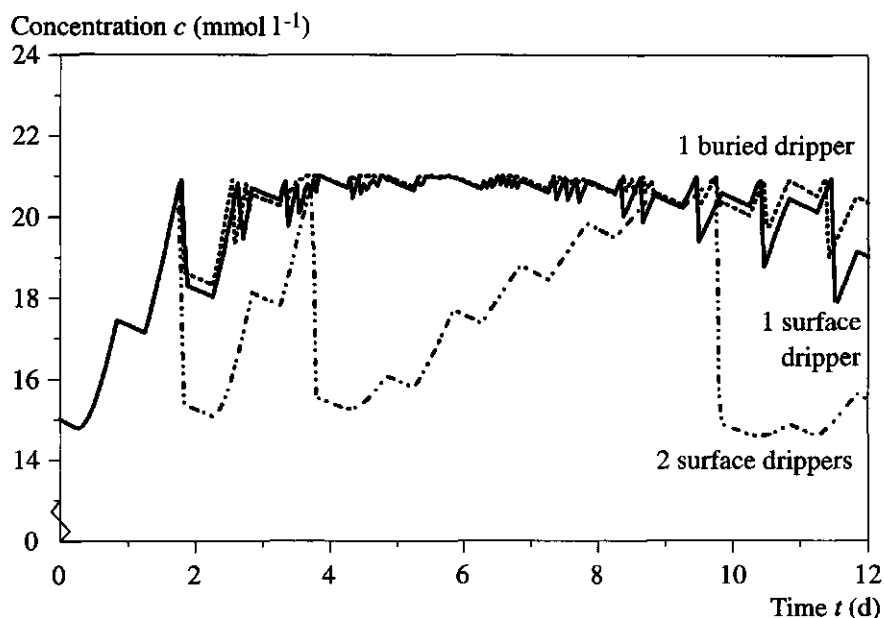
Figure 8-7 Simulation time course of concentration c at $(x, z) = (8.75$ cm, 2.5 cm) in case at this position fertigation is controlled by a threshold concentration of 21 mmol l^{-1}. Three cases are considered with different dripper locations (Figure 8-6; see text for explanation).

Table 8-8 Amounts of water (ml) that entered the substrate slab through irrigation and left the substrate through drainage and the amount of N (mmol) that left the substrate with the drainage water. The input concentration was $c_f = 15$ mmol l^{-1}.

Case	Irrigation	Drainage	N outflow
1 surface dripper	165	63	0.78
2 surface drippers	141	46	0.58
1 buried dripper	~165	~65	~0.87

[1] The data for the third case are approximated values, since only net results at the bottom boundary were available. Since in the first and third case the fertigation regimes were similar it was assumed that the same amount of nutrient solution was applied in both cases, so that the data for the third case could be computed.

This example shows that, with fertigation based on an on-line measurement in the sand bed, it is possible to keep *c* at a certain location below a threshold value. However, when in that case the amount of water applied each time is based on the amount of water use since the previous fertigation, this may result in near continuous fertigation events, i.e. when only one dripper was present. Shortage of water never occurred. During these near continuous fertigation events, which sometimes lasted for 0.5 d, a permanent saturated zone exists. For example, for the case presented in Figure 7-7, the saturated zone amounted to 16% of the total volume of the sand bed slab, thus reducing the effective root zone which may be harmful. Another control mechanism could be to initiate fertigation whenever an upper threshold value is reached at a certain point, and stop fertigation whenever a lower threshold value is reached. Drawbacks of this method are that large amounts of fertigation and drainage can occur. Long fertigation periods may be undesirable (see above), and large amounts of drainage water is also undesirable with respect to sterilization of the drainage water. What the best threshold values are must still be determined, e.g. with the help of this simulation model.

8.3 Leaching accumulated solutes from the substrate

after a growth period

After a growth period when the crop is removed from the substrate, usually the remaining nutrients and salts in the substrate result in a too high initial concentration for a new crop. Then the substrate must be flushed to obtain good initial conditions. Of course, this results in a waste problem, and it is desirable to prevent accumulation in the first place. However, when the initial conditions are not acceptable, the question is *how much of the new solution must be applied, and what kind of application system, i.e. drippers or sprinklers, is needed to obtain good starting conditions for the new growth period.* The same question arises when during the growth period a substrate solution of wrong composition has to be replaced by a solution with a good composition.

In this example I assume a specific final distribution for a solute (Figure 8-8), which could have resulted for a bedding system with surface drip fertigation at horizontal distance $x = 30$ cm. The highest solute concentration is present at $(x, z) = (10$ cm, 0 cm). Two cases are considered: flushing by drip application at $x = 30$ cm, or by overhead sprinkling application across the whole substrate surface. The input parameters for the simulation model are given in Appendix 6.

Depth z (cm)

Horizontal distance x (cm)
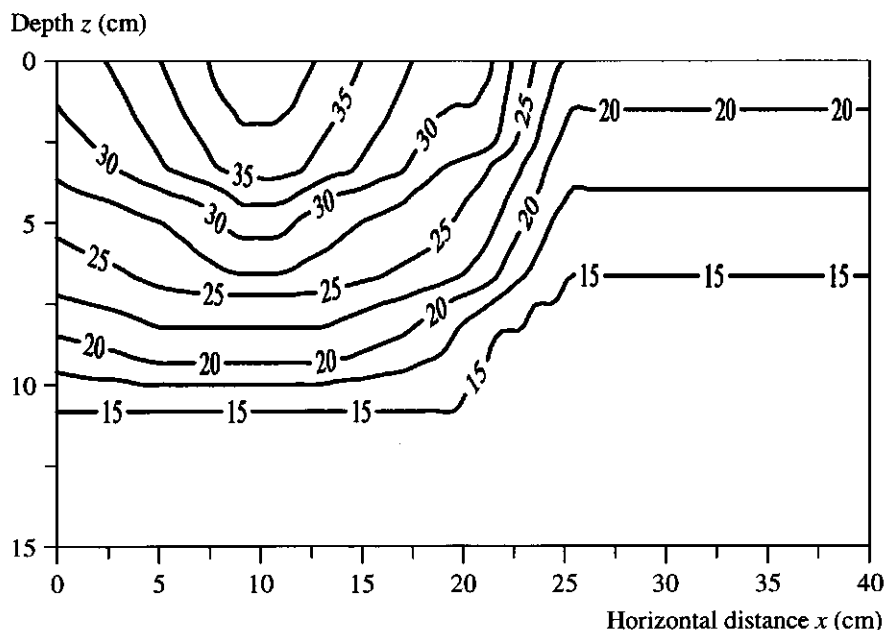
Figure 8-8 Distribution of concentration c for a bedding cropping system used as starting conditions for the cleaning example of Section 8.2.

The results (Figure 8-9) refer to
a) the concentration of the effluent relative to the influent concentration c/c_f, where c_f is the desired initial concentration of the solute for the new crop,
b) the concentration of the upper left corner of the substrate relative to the influent concentration $c(ul)/c_f$, which is the worst position for the case of drip application, and
c) the total amount of the solute present in the substrate relative to the final desired homogeneous distribution Q/Q_f.
The results are shown as a function of the total volume of solution applied relative to the volume of solution present in the substrate: V_s/V_i. The differences between the two cases are clear. The total amount Q decreases continuously in both cases. For $V_s/V_i > 0.5$ the decrease with drip application is faster than with sprinkling application. However, not at all positions c drops faster, like in the upper left corner of the sand slab (Figure 8-9b). The increase in c in the beginning at the upper left corner is due to diffusion and mass flow from $x = 10$ cm to $x = 0$ cm where initially c was lower. The initial Q for the sprinkler case was lower then for the dripper case since the final amount of water, and hence Q_f, was higher for the sprinkler case. Also for the sprinkler case, Q/Q_f increased at first as a result of the fact that the total water content, i.e. V_i decreased in the beginning. In Table 8-9 the values for V_s/V_i are given for which c/c_f of effluent or upper left corner and

Relative drain effluent concentration c/c_f or total amount Q/Q_f (-)

Relative concentration in upper left corner $c(ul)/c_f$ (-)

Relative volume of applied solution V_s/V_i (-)
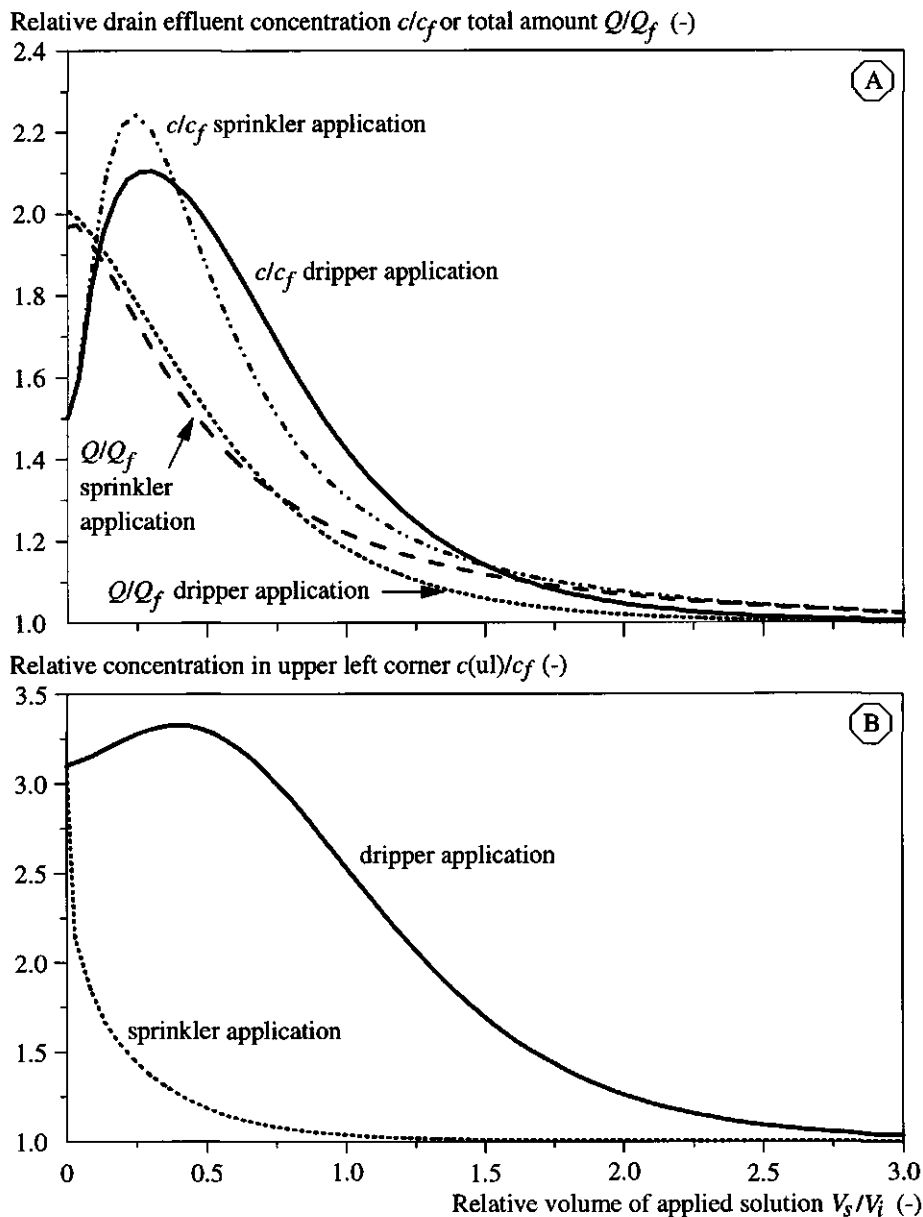
Figure 8-9 (A) Change of concentration c of the drain effluent relative to the input concentration c_f and change of total amount present in the substrate slab Q relative to the final total amount Q_f for the cleaning experiment with either drip or sprinkler application. The x-axis represents the volume V_s of solution applied relative to the volume V_i present in the substrate. In (B) the change of the concentration at the upper left corner of the slab is presented.

Q/Q_f for both cases reaches the new equilibrium condition within 5%. For example, after 1.58 times V_i is applied for the dripper case $Q = 1.05\,Q_f$. However, in the upper left corner c then is still 1.61 times larger then the desired value. With respect to c at the upper left corner 2.77 times V_i must be applied to reach $c/c_f = 1.05$.

Table 8-9 Required volume of cleaning solution relative to volume present in substrate slab V_s/V_i so that the concentration of the drain effluent c or the concentration at the upper left corner $c(ul)$ reach are 1.05 times the input concentration c_f, and so that the total amount Q of solute in the substrate slab reaches 1.05 times the new maximum amount Q_f for the cases of dripper and sprinkler application in the cleaning example.

Dripper			Sprinkler		
c/c_f	Q/Q_f	$c(ul)/c_f$	c/c_f	Q/Q_f	$c(ul)/c_f$
1.97	1.58	2.77	2.37	2.30	0.90

One could expect that a homogeneous supply over the whole surface is much more efficient than a local application. However, it is remarkable to observe that at the end the conditions for the sprinkling case are less favourable than those for the dripper case. In the sprinkling case different dispersion occurs due to the higher water velocities, and water that enters far from the drain has to compete with water that enters above the drain to flow towards and into the drain. Further experimentation and simulation is needed to fully explain why the sprinkling case seems less efficient. A drawback for the dripper case is that at the upper left corner not a complete refreshment is achieved. But if it this zone was refreshed, it would become concentrated in a very short time during the next growth period anyway.

Note that the time scales for the two cases differ. One unit of V_s/V_i corresponds to 230 min or 48 min for the dripper or sprinkler cases, respectively. Based on the different application intensities and different areas of application, ideally the difference should be a factor 5. Since the volume of solution in the sand bed in the sprinkling example initially decreased this is not the case.

8.4 Water and solute distributions in a rockwool slab

The simulation model can also be used to study the dynamics of water and nutrients in other types of cropping systems. Here I consider rockwool slabs. This example is meant for demonstration purposes only. I will give a short introduction (Subsection 8.4.1) followed by some simulation results (Subsection 8.4.2).

8.4.1 Introduction

A rockwool cropping system consists of a slab of 7.5 cm height on top of which small planting cubes are positioned. The volume of rockwool occupied by one plant, e.g. tomato, is typically $50 \times 30 \times 7.5 + 5 \times 5 \times 5 = 11375$ cm^3. Due to symmetry I only consider half the region between two plants (Figure 8-10). Note that, due to an error, the width of half the cube was taken as 5 cm. I simplified the system to a two-dimensional system by assuming that the planting cube extended over the whole width of the slab. In most systems drainage occurs through slits cut in the surrounding plastic sheet about 2 cm above the bottom of the rockwool. Such drainage processes cannot be treated in the simulation model. Here I consider the drain at the bottom of the rockwool as a seepage face. I consider two drain positions (Figure 8-10): either between two plants further denoted as case RW1, or below a plant further denoted as case RW2. The rockwool is surrounded by a plastic sheet, except at the top of the planting cube, where evaporation occurs and fertigation takes place. Thus all other boundaries are no flow boundaries, except for the drain. The simulation model can only consider full rectangular flow domains, which does not hold in this example. However, the region above the rockwool slab and to the left from the planting cube is characterized with the following parameters:
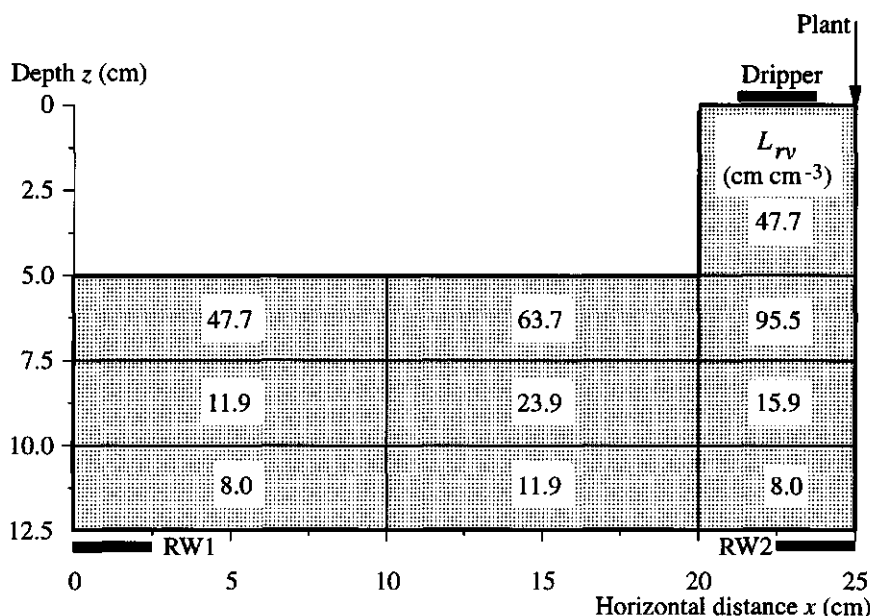
Figure 8-10   Two-dimensional representation of a rockwool slab of 7.5 cm thickness plus a rockwool planting cube. The dripper is located on top of the planting cube, and the drain is either located at lower left corner, i.e between two plants (RW1) or at lower right corner, i.e. below a plant (RW2). Regions of equal root length density L_{rv} are indicated.

$K_s = D_0 = a_L = a_T = 0$, where K_s is the hydraulic conductivity at saturation, D_0 is the diffusion coefficient in free water, and a_L and a_T are the longitudinal and transversal dispersivities, respectively. Due to geometric averaging of these quantities at the interfaces of two control volumes, it is guaranteed that no flow of water or transport of nutrients occurs across the interface between the control volumes in the rockwool and those in the blocked-off region. Thus, no-flow boundaries are guaranteed. The incomplete Cholesky conjugate gradient solution method (Subsection 3.3.2) was slightly modified. For the blocked-off region all elements of matrix **L** were set to zero, so that the solutions of Eqs. [3-50] and [3-51] did not need to be computed. Another example where a blocked-off region was considered with this simulation model was in a study of water and nutrient uptake by potato growing on a ridge (de Willigen *et al.*, 1995).

All input data used in the simulation model are presented in Appendix 6. There are no quantitative data available in the literature for comparison with the simulation results. Some experimental data on *EC* and L_{rv} distributions were presented by van Noordwijk and Raats (1978, 1980). Unfortunately, the rockwool cropping systems at that time differ from the current systems, since the top of the rockwool was partly not covered with plastic, so that evaporation occurred. Thus the *EC* and L_{rv} distributions of their system is different from the system used in this study. Nevertheless, I used their L_{rv} distribution as input, since no other data are available. Van Noordwijk and Raats (1980) gave also a visualization of the flow process with the help of a dye tracer. They showed that for the RW2 case water movement mainly occurred in the region vertically below the planting cube towards the drain, and they concluded that the leaching efficiency was low.

8.4.2 Results

It is not my purpose to describe all outcomes of the simulation runs. I only present some characteristic results and show solute flux density and solute distributions.

At all times, *h* distributions suggest near unit gradient conditions in *h*. At the plant position at the top, *h* ranges from about -20 cm to -10 cm. At the bottom *h* ranges from 0.25 cm to -8 cm. The maximum height of the saturated zone during irrigation is very small with a maximum of about 0.25 cm for case RW1, or less than 0.05 cm for case RW2. Except during and just after an irrigation and drainage event, there are negligible gradients in *h* in the horizontal plane. During the day h_r is about 2500 cm in both cases RW1 and RW2, and water uptake could meet the potential transpiration demand. The total amount of water present in the rockwool slab decreases during the first 5 days. After that, there is a constant pattern of drying out due to evapotranspiration and wetting up due to irrigation. For case RW2 the total water storage is on average slightly higher. The cumulative drainage after twelve days is 2% higher for the case RW1, but the differences between the two cumulative outflows tend towards a constant value in course of time. Thus, it can be concluded that *the position of the drain does not affect total water storage and drainage amount.*

The flux density distribution of a solute, e.g. N, during a fertigation-drainage event shows that there is little difference between the two cases RW1 and RW2 when there is only input of solution (Figure 8-11 A,B). When drainage starts, there is a big difference in flow pattern (Figure 8-11 C,D). The first situation lasts for about one hour, while the second situation lasts about half an hour; drainage stops six minutes after fertigation stops. As is obvious from Figure 8-11, the upper left corner of the rockwool slab hardly participates in the flow process, so that it is a so-called dead corner in the system. Within five days at that corner the concentration c drops to zero. At day six in more than 40% of the volume $c < c_f$ (Figure 8-12). In case RW2 during drainage, most of the solution applied directly leaves the system through the drain, while in case RW1 it passes the whole rockwool substrate, as was also observed by van Noordwijk and Raats (1980). Corresponding with the c distribution (Figure 8-12), it is not surprising that the drain water of case RW2 contains more N than that of case RW1 (Figure 8-13). The total amount of N stored in the rockwool system continuously drops in case RW2, while for case RW1, after an initial drop in total amount, a constant pattern with decreasing c due to uptake and increasing c due to fertigation is established (Figure 8-12). The larger outflow of N in case RW2 cannot be attributed to a larger amount of drainage outflow, since this is nearly the same as for case RW1, as presented in the previous paragraph.

Although realistic input data were used and c_f was that recommended for tomatoes grown on rockwool, depletion of N occurs. This is not expected since the recommended c_f is based on the fact that c in the root zone increases to assure ample availability of nutrient to the root and optimal osmotic conditions (see Chapter 1). According to Sonneveld and Straver (1988) the desired c for N in the root zone is 17 mmol l^{-1}. It should be noted that with the simulation model no recirculation is considered. For case RW1 c of the collected drain water is 9.0 mmol l^{-1} and for case RW2 this is 14.7 mmol l^{-1}, so that for case RW2 c of the applied nutrient solution would increase in time and for case RW1 it would decrease.
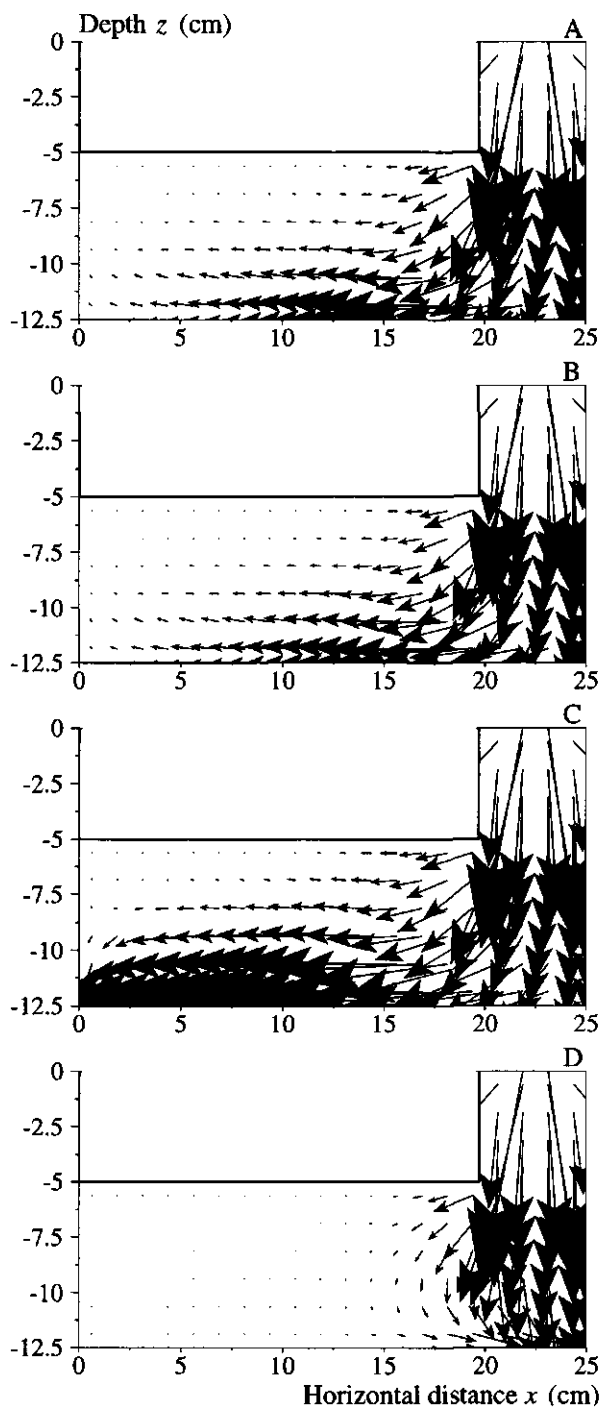
Figure 8-11
Simulated solute flux density distribution in a rockwool slab plus planting cube at day six during the period of fertigation (A,B) and fertigation plus drainage (C,D) for two cases of drain position: between two plants (RW1, A,C) or below a plant (RW2, B,D). A solute flux density with a magnitude of 0.05 mmol $cm^{-2} h^{-1}$ corresponds with an arrow length of 10 *x*-axis units.

Depth z (cm)
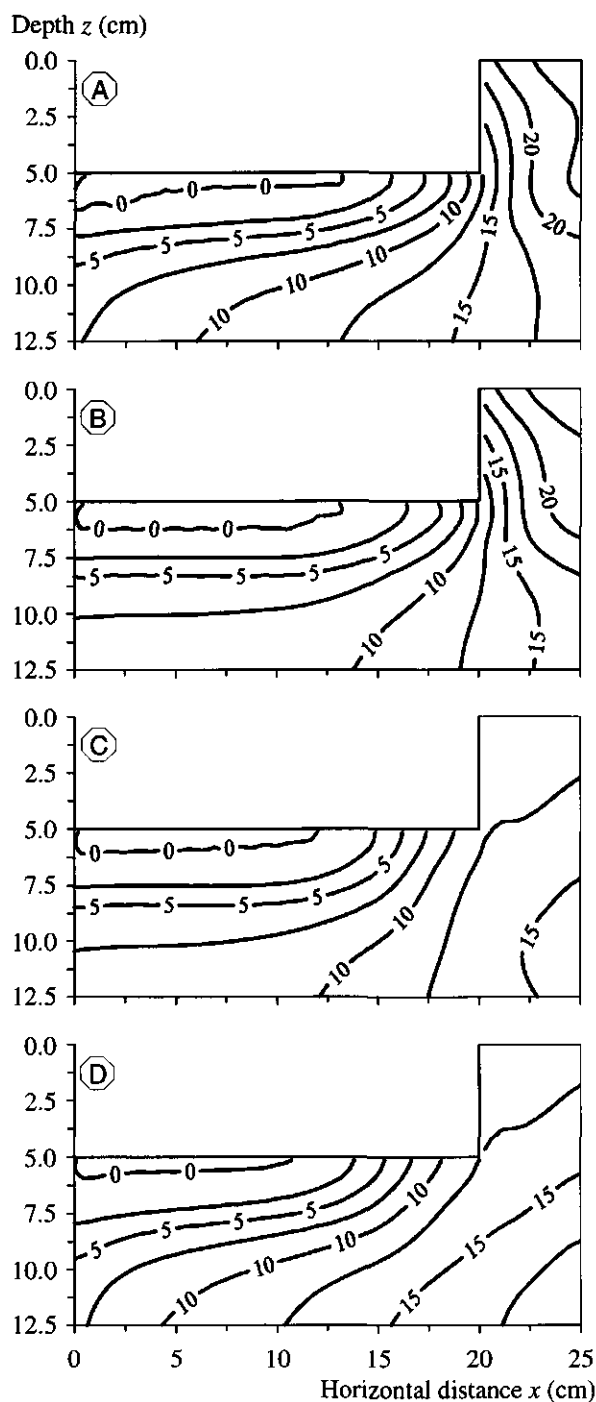
Figure 8-12
Simulated distributions of the concentration c of nitrogen (mmol l^{-1}) in a rockwool slab plus planting cube at day 6 just before the start (A,B) and just after (C,D) a fertigation-drainage event for the case where the drain is located between two plants (RW1, A,C) or below a plant (RW2, B,D). The contour line zero is doubtful and is the result of the Kriging interpolation method used.

Horizontal distance x (cm)

N storage or cumulative outflow (mmol)
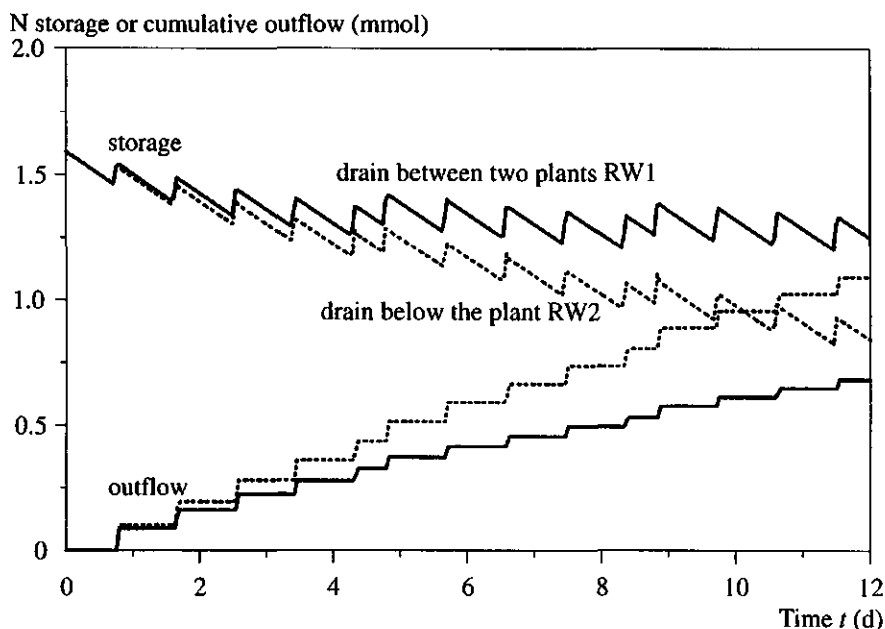
Figure 8-13 Simulated time course of storage of N in a rockwool slab plus planting cube and cumulative outflow of N for the cases where the drain was located between two plants (RW1) and below a plant (RW2).

8.5 Conclusions

In this chapter I have applied the simulation model of Chapter 3 in case studies. In general, the simulation model can be used for a wide range of problems and it is not restricted solely to rectangular bedding systems.

The following conclusions are drawn.

- In designing bedding systems with an optimal drain distance, two analytical equations can be used to estimate as a first approximation, respectively, the maximum height of the phreatic surface and the rate of disappearance of the phreatic surface. These equations overestimate these properties. A better estimate of the maximum height can be obtained when it is adapted for horizontal movement in the unsaturated zone, i.e. by assuming that this movement also occurs in a capillary fringe above the phreatic surface.

- Saturated conditions in the sand occur only for very short periods. Thus, under practical conditions, saturated conditions will not persist for too long periods, and, due to the shape of $\theta(h)$, aeration problems are unlikely. This is also true for other coarse substrates. For a natural loam soil it can be shown that the system remains too wet,

even for very small drain distances and irrigation intensities. This means that natural soils cannot be used in thin layer substrate systems.

■ Based on water storage, estimated from the water retention characteristic, and root water pressure head, it is concluded that it is not necessary to irrigate frequently in the sand bed system. However, when the system is allowed to dry out for a long period, too high nutrient concentrations may occur in the root zone. Thus, fertigation scheduling must be based on control of concentration in the sand bed instead of being based solely on resupplying water lost by evapotranspiration. It is shown that such a control procedure is possible.

■ For coarse porous substrates the change in pressure head due to water removal is small. Therefore, it requires sensitive tensiometers when water supply is based on change in pressure head. It is advised to use water content measurements instead. This has the benefit that the change in actual storage of water is determined and that hysteresis does not play a role.

■ Leaching accumulated solutes originating from drip application can best be done by the same drip system. When using a sprinkling system more new solution has to be applied in order to obtain the desired new situation. However, with the drip system not at all positions in the root zone the desired concentration will be reached.

■ In a rockwool slab cropping system, the position of the drain has a large effect on the flow pattern inside the rockwool. Drains should not be located below the dripper, but situated between two drippers.

The goal of this thesis (Chapter 1) was to formulate and validate a simulation model for water movement and nutrient transport in closed, recirculating cropping systems. Now that it is available, the simulation model can be used to develop closed cropping systems with special attention to fertigation strategies. The model was developed in Chapters 2, 3 and 4, and it was validated in Chapter 7. In this chapter the simulation model was used to show the capabilities of the simulation model. Due to the complexity of the model and the fact that it is a two-dimensional representation of reality, the outcome must be considered with care, and preferably tested with experimentation.

It has been shown that a thorough description combined with detailed measurements of water content, solute transport and root water and nutrient uptake is required to understand the dynamics of water and nutrients in closed, recirculating cropping systems. The present model will be documented in due time. It can be used by researchers to develop fertigation strategies based on physical properties of the substrate. Nevertheless, there are still aspects that need further investigation. These are, for example:

- how appropriate is a two-dimensional approach for three-dimensional problems;
- inclusion of other sources and sinks, such as adsorption and desorption, in the solute transport module;
- sensitivity analysis of the main parameters appearing in the simulation model;
- effect of hysteresis on root water uptake.

Appendix 1

On the function *P*

The definition of the function *P* in the text follows from Mualem (1984) from whom I quote:

> *"... The independent domain theory assumes that all pore domains are free to drain independently, though in reality pores can drain only when free access to outside air is formed. Thus, the pore domain ability to drain is rather dependent on the state of the surrounding pores. To account for this phenomenon, a domain dependence factor (P_d) is applied. Following Everett (1975) and Mualem and Dagan (1975), P_d is considered to be a macroscopic variable that depends on the actual θ. By definition, P_d describes the relative portion of the drainable pores...".*

Mualem (1984) defined P_d as follows

$$P_d = \frac{\Delta\theta}{\Delta\theta_0}, \qquad\qquad [\text{A1-1}]$$

where $\Delta\theta$ represents the change in θ of the latest drying process that has occurred, and $\Delta\theta_0$ represents the change in θ corresponding to the identical process, but in the absence of blockage of air access - namely, $P_d = 1$, as if the pore water domains were actually independent. Mualem (1984) then gives the domain dependence factor in explicit form, using the main drying characteristic and main wetting characteristic. This is given as Eq. [4-10] in the text.

Some special attention is given here to evaluating the function *P*, defined in Eq. [4-10] of the main text, in case of the scanning drying curve. The water content for which Eq. [4-8] of the main text is valid is found iteratively using Brent's method (Press *et al.*, 1986; function ZBRENT described in their chapter 9.3). Although the derivative of Eq. [4-8] of the main text is known, Eqs. [4-14] of the main text, and thus a fast Newton-Raphson method could be used as well, this is not done because of the complexity of the derivative expression. Brent's method finds the root of the function

$$f(\theta) = \theta(h) - \theta_\Delta + P(\theta)\big[\,\theta_s - \theta_w(h)\,\big]\big[\,\theta_w(h_\Delta) - \theta_w(h)\,\big], \qquad [\text{A1-2}]$$

for which $f(\theta) = 0$. The accuracy at which *x* is to be obtained is given as ϵ_a, i.e. $\epsilon_a = 10^{-4}$. The range where *x* is to be found is obviously $[\,\theta_r, \theta_s\,]$. Unfortunately, Brent's method fails at the boundary values, so that a somewhat smaller initial guess of the range is used as input: $[\,\theta_r + \epsilon_1, \theta_s - \epsilon_1\,]$, with ϵ_1 set to a small number, i.c. $\epsilon_1 = 10^{-6}$. However,

$f(\theta)$ as defined in Eq. [A1-2] (-)
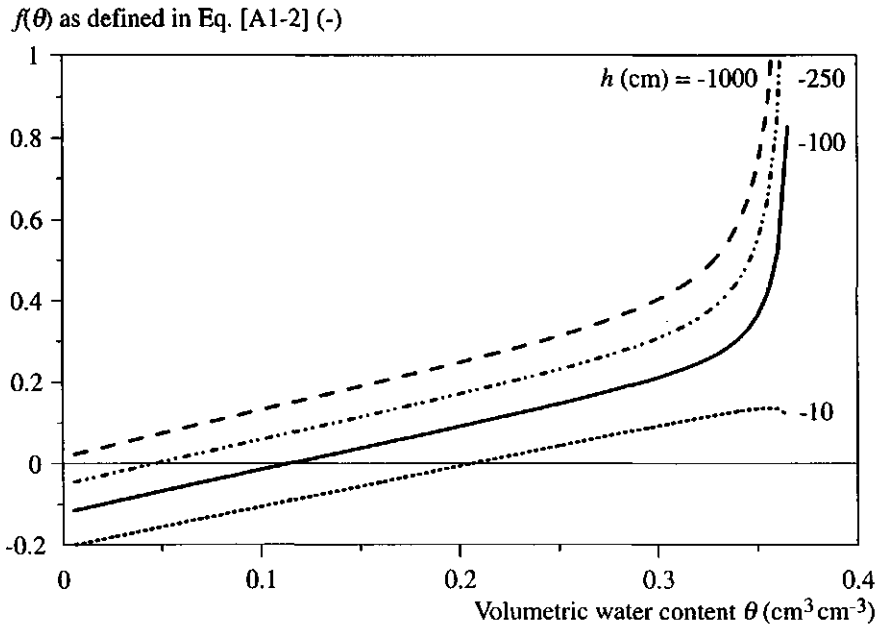
Figure A1-1   Example of function $f(\theta)$ (Eq. [A1-2]) for a fictive soil with $\theta_\Delta = 0.2$ cm^3·cm^{-3} and $h_\Delta = -54.1$ cm.

the length of the range can be decreased, since we know the last reversal point and a scanning drying curve is followed. The new range than becomes [$\theta_r + \epsilon_1$, $\theta_\Delta + \epsilon_2$], with ϵ_2 set to some value because of safety reasons, i.c. $\epsilon_2 = 0.01$. These new boundaries may not exceed the maximum boundaries $\theta_r + \epsilon_1$ or $\theta_s - \epsilon_1$. An example of the function $f(\theta)$ for a fictive soil with $\theta_\Delta = 0.2$ cm^3·cm^{-3} and $h_\Delta = -54.1$ cm is given in Figure A-4. It is obvious that there is only one root for which $f(\theta) = 0$, and thus ZBRENT's module will yield a unique estimate for θ. Since the scanning drying curve is followed, $|h| > |h_\Delta|$, and thus the curve for $h = -10$ in Figure A-4 is meaningless. For a very large pressure head, i.c. $h = -1000$ cm in Figure A1-1, the function $f(\theta)$ is always larger than zero, and no value for θ will be obtained, and thus ZBRENT's method will fail. Presumably, this situation never occurs, and the scanning drying curve will have crossed the main drying curve and the function $f(\theta)$ needs not to be evaluated anymore. Moreover, it is still possible that the true new water content value searched for is in the range [θ_r, $\theta_r + \epsilon_1$] or [$\theta_s - \epsilon_1$, θ_s]. In that case nothing happens, i.e. $\theta^{t+\Delta t} = \theta^t$.

When the status κ_h of a node changes to 1 or + 1, some constants in Eqs. [4-8] and [4-9], respectively, are computed. For the node under consideration the constants θ_Δ and $\theta_w(h_\Delta)$ occurring in Eq. [4-8] (when $\kappa_h = -1$) are computed and stored, while for Eq. [4-9] (when $\kappa_h = +1$) the constants θ_Δ, $\theta_w(h_\Delta)$ and $P(\theta_\Delta)(\theta_s - \theta_w(h_\Delta))$ are computed and stored.

Appendix 2

Simultaneous fit of drying and wetting data using Mathematica

The Mathematica (Wolfram, 1991) statements used in order to obtain the hysteretic properties simultaneously are listed below. The parameters θ_r, θ_s, α_d, α_w and n are represented by r, s, a1, a2 and n, respectively. The data are read from files. Mathematica statements are printed as Courier.

Read data: drying data in X1.DAT (applied *h*) and Y1.DAT (measured θ), and wetting data from X2.DAT and Y2.DAT:

```
x1:=<<x1.dat
x2:=<<x2.dat
y1:=<<y1.dat
y2:=<<y2.dat
```

Defining the two water retention functions:

```
t1[r_,s_,a1_,n_,x1_]:=r+(s-r)/(1+(a1*x1)^n)^(1-1/n)
t2[r_,s_,a2_,n_,x2_]:=r+(s-r)/(1+(a2*x2)^n)^(1-1/n)
```

Defining the optimization criterion, i.e. the sum of squares of differences between observations and fitted values:

```
ssq[r_,s_,a1_,a2_,n_]:=
    Sum[(t1[r,s,a1,n,x1[[I]]]-y1[[I]])^2,{i,24}]+
    Sum[(t2{r,s,a2,n,x2[[I]]]-y2[[I]])^2,{i,24}]
```

The solution is found with the directive FindMinimum according to:

```
FindMinimum[ssq[r,s,a1,a2,n],{r,r0},{s,s0},{a1,a10},
    {a2,a20},{n,n0}]
```

where r0, s0, a10, a20, and n0 are initial guesses supplied by the user. By supplying different initial guesses, or the results from a previous estimate, it can be determined whether a true global minimum is obtained.

Table A2-1. Hydraulic parameters θ_r (-), θ_s (-), n (-), α_d (cm^{-1}), and α_w (cm^{-1}) as obtained from a simultaneous fit of the drying and wetting data using Mathematica (Wolfram, 1991) for the layers 0-5 cm and 5-15 cm; it is assumed *a priori* that $m = 1 - 1/n$ (-). The sum of squares of differences between observations and fit is given as *ssq*.

Depth	θ_r	θ_s	n	α_d	α_w	*ssq*
0-5 cm	0.01438	0.2806	3.7631	0.062236	0.11633	0.0230
5-15 cm	0.02470	0.2802	4.2284	0.052189	0.10087	0.0203

Appendix 3

Description of note numbers occurring in Chapter 5

Description of notes occurring in Chapter 5. The use of trade names is for informational purposes only and should not be considered an endorsement.

1   Grundfos P5.

2   Dan Sprinklers type 8855, 2.88 m^3d^{-1} discharge at operating pressure of $2 \cdot 10^5$ Pa.

3   Netafim type Typhoon, 0.042 m^3d^{-1} discharge at operating pressure of $1 \cdot 10^5$ Pa.

4   Keller type PR46, range 0 Pa to $1 \cdot 10^4$ Pa.

5   Outside diameters of $31 \cdot 10^{-3}$ and $35 \cdot 10^{-3}$ m; the ridges were spaced $5.5 \cdot 10^{-3}$ m apart. Three rows of slits were located along the length of the drain between every other ridge, with average slit dimensions of $6 \cdot 10^{-3}$ x 10^{-3} m (length x width).

6   Grundfos KP200.

7   Keithley Instruments Workhorse Data Acquisition System with serial interface board.

8   Compaq deskpro 386s/16.

9   Tektronix short range cable tester 1502C metric version with internal battery and serial interface SP232.

10   Telemeter Electronics, Donauwörth, Germany, multi-position coaxial switch model SR-6C-H.

11   SMA connector type Radiall R-125-025.

12   Impedance 50 Ω, damping 48 dB/100 m at 1 GHz.

13   Philips *EC* electrode PW9554/00 connected to a Philips digital conductivity meter PW9526.

14   Micro Switch, Honeywell, type 141-PC-15G, 0 Pa to $-1 \cdot 10^5$ Pa giving 1 V to 6 V output at 8 V excitation supply.

15   Soil Moisture Equipment type 652X03-B1M3. Dimensions: length $65 \cdot 10^{-3}$ m, outside diameter $6 \cdot 10^{-3}$ m, and wall thickness 10^{-3} m. The air entry value was 10^5 Pa.

16   Mallinckrodt, Germany.

17   Superb PCC-3-2-2, $-1 \cdot 10^5$ Pa to $2 \cdot 10^5$ Pa, 0.05% full scale accuracy.

18   Unicurve thermistors, 3000 Ω at 25 °C, ± 0.2 °C.

19   MGW Lauda RK 20, -40 °C to 150 °C, ± 0.1 °C.

Appendix 4

Background information about dimensioning the TDR probe

In choosing the configuration of the TDR probes several aspects were considered, i.e. minimal disturbance during insertion, rod spacing and diameter ratio, probe dimension and measured volume, and rod length related to EC measurement. These aspects will be discussed briefly below. Note that the effect of cable length is not taken into account.

Minimal disturbance during insertion.
In order to minimize disturbance of the soil around the probe rods, the rod diameter and length should be kept small.

Rod spacing and diameter ratio.
It is desirable that the impedance of the probe that is exposed to the medium for which the dielectric permittivity is to be measured is approximately equal to that of the coaxial cable, i.e. 50 Ω (De Vos, 1990). A slight change in impedance at the beginning of the probe is advisable, since then the beginning of the signal can be easily determined. The impedance of a three rod probe is given by (Topp *et al.*, 1988; De Vos, 1990)

$$Z_i = \frac{60 \ln\left(\dfrac{2s_r}{d_r}\right)}{\sqrt{K_a}} \qquad\qquad [A4\text{-}1]$$

where Z_i is the impedance (Ω), s_r is the rod spacing (m), d_r is the rod diameter (m), and K_a is the dielectric permittivity (-). However, K_a is not constant in the porous medium, since it depends on volumetric water content, θ, and temperature. Using the relationship between θ and K_a as proposed by Topp *et al.* (1980) one can obtain a relationship between the s_r/d_r ratio as a function of θ for several desired impedances (Figure A4-1). Thus with varying θ the probe dimensions should change in order to keep Z_i constant. A small s_r/d_r ratio is needed when Z_i should remain constant over a large range of θ. However, too small s_r/d_r ratios would mean too small measuring volumes and contact problems between rod and porous medium, so that erroneous results may be obtained. Knight (1992) showed that for small rod diameters a so-called 'skin-effect' occurs, i.e. the measurement is determined by the local conditions around the inner rod, and thus a non-representative part of the substrate is sampled. Therefore, d_r should be as large as possible compared to s_r. Knight (1992) suggested that the s_r/d_r ratio should not be greater than about 10. Heimovaara (1993) used s_r/d_r ratios of about 10, and Zegelin *et al.* (1989) used s_r/d_r ratios of 6.3. It is obvious that no unique probe dimensions can be given. In this study I decided to choose $s_r/d_r = 6$.

Ratio of rod spacing and rod diameter s_r/d_r (-)
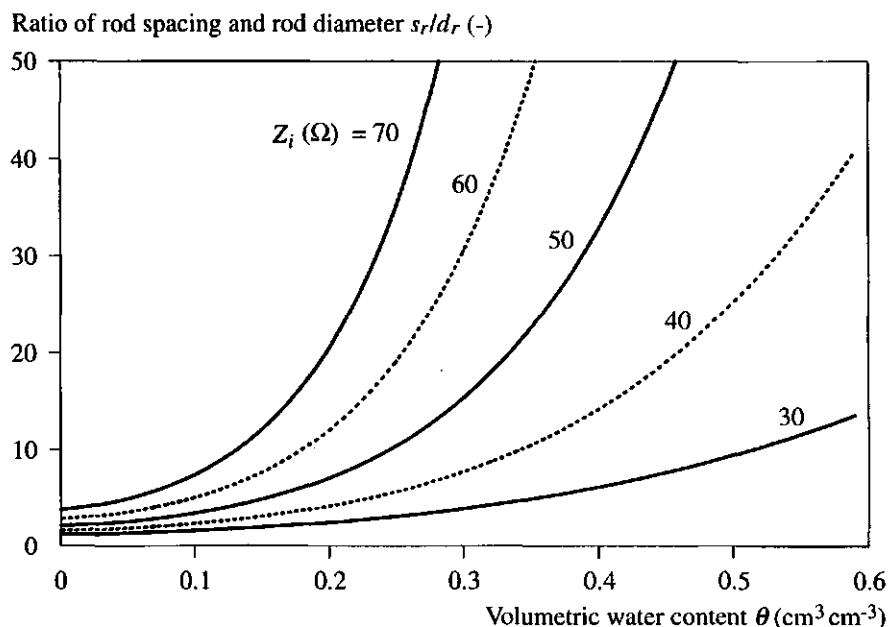
Figure A4-2   The relation between the rod spacing s_r and rod diameter d_r s_r/d_r ratio and volumetric water content θ for different values of Z_i.

Probe dimension and measured volume.
Zegelin *et al.* (1989) showed dimensionless areas of influence around three-rod probes. The extent of the outer curves of their Figure 3 are of dimensions 4.5 s_r by 5.7 s_r. The curve before the outermost curve given by Zegelin *et al.* (1989) yields a much smaller area of influence of dimensions 2.5 s_r by 3.4 s_r. An analysis by Knight *et al.* (1994) on the sampling volume of multi-wire TDR probes confirms these data. For the three-wire probe Knight *et al.* (1994; his Figure 5) obtained contour levels of the relative spatial sensitivity. The extent of the area of influence at contour levels 1/64 and 1/16 is 3.7 s_r by 4.3 s_r and 2.8 s_r by 3.6 s_r, respectively. For horizontally installed probes with a desired vertical extent of the measurement volume of 5 cm, s_r should be smaller than 1.1 to 2 cm. With $s_r/d_r = 6$ it was decided to have $s_r = 12$ mm and $d_r = 2$ mm.

Rod length related to EC measurement.
TDR can also be used to measure the electrical conductivity (*EC*) of the soil. Dalton and Van Genuchten (1986) showed that there exists a relationship between the maximum probe length, θ and *EC*. Assuming maximum *EC* values of 1 S m^{-1} the maximum lengths for $\theta = 0.1$ and 0.4 are 58 and 16 cm, respectively. It was expected that these values are the most extreme to be expected, so that the rod length was chosen to be 15 cm.

Appendix 5

Parameter optimization of the logistic growth function

with GENSTAT 5

The parameters of the logistic growth function, Eq. [6-1] in text, can be obtained from experimental data. Genstat 5 (Genstat 5 Committee, 1993) has a standard procedure to do this. However, in Genstat 5 the logistic function is given by

$$y_G = a_G + \frac{c_G}{1 + \exp\left(-b_G\left(t - m_G\right)\right)}. \tag{A5-1}$$

Heinen (1990) gave the relations between the parameters of Eq. [6-1] and the Genstat 5 formulation of the logistic function. These are

$$W = y_G, \quad 0 = a_G, \quad k_L = b_G, \quad W_f = c_G, \quad W_i = \frac{c_G}{1 + \exp\left(b_G m_G\right)}. \tag{A5-2}$$

The parameter m_G is the time of inflection.

Appendix 6

Input data in the simulation model for all simulation runs

Summary of input data used to validate the simulation model in chapter 7 for the cases of volumetric water content (section 7.3.2) and pressure head (section 7.4.2) and for the example of simulated nitrogen distribution in the sand bed (section 7.6).

Basic units	
Length, time	cm, min
Flow domain configuration	
N, M	15, 9
Δx_I (N values)	3*1.0, 2.0, 4*2.5, 2*5.0, 4*2.5, 5.0 cm
Δz_J (M values)	1.25, 2.5, 2*1.25, 2.5, 2*1.25, 2.5, 1.25 cm
Substrate	coarse sand, hydraulic properties listed in Table 4-6
Top boundary condition: q_0 (N values)	$11*q_0 = -E_p$, $2*q_0$ = irrigation rate - E_p, $2*q_0 = -E_p$
Bottom boundary condition: q_Z, h_Z (N values)	2*seepage drainage, i.e $q_Z = 0$ cm min^{-1} or $h_Z = 0$ cm, $13*q_Z = 0$ cm min^{-1}
h_0 (MxN values, or equilibrium)	equilibrium with $h = -8.5$ cm at the bottom
Weather data	
Irrigation rate	742*0,31*0.153,667*0, 886*0,31*0.153,523*0, 1005*0,31*0.153,404*0, 1095*0,31*0.153,314*0, 1440*0, 788*0,31*0.153,621*0, 1440*0, 1114*0,31*0.153,295*0, 1440*0, 846*0,31*0.153,563*0, 1440*0, 608*0,31*0.153,422*0,31*0.153,348*0 cm min^{-1}

T_p	360*0,840*2.728·10⁻⁵,240*0,
	360*0,840*3.111·10⁻⁵,240*0,
	360*0,840*4.854·10⁻⁵,240*0,
	360*0,840*4.533·10⁻⁵,240*0,
	360*0,840*4.120·10⁻⁵,240*0,
	360*0,840*4.120·10⁻⁵,240*0,
	360*0,840*4.182·10⁻⁵,240*0,
	360*0,840*4.182·10⁻⁵,240*0,
	360*0,840*5.580·10⁻⁵,240*0,
	360*0,840*5.580·10⁻⁵,240*0,
	360*0,840*9.393·10⁻⁵,240*0,
	360*0,840*9.393·10⁻⁵,240*0 cm min⁻¹
E_p	360*0,840*25.114·10⁻⁵,240*0,
	360*0,840*23.566·10⁻⁵,240*0,
	360*0,840*30.163·10⁻⁵,240*0,
	360*0,840*23.164·10⁻⁵,240*0,
	360*0,840*14.232·10⁻⁵,240*0,
	360*0,840*14.232·10⁻⁵,240*0,
	360*0,840*9.812·10⁻⁵,240*0,
	360*0,840*9.812·10⁻⁵,240*0,
	360*0,840*8.949·10⁻⁵,240*0,
	360*0,840*8.949·10⁻⁵,240*0,
	360*0,840*10.406·10⁻⁵,240*0,
	360*0,840*10.406·10⁻⁵,240*0 cm min⁻¹

Timer control data

Δt_i, Δt_{max}, Δt_{min}, t_p, ζ, t_m	0.1 min, 0.2 min, 10^{-15} min, 17280 min, 0.01, 1.5

Solution procedure

Procedure	ADI when completely unsaturated and ICCG when partially saturated; switch between the two at $h = -0.5$ cm
ϵ_c, max. # iterations	10^{-4}, 20; convergence based on K and h
ICCG: ϵ_i, max. # iterations	10^{-8}, 200

Hysteresis

Initial κ_h (*MxN* values), ϵ_κ	-2 (all nodes), 0.01

Solute transport

a_L, a_T, D_0, f_1, f_2, θ_l, c_f	2.0 cm, 0.2 cm, $1.11 \cdot 10^{-3}$ cm^2 min^{-1}, 1.58, -0.17, 0.12, 15 mmol l^{-1}
c_0 (*M*x*N* values)	15 mmol l^{-1} (all nodes)
Root data	
Root growth	yes
$L_{rv,f}$ (*M*x*N* values)	3* [4*3.4927, 2*0.906, 2*1.0587, 5.3033, 5.6787, 2*2.2437, 2*2.277, 5.055], 3* [4*2.44, 2*1.8383, 2*2.5173, 4.6547, 4.322, 2*3.3817, 2*3.5573, 5.266], 3* [4*0.7983, 2*0.7433, 2*0.753, 1.0767, 0.462, 2*0.6073, 2*0.639, 0.3997] cm cm^{-3}
k_L, t^*, start time	$1.498 \cdot 10^{-4}$ min^{-1}, 30240 min, 17280 min
Root water uptake	
K_1, R_0, a, $h_{r,1/2}$	$2.5 \cdot 10^{-9}$ cm min^{-1} (see Table 5-3), 0.017 cm (Schwarz *et al.*, 1995), 10 (see Table 5-3), -9500 cm (see Table 5-3)
Root nutrient uptake	
S_{sr}	$3.0 \cdot 10^{-5}$ mmol min^{-1} (per plant; the three crop rows result in two plants)
Irrigation control unit: n.a.	
n.a. = not applicable	

Breakthrough curve (BTC) calibration experiment (section 7.5). First the steady state conditions in θ, h, F_x, and F_z were obtained. With these conditions the solute transport module was used for certain combinations of a_L and a_T values, i.e. the combinations with $a_L \geq a_T$.

Basic units	
Length, time	cm, min
Flow domain configuration	
N, M	20, 15
Δx_I (N values)	20*2.0 cm
Δz_J (M values)	15*1.0 cm
Substrate	coarse sand, hydraulic properties of 5-15 cm layer as listed in Table 4-6
Top boundary condition: q_0 (N values)	$16*q_0 = 0$ cm min^{-1}, $2*q_0 =$ irrigation rate, $2*q_0 = 0$ cm min^{-1}
Bottom boundary condition: q_Z, h_Z (N values)	seepage drainage, i.e $q_Z = 0$ cm min^{-1} or $h_Z = 0$ cm, $19*q_Z = 0$ cm min^{-1}
h_0 (MxN values, or equilibrium)	equilibrium with $h = 0$ cm at the bottom
Weather data	
Irrigation rate	0.2 cm min^{-1} (constant)
T_p	n.a.
E_p	n.a.
Timer control data	
Δt_i, Δt_{max}, Δt_{min}, t_p, ζ, t_m	0.01 min, 0.1 min, 10^{-15} min, 1500 min to obtaine steady state condition, 500 min to obtain BTC, 0.01, 1.5
Solution procedure	
Procedure	ADI when completely unsaturated and ICCG when partially saturated; switch between the two at $h = -0.5$ cm
ϵ_c, max. # iterations	10^{-4}, 40; convergence based on K and h

ICCG: ϵ_i, max. # iterations	10^{-8}, 400
Solute transport	
a_L, a_T, D_0, f_1, f_2, θ_l, c_f	0, 0.2, 0.5, 1, 2, 3, 4, 5, 10 (see text); 0, 0.1, 0.2, 0.5, 1, 2, 3, 4, 5 10 (see text); $1.11 \cdot 10^{-3}$ cm^2 min^{-1}; 1.58; -0.17; 0.12; 20 mmol l^{-1}
c_0 (*M*x*N* values)	0 mmol l^{-1} (all nodes)
Hysteresis, Root data, Root water uptake, Root nutrient uptake, Irrigation control unit: n.a.	
n.a. = not applicable	

Example 8.1. Nine different cases are considered (see text):

a: Coarse sand, $L_D = 40$ cm　　**d**: Coarse sand, $L_D = 160$ cm　**g**: Clay beads, $L_D = 120$ cm
b: Coarse sand, $L_D = 80$ cm　　**e**: Rockwool, $L_D = 120$ cm　　**h**: Cocos peat, $L_D = 120$ cm
c: Coarse sand, $L_D = 120$ cm　**f**: Peat-perlite, $L_D = 120$ cm　**i**: Zavel-b8, $L_D = 12$ cm

Basic units	
Length, time	cm, min
Flow domain configuration	
N, M	**(a)**: 12, 9; **(b)**: 22, 9; **(c,e,f,g,h)**: 18, 9; **(d)**: 20, 9; **(i)**: 6, 9
Δx_I (*N* values)	**(a)**: 4*1.0, 8*2.0; **(b)**: 4*1.0, 18*2.0; **(c,e,f,h)**: 4*1.0, 14*4.0; **(d)**: 5*1.0, 15*5.0; **(g)**: 2*1.0, 16*1.75; **(i)**: 6*1.0 cm
Δz_J (*M* values)	0.5, 7*2.0, 0.5 cm
Substrate	**(a,b,c,d)**: coarse sand 0-5 cm layer (hydraulic properties listed in Table 4-6); **(e)**: rockwool (Table 8-2); **(f)**: peat-perlite mixture (Table 8-2); **(g)**: clay beads (Table 8-2); **(h)**: cocos peat (Table 8-2); **(i)**: zavelb8 (Table 8-2)
Top boundary condition: q_0 (*N* values)	N * irrigation rate
Bottom boundary condition: q_Z, h_Z (*N* values)	2*seepage drainage, i.e $q_Z = 0$ cm min^{-1} or $h_Z = 0$ cm, (N-2)*$q_Z = 0$ cm min^{-1}
h_0 (*MxN* values, or equilibrium)	equilibrium with $h = 0$ cm at the bottom
Weather data	
Irrigation rate	**(a,b,c,d,e,f,g,h)**: 1000*0.05 cm min^{-1}, 1000*0; **(i)**: 1000*0.001 cm min^{-1}, 1000*0
T_p	n.a.
E_p	n.a.
Timer control data	
$\Delta t_i, \Delta t_{max}, \Delta t_{min}, t_f, \zeta, t_m$	10^{-4} min, $2.5 \cdot 10^{-2}$ min, 10^{-15} min, 2000 min, 0.01, 1.5
Solution procedure	

Procedure	ADI when completely unsaturated and ICCG when partially saturated; switch between the two at $h = -0.5$ cm
ϵ_c, max. # iterations	10^{-4}, 20; convergence based on K and h
ICCG: ϵ_i, max. # iterations	10^{-8}, 200

Hysteresis, Solute transport, Root data, Root water uptake, Root nutrient uptake, Irrigation control unit: n.a.

n.a. = not applicable

Example 8-2.Water storage and irrigation scheduling. Eight cases considered (see text):
a: Irrigate when ET_p exceeds threshold value of 0.15 cm
b: Irrigate when ET_p exceeds threshold value of 0.5 cm
c: Irrigate when ET_p exceeds threshold value of 1.0 cm
d: Irrigate when ET_p exceeds threshold value of 2.0 cm
e: Irrigate when ET_p exceeds threshold value of 4.0 cm
f: Irrigate when c at x, z = 8.75 cm, 2.5 cm exceeds threshold value of 19 mmol l^{-1}, using 1 surface dripper at x, z = 30 cm, 0 cm
g: Irrigate when c at x, z = 8.75 cm, 2.5 cm exceeds threshold value of 19 mmol l^{-1}, using 2 surface drippers at x, z = 10 cm, 0 cm and x, z = 30 cm, 0 cm
h: Irrigate when c at x, z = 8.75 cm, 2.5 cm exceeds threshold value of 19 mmol l^{-1}, using 1 buried dripper at x, z = 30 cm, 15 cm

Basic units	
Length, time	cm, h
Flow domain configuration	
N, M	15, 9
Δx_I (*N* values)	3*1.0, 2.0, 4*2.5, 2*5.0, 4*2.5, 5.0 cm
Δz_J (*M* values)	1.25, 2.5, 2*1.25, 2.5, 2*1.25, 2.5, 1.25 cm
Substrate	coarse sand (hydraulic properties listed in Table 4-6)
Top boundary condition: q_0 (*N* values)	(**a,b,c,d,e,f**): 11*q_0 = -E_p, 2*q_0 = irrigation rate - E_p, 2*q_0 = -E_p; (**g**): 5*q_0 = -E_p, 2*q_0 = irrigation rate - E_p, 4*q_0 = -E_p, 2*q_0 = irrigation rate - E_p, 2*q_0 = -E_p; (**h**): 15*q_0 = -E_p
Bottom boundary condition: q_Z, h_Z (*N* values)	(**a,b,c,d,e,f,g**): 2*seepage drainage, i.e q_Z = 0 cm h^{-1} or h_Z = 0 cm, 13*q_Z = 0 cm h^{-1}; (**h**): 2*seepage drainage, i.e q_Z = 0 cm h^{-1} or h_Z = 0 cm, 9*q_Z = 0 cm h^{-1}, 2*q_Z = -irrigation rate, 2*q_Z = 0 cm h^{-1}
h_0 (*MxN* values, or equilibrium)	equilibrium with h = -8.5 cm at the bottom
Weather data	
Irrigation rate	see irrigation intensity given at section **Irrigation control unit**

T_p	**(a,b,c,d,f,g,h)**: 6*0,14*1.637·10⁻³,4*0, 6*0,14*1.867·10⁻³,4*0, 6*0,14*2.912·10⁻³,4*0, 6*0,14*2.720·10⁻³,4*0, 6*0,14*2.472·10⁻³,4*0, 6*0,14*2.472·10⁻³,4*0, 6*0,14*2.509·10⁻³,4*0, 6*0,14*2.509·10⁻³,4*0, 6*0,14*3.348·10⁻³,4*0, 6*0,14*3.348·10⁻³,4*0, 6*0,14*5.636·10⁻³,4*0, 6*0,14*5.636·10⁻³,4*0; **(e)** 12 * [6*0,14*0.05,4*0] cm h⁻¹
E_p	**(a,b,c,d,f,g,h)**: 6*0,14*15.068·10⁻³,4*0, 6*0,14*14.140·10⁻³,4*0, 6*0,14*18.098·10⁻³,4*0, 6*0,14*13.898·10⁻³,4*0, 6*0,14*8.539·10⁻³,4*0, 6*0,14*8.539·10⁻³,4*0, 6*0,14*5.887·10⁻³,4*0, 6*0,14*5.887·10⁻³,4*0, 6*0,14*5.369·10⁻³,4*0, 6*0,14*5.369·10⁻³,4*0, 6*0,14*6.244·10⁻³,4*0, 6*0,14*6.244·10⁻³,4*0; **(e)**: 12 * [6*0,14*0.01,4*0] cm h⁻¹

Timer control data

Δt_i, Δt_{max}, Δt_{min}, t_p, ζ, t_m	10^{-4} h, $2.5 \cdot 10^{-3}$ h, 10^{-15} h, 288 h, 0.01, 1.5

Solution procedure

Procedure	ADI when completely unsaturated and ICCG when partially saturated; switch between the two at h = -0.5 cm
ϵ_c, max. # iterations	10^{-3}, 20; convergence based on K and h
ICCG: ϵ_i, max. # iterations	10^{-8}, 200

Hysteresis

Initial κ_h (*M*x*N* values), ϵ_κ	-2 (all nodes), 10^{-2}

Solute transport

a_L, a_T, D_0, f_1, f_2, θ_t, c_f	2.0 cm, 0.2 cm, $6.67 \cdot 10^{-2}$ cm^2 h^{-1}, 1.58, -0.17, 0.12, 15 mmol l^{-1}
c_0 (*M*x*N* values)	15 mmol l^{-1} (all nodes)

Root data

Root growth	yes

$L_{rv,f}$ (*M*x*N* values)	3* [4*3.4927, 2*0.906, 2*1.0587, 5.3033, 5.6787, 2*2.2437, 2*2.277, 5.055], 3* [4*2.44, 2*1.8383, 2*2.5173, 4.6547, 4.322, 2*3.3817, 2*3.5573, 5.266], 3* [4*0.7983, 2*0.7433, 2*0.753, 1.0767, 0.462, 2*0.6073, 2*0.639, 0.3997] cm cm^{-3}
k_L, t^*, start time	8.9875·10^{-3} h^{-1}, 504 h, 288 h
Root water uptake	
K_1, R_0, a, $h_{r,1/2}$	1.5·10^{-7} cm h^{-1} (see Table 5-3), 0.017 cm (Schwarz *et al.*, 1995), 10 (-9500 cm (see Table 5-3) see Table 5-3),
Root nutrient uptake	
S_{sr}	1.8·10^{-3} mmol h^{-1} (per plant; the three crop rows result in two plants)
Irrigation control unit	
Method	(**a,b,c,d,e**): irrigate when ET_p exceeds threshold value; (**f,g,h**): irrigate when c exceeds threshold value
Irrigation intensity, *EX*	4.5 cm h^{-1}, 1.0
Threshold: ET_p or h or c, node number (column, row) (if h, c)	(**a**): ET_p = 0.15; (**b**): ET_p = 0.5; (**c**): ET_p = 1.0; (**d**): ET_p = 2.0; (**e**): ET_p = 4.0 cm; (**f,g,h**): c = 19 mmol l^{-1}, (6,2)
n.a. = not applicable	

Substrate bed leaching example (section 8.3).

Basic units	
Length, time	cm, min
Flow domain configuration	
N, M	20, 15
Δx_I (*N* values)	20*2.0 cm
Δz_J (*M* values)	15*1.0 cm
Substrate	coarse sand, 5-15 cm layer (Table 4-6)
Top boundary condition: q_0 (*N* values)	$16*q_0 = 0$ cm min^{-1}, $2*q_0$ = irrigation rate, $2*q_0 = 0$ cm min^{-1}
Bottom boundary condition: q_Z, h_Z (*N* values)	seepage drainage, i.e $q_Z = 0$ cm min^{-1} or $h_Z = 0$ cm, $19*q_Z = 0$ cm min^{-1}
h_0 (*MxN* values, or equilibrium)	equilibrium with $h = 0$ cm at the bottom
Weather data	
Irrigation rate	0.05 cm min^{-1} (constant)
T_p	n.a.
E_p	n.a.
Timer control data	
Δt_i, Δt_{max}, Δt_{min}, t_p, ζ, t_m	0.01 min, 1 min, 10^{-15} min, 500 min, 0.01, 1.5
Solution procedure	
Procedure	ADI when completely unsaturated and ICCG when partially saturated; switch between the two at $h = -0.5$ cm
ϵ_c, max. # iterations	10^{-4}, 20; convergence based on K and h
ICCG: ϵ_i, max. # iterations	10^{-8}, 200
Hysteresis	
Initial κ_h (*MxN* values), ϵ_κ	-2 (all nodes), 10^{-2}

Solute transport	
a_L, a_T, D_0, f_1, f_2, θ_l, c_f	2.0 cm, 0.2 cm, $1.11 \cdot 10^{-3}$ cm^2 min^{-1}, 1.58, -0.17, 0.12, 10 mmol l^{-1}
c_0 (*M*x*N* values)	31, 33, 35, 37, 40, 40, 37, 35, 33, 31, 31, 26, 8*22, 30, 32, 34, 36, 38, 38, 36, 34, 32, 30, 30, 25, 8*20, 29, 31, 33, 35, 37, 37, 35, 33, 31, 29, 29, 24, 8*19, 28, 30, 32, 34, 36, 36, 34, 32, 30, 27, 25, 22, 8*18, 26, 27, 28, 29, 32, 32, 29, 28, 27, 26, 24, 21, 8*17, 25, 26, 27, 28, 30, 30, 28, 27, 26, 25, 23, 19, 8*16, 24, 25, 26, 27, 28, 28, 27, 26, 25, 24, 22, 18, 8*15, 22, 23, 24, 24, 24, 24, 24, 23, 22, 20, 18, 9*15, 20, 21, 22, 22, 22, 22, 21, 20, 18, 10*15, 18, 19, 20, 20, 20, 20, 20, 19, 18, 17, 10*15, 20*15, 20*15, 20*15, 20*15, 20*15 mmol l^{-1}
Root data, Root water uptake, Root nutrient uptake, Irrigation control unit: n.a.	
n.a. = not applicable	

Summary of input data for the example of water and salt distributions in a rockwool slab (section 8.4; refer to Figure 8-8 for schematic view of flow domain). The two cases **RW1** and **RW2** refer to the drain position at $x, z = 0$ cm, 15 cm and 40 cm, 15 cm, respectively.

Basic units	
Length, time	cm, h
Flow domain configuration	
N, M	20, 10
Δx_I (N values)	20*1.25 cm
Δz_J (M values)	10*1.25 cm
Substrate	rockwool, hydraulic properties listed in Table 8-2; $K_s = 0$ cm h^{-1} in blocked-off region
Top boundary condition: q_0 (N values)	16*$q_0 = 0$ cm h^{-1}, $q_0 = -E_p$, 2*$q_0 =$ irrigation rate - $_{Ep}$, $q_0 = -E_p$
Bottom boundary condition: q_Z, h_Z (N values)	(**RW1**) 2*seepage drainage, i.e $q_Z = 0$ cm h^{-1} or $h_Z = 0$ cm, 18*$q_Z = 0$ cm h^{-1}; (**RW2**) 18*$q_Z = 0$ cm h^{-1}, 2*seepage drainage, i.e $q_Z = 0$ cm h^{-1} or $h_Z = 0$ cm,
h_0 (MxN values, or equilibrium)	equilibrium with $h = -5$ cm at the bottom
Weather data	
Irrigation intensity	see irrigation intensity given at section **Irrigation control unit**
T_p	12 * [6*0 cm h^{-1}, 14*0.04 cm h^{-1},6*0 cm h^{-1}]
E_p	12 * [6*0 cm h^{-1}, 14*0.004 cm h^{-1},6*0 cm h^{-1}]
Timer control data	
Δt_i, Δt_{max}, Δt_{min}, t_f, ζ, t_m	10^{-4} h, $2.5 \cdot 10^{-3}$ h, 10^{-15} h, 288 h, 0.01, 1.5
Solution procedure	
Procedure	ADI when completely unsaturated and ICCG when partially saturated; switch between the two at $h = -0.5$ cm
ϵ_c, max. # iterations	10^{-3}, 40; convergence based on K and h
ICCG: ϵ_i, max. # iterations	10^{-7}, 400

Hysteresis	
Initial κ_h (*MxN* values), ϵ_κ	-2 (all nodes), 0.01
Solute transport	
a_L, a_T, D_0, f_1, f_2, θ_l, c_f	2.0 cm (0 cm in blocked-off region), 0.2 cm (0 cm in blocked-off region), $6.67\cdot10^{-2}$ cm^2 h^{-1} (0 cm^2 h^{-1} in blocked-off region), 1.58, -0.17, 0.12, 11 mmol l^{-1} (Sonneveld and Straver, 1988)
c_0 (*MxN* values)	11 mmol l^{-1} (all nodes)
Root data	
Root growth	no
$L_{rv,f}$	4 * [16*0 (blocked-off region),4*47.7], 2 * [8*47.7,8*63.7,4*95.5], 2 * [8*11.9,8*23.9,4*15.9], 2 * [8*8.0,8*11.9,4*8.0] cm cm^{-3} (van Noordwijk and Raats, 1978; 1980)
k_L, t^*, start time	n.a.
Root water uptake	
K_1, R_0, a, $h_{r,1/2}$	$1.5\cdot10^{-7}$ cm h^{-1}, 0.017 cm (van Noordwijk and Brouwer, 1991), 10, -10^{-4} cm
Root nutrient uptake	
S_{sr}	$7.5\cdot10^{-3}$ mmol h^{-1} (based on Sonneveld, 1994; 1000 kg ha^{-1}, assuming 300 days of uptake, at planting density of 2.2 pl m^{-2}, and 1 cm of profile width)
Irrigation control unit	
Method	irrigate when ET_p exceeds threshold
Irrigation intensity, *EX*	4.5 cm h^{-1}, 0.3
Threshold: ET_p or h or c, node number (column, row) (if h, c)	$ET_p = 0.5$ cm
n.a. = not applicable	

Appendix 7

Computation of ϕ

The computation of ϕ in Eq. [2-7], with $K(h)$ given by Mualem's (1976) expression Eq. [4-6] is not directly possible, since the integral $\int K(h)dh$ is unknown. The solution can be obtained by using a numerical integration method, e.g. the Romberg integration routine of Press *et al.* (1986). For computational simplicity reasons a transformed expression for $K(h)$ is used. The new integration variable h' is defined as

$$h' = \ln | \alpha h | .$$ [A7-3]

Thus

$$dh = \frac{e^{h'}}{\alpha} dh' .$$ [A7-4]

Then ϕ is obtained from

$$\phi = \frac{K_s}{\alpha} \int_{h_1'}^{h_2'} \frac{\left[\left(1 + e^{nh'} \right)^m - e^{(n-1)h'} \right]^2}{\left(1 + e^{nh'} \right)^{m(\lambda+2)}} e^{h'} dh' .$$ [A7-5]

In order to avoid large computational times in evaluating ϕ in the root water uptake module, use is made of tabulated $\phi(h)$ obtained once before the start of simulation. In the simulation model ϕ is obtained by linear interpolation.

Appendix 8

Computation of *EC* of a solution

According to the theory of ionic mobilities and ionic conductance in electrolyte solutions the electrical conductivity *EC* of a solution can be given as a function of the concentration (Atkins, 1978; Bard and Faulkner, 1980, Chang, 1981). In fact activities instead of concentrations should be used (Kamphorst and Bolt, 1981). In that case EC (dS m^{-1}) is given by (see also Heinen, 1990b)

$$EC = F \sum_{i=1}^{m_s} \rho_s c_i n_{v,i} \mu_{m,i} f_{a,i},$$ [A8-1]

where F is Faraday's constant (96485 C mol^{-1}), m_s is the number of solutes, ρ is the density of the solvent (kg m^{-3}), c_i is the concentration of ion i (mol kg^{-}), $n_{v,i}$ is the absolute valence of ion i (-), $\mu_{m,i}$ is the ionic mobility of ion i (cm^2 s^{-1} V^{-1}; Table 8-A), and $f_{a,i}$ is the activity coefficient of ion i (-), and . The activity coefficient $f_{a,i}$ depends on the total concentration, i.e. ionic strength I_s (mol kg^{-1}) of the solution, where I_s is defined as

$$I_s = 0.5 \sum_{i=1}^{m_s} c_i n_{v,i}^2.$$ [A8-2]

This dependence $f_{a,i}(I)$ is described by the extended Debye-Hückel theory according to (Atkins, 1978; Chang, 1981; Novozamsky *et al.*, 1981)

$$\log f_{a,i} = -\frac{A_f n_{v,i}^2 \sqrt{I_s}}{1 + B_f d_{i,i} \sqrt{I_s}},$$ [A8-3]

with (Atkins, 1978)

$$A_f = \frac{N_a^2 e^3 \sqrt{2 \rho_s}}{8 \pi \left(\epsilon_0 \epsilon R_g T \right)^{1.5} \ln 10},$$ [A8-4]

and

$$B_f = \frac{N_a e \sqrt{2 \rho_s}}{\left(\epsilon_0 \epsilon R_g T \right)^{0.5}},$$ [A8-5]

where d_i is the effective diameter of the ion (m; Table 8-A), N_a is Avogadro's number (= 6.022 10^{23} mol^{-1}), e is the electron charge (= 1.6022 10^{-19} C), ϵ_0 is the dielectric permittivity of vacuum (= 8.8542 10^{-12} C V^{-1} m^{-1}), ϵ is the dielectric permittivity of the solvent, R_g is the universal gas constant (= 8.3144 J mol^{-1} K^{-1}), and T is the temperature (K). The Debye-Hückel theory assumes that the electrolytes are completely dissociated

into ions in solution and that each ion is surrounded by ions of opposite charge. For $T = 298$ K and water as solvent ($\epsilon = 78.54$, $\rho = 1000$ kg m^{-3}) the parameters A_f and B_f become $A_f = 0.51$ (mol kg^{-1})$^{0.5}$ and $B_f = 3.3\ 10^9$ (mol kg^{-1})$^{0.5}$ m^{-1}. For very dilute solution ($I_s < 0.005$ mol kg^{-1} according to Bates (1978); $I_s < 0.01$ mol kg^{-1} according to Chang (1981)) or when ions are assumed to be points, i.e. $d_i = 0$ m, one obtains the limiting Debye-Hückel law:

$$\log f_{a,i} = -A_f n_{v,i}^2 \sqrt{I_s}.$$
[A8-6]

In case d_i is assumed to be $d_i = 3\ 10^{-10}$ m and equal for all ions in the solution, the Debye-Hückel law becomes (Günterberg approximation)

$$\log f_{a,i} = -\frac{A_f n_{v,i}^2 \sqrt{I_s}}{1 + \sqrt{I_s}}.$$
[A8-7]

For high values of I_s, say $I_s > 0.1$ mol kg^{-1}, one can use the Davies extension (Bates, 1978):

$$\log f_{a,i} = -\frac{A_f n_{v,i}^2 \sqrt{I_s}}{1 + \sqrt{I_s}} + 0.1\ n_{v,i}^2 I_s.$$
[A8-8]

As a rough approximation EC (dS m^{-1}) is equal to the sum of the concentration of all ions (in mmol l^{-1} !!!) divided by 10, where this factor 10 follows from $10^{-3} F f_a n_v \mu_m$ with f_a, n_v and μ_m representing some average values for $f_{a,i}$ (say 0.9), $n_{v,i}$ (say 1.5) and $\mu_{m,i}$ (say 7.5 10^{-4} cm^2 s^{-1} V^{-1}), respectively, and 10^{-3} is the correction for mmol to mol.

Table A8-1. Values for ionic mobility μ_m (10^{-4} cm^2 s^{-1} V^{-1}; from Chang, 1981 or Bard and Faulkner, 1980) and ion diameter d_i (10^{-10} m; from Novozamsky *et al.*, 1981) for several ions commonly present in nutrient solutions.

	NO_3	H_2PO_4	SO_4	Cl	NH_4	K	Ca	Mg
μ_m	7.40	7.84[1]	8.27	7.91	7.61	7.62	6.16	5.50
d_i	3.0	4.0	4.0	3.0	3.0	3.0	6.0	8.0

[1] since no value is known it is set equal to the average of the values for NO_3 and SO_4

Summary

A considerable fraction of the applied amounts of water and nutrients in glasshouse horticulture is not utilized. The excess of water and nutrients is a hazard for the environment. Therefore, around 1990 the Dutch government established the policy that all commercial growers had to change to closed management systems by the year 2000. Part of closed management systems are closed cropping systems. Around 1990 several crops were already grown in closed, recirculating cropping systems. For other crops, mainly crops with a high planting density such as lettuce, radish and some flowers, closed cropping systems were still lacking or under development. Roughly, the two possible ways of approach in developing cropping systems are:
1) by trial and error experimentation on small scale systems, and
2) by a modelling approach in combination with a few detailed experiments.
This latter, new approach was employed in this thesis. The benefit of a model, once in operation, is that in a short period several scenarios can be screened on their usefulness for practice. The most promising cases can then be tested in experiments. In this thesis I focus on closed bedding systems, i.e. large area systems with a thin layer of a substrate. The reason for choosing only one system is that it allows an in-depth analysis. A two-dimensional simulation model is developed for describing water movement, solute transport, and root uptake. The simulation model is validated and parameterised using experimental data obtained in a sand bed system. As a demonstration the model is applied to answer some questions from practice.

In Chapter 1 some general aspects about glasshouse horticulture in The Netherlands are described. Due to the large excess amounts of water and nutrients applied in glasshouse horticulture, environmental pollution is evidently one main matter of concern. Soilless culture with recirculating systems offers a good alternative for natural soil cropping systems. There is a need to understand what happens with water and nutrients in closed cropping systems with their coarse porous media. Especially for crops with a high planting density such systems were still lacking around 1990. In this thesis I give a demonstration of a modelling approach in understanding the dynamics of water and nutrients in such systems. *The aim of this thesis is to formulate and validate a simulation model for water movement and nutrient transport in closed, recirculating cropping systems.* It should be a starting point for management models that can be used to obtain growth systems with minimal input of water, nutrients and pesticides, with a high production of good quality, and with a minimal nuisance to the environment. Of course, this approach is not restricted to closed, recirculating cropping systems, but it can also be applied to open, soil-based systems. The reasons for choosing closed systems as the main object is that these systems are better defined and controllable. As a central test case I used a sand bed system as schematically presented in Figure 1-1. For this system a one-

dimensional approach is obviously not valid. For practical reasons, I used a two-dimensional approach. Due to symmetry, I only consider half the region between two drains. The sand bed was 15 cm in height and the drain distance was about 80 cm.

In Chapter 2 I present the general theory of water movement in porous media, i.e. the Richards equation including root water uptake. The main parameters are the hydraulic conductivity K, volumetric water content θ, and pressure head h. The relationships between K-θ-h are discussed and determined in Chapter 4. Root water uptake is described by a model for single root uptake. If at a certain time in the root zone regions exist with equal root length density, i.e. root length per unit volume of porous medium, this single root uptake model can be used for each of these regions (upscaling). Root uptake is based on potential transpiration, a steady-rate distribution of the matric flux potential in the porous medium around the root, and a transpiration reduction function as a function of the root water pressure head.

Solute transport is considered to occur with the moving water (convection) and by the concentration gradient driven processes of dispersion and diffusion. The main parameters are the longitudinal and transversal dispersivities as determined in Chapter 7. The root nutrient uptake model is analogous to that used for water uptake. The maximum nutrient uptake rate is based on a steady-rate approximation for the concentration distribution around the root.

For the specific case of the sand bed system the boundary conditions for water and solute transport are defined. The Richards equation is a nonlinear equation, being mostly solved numerically (Chapter 3).

In Chapter 3 a Control Volume (CV) finite element method is used to solve the nonlinear Richards equation. The CV method is simple, easy to understand, and, most important, mass-conservative. Since it is not often applied, it is described in detail in this chapter. In succession, the different terms of the Richards equation are treated. The storage term is treated according to the mass-conservative method proposed by Celia *et al.* (1990). With this method the mass conservation problems often observed in the numerical solution of the Richards equation are no longer present. The resulting set of numerical equations is written in matrix notation. The solution of this matrix problem is obtained either with the Alternating Direction Implicit (ADI) method or with the Incomplete Cholesky Conjugate Gradient (ICCG) method. When the substrate is completely unsaturated the faster ADI method is used, while only during partially saturated conditions the slower ICCG method is used (the ADI method then fails). For the two-dimensional system with rectangular CV's, the coefficient matrix has a simple sparsity pattern, with only five bands filled with parameters. This makes storage and the ICCG computations easy.

Nutrient transport and root water and nutrient uptakes are treated explicitly. Nutrient transport uses the new values of volumetric water content and water flux densities as obtained from the solution of the Richards equation, and old values of concentration. Root

water and nutrient uptake are based on pressure head and concentration of the previous time step, respectively. The method of time-stepping during the solution procedure is based on minimizing numerical errors.

The analytical equations for the $\theta(h)$ (van Genuchten, 1980) and $K(\theta)$ (Mualem, 1976) relationships are given in Chapter 4. Since any porous medium shows a hysteretic behaviour in $\theta(h)$, and frequent irrigations take place in the cropping systems considered in this thesis, i.e. frequent cycles of drying and wetting occur in the substrate, hysteresis is considered as well. The relationship $K(\theta)$ is considered not hysteretic. The modified dependent domain model of Mualem (1984) is used to describe the scanning curves in the $\theta(h)$ domain.

The following properties were determined for the coarse sand substrate: particle weight fractions, dry bulk density ρ_d, hydraulic conductivity at saturation K_s, as well as the water retention $\theta(h)$ and hydraulic conductivity $K(\theta)$ characteristics. The median particle diameter was 0.6 mm. For the top layer of 5 cm ρ_d was 1680 kg m^{-3} which was significantly lower than ρ_d = 1720 kg m^{-3} of the bottom 10 cm. The laboratory determination of K_s was affected by microbial growth. The initial K_s was 12.56 m d^{-1}. The $\theta(h)$ relationships were determined by the standard laboratory equilibrium method. Two cycles of drying and wetting were performed. The second cycle yielded much drier conditions than the first cycle. The saturated water content θ_s predicted by the second cycle was much lower than the water contents observed in the experiments (see Chapters 5 and 7). In the cropping system water is entering from the top, while in the laboratory setup water is removed/entering from the bottom. Due to hysteresis this results in wetter conditions in the experimental system than in the laboratory system. Therefore, I used the data from the first cycle as the $\theta(h)$ relationships. The fast transient multi-step outflow method was used to determine simultaneously the $\theta(h)$ (only main drying) and $K(\theta)$ relationships. Using samples of equal ρ_d, this method resulted in large variability in obtained physical characteristics. The average of all $\theta(h)$ relationships obtained with the multi-step outflow method was in good agreement with the ones obtained with the equilibrium method, except near saturation. This is not surprising, since near saturation no outflow information is present because the samples need to be completely unsaturated at the beginning of the experiment. Since the main drying curves obtained by both methods were alike, the average $K(\theta)$ relationship was employed as the required $K(\theta)$ relationship. Due to the differences in ρ_d in the sand bed, the top 5 cm layer had hydraulic properties different from the bottom 10 cm. The main drying curve is described by the van Genuchten equation. Contrary to a proposal by Kool and Parker (1987b) the main wetting curve described by the van Genuchten equation, with the same parameters as those for the main drying curve, exclusive for the α parameter, was not able to describe the main wetting data well. Therefore, this curve was described by tabulated measured data, with intermediate values obtained through linear interpolation.

Chapter 5 presents a detailed description of the experimental system. The experiments were carried out at the Glasshouse Crops Research Station (GCRS) at Naaldwijk. An automatic data acquisition system was used to collect all measured data. Measurements were carried out to determine volumetric water content (by Time Domain Reflectometry, TDR), pressure head, substrate temperature, and the volumes of solution in the supply and drain vessels. To estimate evapotranspiration the incoming radiation and the greenhouse temperature were monitored at a central location at GCRS. The equipment was calibrated before and after the experimental period. For TDR calibration lines were obtained for water content and total electrical conductivity. The water content calibration curve differed from the so-called 'universal' calibration curve by Topp *et al.* (1980). A description of the most important experiments carried out is given in Table 5-2. Finally, values for some parameters occurring in the model of Chapter 2, which were not independently determined, were obtained from the literature (Table 5-3).

Chapter 6 describes results of measurements carried out in the greenhouse sand bed production system. Some of these data are used as input or boundary conditions for the validation of the simulation model as described in Chapter 7. The following data are discussed:
- lettuce production as a function of time, cumulative radiation and heat sum;
- root length density distribution and root radius;
- total water use and its partitioning into transpiration and evaporation;
- relationships between dry weight, evapotranspiration, transpiration as well as radiation;
- nutrient uptake;
- nutrient balance.

The hypothesis was that lettuce production and nutrient uptake are independent of the growth system. Developing a growth system is then possible based on root zone characteristics only (i.e. the model of Chapter 2), without having to deal with differences in crop reaction. To find out whether this hypothesis is valid, in some sections the results were compared with data obtained for lettuce grown in a Nutrient Film Technique (NFT) system (Heinen *et al.*, 1991; Heinen, 1994). Although comparison concerns lettuce grown in the same period of the year, the actual glasshouse climatic conditions were different, and in the NFT experiments a different cultivar was used. Thus, a true comparison is not possible.

Lettuce growth in sand beds was similar to lettuce production in NFT and other data from the literature, and could be well described by a logistic model. Nutrient uptake differed between sand bed and NFT. So, no definitive conclusions can be drawn about the hypothesis that crop growth and uptake is system-independent.

During a summer growth period restricted supply of fertigation water negatively affected lettuce production in sand beds. For this cropping system it is advised that the dripper density should be equal to the planting density, and that a high surplus of fertigation water must be used. A high surplus of fertigation water also results in a more even horizontal distribution of the roots.

The total contribution of transpiration by the crop to total water use for an autumn experiment was 55%. Transpiration was determined as the water use in a sand bed covered with a plastic sheet. Dry matter production in the covered sand bed was not different from that obtained in an uncovered sand bed. A good exponential relationship was found between the contribution of transpiration to evapotranspiration and the fractional substrate coverage.

The nutrient balance during one experiment was determined by following the change in total content of the nutrients in the crop and in the different system components. For neither of the nutrients a perfect mass balance was obtained. For example, for nitrogen (N) the process of denitrification may be a cause of the non-perfectness of the N balance. However, denitrification measurements by Postma *et al.* (1994) cannot explain the missing N in the mass balance.

During a summer experiment high root zone temperatures of more than 30 °C were observed, which may explain the low final dry matter production obtained in this experiment.

In Chapter 7 simulated data obtained with the model of Chapters 2 to 4 are compared with experimental data. Measured volumetric water content θ and pressure head h distributions in space and time and cumulative outflow from the drain serve as data to validate the water movement part of the simulation model. All data needed as boundary conditions and potential evapotranspiration were obtained from corresponding measured data as presented in Chapter 6. The *in-situ* obtained $\theta(h)$ characteristics fall within the laboratory obtained $\theta(h)$ main drying and wetting characteristics. Good agreement was obtained between simulated and measured data (validation), i.e. for θ and h distributions and cumulative outflow from the drain. A simulation model gives possibilities to extract more information. In that way more insight in the dynamics of water movement can be obtained. For example, net flux density patterns are used to visualize water movement during a short period around an irrigation-drainage event. When irrigation occurs but not yet drainage, water moves downwards below the dripper whereas in the zone far from the dripper it moves upward due to capillary rise. In that way the dead corner at the top of the sand bed far from the dripper location is supplied with water. When drainage starts this upward movement of water vanishes.

For the solute transport part of the simulation model, the two dispersivity parameters are obtained by comparing measured and simulated breakthrough curves (BTC). Taking into account that the true transport process is three-dimensional and the model is only two-dimensional, a good agreement between measured and simulated BTC was obtained, with the longitudinal dispersivity being the dominating dispersivity. Simulated dynamics of solute transport show that solute transport is mainly by mass flow with the water. The net solute flux density patterns are similar to the ones for water movement.

In Chapter 8 the simulation model is used to give answers to several practical questions. Here it is just meant as a demonstration, and many more aspects can be studied of course.

- What is the maximum height of a phreatic surface and its time of disappearance during an irrigation-drainage cycle in a bedding system, and can these features be predicted by existing analytical solutions?

  Simple analytical equations overestimate these properties, which is mainly because water movement above the phreatic surface is not taken into account. The analytical solutions may serve as a first guess. Saturated conditions occur only for short periods, and due to the shape of the $\theta(h)$ relationship aeration problems in frequently irrigated substrate beds are unlikely. For comparison, a natural loam soil is considered in this section as well. For the loam soil, regarded as a representative for the fine-textured natural soils, the root zone remains too wet, even for very small drain distances and small irrigation intensities. This explains why coarse porous media are needed in thin layer cropping systems.

- What is the maximum allowable time span between two fertigation events and what should determine that? In other words, how much water is available in the cropping system, and how are the concentrations of solutes affected when the substrate dries out?

  The total amount of water stored in a cropping system under wet conditions can be approximated from the water retention characteristic. From that it can be estimated how much water can leave the system before replenishment by irrigation is needed. The effect on root water pressure head for mature crops is negligible, and water stress is not likely to occur. For coarse porous substrates the change in pressure head h due to water removal is small. Therefore, it requires sensitive tensiometers when water supply is based on change in h. It is advised to use water content measurements instead. This has the benefit that the change in actual water storage is determined and that hysteresis does not play a role.

  When the substrate is allowed to dry out far, it is shown that this has a large impact on the concentration of a solute in the system. It is concluded that fertigation must be based on control of the concentration in the root zone instead of being based solely on replenishing water lost by evapotranspiration. As an example it is shown that keeping the concentration at a certain position below a threshold value for different application positions is possible.

- How much new solution must be flushed through the substrate to replace a resident solution by the new solution?

  Sometimes the substrate solution must be refreshed. For example, between two growth periods the existing concentrations may be too high as start conditions for a new crop. Flushing by the new solution replaces the old solution. An arbitrary initial distribution that could result from drip irrigation can well be replaced by drip irrigation with the new solution. However, the final concentration is not rapidly reached at all positions. There is no reason to advise to use an overhead sprinkling system, since it is not as effective.

■ Can the simulation model be used for other substrates and other cropping systems as well?
In the first section of this chapter different substrates are used, and the last section of this chapter presents some simulation results for a rockwool slab cropping system. In the rockwool system it is shown that the position of the drains with respect to the dripper location affects the flow pattern. Drains should be located between two drippers to assure flow throughout the rockwool slab during fertigation.

The goal of this thesis was to formulate and validate a simulation model for water movement and nutrient transport in closed, recirculating cropping systems. Now that it is available, the simulation model can be used to develop closed cropping systems with special attention to fertigation strategies. The model was developed in Chapters 2, 3 and 4, and it was validated in Chapter 7. In Chapter 8 the simulation model was used to show the capabilities of the simulation model. Due to the complexity of the model and the fact that it is a two-dimensional representation of reality, the outcome must be considered with care, and preferably tested with experimentation.

It has been shown that a thorough description combined with detailed measurements of water content, solute transport, and root water and nutrient uptake is required to understand the dynamics of water and nutrients in closed, recirculating cropping systems. The present model will be documented in due time. It can be used by researchers to develop fertigation strategies based on physical properties of the substrate. Nevertheless, some aspects still need further investigation. These are, for example:
- how appropriate is a two-dimensional approach for three-dimensional problems;
- inclusion of other sources and sinks, such as adsorption and desorption, in the solute transport module;
- sensitivity analysis of the main parameters appearing in the simulation model;
- effect of hysteresis on root water uptake.

Samenvatting

Een groot deel van de toegediende hoeveelheden water en meststoffen in de glastuinbouw komt niet ten goede aan het gewas. De overmaat aan water en meststoffen is een gevaar voor het milieu. Rond 1990 werd in het Nederlandse beleid vastgesteld dat alle commerciële tuinders voor het jaar 2000 moeten overstappen op gesloten bedrijfs-systemen, waarvan een gesloten teeltsysteem een onderdeel is. In die periode bestonden voor een aantal gewassen al gesloten, recirculerende teeltsystemen. Maar voor andere gewassen, voornamelijk gewassen met een hoge plantdichtheid zoals sla, radijs en sommige bloemen, ontbraken dergelijke systemen of waren ze nog in ontwikkeling. Grofweg kunnen twee methoden onderscheiden worden om nieuwe teeltsystemen te ontwikkelen:
1) de 'trial and error' experimentele aanpak met vele kleine systemen, en
2) een aanpak via modellering, gekoppeld met enkele gerichte experimenten.
Deze laatste, nieuwe aanpak is toegepast in dit proefschrift. Het voordeel van een model is dat in een korte periode een aantal scenario's doorgerekend en beoordeeld kan worden op hun bruikbaarheid in de praktijk. De meest veelbelovende scenario's kunnen vervolgens in experimenten getoetst worden. In dit proefschrift richt ik mij op substraat-bed-systemen. Dit zijn teeltsystemen met een groot oppervlak bestaande uit een dunne laag substraat. De reden om me te beperken tot één type systeem is dat het de mogelijkheid biedt om dit type diepgaand te analyseren.

In dit proefschrift wordt een tweedimensionaal simulatiemodel opgesteld voor de beschrijving van de waterbeweging, stoffentransport en wortelopname. Het model wordt vervolgens gevalideerd en de waarden van een aantal parameters worden bepaald. Dit gebeurt aan de hand van meetdata verkregen in diverse laboratorium- en kasexperi-menten. Tenslotte wordt het model als demonstratie gebruikt bij het beantwoorden van een aantal mogelijke vragen uit de praktijk.

In Hoofdstuk 1 wordt een aantal aspecten van de Nederlandse glastuinbouw beschreven. Er wordt een overmaat aan water en meststoffen toegediend aan het gewas. Deze overmaat is echter belastend voor het milieu. Teelten los van de ondergrond met hergebruik van drainagewater bieden een alternatief. Hiervoor is het nodig te begrijpen wat er met het water en de voedingsstoffen in de grove substraten in deze teeltsystemen gebeurt. Rond 1990 ontbraken dergelijke systemen nog voor gewassen met een hoge plantdichtheid. In dit proefschrift laat ik zien hoe met een simulatiemodel de dynamiek van water en voedingsstoffen kunnen worden bestudeerd in dergelijke teeltsystemen. *Het doel van dit proefschrift is het formuleren en valideren van een simulatiemodel voor de beschrijving van de waterbeweging en stoffentransport in gesloten, recirculerende teeltsystemen.* Dit model kan dan als uitgangspunt dienen voor het opstellen van managementmodellen welke gebruikt kunnen worden om teeltstrategieën te ontwikkelen

waarbij zo gering mogelijke hoeveelheden water, meststoffen en pesticiden gebruikt worden, met behoud van hoge productie met goede kwaliteit, en minimale belasting voor het milieu. Deze aanpak is natuurlijk niet alleen toepasbaar op gesloten, recirculerende teeltsystemen, maar kan ook worden toegepast op open grondsystemen. Een teeltbedsysteem is als studieobject is gekozen omdat zo'n systeem goed gedefinieerd is en beter beheersbaar is in experimenten. Centraal staat een zandbed-teeltsysteem zoals schematisch weergegeven in Figuur 1-1. Voor dit systeem is het duidelijk dat een eendimensionale analyse niet volstaat. Om praktische redenen gebruik ik een tweedimensionale analyse. Vanwege de symmetrie in het systeem beperk ik me tot het halve gebied tussen twee drains. Het zandbed was 15 cm hoog en de drainafstand was ongeveer 80 cm.

In Hoofdstuk 2 geef ik de algemene theorie voor de beschrijving van waterbeweging in een poreus medium, de zogenaamde Richards vergelijking. De parameters die hierin voorkomen zijn de doorlatendheid K, het volumetrisch watergehalte θ en de drukhoogte h. De onderlinge relaties tussen K, θ en h worden beschreven en bepaald in Hoofdstuk 4. Wateropname door de wortels wordt beschreven op basis van een model voor opname door een enkele wortel. Wanneer op een bepaald tijdstip in de wortelzone zones aanwezig zijn met gelijke wortellengtedichtheid (wortellengte per volume eenheid substraat), dan kan dit wortelopnamemodel voor elk van deze zones toegepast worden. De wateropname door de wortels is gebaseerd op de potentiële transpiratie, een 'steady-rate' verdeling van de matrix-fluxpotentiaal in het substraat als functie van de radiale afstand tot de wortel en een transpiratie-reductiefunctie welke afhangt van de wortelpotentiaal.

Opgeloste stoffen worden met het water mee getransporteerd (convectie), maar er vindt ook transport plaats via dispersie en diffusie als gevolg van gradiënten in de concentratie. De parameters die hierin voorkomen zijn de longitudinale en transversale dispersiviteiten, welke worden bepaald in Hoofdstuk 7. Nutriëntenopname door de wortels wordt door een model beschreven dat analoog is aan dat voor de wateropname. De maximaal mogelijke opname door de wortel is gebaseerd op een 'steady-rate' verdeling van de concentratie als functie van de radiale afstand tot de wortel.

Voor het zandbed-teeltsysteem worden de randvoorwaarden voor de waterbeweging en het stoffentransport gegeven. De Richards vergelijking is niet lineair en moet daarom vaak numeriek worden opgelost (Hoofdstuk 3).

In Hoofdstuk 3 wordt de 'Control Volume' (CV) eindige-elementenmethode gebruikt om de Richards vergelijking numeriek op te lossen. De CV-methode is eenvoudig te begrijpen en bovendien massa-conservatief. Omdat de methode niet vaak wordt toegepast, wordt deze in detail beschreven. De diverse termen in de Richards vergelijking worden achtereenvolgens behandeld. De capaciteitsterm wordt behandeld volgens de methode zoals voorgesteld door Celia *et al.* (1990). Met deze laatste methode komen de massabalansproblemen die vaak bij de numerieke oplossing van de Richards vergelijking worden waargenomen niet voor. Het uiteindelijk verkregen stelsel van impliciete

vergelijkingen kan in een matrixvorm worden geschreven. De oplossing van deze matrixvergelijking wordt verkregen ofwel via de 'Alternating Direction Implicit' (ADI) methode ofwel met de 'Incomplete Cholesky Conjugate Gradient' (ICCG) methode. Wanneer het substraat volledig onverzadigd is wordt de snelle ADI-methode toegepast, maar wanneer er sprake is van partiële verzadiging wordt de tragere ICCG-methode gebruikt (de ADI-methode faalt in dat geval). Voor het tweedimensionale probleem met de rechthoekige CV's bestaat de coëfficiëntenmatrix uit vijf banden. Dit resulteert in minder opslagruimte en efficiëntere berekeningen.

Stoffentransport en wortelopname van water en voedingsstoffen worden expliciet berekend. Voor stoffentransport wordt gebruik gemaakt van de meest recente waarden van watergehalte en waterfluxdichtheden en de oude waarden van de concentratie. Wateropname is gebaseerd op de oude waarde van de drukhoogte, en de opname van nutriënten is gebaseerd op de oude waarde van de concentratie. De methode van tijdstapregeling tijdens de berekeningen is gebaseerd op het minimaliseren van numerieke fouten.

In Hoofdstuk 4 worden de analytische vergelijkingen voor de waterretentiecurve $\theta(h)$ (van Genuchten, 1980) en de doorlatendheidscurve $K(\theta)$ (Mualem, 1976) gegeven. Omdat elk poreus medium hysterese in $\theta(h)$ vertoont en omdat in de glastuinbouwteeltsystemen frequente cycli van watergeven en uitdrogen voorkomen, is hysterese ook in beschouwing genomen. De $K(\theta)$-relatie kent geen hysterese. De 'modified dependent domain' model van Mualem (1984) wordt gebruikt om de scanning curves in het $\theta(h)$-domein te beschrijven.

De volgende eigenschappen van het grove zand werden bepaald: gewichtsfracties van de korrelgrootteverdeling, de droge bulkdichtheid ρ_d, de doorlatendheid bij verzadiging K_s, en de relaties $\theta(h)$ en $K(\theta)$. De mediaan diameter van het zand was 0.6 mm. Voor de toplaag van 5 cm in het zandbed is ρ_d 1680 kg m^{-3}. De onderste 10 cm van het zandbed had een significant hogere dichtheid: ρ_d = 1720 kg m^{-3}. De bepaling van K_s werd beïnvloed door microbiële groei. De initiële waarde voor K_s was 12.56 m d^{-1}. De $\theta(h)$-relatie werd bepaald via een evenwichtsmethode. Twee cycli van uitdrogen plus bevochtigen werden uitgevoerd. De tweede cyclus resulteerde in een drogere toestand. Het verzadigde watergehalte van de tweede cyclus was veel lager dan waarden die in experimenten werden gemeten (zie Hoofdstukken 5 en 7). In het teeltsysteem wordt water gegeven aan de bovenkant, terwijl in de laboratoriumopstelling water aan de onderkant wordt toegediend of afgezogen. Als gevolg van hysterese mag verwacht worden dat in het teeltsysteem nattere omstandigheden heersen dan in de laboratoriumopstelling. Daarom heb ik de resultaten van de eerste cyclus gebruikt als de $\theta(h)$-relaties. De snelle 'multi-step outflow' methode werd gebruikt om simultaan de hoofduitdrogingscurve te bepalen en de $K(\theta)$-relatie. De spreiding voor deze relaties was groot, maar de gemiddelde $\theta(h)$-relatie kwam goed overeen met de via in de evenwichtsmethode verkregen relatie, behalve nabij verzadiging. Dit laatste is niet zo verwonderlijk omdat met een onverzadigd monster werd begonnen aan de meting, en dus uitstroming bij

verzadiging niet is gemeten. Omdat de $\theta(h)$-relaties bij beide methoden gelijk waren is de verkregen gemiddelde $K(\theta)$-relatie gebruikt als de benodigde $K(\theta)$-relatie. Het verschil in ρ_d in het zandbed leidde to verschillende $\theta(h)$- en $K(\theta)$-relaties voor de top 5 cm en voor de onderste 10 cm. De hoofduitdrogingscurve van het grove zand wordt door de van-Genuchten-vergelijking gegeven. In tegenstelling tot het voorstel van Kool en Parker (1987b) kan de hoofdbevochtigingscurve niet beschreven worden door dezelfde set parameters, uitgezonderd de α-parameter, die de uitdrogingscurve beschrijven. Daarom wordt de bevochtigingscurve beschreven door de meetwaarden in tabelvorm, waarbij tussenwaarden via lineaire interpolatie worden verkregen.

In Hoofdstuk 5 is het experimentele systeem in detail beschreven. De kasexperimenten werden uitgevoerd op het Proefstation voor Tuinbouw onder Glas (PTG) te Naaldwijk. Een geautomatiseerd data-acquisitie systeem werd gebruikt voor het verzamelen van de meetwaarden. Gemeten werden: het volumetrisch watergehalte (met behulp van de 'Time Domain Reflectometry' methode, TDR), de drukhoogte, de temperatuur in het substraat, en de volumina voedingsoplossing in de voorraad- en drainvaten. Fertigatie werd gestuurd door de centrale klimaatcomputer van het PTG op basis van de evapotranspiratie welke werd geschat uit de inkomende straling en de kastemperatuur. Alle meetsystemen werden voorafgaande aan en aan het eind van de experimentele periode geijkt. Voor TDR werden de ijklijnen voor watergehalte en geleidbaarheid bepaald. De ijklijn voor water verschilde van de zogenaamde 'universele' ijklijn van Topp *et al.* (1980). De meest relevante zaken van de uitgevoerde experimenten zijn gegeven in Tabel 5-2. De waarden van een aantal parameters van Hoofdstuk 2, die niet in experimenten zijn bepaald, zijn afgeleid uit de literatuur (Tabel 5-3).

In Hoofdstuk 6 zijn de resultaten uit de kasexperimenten beschreven. Veel van deze data worden als input gebruikt voor de validatie van het simulatiemodel, zoals uitgevoerd in Hoofdstuk 7. De volgende gegevens worden behandeld:
- groei van sla als functie van de tijd, cumulatieve straling en warmtesom;
- verdeling van wortellengtedichtheid en wortelstraal;
- waterverbruik en de opsplitsing hiervan in verdamping aan het substraatoppervlak en transpiratie door het gewas;
- onderlinge relaties tussen droog gewicht, evapotranspiratie, transpiratie en straling;
- nutriëntenopname;
- massabalans van nutriënten.

De hypothese was dat de productie en nutriëntenopname in alle teeltsystemen gelijk zijn. Het ontwikkelen van teeltstrategieën kan dan plaatsvinden enkel op basis van de condities in de wortelzone. Deze hypothese werd getoetst door een aantal resultaten te vergelijken met overeenkomstige resultaten verkregen voor sla geteeld op een voedingsfilmsysteem ('Nutrient Film Technique', NFT; Heinen *et al.*, 1991; Heinen, 1994). Hoewel in beide systemen sla werd geteeld in dezelfde periode van het jaar, zullen toch de werkelijke klimaatsomstandigheden verschillend zijn geweest, en tevens werden verschillende

cultivars gebruikt.

Slaproductie op zandbed en NFT was overeenkomstig, en kon goed beschreven worden door een logistische curve. Nutriëntenopname verschilde voor beide systemen. Er kunnen dus geen definitieve conclusies getrokken worden over de hypothese dat productie en opname systeem-onafhankelijk zijn.

Tijdens een zomerteelt bleek dat een beperkte toediening van fertigatiewater in het zandbed een negatief effect had op de productie. Het advies is dan ook om de dichtheid van het aantal druppelaars gelijk te hebben aan de plantdichtheid, maar ook dat een grote doorspoelfractie gehanteerd moet worden. In die situatie wordt de hoogste productie verkregen en is de wortelverdeling homogeen.

De total bijdrage van de transpiratie aan het totale waterverbruik tijdens een najaarsteelt was 55%. De transpiratie werd bepaald als het waterverbruik in een met plastic afgedekt zandbed. De droge-stofproductie in het afgedekte zandbed was niet significant verschillend van die verkregen op een onafgedekt zandbed. Er werd een goede exponentiële relatie gevonden tussen de bedekkingsgraad door het gewas en de verhouding tussen transpiratie en evapotranspiratie.

De massabalans van nutriënten werd bepaald voor één teelt. Hiertoe werden de veranderingen in gehalten aan nutriënten in het gewas en in de verschillende systeemcomponenten bepaald. Voor geen enkel element kon een gesloten balans worden opgesteld. In het geval van stikstof (N) kan gedacht worden aan denitrificatie als oorzaak van het waargenomen verschil tussen opname door het gewas en afname van N in het systeem. Denitrificatiemetingen door Postma *et al.* (1994) kunnen dit verschil echter bij lange na niet verklaren.

Tijdens een zomerteelt werden temperaturen in de wortelzone gemeten van meer dan 30 °C. Dit is mogelijk een oorzaak van de lage verkregen droge-stofproductie tijdens deze teelt.

In Hoofdstuk 7 worden gesimuleerde data en experimentele data met elkaar vergeleken. Gemeten ruimtelijke en temporele verdelingen van watergehalte θ en drukhoogte h, en hoeveelheden drainagewater dienen als validatiegegevens. Alle gegevens voor de randvoorwaarden zijn bepaald in Hoofdstuk 6. De *in-situ* verkregen $\theta(h)$-relaties stemmen overeen met de relaties zoals bepaald in het laboratorium (Hoofdstuk 4). Er was een goede overeenkomst tussen de gesimuleerde en gemeten data (validatie) voor zowel θ en h als drainage. Het simulatiemodel levert extra informatie. Ter illustratie worden verdelingen van de waterfluxdichtheden gegeven welke het stromingsproces visualiseren. Wanneer er wordt geïrrigeerd, maar er nog geen drainage plaatsvindt, stroomt het water onder een druppelaar naar beneden en opwaarts in de zone ver van de druppelaar. Op deze manier wordt de zone ver van de druppelaar aan het oppervlak van nieuw water voorzien. Op het moment dat drainage start stopt deze opwaartse beweging.

De twee dispersiviteitsparameters werden bepaald door een gesimuleerde doorbraak-curve ('Breakthrough curve', BTC) te fitten door een gemeten dataset. Een redelijke overeenkomst tussen de gesimuleerde en gemeten BTC kon verkregen worden. De

longitudinale dispersiviteit was de bepalende parameter. Uit simulatieberekeningen van stoffentransport blijkt dat in het zandbed het transport met het water de meest dominante factor is. De verdelingen van de stof-fluxdichtheden zijn dus vergelijkbaar met die van de waterfluxdichtheden.

In Hoofdstuk 8 wordt het simulatiemodel gebruikt om een aantal praktische vragen te beantwoorden. Het is hier bedoeld als een demonstratie van wat je met het model zou kunnen doen. Er zijn veel meer zaken die aangepakt kunnen worden.

- Wat is de maximale hoogte die het freatisch vlak bereikt en hoe snel verdwijnt dit weer in een bedsysteem, en kunnen deze twee eigenschappen door bestaande analytische vergelijkingen gegeven worden?

  Eenvoudige analytische vergelijkingen overschatten deze twee eigenschappen, hetgeen voornamelijk te wijten valt aan het feit dat de horizontale stroming boven het freatisch vlak niet beschouwd wordt. Ze kunnen dus alleen als een eerste schatting gebruikt worden. Uit de simulatieberekeningen blijkt dat de verzadigde condities slechts gedurende een korte periode aanwezig zijn. Dankzij de vorm van de $\theta(h)$-relatie zijn aëratieproblemen in frequent geïrrigeerde substraatbedden niet waarschijnlijk. Ter vergelijking is dezelfde analyse uitgevoerd voor een natuurlijke leemgrond. Hiervoor blijkt dat in een dunne laag de toestand te nat blijft, zelfs bij zeer geringe drainafstand en irrigatie-intensiteit. Dit verklaart waarom de natuurlijke grond niet in dergelijke dunne lagen toegepast kan worden.

- Wat is de maximaal toelaatbare tijdsspanne tussen twee fertigatiebeurten en waardoor wordt dat bepaald? Met andere woorden, hoeveel water is er beschikbaar in het teeltsysteem en hoe verloopt de concentratie tijdens het uitdrogen?

  De totale hoeveelheid water onder natte omstandigheden die in de wortelzone aanwezig is kan worden berekend uit de waterretentiecurve. Hieruit kan worden bepaald hoeveel water het systeem kan verlaten voordat aanvulling noodzakelijk is. Het effect op de wortelpotentiaal van een volwassen gewas blijkt gering te zijn, en waterstress zal niet optreden. Voor grove substraten is de verandering van de drukhoogte h onderin het systeem als gevolg van wateronttrekking klein. Daarom moeten zeer gevoelige tensiometers gebruikt worden om de watergift te regelen op basis van veranderingen in h. Het advies is om de watergift te sturen op basis van metingen van het watergehalte. Het voordeel hierbij is dat de verandering in hoeveelheid water direct wordt gemeten, en dat deze meting niet door hysterese wordt beïnvloed.

  Wanneer het substraat ver uitdroogt heeft dat een groot effect op de concentraties in de wortelzone. Het is dus beter om het moment van fertigeren te laten bepalen door de beheersing van de concentratie in plaats van alleen op basis van de waterbehoefte. Ter illustratie is een voorbeeld gegeven waarin fertigatie wordt gestuurd op basis van het handhaven van een bepaalde concentratie ergens in het systeem.

■ Hoeveel verse oplossing moet door een substraat gespoeld worden om een bestaande oplossing te vervangen?

Soms is het nodig om een aanwezige oplossing in het substraat te vervangen door een nieuwe. Bij aanvang van een nieuwe teelt kan bijvoorbeeld de eindtoestand van de voorafgaande teelt ongunstig zijn voor het nieuwe gewas. Een bepaalde verdeling van de concentraties, welke resulteerde bij druppelfertigatie, kan het beste met hetzelfde druppelsysteem vervangen worden. Niet op alle posities kan echter een volledige verversing in korte tijd gerealiseerd worden. Het gebruik van een beregeningsinstallatie blijkt in dat geval niet effectiever te zijn.

■ Kan het simulatiemodel ook voor andere substraten dan grof zand en voor andere systemen toegepast worden?

In de eerste sectie van dit hoofdstuk worden substraten met verschillende fysische eigenschappen gebruikt; in de laatste sectie wordt een steenwolmat beschouwd. Aan de hand van de fluxdichtheidverdelingen tijdens een fertigatie-drainage periode wordt vastgesteld dat de drains niet direct onder druppelpunten moeten worden aangebracht, maar precies tussen twee druppelpunten. Dit garandeert een goede doorstroming van de hele steenwolmat.

Het doel van dit proefschrift was het formuleren en valideren van een simulatiemodel voor de beschrijving van de waterbeweging en het stoffentransport in een tuinbouwteeltsysteem. Nu dat model beschikbaar is kan het worden gebruikt om teeltsystemen en fertigatiestrategieën te ontwikkelen. Het model is opgezet in Hoofdstukken 2, 3 en 4, en het is gevalideerd in Hoofdstuk 7. In Hoofdstuk 8 liet ik zien wat zoal met het model mogelijk is. Vanwege de complexiteit en het feit dat het een tweedimensionale representatie van de werkelijkheid is, moeten de uitkomsten altijd met voorzichtigheid behandeld worden, en het liefst in experimenten getoetst.

Dit proefschrift laat zien dat grondige beschrijvingen, aangevuld met nauwkeurige metingen van watergehalte, stoffentransport, en wortelopname van water en voedings- stoffen noodzakelijk zijn om de dynamiek van water en nutriënten in gesloten, recirculerende teeltsystemen te begrijpen. Het simulatiemodel zal binnenkort gedocumenteerd worden. Dan zal het door onderzoekers gebruikt kunnen worden, bijvoorbeeld om fertigatiestrategieën te ontwikkelen op basis van de fysische eigenschappen van een substraat. Maar er zijn nog steeds aspecten die nadere studie vragen. Deze zijn, bijvoorbeeld:
- hoe passend is een tweedimensionale aanpak van driedimensionale problemen;
- het inbouwen van andere bronnen, zoals adsorptie en desorptie, in de module van stoffentransport;
- gevoeligheidsanalyse voor de belangrijkste parameters in het simulatiemodel;
- effect van hysterese op de wateropname door wortels.

References

Adams P. and D.M. Massey, 1984. Nutrient uptake by tomatoes from recirculating solutions. *Proceedings Sixth International Congress on Soilless Culture*, Lunteren, The Netherlands, p. 71-79.

Atkins P.W., 1978. *Physical chemistry*. Oxford University Press, Oxford, 1022 p.

Baille M., J.C. Laury, and A. Baille, 1992. Some comparative results on evapotranspiration of greenhouse ornamental crops, using lysimeter, greenhouse H_2O balance and lvdt sensors. *Acta Horticulturae* 304: 199-208.

Baker J.M. and R.R. Allmaras, 1990. System for automating and multiplexing soil moisture measurement by time-domain reflectometry. *Soil Science Society of America Journal* 54: 1-6.

Bakker J.C., 1986. Measurement of canopy transpiration or evapotranspiration in greenhouses by means of a simple vapour balance model. *Agricultural and Forest Meteorology* 37: 133-141.

Bard A.J. and L.R. Faulkner, 1980. *Electrochemical methods. Fundamentals and applications*. John Wiley and Sons, New York, 718 p.

Barraclough P.B. and P.B. Tinker, 1981. The determination of ionic diffusion coefficients in field soils. I. Diffusion coefficients in sieved soils in relation to water content and bulk density. *Journal of Soil Science* 32: 225-236.

Bates R.G., 1978. *Electrode potentials*. IN: I.M. Kolthoff and P.J. Elving (eds.), Treatise on analytical chemistry 2nd edition, part 1 volume 1, p. 245-267. John Wiley and Sons, New York.

Bear J. and A. Verruijt, 1987. *Modeling groundwater flow and pollution. With computer programs for sample cases*. D. Reidel Publishing Company, Dordrecht, The Netherlands, 414 p.

Bernstein L., 1964. *Salt tolerance of plants*. Agricultural Information Bulletin No. 283. US Department of Agriculture, Washington, 23 p.

Beven K.J., D.E. Henderson and A.D. Reeves, 1993. Dispersion parameters for undisturbed partially saturated soil. *Journal of Hydrology* 143: 19-43.

Bierhuizen J.F., 1960. De relatie tussen temperatuur en licht, en de opbrengst van tuinbouwgewassen in kassen (in Dutch). *Mededelingen Directeur Tuinbouw* 23: 822-831.

Bierhuizen J.F. and R.A. Feddes, 1963. Use of temperature and short wave radiation to predict the rate of seedling emergence and the harvest date. *Acta Horticulturae* 27: 269-277.

Blake G.R. and K.H. Hartge, 1986. *Particle density*. IN: A. Klute (ed.), Methods of soil analysis, Part 1, physical and mineralogical methods, 2nd edition. Agronomy 9 (1), American Society of Agronomy, Madison, Wisconsin, p. 377-382.

Bolt G.H., 1982. *Movement of solutes in soil: principles of adsorption/exchange chromatography*. IN: G.H. Bolt (ed.), Soil chemistry. B. Physico-chemical models. Elsevier Scientific Publishing Company, Amsterdam, The Netherlands, p. 285-348.

Bolt G.H., M.G.M. Bruggenwert and A. Kamphorst, 1978. *Adsorption of cations by soils*. IN: G.H. Bolt and M.G.M. Bruggenwert (eds.), Soil chemistry. A. Basic elements. Elsevier Scientific Publishing Company, Amsterdam, The Netherlands, p. 54-90.

Bot G.P.A., 1991. *Physical modeling of greenhouse climate*. IN: Y. Hashimoto and W. Day (eds.), Mathematical and Control Applications in Agriculture and Horticulture, Proceedings of the IFAC/ISHS workshop, p. 7-12. Pergamon Press, Oxford.

Campbell, G.S., 1985. *Soil physics with BASIC*. Elsevier, Amsterdam, The Netherlands, 148 p.

Campbell, G.S., 1991. *Simulation of water uptake by plant roots*. IN: J. Hanks and J.T. Ritchie (eds.), Modeling Plant and Soil Systems. Agronomy Monograph 31, American Society of Agronomy, Madison, Wisconsin., p. 273-285.

Cassell D.K. and A. Klute, 1986. *Water potential: tensiometry*. IN: A. Klute (ed.), Methods of soil analysis. Part 1. Physical and mineralogical methods, 2nd ed. Agronomy Monograph 9, American Society of Agronomy, Madison, Wisconsin, p. 563-596.

Challa H. and G. van Straten, 1991. *Reflections about optimal climate control in greenhouse cultivation*. IN: Y. Hashimoto and W. Day (eds.), Mathematical and Control Applications in Agriculture and Horticulture, Proceedings of the IFAC/ISHS workshop, p. 13-18. Pergamon Press, Oxford.

Chang R., 1981. *Physical chemistry with applications to biological systems, 2nd edition*. Macmillan, New York, 659 p.

Celia M.A., E.T. Bouloutas and R.L. Zarba., 1990. A general mass-conservative numerical solution for the unsaturated flow equation. *Water Resources Research* 26: 1483-1496.

Charles-Edwards, D.A., D. Doley and G.M. Rimmington, 1986. *Modelling plant growth and development*. Academic Press, Sydney, 235 p.

Chen Y., A. Banin and Y. Ataman. 1980 Characterization of particles and pores, hydraulic properties and water-air ratios of artificial growth media and soils. *Proceedings Fifth International Congress on Soilless Culture*, Wageningen, The Netherlands, p. 63-82.

Chotai A. and P.C. Young, 1991. *Self-adaptive and self-tuning control of a nutrient film technique (NFT) system*. IN: Y. Hashimoto and W. Day (eds.), Mathematical and Control Applications in Agriculture and Horticulture, Proceedings of the IFAC/ISHS workshop, p. 33-40. Pergamon Press, Oxford.

Chotai A., P.C. Young, P. Davis and Z.S. Chalabi, 1991. *True digital control of glasshouse systems*. IN: Y. Hashimoto and W. Day (eds.), Mathematical and Control Applications in Agriculture and Horticulture, Proceedings of the IFAC/ISHS workshop, p. 41-45. Pergamon Press, Oxford.

Collins W.L. and M.H. Jensen, 1983. *Hydroponics. A 1983 technical overview*. A report on the current status and long-term interdisciplinary needs for research on hydroponics; submitted to The national Science Foundation Report 82-SP-1009. The environmental Research Laboratory of the University of Arizona, Tucson, 119 p. + figures.

Cooley R.L., 1983. Some new procedures for numerical solution of variably saturated flow problems. *Water Resources Research* 19: 1271-1285.

Da Silva F.F., R. Wallach and Y. Chen, 1995. Hydraulic properties of rockwool slabs used as substrates in horticulture. *Acta Horticulturae* 401, p. 71-75.

Dalton F.N. and M.Th. van Genuchten, 1986. The time-domain reflectometry method for measuring soil water content and salinity. *Geoderma* 38: 237-250.

Darcy H., 1856. *Les fontaines publique de la ville de Dijon*. Dalmont, Paris.

Daus A.D. E.O. Frind and E.A. Sudicky, 1985. Comparative error analysis in finite element formulations of the advective-dispersive equation. *Advances in Water Resources* 8: 86-95.

Day W., 1986. A simple model to describe variation between years in the early growth of sugar beet. *Field Crops Research* 14: 213-220.

De Kreij C., C.W. van Elderen, E. Meincke and P. Fischer, 1995. Extraction methods for chemical quality control of mineral substrates. *Acta Horticulturae* 401, p. 61-70.

De Graaf, R., 1980. Beter inzicht in het watergeven bij sla (in Dutch). *Tuinderij* 20, 38-39.

De Graaf R. and J. van den Ende, 1981. Transpiration and evapotranspiration of the glasshouse crops. *Acta Horticulturae* 119: 147-158.

De Graaf R. and L. Spaans, 1989. *Automatisering watergeven bij teelten op substraat met behulp van een watergeefrekenmodel* (in Dutch). Glasshouse Crops Research Station, Naaldwijk, The Netherlands, Internal Report Nr. 33, 15 p.

De Jager A., 1985. *Response of plants to a localized nutrient supply*. PhD Thesis, University of Utrecht, Utrecht, The Netherlands, 137 p.

De Vos J.A., 1990. *Watergehaltemetingen met behulp van time domain reflectometry* (in Dutch). DLO Institute for Soil Fertility Research, Nota 231, 43 p.

De Willigen P., M. Heinen and B.J. van den Broek, 1995a. *Modeling water and nitrogen uptake of a potato crop growing on a ridge*. IN: A.J. Haverkort and D.K.L. MacKerron, Potato ecology and modelling of crops under conditions limiting growth. Kluwer Academic Publishers, Dordrecht, The Netherlands, p. 75-88.

De Willigen P., M. Heinen and M. van Noordwijk, 1995b. Availability and uptake of water from multilayered soils: a model. *in prep.*

De Willigen P. and M. van Noordwijk, 1987. *Roots, plant production and nutrient use efficiency*. PhD Thesis, Agricultural University, Wageningen, The Netherlands, 282 p.

De Willigen P. and M. van Noordwijk, 1989. Model calculations on the relative importance of internal longitudinal diffusion for aeration of roots of non-wetland plants. *Plant and Soil* 113: 111-119.

De Willigen P. and M. van Noordwijk, 1994a. Mass flow and diffusion of nutrients to a root with constant or zero-sink uptake I. Constant uptake. *Soil Science* 157: 162-170.

De Willigen P. and M. van Noordwijk, 1994b. Mass flow and diffusion of nutrients to a root with constant or zero-sink uptake II. Zero-sink uptake. *Soil Science* 157: 171-175.

Dirksen C. and S. Dasberg, 1993. Improved calibration of time domain reflectometry soil water content measurements. *Soil Science Society of America Journal* 57:660-667.

Dirksen C., J.B. Kool, P. Koorevaar and M. Th. van Genuchten, 1993. *HYSWASOR - Simulation model of hysteretic water and solute transport in the root zone*. IN: D. Russo and G. Dagan (eds.). Water flow and solute transport in soils. Developments and applications. Springer Verlag, Berlin, p. 99-122.

Doering E.J., 1965. Soil-water diffusivity by the one-step method. *Soil Science* 99: 322-326.

Douglas Jr., J., D.W. Peaceman and H.H. Rachford, 1959. A method for calculating multi-dimensional immiscible displacement. *Trans. AIME* 216: 297-306.

Eching S.O., J.W. Hopmans and O. Wendroth, 1994. Unsaturated hydraulic conductivity from transient multistep outflow and soil water pressure data. *Soil Science Society of America Journal* 58: 687-695.

Eijkelkamp, 1987. *Soil moisture equipment porous ceramics 600 series.* Eijkelkamp, Giesbeek, The Netherlands, 19 p.

El-Kadi A. and G. Ling, 1993. The Courant and Peclet number criteria for the numerical solution of the Richards equation. *Water Resources Research* 29: 3485-3494.

FAO, 1990. *Soilless culture for horticultural crop production.* FAO Plant Production and protection Paper 101, Rome, 188 p.

Feddes R.A. 1987. *Simulating water management and crop production with the SWACRO-model.* IN: Proceedings of the Third International Workshop on Land Drainage, p. A27-A40, Ohio.

Gabriels R., W. van Keirsbulck and H. Engels, 1995. A rapid method for the determination of chemical properties of growing media. *Acta Horticulturae* 401, p. 57-59.

Gardner W.R., 1956. Calculation of capillary conductivity from pressure plate outflow data. *Soil Science Society of America Proceedings* 20: 317-320.

Gardner W.R., 1958. Some steady state solutions of the unsteady state moisture flow equation with application to evaporation from a water table. *Soil Science* 85: 228-232.

Gardner W.R., 1960. Dynamic aspects of water availability to plants. *Soil Science* 89: 63-73.

Genstat 5 Committee, 1993. *Genstat*[TM] *5 release 3 reference manual.* Clarendon Press, Oxford, 796 p.

Gijsman A.J., J. Floris, M. van Noordwijk and G. Brouwer, 1991. An inflatable minirhizotron system for observations with improved soil/tube contact. *Plant and Soil* 134: 261-269.

Golub G.H. and C.F. van Loan, 1989. *Matrix computations, 2nd ed.* The Johns Hopkins University Press, Baltimore, 642 p.

Gustafsson I., 1984. *Modified incomplete Cholesky (MIC) methods.* IN: D.J. Evans (ed.), Preconditioning Methods, Theory and Applications, p. 265-293. Gordon and Breach, New York.

Hamaker P., 1989. *Centraal afvoersysteem voor drainagewater van de glastuinbouw in Delfland: onderzoek naar de invloed op de kwaliteit van het oppervlaktewater als gietwaterbron en naar de baten voor de glastuinbouw binnen het beheersgebied van het Hoogheemraadschap Delfland* (in Dutch). Report 21, Winand Staring Centre, Wageningen, The Netherlands, 65 p.

Hamaker P., 1992. *Effect van de gietwatervoorziening en teeltmethode op de waterbehoefte en de nutriëntenemissie van de glastuinbouw in het Zuidhollands Glasdistrict: modelberekeningen van de bestaande en toekomstige situatie* (in Dutch). Report 235, Winand Staring Centre, Wageningen, The Netherlands, 113 p.

Hanks R.J. and G.L. Ashcroft, 1980. *Applied soil physics.* Advanced Series in Agricultural Sciences 8. Springer-Verlag, Berlin, 159 p.

Hasted, J.B., 1973. *Aqueous dielectrics.* Chapman and Hall Ltd., London, 302 p.

Haverkamp R. and M. Vauclin, 1979. A note on estimating finite difference interblock hydraulic conductivity values for transient unsaturated flow problems. *Water Resources Research* 15: 181-187.

Heimovaara T.J., 1993. *Time domain reflectometry in soil science: theoretical backgrounds, measurements and models.* PhD Thesis, University of Amsterdam, The Netherlands, 169 p.

Heimovaara T.J. and W. Bouten, 1990. A computer-controlled 36-channel time domain reflectometry system for monitoring soil water contents. *Water Resources Research* 26: 2311-2316.

Heinen M., 1990a. *Analytical growth equations and their Genstat 5 equivalents.* Nota 223, Institute for Soil Fertility, Haren, The Netherlands, 48 p.

Heinen M., 1990b. *The use of ion-selective electrodes in NFT systems.* Nota 222, Institute for Soil Fertility, Haren, The Netherlands, 29 p.

Heinen M., 1992. Control of the composition of the nutrient solution in an automated NFT system: a simulation study. *Acta Horticulturae* 304: 281-289.

Heinen M., 1994. *Growth and nutrient uptake by lettuce grown on NFT.* Research Institute for Agrobiology and Soil Fertility (AB-DLO), Haren, The Netherlands, Report 1, 74 p.

Heinen M., A. de Jager, and H. Niers, 1991. Uptake of nutrients by lettuce on NFT with controlled composition of the nutrient solution. *Netherlands Journal of Agricultural Science*, 39: 197-212.

Heinen M. and P. de Willigen, 1992. *FUSSIM2. A simulation model for two-dimensional flow of water in unsaturated soil.* Nota 260, Research Institute for Agrobiology and Soil Fertility, Haren, The Netherlands, 146 p.

Heinen M. and K. Harmanny, 1992. Evaluation of the performance of ion-selective electrodes in an automated NFT system. *Acta Horticulturae* 304: 273-280.

Heinen M., C. Sonneveld, W. Voogt, R. Baas, W.G. Keltjens and B. Veen, 1996. *Mineral balance of young tomato grown on nutrient solution.* Report 66, Research Institute for Agrobiology and Soil Fertility, Haren, The Netherlands, 47 p.

Heinen M. and J. van Moolenbroek, 1995. Water balance of lettuce grown on sand beds. *Acta Horticulturae* 401: 517-524.

Herkelrath W.N., S.P. Hamburg and F. Murphy, 1991. Automatic, real-time monitoring of soil moisture in a remote field area with time domain reflectometry. *Water Resources Research* 27: 857-864.

Hestenes M.R. and E. Stiefel, 1952. Methods of conjugate gradients for solving linear systems. *Journal of Research of the Bureau of Standards* 49: 409-436.

Hillel D., 1980a. *Fundamentals of soil physics.* Academic Press, New York, 413 p.

Hillel D., 1980b. *Applications of soil physics.* Academic Press, New York, 385 p.

Hooghoudt S.B., 1937. *Bijdragen tot de kennis van eenige natuurkundige grootheden van den grond. 6. Bepaling van de doorlatendheid in gronden van de tweede soort; theorie en toepassingen van de kwantitatieve strooming van het water in ondiep gelegen grondlagen, vooral in verband met ontwaterings- en infiltratievraagstukken* (in Dutch). Verslagen van Landbouwkundige Onderzoekingen No 43 (13) B, p. 13-216, 's-Gravenhage.

Hooghoudt S.B., 1940. *Bijdragen tot de kennis van eenige natuurkundige grootheden van den grond. 7. Algemeene beschouwing van het probleem van de detailontwatering en de infiltratie door middel van parallel loopende drains, greppels, slooten en kanalen* (in Dutch). Verslagen van Landbouwkundige Onderzoekingen No 46 (4) B, p. 515-707, 's-Gravenhage.

Ikeda H. and T. Osawa, 1984. Lettuce growth as influenced by N source and temperature of the nutrient solution. *Proceedings of the Sixth International Congress on Soilless Culture*, 273-284.

Jaynes, D.B., 1984. Comparison of soil-water hysteresis models. *Journal of Hydrology* 75: 287-299.

Jensen M.H. and W.L. Collins, 1985. Hydroponic vegetable production. *Horticultural Reviews* 7: 483-558.

Kamphorst A. and G.H. Bolt, 1981. *Saline and sodic soils*. IN: G.H. Bolt and M.G.M. Bruggenwert (eds.), Soil Chemistry. A. Basic Elements, p. 171-191. Elsevier Scientific Publishing Company, Amsterdam, The Netherlands.

Keithley, 1991. *Data acquisition and control. Hardware and software for IBM PC/XT/AT, PS/2 and microchannel computers.* Keithley Metrabyte/Asyst/DAC, Taunton, Massachusetts, 272 p.

Kershaw D.S., 1978. The incomplete Cholesky-conjugate gradient method for the iterative solution of systems of linear equations. *Journal for Computational Physics* 26: 43-65.

Kipp J.A. and G. Wever, 1993. *Wortelmedia* (in Dutch). Informatiereeks No. 103, Proefstation voor Tuinbouw onder Glas, Naaldwijk, The Netherlands, 48 p.

Kirkland M.R., R.G. Hills and P.J. Wierenga, 1992. Algorithms for solving Richards' equation for variably saturated soils. *Water Resources Research* 28: 2049-2058.

Klute A., 1986. *Water retention: laboratory methods*. IN: A. Klute (ed.), Methods of soil analysis, Part 1, physical and mineralogical methods, 2nd edition. Agronomy 9 (1), American Society of Agronomy, Madison, Wisconsin, p. 635-662.

Klute A. and C. Dirksen, 1986. *Hydraulic conductivity and diffusivity: laboratory methods*. IN: A. Klute (ed.), Methods of soil analysis, Part 1, physical and mineralogical methods, 2nd edition. Agronomy 9 (1), American Society of Agronomy, Madison, Wisconsin, p. 686-732.

Knight J.H., 1992. Sensitivity of time domain reflectometry measurements to lateral variations in soil water content. *Water Resources Research*, 28: 2345-2352.

Knight J.H., I. White and S.J. Zegelin. *Sampling volume of TDR probes used for water content monitoring*. IN: K.M. O'Connor, C.H. Dowding and C.C. Jones (eds.), Proceedings of the symposium and workshop on time domain reflectometry in environmental, infrastructure, and mining applications. United States Department of Interior Bureau of Mines, Special Publication SP 19-94, p. 93-104, Minneapolis, MN.

Kool J.B. and J.C. Parker, 1987a. *Estimating soil hydraulic properties from transient outflow experiments: SFIT user's guide*. Department of Soils and Environmental Sciences, Virginia Polytechnic Institute and State University, Blacksburg, Virginia 24061, USA, 59 p.

Kool J.B. and J.C. Parker, 1987b. Development and evaluation of closed-form expressions for hysteretic soil hydraulic properties. *Water Resources Research* 23: 105-114.

Kool J.B., J.C. Parker and M.Th. van Genuchten, 1985. Determining soil hydraulic properties from one-step outflow experiments by parameter estimation: I. Theory and numerical studies. *Soil Science Society of America Journal* 49: 1348-1354.

Koorevaar P., G. Menelik and C. Dirksen, 1983. *Elements of soil physics*. Elsevier, Amsterdam, The Netherlands, 228 p.

Kuiper L.K., 1981. A comparison of the incomplete Cholesky-conjugate gradient method with the strongly implicit method as applied to the solution of two-dimensional groundwater flow equations. *Water Resources Research* 17: 1082-1086.

Larabi A. and F. de Smedt, 1994. Solving three-dimensional hexahedral finite element groundwater models by preconditioned conjugate gradient methods. *Water Resources Research* 30: 509-521.

Ledieu J.P., P. de Ridder, P. de Clerck and S. Dautrebande, 1986. A method of measuring soil moisture by time-domain reflectometry. *Journal of Hydrology* 88:319-328.

LEI and CBS, 1992. *Landbouwcijfers 1992* (in Dutch). Landbouw Economisch Instituut (LEI-DLO), Den Haag, en Centraal Bureau voor de Statistiek (CBS), Voorburg, 271 p.

Leij F.J., M. Th. van Genuchten, S.R. Yates, W.B. Russell and F. Kaveh, 1992. *RETC: A computer program for analyzing soil water retention and hydraulic conductivity data.* IN: M. Th. van Genuchten, F.J. Leij and L.J. Lund (eds.), Indirect methods for estimating the hydraulic properties of unsaturated soils. University of California, Riverside, Ca 92521, USA, p. 263-272.

Maas E.V. and G.J. Hoffman, 1977a. Crop salt tolerance - current assessment. *Journal of Irrigation and Drainage Division ASCE* 103(IR2): 115-134.

Maas E.V. and G.J. Hoffman, 1977b. *Crop salt tolerance: an evaluation of existing data.* IN: H.E. Dregne (ed.), Managing Saline Water for Irrigation, Proceedings of the International Salinity Conference, p. 187-198. Texas Tech University, Lubbock, Texas.

McCord J.T., 1991. Application of second-type boundaries in unsaturated flow modeling. *Water Resources Research* 27: 3257-3260.

McNeal B.L., J.D. Oster and J.T. Hatcher, 1970. Calculation of electrical conductivity from solution composition data as an aid to in-situ estimation of soil salinity. *Soil Science* 110: 405-414.

Meijerink J.A. and H.A. van der Vorst, 1977. An iterative solution method for linear systems of which the coefficient matrix is a symmetric M-matrix. *Mathematics of Computation* 31: 148-162.

Meurs G.A.M., 1985. *Seasonal heat storage in the soil.* PhD Thesis, Technical University, Delft, The Netherlands, 217 p.

Micro Switch, 1986. *Specifier's guide for pressure sensors, Catalog 15, Issue 4.* Micro Switch, Freeport, Illinois, 84 p.

Milks R.R., W.C. Fonteno and R.A. Larson, 1989. Hydrology of horticultural substrates: I. Mathematical models for moisture characteristics of horticultural container media. *Journal of the American Society of Horticultural Science* 114: 48-52.

Miller E.E. and Miller R.D., 1956. Physical theory for capillary flow phenomena. *Journal of Applied Physics* 27: 324-332.

Milly P.C.D., 1985. A mass-conservative procedure for time-stepping in models of unsaturated flow. *Advances in Water Resources* 8: 32-36.

Moldrup P., T. Yamaguchi, J. Aa. Hansen and D.E. Rolston, 1992. An accurate and numerically stable model for one-dimensional solute transport in soils. *Soil Science* 153: 261-273.

Moldrup P., T. Yamaguchi, D.E. Rolston, K. Vestergaard and J.Aa. Hansen, 1994. Removing numerically induced dispersion from finite difference models for solute and water transport in unsaturated soils. *Soil Science* 157: 153-161.

Mongeau R and K.A. Stewart, 1984. Effect of solution temperature on the growth and development of lettuce cv. Ostinata. *Proceedings of the Sixth International Congress on Soilless Culture*, 387-392.

Morgan J.V., A.T. Moustafa and A. Tan, 1980. Factors affecting the growing-on stages of lettuce and chrysanthemum in nutrient solution culture. *Acta Horticulturae*, 98: 253-261.

Mous S.L.J., 1993. Identification of the movement of water in unsaturated soils: the problem of identifiability of the model. *Journal of Hydrology* 143: 153-167.

Mualem Y., 1976. A new model for predicting the hydraulic conductivity of unsaturated porous media. *Water Resources Research* 12: 513-522.

Mualem Y., 1984. A modified dependent-domain theory of hysteresis. *Soil Science* 137: 283-291.

Mualem Y. and S.P. Friedman, 1991. Theoretical prediction of electrical conductivity in saturated and unsaturated soil. *Water Resources Research* 27: 2771-2777.

Narasimhan T.N. and P.A. Witherspoon, 1976. An integrated finite difference method for analyzing fluid flow in porous media. *Water Resources Research* 12: 57-64.

Narasimhan T.N. and P.A. Witherspoon, 1977. Numerical model for saturated-unsaturated flow in deformable porous media 1. Theory. *Water Resources Research* 13: 657-664.

Narasimhan T.N., P.A. Witherspoon and A.L. Edwards, 1977. Numerical model for saturated-unsaturated flow in deformable porous media 2. The algorithm. *Water Resources Research* 13: 255-261.

NEN 999, 1977. *The international system of units (SI)* (in Dutch). Nederlands Normalisatie Instituut, Delft, The Netherlands, 35 p.

NEN 5786, 1991. *Soil - Unsaturated zone - Determination of water retention characteristic - Underpressure method until h = -200 cm - Determination with a porous plate in combination with a buret* (in Dutch). Nederlands Normalisatie Instituut, Delft, The Netherlands, 4 p.

NEN 5789, 1991. *Soil - Unsaturated zone - Determination of the saturated hydraulic conductivity* (in Dutch). Nederlands Normalisatie Instituut, Delft, The Netherlands, 4 p.

Neuman S.P., R.A. Feddes and E. Bresler, 1974. *Finite element simulation of flow in saturated-unsaturated soils considering water uptake by plants*. AIO-SWC-77, Technion, Institute of Technology, Haifa, Israel, 104 p.

Nieber J.L. and R.A. Feddes, 1996. *Solutions for combined saturated and unsaturated flow*. To appear in: J. van Schilfgaarde and W. Skaggs (eds.), Drainage in Agriculture. Agronomy Monograph, American Society of Agronomy, Madison, Wisconsin.

Novozamsky I., J. Beek and G.H. Bolt, 1981. *Chemical equilibria*. IN: G.H. Bolt and M.G.M. Bruggenwert (eds.), Soil Chemistry. A. Basic Elements, p. 13-42. Elsevier Scientific Publishing Company, Amsterdam, The Netherlands.

NRLO, 1990. *Onderzoekprogramma gesloten bedrijfssytemen glastuinbouw* (in Dutch). Nationale Raad voor Landbouwkundig Onderzoek (NRLO), 's-Gravenhage, The Netherlands, 31 p. + Appendices.

Nyhan J.W. and B.J. Drennon, 1990. Tensiometer data acquisition system for hydrologic studies requiring high temporal resolution. *Soil Science Society of America Journal* 54: 293-296.

Okuya A. and T. Okuya, 1991. *Development of an ion controlled feeding method in hydroponics*. IN: Y. Hashimoto and W. Day (eds.), Mathematical and Control Applications in Agriculture and Horticulture, Proceedings of the IFAC/ISHS workshop, p. 355-359. Pergamon Press, Oxford.

Otten W., 1994. *Dynamics of water and nutrients for potted plants induced by flooded bench fertigation: experiments and simulation.* PhD Thesis, Wageningen Agricultural University, Wageningen, The Netherlands, 115 p.

Otten W., P. Kabat and P.A.C. Raats, 1996. Hysteretic water retention and hydraulic conductivity characteristics of a peat based potting medium. *Submitted to Journal of American Society of Horticultural Science.*

Parker J.C, J.B. Kool and M.Th. van Genuchten, 1985. Determining soil hydraulic properties from one-step outflow experiments by parameter estimation: II. Experimental studies. *Soil Science Society of America Journal* 49: 1354-1359.

Passioura J.B., 1976. Determining soil water diffusivities from one-step outflow experiments. *Australian Journal of Soil Research* 15: 1-8.

Patankar S.V., 1980. *Numerical heat transfer and fluid flow.* Hemisphere Publishing Corporation, New York, 197 p.

Peaceman D.W. and H.H. Rachford Jr., 1955. The numerical solution of parabolic and elliptic differential equations. *Journal of the Society of Industrial and Applied Mathematics.* 3: 28-41.

Postma R., O. Oenema, D.W. Bussink, M. Heinen and J. van Moolenbroek, 1994. Gasvormige stikstofverliezen bij de substraatteelt van sla op een zandbed onder glas. *Meststoffen 1994*: 28-34 (in Dutch, with English abstract and legends to figures and tables).

Press W.H., B.P. Flannery, S.A. Teukolsky and W.T. Vetterling, 1986. *Numerical recipes. The art of scientific computing.* Cambridge University Press, Cambridge, 818 p.

Pullan A.J. and I.F. Collins, 1987. Two- and three-dimensional steady quasi-linear infiltration from buried and surface cavities using boundary element techniques. *Water Resources Research* 23: 1633-1644.

Raats P.A.C., 1970. Steady infiltration from line sources and furrows. *Soil Science Society of America Proceedings* 34: 709-714.

Raats P.A.C., 1980. The supply of water and nutrients in soilless culture. *Proceedings Fifth International Congress on Soilless Culture*, Wageningen, The Netherlands, p. 53-62.

Raats P.A.C., 1992. *A superclass of soils.* IN: M. Th. van Genuchten, F.J. Leij and L.J. Lund (eds.), Indirect methods for estimating the hydraulic properties of unsaturated soils. University of California, Riverside, Ca 92521, USA, p. 45-51.

Raats P.A.C. and W.R. Gardner, 1974. *Movement of water in the unsaturated zone near a water table.* IN: J. van Schilfgaarde (ed.), Drainage for Agriculture, p. 311-357. Series in Agronomy Nr. 17, American Society of Agronomy, Madison, Wisconsin.

Rappoldt C., 1992. *Diffusion in aggregated soil.* PhD Thesis, Agricultural University, Wageningen, The Netherlands, 162 p.

Rathfelder K. and L.M. Abriola, 1994. Mass conservative numerical solutions of the head-based Richards equation. *Water Resource Research* 30: 2579-2586.

Rhoades J.D. and J. Loveday, 1990. *Salinity control in irrigated agriculture.* IN: B.A. Stewart and D.R. Nielsen (eds.), Irrigation of Agricultural Crops, p. 1089-1142. Series in Agronomy 30, American Society of Agronomy, Madison, Wisconsin.

Richards L.A., 1931. Capillary conduction of liquids through porous mediums. *Physics* 1: 318-333.

Ritchie J.T., 1983. *Efficient water use in crop production: discussion on the generality of relations between biomass production and evapotranspiration.* IN: H.M. Taylor, W.R. Jordan and T.R. Sinclair (eds.), Limitations to efficient water use in crop production. American Society of Agronomy, Madison, Wisconsin, p. 29-44.

Roorda van Eysinga, J.P.N.L., and Smilde, K.W., 1971. *Nutritional disorders in glasshouse lettuce.* PUDOC, Wageningen, The Netherlands, 56 p.

Rosenberg D.U., 1969. *Methods for the numerical solution of partial differential equations.* American Elsevier Publishing Company Inc., New York, 128 p.

Ross P. and K.L. Bristow, 1990. Simulating water movement in layered and gradational soils using the Kirchoff transform. *Soil Science Society of America Journal* 54: 1519-1524.

Rubin J., 1968. Theoretical analysis of two-dimensional, transient flow of water in unsaturated and partly unsaturated soils. *Soil Science Society of America Proceedings* 32: 607-615.

Ruijs M.N.A., E.A. van Os, A.T.M. Hendrix, A.P. van der Hoeven, F. Koning and P.A. van Weel, 1990. *Bedrijfseconomische aspecten van milieuvriendelijkere bedrijfssystemen in de glastuinbouw. Simulatie van milieuvriendelijkere bedrijfssystemen voor de gewasgroep 'eenmalig oogstbare snijbloemen' (chrysant)* (in Dutch). Verslag nr. 2, Proefstation voor Tuinbouw onder Glas, Naaldwijk, The Netherlands, 45 p. + appendices.

Russo D., J. Zaidel and A. Laufer, 1994. Stochastic analysis of solute transport in partially saturated heterogeneous soil. 1. Numerical experiments. *Water resources Research* 30: 769-779.

Schuurman J.J., and B.E. Schäffner, 1974. *De wortelontwikkeling van enige tuinbouwgewassen op zandgrond* (in Dutch). Rapport 11-74, Instituut voor Bodemvruchtbaarheid, Haren ,The Netherlands, 62 p.

Schwarz D., M. Heinen and M. van Noordwijk, 1995. Rooting intensity and root distribution of lettuce grown in sand beds. *Plant and Soil* 176: 205-217.

Simunek J., T. Vogel and M.Th. van Genuchten, 1994. *The SWMS_2D code for simulating water flow and solute transport in two-dimensional variably saturated media.* Research Report 132, US Salinity Laboratory, ARS, USDA, Riverside, Ca, 169 p.

Sonneveld C., 1994. *Mineralenopname van teelten onder glas (voorlopige uitgave)* (in Dutch). Intern Verslag no. 6. Proefstation voor Tuinbouw onder Glas, Naaldwijk, 25 p.

Sonneveld C., 1995. Fertigation in the greenhouse industry. *Proceedings of the Dahlia Greidinger International Symposium on Fertigation,* p. 121-140, Technion - Israel Institute of Technology, Haifa, Israel.

Sonneveld C. and N. Straver, 1988. *Nutrient solutions for vegetables and flowers grown in water or substrates.* Voedingsoplossing Glastuinbouw No. 8, Proefstation voor Tuinbouw onder Glas, Naaldwijk, The Netherlands, 19 p.

Sonneveld C., J. van den Ende and S.S. de Bes, 1990. Estimating the chemical composition of soil solutions by obtaining saturation extracts or specific 1:2 by volume extracts. *Plant and Soil* 122: 169-175.

Spiegel M.R., 1968. *Mathematical handbook of formulas and tables.* Schaum's outline series in mathematics, McGraw-Hill Book Company, New-York, 271 p.

Stanghellini C., 1987. *Transpiration of greenhouse crops; an aid to climate management.* PhD Thesis, Wageningen Agricultural University, Wageningen, The Netherlands, 150 p.

Steiner A.A., 1984. The universal nutrient solution. *Proceedings Sixth International Congress on Soilless Culture*, Lunteren, The Netherlands, 633-649.

Steiner A.A., 1985. The history of mineral plant nutrition till about 1860 as source of the origin of soilless culture methods. *Soilless Culture*, Vol. 1 No. 1, p. 7-24.

Stolte J., J.I. Freyer, W. Bouten, C. Dirksen, J.M. Halbertsma, J.C. van Dam, J.A. van den Berg, G.J. Veerman and J.H.M. Wösten, 1994. Comparison of six methods to determine unsaturated hydraulic conductivity. *Soil Science Society of America Journal* 58: 1596-1603.

Taylor S.A. and G.L. Ashcroft, 1972. *Physical edaphology. The physics of irrigated and non-irrigated soils.* W.H. Freeman Co., San Francisco, CA, 533 p.

Taylor H.M. and B. Klepper, 1978. The role of rooting characteristics in the supply of water to plants. *Advances in Agronomy* 30, 99-128.

Toorman A.F., P.J. Wierenga and R.G. Hills, 1992. Parameter estimation of hydraulic properties from one-step outflow data. *Water Resources Research* 28: 3021-3028.

Topp G.C., 1969. Soil-water hysteresis measured in a sandy loam and compared with the hysteretic domain model. *Soil Science Society of America Proceedings* 33:645-651.

Topp G.C., J.L. Davis and A.P. Annan, 1980. Electromagnetic determination of soil water content: measurements in coaxial transmission lines. *Water Resources Research* 16: 574-582.

Topp G.C., M. Yanuka, W.D. Zebchuk and S. Zegelin, 1988. Determination of electrical conductivity using time domain reflectometry: soil and water experiments in coaxial lines. *Water Resources Research* 24: 945-952.

US Salinity Laboratory Staff, 1954. *Diagnosis and improvement of saline and alkali soils* (ed. L.A. Richards). United States Department of Agriculture, Handbook 60, Washington, 160 p.

Van Dam J.C., J.N.M. Stricker and P. Droogers, 1994. Inverse method to determine soil hydraulic functions from multistep outflow experiments. *Soil Science Society of America Journal* 58: 647-652.

Van den Elsen H.G.M. and J.W. Bakker, 1992. A universal device to measure the pressure head for laboratory use or long-term stand-alone field use. *Soil Science* 154: 458-464.

Van den Vlekkert, 1992. Ion-sensitive field effect transistors. *Acta Horticulturae* 304: 113-126.

Van der Boon J., J.W. Steenhuizen and E.G. Steingröver, 1990. Growth and nitrate concentration of lettuce as affected by total nitrogen and chloride concentration, NH_4/NO_3 ration and temperature of the recirculating nutrient solution. *Journal of Horticultural Science*, 65: 309-321.

Van der Burg A.M.M. and Ph. Hamaker, 1986. *Water- en mineralenhuishouding bij teelten op substraat in de praktijk* (in Dutch). Nota 1520, Instituut voor Cultuurtechniek en Waterhuishouding, Wageningen, 44 p.

Van der Schans D.A., M. de Graaf and A.J. Hellings, 1984. *De relatie tussen wateraanvoer, verdamping en produktie bij het gewas aardappelen* (in Dutch). Nota 1539, Instituut voor Cultuurtechniek en Waterhuishouding, Wageningen, The Netherlands, 47 p.

Vandevivere Ph. and Ph. Baveye, 1992. Saturated hydraulic conductivity reduction caused by aerobic bacteria in sand columns. *Soil Science Society of America Journal* 56: 1-13.

Van Genuchten M.T., 1980. A closed form equation for predicting the hydraulic conductivity of unsaturated soils. *Soil Science Society of America Journal* 44: 982-989.

Van Genuchten M. Th., F.J. Leij and S.R. Yates, 1991. *The RETC code for quantifying the hydraulic functions of unsaturated soils*. Report No. EPA/600/2-91/065, Robert S. Kerr Environmental Research Laboratory, Office of Research and Development, US Environmental Protection Agency, Ada, Oklahoma, 83 p.

Van Heerden C and A. Tiktak, 1994. *Het grafisch programma XY. Een programma voor visualisatie van de resultaten van rekenprogramma's* (in Dutch). Rapport nr. 715501002, SOTRAS deelrapport nr. 2, Rijksinstituut voor Volksgezondheid en Milieuhygiëne, Bilthoven, The Netherlands, 82 p.

Van Moolenbroek J., 1995. *Water- en mineralenbalans bij roos in een gesloten teeltsysteem* (in Dutch). Rapport 18, Proefstation voor Bloemisterij en Glasgroenten, Naaldwijk, 19 p.

Van Moolenbroek J. and M. Heinen, 1994. *Dynamiek van water en nutriënten in gesloten, recirculerende teeltsystemen, met name systemen gebaseerd op zandbedden* (in Dutch). Proefstation voor Tuinbouw onder Glas, Intern Verslag Nr. 14, 28 p. + bijlagen.

Van Noordwijk M., 1978. *Zout ophoping en beworteling bij de teelt van tomaten op steenwol* (in Dutch, with a summary: Distribution of salts and root development in the culture of tomatoes on rock wool). Rapport 3-78, Instituut voor Bodemvruchtbaarheid, Haren, 21 p.

Van Noordwijk M., 1990. *Synchronization of supply and demand is necessary to increase efficiency of nutrient use in soilless culture*. IN: M.L. van Beusichem (ed.), Plant Nutrition - Physiology and applications, p. 525-531. Kluwer Academic Publishers, Dordrecht, The Netherlands.

Van Noordwijk M. and G. Brouwer, 1991. *Review of quantitative root length data in agriculture*. IN: B.L. McMichael and H. Persson (eds.), Plant Roots and their Environment, p. 515-525, Elsevier Science Publishers.

Van Noordwijk M. and G. Brouwer, 1993. Gas-filled root porosity of crop plants in response to temporary low oxygen supply in different growth stages. *Plant and Soil* 152: 187-199.

Van Noordwijk M. and P.A.C. Raats, 1980. Drip and drainage systems for rockwool cultures in relation to accumulation and leaching of salts. *Proceedings Fifth International Congress on Soilless Culture*, Wageningen, The Netherlands, p. 279-287.

Van Noordwijk M. and P.A.C. Raats, 1981. *Zoutophoping en -uitspoeling in samenhang met het druppelsysteem bij de teelt op steenwol* (in Dutch, with a summary: The influence of the drip system upon accumulation and leaching of salts in rockwool cultures). Rapport 9-81, Instituut voor Bodemvruchtbaarheid, Haren, 37 p.

Van Schilfgaarde J., 1974. *Nonsteady flow to drains*. IN: J. van Schilfgaarde (ed.), Drainage for Agriculture, p. 245-270. Series in Agronomy Nr. 17, American Society of Agronomy, Madison, Wisconsin.

Vauclin M., D. Khanji and G. Vachaud, 1979. Experimental and numerical study of a transient, two-dimensional unsaturated-saturated water table recharge problem. *Water Resources Research* 15: 1089-1101.

Vellidis G. and A.G. Smajstrla, 1992. Modeling soil water redistribution and extraction patterns of drip-irrigated tomatoes above a shallow water table. *Transactions of the American Society of Agricultural Engineers* 35: 183-191.

Viaene P., H. Vereecken, J. Diels and J. Feyen, 1994. A statistical analysis of six hysteresis models for the moisture retention characteristic. *Soil Science* 157: 345-355.

Voogt W., 1992. *Mineralenbalans bij komkommer in watercultuur* (in Dutch). Intern Verslag nr. 47, Proefstation voor Tuinbouw onder Glas, Naaldwijk, 8 p.

Voogt W., 1993. Nutrient uptake of year round tomato crops. *Acta Horticulturae* 339: 99-112.

Wallach R., F.F. da Silva and Y. Chen, 1992a. Hydraulic characteristics of tuff (Scoria) used as a container medium. *Journal of the American Society of Horticultural Science* 117: 415-421.

Wallach R., F.F. da Silva and Y. Chen, 1992b. Unsaturated hydraulic characteristics of composted agricultural wastes, tuff and their mixtures. *Soil Science* 153: 434-441.

Wang H.F. and M.P. Anderson, 1982. *Introduction to groundwater modeling. Finite difference and finite element methods*. W.H. Freeman and Company, New York, 237 p.

Weast R.C. (ed.), 1975. *Handbook of chemistry and physics, 56th edition*. CRC Press, Cleveland, Ohio.

Whalley W.R., 1993. Considerations on the use of time-domain reflectometry (TDR) for measuring soil water content. *Journal of Soil Science* 44: 1-9.

Willumsen J., 1980. pH of the flowing nutrient solution. *Acta Horticulturae* 98: 51-62.

Willumsen J., 1984. Nutritional requirements of lettuce in water culture. *Proceedings Sixth International Congress on Soilless Culture*, p. 777-791, ISOSC, Wageningen, The Netherlands.

Wind G.P., 1955. Flow of water through plant roots. *Netherlands Journal of Agricultural Science* 3: 259-264.

Wolfram S., 1991. *Mathematica. A system for doing mathematics by computer, 2nd edition*. Addison-Wesley Publishing Company Inc., Redwood City, CA, 961 p.

Wösten J.H.M., G.J. Veerman and J. Stolte, 1994. *Waterretentie- en doorlatendheidskarakteristieken van boven- en ondergronden in Nederland: de Staringreeks; vernieuwde uitgave 1994* (in Dutch). Technical Document 18, Agricultural Research Department Winand Staring Centre for Integrated Land, Soil and Water Research, Wageningen, The Netherlands, 66 p.

Young P.C., W. Tych and A. Chotai, 1991. *Identification, estimation and control of glasshouse systems*. IN: Y. Hashimoto and W. Day (eds.), Mathematical and Control Applications in Agriculture and Horticulture, Proceedings of the IFAC/ISHS workshop, p. 307-315. Pergamon Press, Oxford.

Zaidel J. and D. Russo, 1992. Estimation of finite difference interblock conductivities for simulation of infiltration into initially dry soils. *Water Resources Research* 28: 2285-2295.

Zegelin S.J., I. White and D.R. Jenkins, 1989. Improved field probes for soil water content and electrical conductivity measurement using time domain reflectometry. *Water Resources Research* 25: 2367-2376.

List of symbols

The following notation conventions were used:

Matrix	**BOLD, ROMAN, CAPITAL**
Vector	**bold, roman, small**
Scalar	*italic*
Integrated scalar	***italic and bold***
Functions, operators	roman
Numbers	roman

The basic SI dimensions 1, A, L, M, T, m and Θ represent dimensionless, strength of current, length, mass, time, molar amount of a species and temperature, respectively, while the deduced dimensions J, V and Ω represent energy, voltage and resistance, respectively (NEN 999, 1977).

In the list below are given: the symbol, its description, its dimension, and the equation number or section number of first occurrence.

Symbol	Description	Dimension	Equation
A	Coefficient matrix	L^2T^{-1}	[3-39]
$\mathbf{A}^{-1}$	Inverse of **A**	$L^{-2}T$	[3-40]
A	Coefficient referring to central node	L^2T^{-1}	[3-22,26]
A_C	Coefficient referring to C of central node	L^2T^{-1}	[3-25]
A_E	K-geometry coefficient between central node (I,J) and its eastern neighbour node $(I+1,J)$	L^2T^{-1}	[3-22,23]
A_N	K-geometry coefficient between central node (I,J) and its northern neighbour node $(I,J-1)$	L^2T^{-1}	[3-22,23,28]
A_S	K-geometry coefficient between central node (I,J) and its southern neighbour node $(I,J+1)$	L^2T^{-1}	[3-22,23]
A_W	K-geometry coefficient between central node (I,J) and its western neighbour node $(I-1,J)$	L^2T^{-1}	[3-22,23,27]
A_{bf}	Amount of nutrient in the sand bed buffer at harvest	M	[6-14]
A_{bi}	Initial amount of nutrient in the sand bed buffer	M	[6-14]
A_{cf}	Amount of nutrient in the crop at harvest	M	[6-13]
A_{ci}	Initial amount of nutrient in the crop	M	[6-13]
A_{df}	Amount of nutrient in the drainage tank	M	[6-14]
A_{di}	Initial amount of nutrient in the drainage tank	M	[6-14]
A_f	Parameter in expression for activity coefficient	$M^{0.5}m^{0.5}$	[A8-3,4]

A_{sf}	Amount of nutrient in the supply tank	M	[6-14]
A_{si}	Initial amount of nutrient in the supply tank	M	[6-14]
B	Boundary condition function	1	[2-8]
B_f	Parameter in expression for activity coefficient	$L^{-1}M^{0.5}m^{0.5}$	[A8-3,5]
B_Γ	Specified hydraulic gradient at Γ	1	[2-11]
$\mathbf{C}$	Preconditioning matrix	L^2T^{-1}	[3-47]
C	Differential moisture capacity	L^{-1}	[2-5,6]
CV	Volume of control volume	L^3	[3-5]
Co	Courant number	1	[3-74]
C_{sd}	C of scanning drying curve	L^{-1}	[4-14]
C_{sw}	C of scanning wetting curve	L^{-1}	[4-19]
C_w	C of main wetting curve	L^{-1}	[4-14,19]
$\mathbf{D}_h$	Hydrodynamic dispersion tensor	L^2T^{-1}	[2-33]
DM	'Degree-minutes' defined as the difference between heating pipeline T and greenhouse air T of one degree during a time span of one minute	$T^{-1}\Theta$	[5-14]
D	Diffusion coefficient	L^2T^{-1}	[2-47]
D_0	Diffusion coefficient in free water	L^2T^{-1}	[2-35,5-16]
D_A	Amount of nutrient added as dosage	M	[6-14]
D_{ij}	Component (i,j) of $\mathbf{D}_h$	L^2T^{-1}	[2-34,35]
D_{max}	Maximum observed D in any control volume	L^2T^{-1}	[3-94]
D_w	Water diffusivity $= K(\theta)/C(h)$	L^2T^{-1}	[2-29]
D_{xx}	Dispersion/diffusion coefficient for transport in x direction due to a gradient of c in the x-direction	L^2T^{-1}	[3-58,80,83]
D_{xz}	Dispersion/diffusion coefficient for transport in x direction due to a gradient of c in the z-direction	L^2T^{-1}	[3-58,82,84]
D_{zx}	Dispersion/diffusion coefficient for transport in z direction due to a gradient of c in the x-direction	L^2T^{-1}	[3-58,82,84]
D_{zz}	Dispersion/diffusion coefficient for transport in z direction due to a gradient of c in the z-direction	L^2T^{-1}	[3-58,81,83]
E	Evaporation rate from the substrate surface	LT^{-1}	[6-6]
E	Cumulative evaporation, i.e. E integrated over t	L	6.3
EC	Electrical conductivity	$L^{-1}\Omega^{-1}$	[5-6,8-15,16, A8-1]
EC_T	EC at specified temperature T	$L^{-1}\Omega^{-1}$	[5-9]
EC_{av}	Some average EC	$L^{-1}\Omega^{-1}$	8.2
EC_b	Bulk substrate EC	$L^{-1}\Omega^{-1}$	[5-10]
EC_e	EC of a saturation extract	$L^{-1}\Omega^{-1}$	[8-16]
$EC_{e,av}$	Some average EC_e	$L^{-1}\Omega^{-1}$	8.2
EC_w	Bulk aqueous solution EC	$L^{-1}\Omega^{-1}$	[5-10]
ET	Evapotranspiration rate	LT^{-1}	[6-6]

ET	Cumulative evapotranspiration, i.e. *ET* integrated over *t*	L	6.3,6.4
ET_f	*ET* at time t_h	L	6.4
ET_c	*ET* of covered plot	LT^{-1}	[6-7]
ET_p	Potential *ET*	LT^{-1}	[6-11]
ET_p	Cumulative potential evapotranspiration, i.e. ET_p integrated over *t*	L	8.2
ET_u	*ET* of uncovered plot	LT^{-1}	[6-8,9]
EX	Excess amount of water application	1	[5-15]
F	Faraday's constant	ATm^{-1}	[A8-1]
Fo	Fourier number	1	[3-75]
F_d	Dilution factor	1	[6-19,A6-1]
G	Dimensionless geometry function	1	[2-49,50]
G_0	Dimensionless geometry function, special case of *G*	1	[2-24,26]
H	Hydraulic head	L	[2-2]
I	Index of column number	1	[3-6]
I_s	Ionic strength	$M^{-1}m$	[A8-2]
I_η	Incomplete beta function of order η	1	[4-3]
J	Index of row number	1	[3-7]
K	Hydraulic conductivity	LT^{-1}	[2-2]
K_1	Root hydraulic conductance	LT^{-1}	[2-21]
K_a	Dielectric permittivity	1	[5-2]
K_e	Ethanol conductivity at saturation	LT^{-1}	[4-23]
K_p	TDR cell constant	L^{-1}	[5-6]
K_r	Relative *K*	LT^{-1}	[4-2]
K_s	*K* at saturation	LT^{-1}	[4-2]
K_x	*K* in *x*-direction	LT^{-1}	[3-9,11]
K_z	*K* in *z*-direction	LT^{-1}	[3-13,14]
K_Γ	Specified *K* normal to the boundary Γ	LT^{-1}	[2-10]
L	Cholesky lower triangular matrix	$LT^{-0.5}$	[3-47,48]
$\mathbf{L}^T$	Transpose of **L**	$LT^{-0.5}$	[3-47]
L	Deviation from perfect mass balance	1	[6-15]
$L_.$	*L* without considering the sand bed buffer	1	[6-18]
LAI	Leaf area index	L^2L^{-2}	6.3
LF	Leaching fraction	1	[5-15]
L_D	Drain distance	L	[8-1]
L_{rv}	Root length density	LL^{-3}	[2-20,7-1]
$L_{rv,f}$	Final L_{rv}	LL^{-3}	[7-1]
M	Number of rows	1	3.2
N	Number of columns	1	3.2
N_a	Avogadro's number	m^{-1}	[A8-4,5]

N_p	Number of plants in the growth system		[6-13]
P	Hysteresis shape function	1	[4-8,9,10]
Pe	Peclet number	1	[3-73]
P_d	Domain dependence factor	1	[A1-1]
Q	Total density of nutrient per unit volume of substrate	$L^{-3}M$	[2-31,32]
Q_f	Q at the end of the cleaning case (section 8.3)	M	8.3
Q_m	Total amount of nutrient	M	[2-45,46]
Q_{m0}	Initial value of Q_m	M	[2-45]
R	Radial coordinate	L	[2-23]
R	Radiation (section 6.4)	JL^{-2}	6.4
R	Cumulative radiation since $t = 0$	JL^{-2}	[5-14],6.1,6.4
R_f	R at time t_h	JL^{-2}	6.4
R_0	Root radius	L	[2-23]
R_1	Radius of porous medium surrounding a root	L	[2-20]
R_c	Combined series resistance of the cable tester, connectors and cable	Ω	[5-6]
R_g	Universal gas constant	$Jm^{-1}\Theta^{-1}$	[A8-4,5]
R_t	Total resistance of TDR system	Ω	[5-6,7]
R_{th}	Thermistor resistance	Ω	[5-12]
R_v	Build-in precision resistance	Ω	[5-12]
S	Supplied excitation	V	[5-12]
S_c	Fractional soil cover	L^2L^{-2}	[6-10]
S_e	Reduced volumetric water content	1	[4-1]
S_s	Sink strength for solute; or root nutrient uptake rate	$L^{-3}MT^{-1}$	[2-31,51]
S_{sm}	Maximum possible root nutrient uptake rate per unit surface area of substrate	$L^{-2}MT^{-1}$	[2-49]
S_{sr}	Required plant nutrient uptake rate	$L^{-3}MT^{-1}$	[2-47]
$S_{sr,c}$	Required uptake per unit root length	$L^{-1}MT^{-1}$	[3-91]
S_w	Sink strength for water or root water uptake rate	$L^3L^{-3}T^{-1}$	[2-1]
T	Transpiration rate	LT^{-1}	[2-19,6-6,7,8]
T	Cumulative transpiration i.e. T integrated over t	L	[5-14],6.3,6.4
T_f	T at time t_h	L	6.4
T	Temperature	Θ	[5-3,16, A8-4,5]
T_h	Heat sum	$T\Theta$	6.1,6.5
$\overline{T}$	Average day temperature	Θ	6.1
T_1	Dummy term	1	[4-14,15]
T_2	Dummy term	1	[4-14,16]
T_3	Dummy term	1	[4-14,17]
T_4	Dummy term	L	[4-18]

T_p	Potential T	LT^{-1}	[2-27,6-11]
U_a	Nutrient uptake determined as accumulation in the crop	M	[6-12,13]
U_d	Nutrient uptake determined as depletion from the growth system	M	[6-12,14]
U_{d-}	U_d without considering the sand bed buffer	M	[6-16]
V	Volume of total flow domain	L^3	[2-46]
V_A	The wave form amplitude of the incoming signal	V	[5-8]
V_d	Volume of drainage water	L^3	[8-6,7]
V_{d1}	Volume of water present in the flow domain when the phreatic surface has reached its maximum height	L^3	[8-7,8]
V_{d2}	Volume of water present in the flow domain when the saturated zone has just disappeared	L^3	[8-7,9]
V_{ds}	Volume of saturated zone	L^3	[8-6,10]
V_i	Volume of water present in the flow domain	L^3	7.5,8.3
V_s	Volume of applied solution	L^3	7.5,8.3
V_v	Measured voltage	V	[5-11,12,13]
V_w	Volume of water used in 1:2-by-volume extraction method	L^3	[6-19]
V_∞	The wave form amplitude the final amplitude	V	[5-8]
W	Weight (or cumulative uptake as in Section 6.5)	M	[6-1,2]
W^*	W at inflection point	M	[6-3]
W_i	Initial W	M	[6-2]
W_f	(Asymptotic) final W	M	[6-1,2]
X	Profile width	L	[2-12]
Z	Profile depth	L	[2-13]
Z_0	The distance between substrate surface and water table	L	[8-13]
Z_c	The characteristic impedance of the cable tester system including the coaxial cable	Ω	[5-7]
Z_i	Impedance	Ω	[A4-1]
a	Crop specific constant in transpiration reduction function	1	[2-27]
a_1	Iteration parameter in conjugate gradient method	1	[3-53]
a_2	Iteration parameter in conjugate gradient method	1	[3-53]
a_G	Parameter in Genstat 5 logistic expression		[A5-1,2]
a_L	Longitudinal dispersivity	L	[2-35]
a_T	Transversal dispersivity	L	[2-35]
b	Vector containing known quantities b	L^3T^{-1}	[3-39]
b	Known quantities in difference equation	L^3T^{-1}	[3-22,24]

b_G	Parameter in Genstat 5 logistic expression		[A5-1,2]
c	Concentration of nutrient in substrate solution	$L^{-3}M$	[2-32]
$c(ul)$	c at upper left corner of the cleaning case	$L^{-3}M$	8.3
$\bar{c}$	Average bulk concentration	$L^{-3}M$	[2-49]
c_0	Initial c	$L^{-3}M$	[2-44]
c_D	c at the drain location	$L^{-3}M$	[2-40]
c_G	Parameter in Genstat 5 logistic expression		[A5-1,2]
c_{av}	Some average c	$L^{-3}M$	8.2
c_f	c in fertigation water	$L^{-3}M$	[2-37],7.5,8.3
d	Maximum relative change during iteration	1	[3-55]
d_1	Maximum relative change in h during main iteration	1	[3-55,56]
d_2	Maximum relative change in K during main iteration	1	[3-55,57]
d_I	Maximum relative change during ICCG iteration	1	[3-54]
d_i	Effective ion diameter	L	[A8-3]
d_r	Rod diameter of TDR probe	L	[A4-1]
e	Electron charge	AT	[5-16,A8-4,5]
f	Drainable porosity or specific yield	$L^3 L^{-3}$	[8-3,6,11,12]
$f(\theta)$	Function defined by Eq. [A1-2] (App. 1 only)	1	[A1-2]
f_1	Dimensionless parameter	1	[2-35]
f_2	Dimensionless parameter	1	[2-35]
f_K	Temperature correction function for K_a	1	[5-3,4,5]
f_T	Temperature coefficient of the medium	Θ^{-1}	[5-9]
f_a	Activity coefficient	1	[A8-1,3,6,7,8]
f_r	Transpiration reduction function	1	[2-27,28]
g	Gravitational field strength	LT^{-2}	[2-22]
$\mathbf{h}$	Vector containing unknown values of h	L	[3-39]
$\mathbf{h}^0$	Initial guess of $\mathbf{h}$	L	[3-52]
h	Pressure head	L	[2-3]
h'	ln transformed variable of ah	1	[A9-1]
h^+	h for which $\theta_d = \theta$	L	[4-10,11,12]
h^*	Approximate solution for h	L	[3-3]
h^0	h at time t	L	[3-21]
h_0	Initial h	L	[2-17]
h_1'	Lower integration boundary for h'	1	[A9-3]
h_2'	Upper integration boundary for h'	1	[A9-3]
h_Z	Prescribed h at bottom boundary	L	[3-35]
h_a	Air entry value	L	2.1
h_{cf}	Height of equivalent saturated capillary fringe region	L	[8-14]
h_r	Root water pressure head	L	[2-21]

$h_{r,1/2}$	h_r where $T_a = 0.5T_p$	L	[2-28]
h_{ref}	Reference value for h	L	[2-7]
h_{rs}	h at root-substrate interface	L	[2-21]
h_Γ	Specified h at boundary Γ	L	[2-9]
h_Δ	h at reversal point	L	[4-8,9]
i	Index referring to CV interface between columns I and $I+1$	1	[3-6]
i	Tensor or matrix index counter		[2-34]
j	Index referring to CV interface between rows J and $J+1$	1	[3-7]
j	Tensor or matrix index counter		[2-34]
k	Iteration counter	1	[3-19]
k_B	Boltzmann constant	$J\Theta^{-1}$	[5-16]
k_L	Inverse time constant in the logistic growth function	T^{-1}	[6-1,5]
k_S	Inverse time constant in logistic expression for S_c	T^{-1}	[6-10]
k_T	Proportionality constant in exponential expression for T_p/ET_p	1	[6-11]
m	Curve-shape parameter	1	[4-1]
m_0	Maximum height of phreatic surface above bottom	L	[8-1]
m_G	Parameter in Genstat 5 logistic expression		[A5-1,2]
m_d	Curve shape parameter of main drying curve	1	4.1,[4-24,25]
m_p	Height of phreatic surface above bottom	L	[8-2]
m_s	Number of solvents	1	[A8-1]
m_w	Curve shape parameter of main wetting curve	1	4.1,[4-24,25]
n	Curve-shape parameter	1	[4-1]
n_d	Curve shape parameter of main drying curve	1	4.1,[4-24,25]
n_v	Valence of ion	1	[5-16,A8-1]
n_w	Curve shape parameter of main wetting curve	1	4.1,[4-24,25]
n_Γ	Coordinate normal to the boundary Γ	L	[2-8]
$\mathbf{p}$	Direction vector	L	[3-53]
$\mathbf{p}^0$	Initial guess of $\mathbf{p}$	L	[3-52]
$\mathbf{q}$	Volumetric water flux density	$L^3L^{-2}T^{-1}$	[2-1]
$\mathbf{q}_s$	Solute or nutrient mass flux density	$L^{-2}MT^{-1}$	[2-31,33]
q	Volumetric water flux density - magnitude of $\mathbf{q}$	$L^3L^{-2}T^{-1}$	[2-34]
q_{sx}^c	Magnitude of convective part of $\mathbf{q}_s$ in horizontal direction	$L^{-2}MT^{-1}$	[3-59,61]
q_{sz}^c	Magnitude of convective part of $\mathbf{q}_s$ in vertical direction	$L^{-2}MT^{-1}$	[3-59,61]

q_{sxx}^{d}	Magnitude of dispersive/diffusive part of q_s in horizontal direction due to a gradient in c in horizontal direction	$L^{-2}MT^{-1}$	[3-59,62]
q_{sxz}^{d}	Magnitude of dispersive/diffusive part of q_s in horizontal irection due to a gradient in c in vertical direction	$L^{-2}MT^{-1}$	[3-59,62]
q_{szx}^{d}	Magnitude of dispersive/diffusive part of q_s in vertical direction due to a gradient in c in horizontal direction	$L^{-2}MT^{-1}$	[3-59,62]
q_{szz}^{d}	Magnitude of dispersive/diffusive part of q_s in vertical direction due to a gradient in c in vertical direction	$L^{-2}MT^{-1}$	[3-59,62]
q^{n}	Net flux density into a control volume	$L^{3}L^{-2}T^{-1}$	[3-73,74]
q_0	Prescribed q at the top boundary	$L^{3}L^{-2}T^{-1}$	[2-12]
q_1	Water flux density across root surface	LT^{-1}	[2-19]
q_2	Water flux density from bulk soil towards root surface	LT^{-1}	[2-19]
q_Z	Prescribed q at the bottom boundary	$L^{3}L^{-2}T^{-1}$	[2-13]
q_{max}	Maximum net flux density into any control volume	$L^{3}L^{-2}T^{-1}$	[3-93]
q_{sx}	Magnitude of q_s in horizontal direction	$L^{-2}MT^{-1}$	[3-60,63]
q_{sz}	Magnitude of q_s in vertical direction	$L^{-2}MT^{-1}$	[2-37,3-60,63]
q_x	Magnitude of horizontal component of q	$L^{3}L^{-2}T^{-1}$	[3-58,8-10]
q_z	Magnitude of vertical component of q	$L^{3}L^{-2}T^{-1}$	[2-12,3-58]
q_Γ	Specified q normal to the boundary Γ	$L^{3}L^{-2}T^{-1}$	[2-10]
r	Residual vector	$L^{3}T^{-1}$	[3-53]
r^0	Initial guess of r	$L^{3}T^{-1}$	[3-52]
r	Residual		[3-3]
r^2	Regression coefficient	1	4.3
r_x	Radius of a xylem vessel	L	[2-22]
s	Plant size factor	1	[5-14]
s_i	Irrigation intensity	LT^{-1}	[8-1]
s_r	Rod spacing of TDR probe	L	[A4-1]
Δs	Characteristic length of control volume	L	[3-73,74,75]
Δs_{min}	Minimum grid spacing	L	[3-93,94]
t	Time	T	[2-1]
t^*	t at inflection point of a logistic function	T	[6-4,6-10]
$t_{0.1}$	t when $m_p = 0.1m_0$	T	[8-4,5]
t_f	End time of simulation	T	3.5
t_h	Time of harvest	T	6.4
t_m	Multiplication factor for Δt	1	3.5
t_{mp}	t when phreatic surface has reached height m_p	T	[8-3]

Δt	Time interval	T	[3-8]
Δt_C	Δt required by Co	T	[3-95]
Δt_F	Δt required by Fo	T	[3-95]
Δt_i	Initial Δt	T	3.5
Δt_{max}	Maximum allowable Δt	T	[3-95]
Δt_{min}	Minimum allowable Δt	T	3.5
Δt_p	Time interval between current time and next printing time	T	[3-95]
v	Water velocity	LT^{-1}	[2-1]
w	Weighing function	1	[3-4]
w_E	Distance weighing factor in x-direction	1	[3-10]
w_S	Distance weighing factor in z-direction	1	[3-15]
w_g	Gravimetric water content	MM^{-1}	[5-1]
x	Horizontal coordinate	L	[2-12]
x_D	Radius of drain	L	[2-13]
Δx_I	Width of column I	L	[3-6]
Δx_i	Distance between nodes in columns I and I+1	L	[3-6]
y	Dummy vector	$L^2T^{-0.5}$	[3-50]
y	Horizontal coordinate	L	2.1
y_G	Parameter in Genstat 5 logistic expression		[A5-1,2]
Δy	Control volume width in y-direction	L	3.2
z	Vertical coordinate positive downwards	L	[2-4]
z_g	Gravitational head	L	[2-3]
Δz	Thickness of a layer or root length	L	[2-21]
Δz_J	Thickness of row J	L	[3-7]
Δz_j	Distance between nodes in rows J and J+1	L	[3-7]
Γ	Boundary of flow domain		[2-8]
α	Curve-shape parameter	L^{-1}	[4-1]
α_1	Coefficient in polynome	1	[5-2,11]
α_2	Coefficient in polynome	1	[5-2,11]
α_3	Coefficient in polynome	1	[5-2]
α_4	Coefficient in polynome	1	[5-2]
α_T	Empirical transpiration crop factor	$J^{-1}L^3$	[5-14]
α_d	α of main drying curve	L^{-1}	4.1, [4-12,24,25]
α_w	α of main wetting curve	L^{-1}	4.1,[4-24,25]
β_T	Empirical transpiration crop factor	$LT\Theta^{-1}$	[5-14]
γ	Matrix index	1	[3-48]
δ_{ij}	Kronecker delta: $\delta_{ij} = 1$ if i=j, $\delta_{ij} = 0$ if $i{\neq}j$	1	[2-35]
ϵ	Dielectric permittivity of solvent	$AL^{-1}TV^{-1}$	[A8-4,5]

ϵ_0	Dielectric permittivity of vacuum	$AL^{-1}TV^{-1}$	[A8-4,5]
ϵ_1	Some small number used in Appendix 1	1	App. 1
ϵ_2	Some small number used in Appendix 1	1	App. 1
ϵ_a	Convergence criterion in root finding procedure of Eq. [A1-2]	1	App. 1
ϵ_c	Convergence criterion	1	3.3
ϵ_i	Convergence criterion ICCG	1	3.3
ϵ_t	Convergence criterion in root water uptake module	1	[3-38]
ϵ_κ	Hysteresis reversal criterion	1	[4-20]
ζ	Maximum permissible change in θ	L^3L^{-3}	[3-93]
η	Dummy variable		[2-7]
η_e	Viscosity of ethanol	$L^{-1}MT^{-1}$	[4-23]
η_l	Viscosity of water	$L^{-1}MT^{-1}$	[2-22,4-23]
θ	Volumetric water content	L^3L^{-3}	[2-1]
θ^0	θ at time t	L^3L^{-3}	[3-18]
θ_d	θ of main drying curve	L^3L^{-3}	[4-11]
θ_w	θ of main wetting curve	L^3L^{-3}	[4-8,9]
θ_i	Dimensionless parameter	1	[2-36]
θ_r	Residual θ	L^3L^{-3}	[4-1]
$\theta_{r,d}$	Residual θ of main drying curve	L^3L^{-3}	4.1
$\theta_{r,w}$	Residual θ of main wetting curve	L^3L^{-3}	4.1
θ_s	Saturated θ	L^3L^{-3}	[4-1]
θ_{sd}	θ of scanning drying curve	L^3L^{-3}	[4-8]
$\theta_{s,d}$	θ_s of main drying curve	L^3L^{-3}	4.1
θ_{sw}	θ of scanning wetting curve	L^3L^{-3}	[4-9]
$\theta_{s,w}$	θ_s of main wetting curve	L^3L^{-3}	4.1
θ_Δ	θ at reversal point	L^3L^{-3}	[4-8,9]
$\Delta\theta$	Change in θ of the latest drying process	L^3L^{-3}	[A1-1]
$\Delta\theta_0$	$\Delta\theta$ in the absence of blockage of air access	L^3L^{-3}	[A1-1]
ι	Matrix index	1	[3-48]
κ	Matrix index	1	[3-48]
κ^*	Hysteresis direction pointer	1	[4-20,21]
κ_h	Hysteresis pointer	1	[4-21]
λ	Local iteration counter in conjugate gradient iterative solution procedure (Eq. [3-53] only)	1	[3-53]
λ	Curve-shape parameter	1	[4-2]
μ	Boundary condition parameter	L^{-1}	[2-8]
μ_m	Ionic mobility	$L^2T^{-1}V^{-1}$	[5-16,A8-1]
ν	Boundary condition parameter	1	[2-8]
π	Number pi	1	[2-20]
ρ	Dimensionless radius of soil cylinder surrounding a root	1	[2-23]

ρ_d	Dry bulk density	$L^{-3}M$	[4-22]
ρ_e	Density of ethanol	$L^{-3}M$	[4-23]
ρ_l	Density of water	$L^{-3}M$	[2-22,4-23]
ρ_s	Particle density	$L^{-3}M$	[4-22]
ρ_s	Density of solvent (App. 8 only)	$L^{-3}M$	[A8-1]
ρ_∞	The reflection coefficient at long times	1	[5-7,8]
σ	Dimensionless root water uptake rate	1	[2-47,48]
τ	Tortuosity factor	1	[2-35,36]
ϕ	Matric flux potential	L^2T^{-1}	[2-7]
$\overline{\phi}$	Average matric flux potential	L^2T^{-1}	[2-24,25]
ϕ_a	Air-filled porosity	L^3L^{-3}	[6-19,A6-1]
ϕ_p	Porosity	L^3L^{-3}	[4-22]
ϕ_{rs}	Matric flux potential at root-porous medium interface	L^2T^{-1}	[2-24]

Mathematical operators

d	Derivative operator	
e, exp	Natural base	
ln	Natural logarithm	
max	Operator yielding the maximum value in argument list	
min	Operator yielding the minimum value in argument list	
∇	Gradient operator	L^{-1}
$\nabla\cdot$	Divergence operator	L^{-1}
∂	Partial derivative operator	
$\partial/\partial n\vert_\Gamma$	The exterior normal derivative operator	L^{-1}
$\mathscr{L}$	Some differential operator (Subsection 3.2.1)	
$\vert\eta\vert$	Represents the absolute value of argument η	
Δ	Small increment	
$\{.,.\}$	In-product of two vectors	

Abbreviations

AB-DLO	DLO Research Institute for Agrobiology and Soil Fertility (DLO Instituut voor Agrobiologie en Bodemvruchtbaarheid)
ADI	Alternating Direction Implicit
BTC	BreakThrough Curve

CEC	Cation Exchange Capacity
CV	Control Volume
D	Drainage
ET	EvapoTranspiration
I	Irrigation
ICCG	Incomplete Cholesky-Conjugate Gradient
NFT	Nutrient Film Technique
GCRS	Glasshouse Crops Research Station
SSQ	Sum of Squared Differences
TDR	Time Domain Reflectometry

Curriculum Vitae

Marius Heinen werd geboren op 13 oktober 1962 te Sint-Michielsgestel. Na beëindiging van het ongedeeld Gymnasium 'Beekvliet' in zijn geboorteplaats, is hij in 1981 aan de toenmalige Landbouwhogeschool, nu Landbouwuniversiteit (LUW), te Wageningen begonnen aan de studie Bodemkunde en Bemestingsleer (nu Bodemkunde en Planten-voeding). In Maart 1988 studeerde hij af in de twee hoofdvakken Bodemnatuurkunde en Agrohydrologie en het bijvak Bodemverontreiniging. Tijdens zijn studie heeft hij zijn praktijktijd doorgebracht aan de New Mexico State University te Las Cruces, New Mexico (USA). Het hoofdafstudeervak Bodemnatuurkunde werd uitgevoerd op het Instituut voor Bodemvruchtbaarheid (nu Instituut voor Agrobiologie en Bodemvrucht-baarheid) te Haren. In augustus 1988 werd hij aangesteld als wetenschappelijk onderzoeker op het Instituut voor Bodemvruchtbaarheid bij de afdeling Bodemfysica. Tijdens zijn werkzaamheden kwam hij in aanraking met de problematiek van gesloten teeltsystemen in de glastuinbouw. In 1990 resulteerde het onderhavige in de formulering van het project 'Dynamiek van water en nutriënten in gesloten, recirculerende teeltsystemen in de glastuinbouw, met name systemen gebaseerd op zandbedden'. Dit project heeft geresulteert in dit proefschrift. Op dit moment is hij als senior wetenschappelijk onderzoeker Bodemfysica en Nutriëntendynamiek werkzaam op het Instituut voor Agrobiologie en Bodemvruchtbaarheid te Haren bij de afdeling Bodem- en Nutriëntenbeheer.

Publicaties

Heinen M. and P.A.C. Raats, 1990. Evaluation of two models describing the steady discharge from a constant head well permeameter into unsaturated soil. *Soil Science* 150: 401-412.

Heinen M., A. de Jager and H. Niers, 1991. Uptake of nutrients by lettuce on NFT with controlled composition of the nutrient solution. *Netherlands Journal of Agricultural Science* 39: 197-212.

Van Noordwijk M., Widianto, M. Heinen, and Kurniatun Hairiah, 1991. *Old tree root channels in acid soils in the humid tropics: Important crop root penetration, water infiltration and nitrogen management.* IN: R.J. Wright et al. (Eds.), Plant-soil interactions at low pH. Kluwer Academic Publishers, The Netherlands, p. 423-430.

Heinen M., 1992. Control of the composition of the nutrient solution in an automated NFT system: A simulation study. *Acta Horticulturae* 304: 281-289.

Heinen M. and K. Harmanny, 1992. Evaluation of the performance of ion-selective electrodes in an automated NFT system. *Acta Horticulturae* 304: 273-280.

Schwarz D., M. Heinen und M. van Noordwijk, 1993a. *Wurzelverteilung bei Salat in einem Kiesbeetsysteem.* IN: W. Merbach (ed.), Ökophysiologie des Wurzelraumes, Nr 4, p. 9-12.

Schwarz D., M. Heinen and M. Van Noordwijk, 1993b. *Root distribution of lettuce in sand bed systems.* IN: Proceedings of the 4th International Symposium on Structure and Function of Root, 20-26 June 1993. Stara Lesna, Slovakia.

Postma R., O. Oenema, D.W. Bussink, M. Heinen en J. van Moolenbroek, 1994. Gasvormige stikstofverliezen bij de teelt van sla op een zandbed onder glas. *Meststoffen*, Dutch/English annual on fertilizers and fertilization. Nutrient Management Institute (NMI), Wageningen, The Netherlands, p. 28-34.

De Willigen P., M. Heinen and B.J. van den Broek, 1994. *Modeling water and nitrogen uptake of a potato crop growing on a ridge. In*: A.J. Haverkort and D.K.L. MacKerron, Potato ecology and modelling of crops under conditions limiting growth. Kluwer Academic Publishers, Dordrecht, The Netherlands, pp. 75-88.

Van Moolenbroek A. en M. Heinen, 1994. Nieuwe stap bij gesloten teeltsystemen. *Groenten + Fruit/Glasgroenten* Week 47 (25-11-1991) p. 13.

Heinen M. and P. De Willigen, 1995. Dynamics of water and nutrients in closed, recirculating sand bed systems: modeling water flow, nutrient transport, and root water and nutrient uptake. *Acta Horticulturae* 401: 501-508.

Heinen M. and J. van Moolenbroek, 1995. Water balance of lettuce grown on sand beds. *Acta Horticulturae* 401: 517-524.

Schwarz D., M. Heinen and M. van Noordwijk, 1995. Rooting intensity and root distribution of lettuce grown in sand beds. *Plant and Soil* 176: 205-217.

Rapporten e.d.

Heinen M., 1985. Solute transport and hydraulic properties in unsaturated soil in laboratory columns and deep field lysimeter. Validation of transport models. Training report in partial satisfaction of the requirements of the MSc degree in soil physics, 67 p. + appendices.

Wierenga P.J., W. Strong, M. Heinen, D. Hudson, and M. Th. van Genuchten, 1985. Validation of stochastic flow and transport models for unsaturated soils. Department of Crop and Soils Sciences, New Mexico State University, Las Cruces, Research Report 85-SS-02, 67 p.

Heinen M., 1987. STRADI, a quasi 3-dimensional saturated transient groundwater flow model for inhomogeneous soils. Report in partial satisfaction of the requirements of the MSc degree in soil physics, 49 p. + appendices.

Heinen M., 1988. Theoretical and experimental evaluation of two models describing steady discharge from the Guelph permeameter. DLO Institute for Soil Fertility Research, Haren, Nota 184, 60 p. + appendices.

Heinen M., 1990. The use of ion-selective electrodes in NFT systems. DLO Institute for Soil Fertility Research, Haren, Nota 222, 29 p.

Heinen M., 1990. Analytical growth equations and their genstat 5 equivalents. DLO Institute for Soil Fertility Research, Haren, Nota 223, 48 p.

Heinen M., 1990. Identification of physical and physico-chemical properties of a partially acetylated cellulose acetate polymer and evaluation of its performance as a substrate for plant roots. DLO Institute for Soil Fertility Research, Haren, The Netherlands, Report of contract research for Hoechst Celanese Corporation Brussels, 29 p.

Heinen M. A. de Jager en H. Niers, 1990. Regeling van het nutriëntenaanbod aan planten in kunstmatige substraten. 1. Systeembeschrijving en oriënterend experiment met sla (with an English summary: Control of nutrient supply to plants on artificial substrates. 1. System description and preliminary experiment with lettuce). DLO Institute for Soil Fertility Research, Haren, Nota 221, 78 p.

De Willigen P. en M. Heinen, 1992. Modellering van tweedimensionaal transport van water in de grond. IN: IB-DLO Jaarverslag 1992, DLO Instituut voor Bodemvruchtbaarheid, Haren, p. 79-81.

Heinen M. and P. de Willigen, 1992. FUSSIM2. A simulation model for two-dimensional flow of water in unsaturated soil. Nota 260, DLO Institute for Soil Fertility Research, Haren, The Netherlands, 146 p.

Raats P.A.C., W. Otten en M. Heinen, 1992. Substraatteelt en fertigatie. IN: IB-DLO Jaarverslag 1992, DLO Instituut voor Bodemvruchtbaarheid, Haren, p. 47-55.

Heinen M. and P. de Willigen, 1993. FUSSIM2: a simulation model for two-dimensional flow of water in soil, coupled with modules for root water uptake and nutrient transport. Abstract, EGS 18th General Assembly of the European Geophysical Society, Wiesbaden, Annales Geophysicae, Supplement II to Volume 11, p. 250.

Raats P.A.C., W.Otten en M. Heinen, 1993. Substraatteelt en fertigatie (Crop production on artificial substrates and fertigation). Jaarverslag 1992, Instituut voor Bodemvruchtbaarheid (IB-DLO), pp. 47-55.

Heinen M., 1994. Growth and nutrient uptake by lettuce grown on NFT. Report 1, Research Institute for Agrobiology and Soil Fertility (AB-DLO), Haren, The Netherlands, 74 p.

Van Moolenbroek J. en M. Heinen, 1994. Dynamiek van water en nutriënten in gesloten, recirculerende teeltsystemen, met name systemen gebaseerd op zandbedden. Verslaglegging van experimenten op het PTG. Intern Verslag 14, Proefstation voor Tuinbouw onder Glas (PTG), Naaldwijk, 28 p. + bijlagen.

Heinen M., W. Voogt, R. Booij, R. van Zuydam en C. de Kreij, 1995. Notitie 'Benutting van water en stikstof in de glastuinbouw'. Interne notitie, AB-DLO, PBG, IMAG-DLO, Haren, 38 p.

Heinen M., 1996. Dynamics of water and nutrients in closed recirculating cropping systems: model, validation, and use of model. Abstract, Annales Geophysicae, part II Hydrology, Oceans, Atmosphere & Nonlinear Geophysics, Supplement II to Volume 14, EGS, Wiesbaden, Germany, p. C321.

Heinen M. And P.A.C. Raats, 1996. Unconventional flow: water flow from dry to wet. Abstract, Annales Geophysicae, part II Hydrology, Oceans, Atmosphere & Nonlinear Geophysics, Supplement II to Volume 14, EGS, Wiesbaden, Germany, p. C321.

Heinen M., C. Sonneveld, W. Voogt, R. Baas, W.G. Keltjens and B. Veen, 1996. Mineral balance of young tomato grown on nutrient solution. Report 66, Research Institute for Agrobiology and Soil Fertility, Haren, The Netherlands, 47 p.